ASPECTS OF
ELECTROMAGNETIC SCATTERING.

A thesis presented for the degree of

Doctor of Philosophy

in Electrical Engineering,

in the University of Canterbury,

Christchurch, New Zealand,

by

J.D. Hunter,

1970.

Se non è vero, è molto ben trovato.

ACKNOWLEDGEMENTS.

I am greatly indebted to my supervisor Mr. R.H.T. Bates whose insight, guidance, and encouragement have contributed so much to this thesis.

Financial support has been provided by the University Grants Committee.

ABSTRACT

An expression for the field scattered by a perfectly conducting wedge with a deformed apex is formulated as a finite matrix equation to illustrate the application of the current density replacement technique. This technique enables the scattering from any size of body to be determined to a given accuracy after the inversion of one finite matrix, provided that the shape of the body can be derived by inwardly deforming a finite part of a body from which the scattering is known explicitly. The size of only the deformed part of the body is limited by available computational facilities.

The field scattered from truncated and rounded wedges is calculated. These results not only enable the effect of edge deformation to be studied, but are also used to evaluate the accuracy of the geometrical theory of diffraction and physical optics estimates of the diffracted field.

Expressions for the field scattered by a perfectly conducting wedge in the presence of transversely polarized line sources are found. These results are used with an iterative current density replacement technique to formulate expressions for the field scattered by a truncated wedge, and thus derive a secondary edge diffraction coefficient for use with the geometrical theory of diffraction. This coefficient is applicable to perfectly conducting bodies with small or large separation between edges. The increased accuracy obtainable with this coefficient, and a modification to the physical optics representation of the current density on a body with edges, are discussed.

SYMBOLS, TERMINOLOGY, AND ABBREVIATIONS

H	magnetic field intensity
E	electric field intensity
B	magnetic flux density
D	electric flux density
J	electric current density
q	electric charge density
A	magnetic vector potential
U	E, H, or A
$K(x)$	surface current density at x
μ	permeability
μ_o	permeability of free space
ε	permittivity
ε_o	permittivity of free space
ω	angular frequency; variable of integration
c	velocity of electromagnetic propagation $c = (\mu\varepsilon)^{-\frac{1}{2}}$
λ	wavelength
k	wavenumber $k = \omega/c = 2\pi/\lambda$
$J_\nu(z)$	Bessel function of the first kind of order ν and argument z
$H_\nu^{(2)}(z)$	Hankel function of the second kind of order ν and argument z
$C_\nu(z), \overline{C}_\nu(z)$	Any cylindrical Bessel function of order ν and argument z
$\delta(z)$	the Dirac delta function

j	$j^2 = -1$
$\dot{X}$	time derivative of X, $\dot{X} = \frac{\partial X}{\partial t}$
$\hat{r}$	unit vector
$\hat{n}$	outward unit normal vector to a surface or contour
$\vec{F}$	the vector of magnitude F
$\nabla \times$	the vector curl operator
$\nabla \cdot$	the vector divergence operator
∇	the vector gradient operator
(ρ, ϕ, z) (s, θ, z) (r, θ, z) (s, δ, z)	cylindrical polar co-ordinate systems

electrically polarized $\vec{E} = \hat{z}E, \quad \vec{A} = \hat{z}A$

magnetically polarized $\vec{H} = \hat{z}H$

G.O.	Geometrical Optics
G.T.D.	Geometrical Theory of Diffraction
P.O.	Physical Optics
P.C.R.	Polarization Current Replacement
S.C.R.	Surface Current Replacement
I.R.	Iterative Surface Current Replacement
M.P.O.	Modified Physical Optics
U.HP.	Upper Half-plane
L.HP.	Lower Half-plane

TABLE OF CONTENTS

CHAPTER 3 (continued)

PREFACE

This thesis is concerned with the computation of electromagnetic scattering, particularly from perfectly conducting bodies.

It is evident from recent volumes of the IEEE Transactions on Antennas and Propagation that considerable attention is being devoted to the application of ray-optical techniques to electromagnetic scattering problems. Diffraction by horns and obstacles in waveguides has received particular attention.

In order to be able to evaluate the accuracy of ray-optical and other approximate methods of determining electromagnetic scattering, it is desirable to have available solutions to other than simple scattering problems. This thesis presents techniques for determining such solutions. These techniques are essentially new and are of interest in their own right.

The field scattered from a perfectly conducting wedge with a deformed apex is calculated by using a current density replacement technique. The results not only enable the effect of edge deformation to be studied, but are also used to evaluate the accuracy of the geometrical theory of diffraction and physical optics estimates of the diffracted field.

Expressions are found for the field scattered by a perfectly conducting wedge in the presence of a transversely

polarized line source. These results are used with an iterative current density replacement technique to formulate expressions for the field scattered by a perfectly conducting truncated wedge, and thus derive secondary edge diffraction coefficients for use with the geometrical theory of diffraction. These coefficients are equally applicable to perfectly conducting bodies with small or large separation between edges. The accuracy of these coefficients, and a suggested improvement to the physical optics representation of the current density on a body with edges, are evaluated.

Chapter 1 is introductory. New results are presented in Chapters 2 - 7.

Chapter 1 contains a brief survey of several well known methods of determining electromagnetic scattering which are relevant to this thesis. Mention is made of papers which show the usefulness and limitations of these methods.

Chapter 2 introduces a method of determining electromagnetic scattering called the current density replacement technique. This technique enables the scattering from any size of body to be determined to a given accuracy after the inversion of one finite matrix, provided that the shape of the body can be derived by inwardly deforming a finite part of a body from which the scattering is known explicitly. The size of only the deformed part of the body is limited by available computational facilities. Thus, the current replacement technique enables the scattering from large

or even infinite bodies to be calculated.

The current replacement technique is used to formulate expressions which describe the field scattered by a perfectly conducting wedge with a deformed apex, and in Chapter 3 this formulation is specialized to the truncated and rounded wedges. Results are presented which illustrate the convergence of the solutions as the matrix order is increased. It is found that the convergence is accelerated if explicit use is made of the analytic properties of the surface current density.

The results of Chapter 3 are used in Chapter 4 to study the accuracy of the physical optics and geometrical theory of diffraction estimates of the field scattered by a perfectly conducting wedge with a deformed apex. Of particular interest is the accuracy of the geometrical theory of diffraction applied to the truncated wedge when the distance between the two edges is less than one wavelength. It is found that when the incident field is magnetically polarized parallel to the wedge axis, the inclusion of the higher order diffracted fields may lead to inaccuracies. However in other cases, such as the prediction of the end-on electrically polarized backscattered field, the geometrical theory of diffraction yields accurate estimates even when the separation of the edges is as small as 0.05 wavelengths.

Expressions for the field surrounding a perfectly conducting wedge in the presence of transversely polarized

electric or magnetic line sources are derived in Chapter 5.

The results of Chapter 5 are used in Chapter 6, where the field surrounding a perfectly conducting truncated wedge is formulated by successive application of the current replacement technique to two separate perfectly conducting wedges. The expressions from the first two such applications are obtained.

It is shown in Chapter 7 that these expressions not only give rise to terms describing the primary field of the geometrical theory of diffraction, but also describe a secondary diffracted field. The resulting secondary diffraction coefficient is identical to that of the geometrical theory of diffraction when the edge separation is large, but is also valid when the distance between the edges is small. Unlike the geometrical theory of diffraction secondary diffraction coefficient, this diffraction coefficient is not zero when the field is electrically polarized parallel to the edges of the body. Results are presented which show the increased accuracy obtained by using this coefficient to approximate the field scattered from the truncated wedge and perfectly conducting strip. The improvement in the representation is particularly noticeable in the vicinity of the direction for which the secondary diffracted field of the geometrical theory of diffraction becomes infinite.

An improvement to the physical optics representation of the surface current density on a perfectly conducting body with edges is suggested in Chapter 7. It is shown that this suggestion is equivalent to representing the diffracted field by the primary diffracted field of the geometrical theory of diffraction and two correction terms for each edge of the body. Results are presented which show the increased accuracy obtained by using the modified physical optics current density.

Chapter 7 concludes with suggestions for further areas of research.

Some results in Chapters 2 and 3 have been published,[1,2] as have the derivations in Chapter 5.[3]

The computer programs required for this thesis were written in the Fortran IV language using the double precision option, and were executed on an IBM 360/44 computer which has 64K bytes of core memory. All programs and subroutines were written by the author of this thesis, with the exception of the IBM subroutine MINV which, after suitable modification for complex double precision operation, was used to invert the matrices of Chapter 3.

CHAPTER 1

Four methods of determining the electromagnetic field surrounding a scattering body are discussed in this chapter. The first of these methods requires the derivation of an explicit solution to the scattering problem, and the second involves the use of modal expansions in conjunction with an integral equation representation of the scattered field. The use of ray tracing techniques including the geometrical theory of diffraction is the third method discussed, and the fourth is the physical optics approximation.

1.1(a) EXPLICIT SOLUTIONS

A rigorous description of an electromagnetic scattering phenomenon requires the solution of Maxwell's field equations

$$\nabla \times \vec{E} = -\dot{\vec{B}}, \qquad \nabla \times \vec{H} = \vec{J} + \dot{\vec{D}},$$
$$\nabla \cdot \vec{D} = q, \qquad \nabla \cdot \vec{B} = 0, \tag{1.1}$$

formulated as a boundary value problem.

Use of the classical separation of variables technique with the Helmholtz equation

$$\nabla^2 U + k^2 U = 0 \tag{1.2}$$

is possible in only eleven separable co-ordinate systems[4] when the surface of the scatterer conforms to

a complete co-ordinate surface. Rigorous solutions can be obtained when the scattered field is described by equations of the Wiener-Hopf type[5], but the total number of known explicit solutions of Maxwell's field equations formulated as boundary value problems remains extremely limited.

One such known solution describes the field scattered by an infinite perfectly conducting wedge. Because much of this thesis is related to the problem of scattering by a wedge, several forms of the solution to this problem will be examined in some detail.

1.1(b) SCATTERING BY A PERFECTLY CONDUCTING WEDGE

Consider the infinite perfectly conducting wedge of interior angle β and surface contour C defined in terms of the (ρ, ϕ, z) cylindrical polar co-ordinate system in Fig. 1.1 by $\phi = 0$ and $\phi = m\pi$, where

$$m\pi = 2\pi - \beta. \qquad (1.3)$$

The wedge is of infinite extent in both the positive and negative z directions. When the incident field exhibits no variation in the z direction it is necessary to consider the variation of field quantities in only the ρ and ϕ directions. The problem then becomes two-dimensional, and even though the fields are described in terms of electromagnetic quantities, the expressions are equally applicable to acoustic scattering.[6]

The wedge is surrounded by a homogeneous, isotropic, time-invariant medium of permeability μ, and permittivity ε. The total field U surrounding the wedge must satisfy the Helmholtz equation (1.1) at all source-free points, and either the Neumann boundary condition

$$\frac{\partial U}{\partial n} = 0, \quad \text{on } C, \tag{1.4}$$

when the field is magnetically polarized ($\vec{H} = \hat{z}H$), or the Dirichelet boundary condition

$$U = 0, \text{ on } C, \tag{1.5}$$

when the field is electrically polarized ($\vec{E} = \hat{z}E$). n is the direction normal to the boundary contour C, and $k^2 = \omega^2\mu\varepsilon$ in (1.2). The suppressed monochromatic time dependence is $\exp(j\omega t)$. The Neumann boundary condition corresponds to the sound-hard boundary, and the Dirichelet boundary condition to the sound-soft boundary in acoustics.

In 1896, Sommerfeld obtained expressions describing the diffraction from a perfectly conducting half plane[7]. Macdonald used the method of separation of variables to obtain both series and integral representations of the field scattered by a perfectly conducting wedge[8,9]. When the incident field $\vec{U}^i$ is the plane wave

$$\vec{U} = \hat{z}U, \qquad U^i = e^{jk\rho\cos(\phi-\psi)}, \tag{1.6}$$

he found that the solutions to (1.2), subject to the boundary conditions in (1.4) and (1.5) respectively, are

given by

$$U(\rho,\phi) = W(\rho,\phi-\psi) \pm W(\rho,\phi+\psi), \tag{1.7}$$

where

$$W(\rho,\xi) = V_1(\rho,\xi) + V_2(\rho,\xi), \tag{1.8}$$

$$V_1(\rho,\xi) = e^{jk\rho\cos(\xi+2p\pi m)}, \quad |\xi + 2p\pi m| < \pi,$$

$$= 0, \quad |\xi + 2p\pi m| > \pi, \tag{1.9}$$

$$V_2(\rho,\xi) = \frac{1}{2\pi m} \int_{C_1} \frac{e^{jk\rho\cos\alpha}}{1 - e^{(\frac{-j}{m}[\alpha+\xi])}}\, d\alpha, \tag{1.10}$$

and p is any integer or zero. The upper (lower) sign in (1.7) applies when the field is magnetically (electrically) polarized.

By performing a contour integration, Pauli obtained $V_2(\rho,\xi)$ in the form[10]

$$V_2(\rho,\xi) = \frac{2\sin(\frac{\pi}{m})\,|\cos(\frac{\xi}{2})\,|}{m[\cos(\frac{\pi}{m})-\cos(\frac{\xi}{m})]} \sqrt{\frac{j}{\pi}}\, e^{jk\rho\cos\xi} \int_{\sqrt{k\rho(1+\cos\xi)}}^{\infty} e^{-j\alpha^2}\, d\alpha$$

$$+(\text{higher order terms in } \rho^{-n-\frac{1}{2}}). \tag{1.11}$$

Pauli showed that the higher order terms in (1.11) are identically zero when $\beta = 0$ (the case of the half plane), and can be neglected if $k\rho(1 + \cos\xi)$ is large. In this latter case, the asymptotic form of the expression in (1.11) is given by

$$V_2(\rho,\xi) = \frac{\sin(\frac{\pi}{m})\ e^{-jk\rho}}{\sqrt{j2\pi k\rho}\ m[\cos(\frac{\pi}{m}) - \cos(\frac{\xi}{m})]}, \quad k\rho(1+\cos\xi) \gg 1, \qquad (1.12)$$

where the first neglected term is of the order of $\rho^{-\frac{3}{2}}$. The expressions for $V_2(\rho,\xi)$ given in (1.11) and (1.12) with $\beta = 0$ are identical to those obtained by Sommerfeld.

Oberhettingher found a different asymptotic expansion of (1.11) involving only trigonometric functions in the higher order terms[11].

Consider a line source situated at (ρ_o,ψ) in Fig. 6.1 such that the incident field $\vec{U}^i$ is given by

$$\vec{U} = \hat{z}U,\ U^i(\rho,\phi) = \frac{-j}{4}H_o^{(2)}\{k[\rho^2 + \rho_o^2 - 2\rho\rho_o\cos(\phi-\psi)]^{\frac{1}{2}}\} \qquad (1.13)$$

Then a solution is required to

$$\nabla^2 U + k^2 U = -\frac{\delta(\rho-\rho_o)\ \delta(\phi-\psi)}{\rho_o}, \qquad (1.14)$$

subject to the appropriate boundary condition (1.4) or (1.5) on C. This problem of the wedge illuminated by a cylindrical wave can be solved by using the Kontorowich-Lebedev transform[12]. Thus[13]

$$U(\rho,\phi) = \frac{-j\nu}{4} \sum_{n=0}^{\infty} \varepsilon_n J_{n\nu}(k\rho)\, H_{n\nu}^{(2)}(k\rho_o)\, \{\cos[n\nu(\phi-\psi)] \pm \cos[n\nu(\phi+\psi)]\}, \qquad (1.15)$$

where $\nu = 1/m$, and ε_n is the Neumann factor defined as $\varepsilon_o = 1$; $\varepsilon_n = 2$, $n \neq 0$. The expression in (1.15) may also be written as[13]

$$U(\rho,\phi) = \Omega(\rho,\phi-\psi) \pm \Omega(\rho,\phi+\psi), \qquad (1.16)$$

where

$$\Omega(\rho,\xi) = \frac{-1}{8\pi} \int_{\infty-j\frac{\pi}{m}}^{\infty+j\frac{\pi}{m}} \frac{H_o^{(2)}\{k[\rho^2+\rho_o^2-2\rho\rho_o\cosh(mv)]^{\frac{1}{2}}\}\, \sinh v}{\cosh v - \cos(\frac{\xi}{m})}\, dv, \qquad (1.17)$$

and the upper sign in (1.16), as in (1.15), is to be taken with the boundary condition (1.4) for a magnetic line source; and the lower sign is to be taken with the boundary condition (1.5) for an electric line source. By deforming the contour of integration in (1.17) into the straight lines joining $\infty - j\frac{\pi}{m}$, $-j\frac{\pi}{m}$, $j\frac{\pi}{m}$, $\infty + j\frac{\pi}{m}$, and accounting for the included poles which occur only on the imaginary axis, Jones showed that

$$\Omega(\rho,\xi) = \omega_1(\rho,\xi) + \omega_2(\rho,\xi), \qquad (1.18)$$

$$\omega_1(\rho,\xi) = \frac{-j}{4} H_o^{(2)}\{k[\rho^2+\rho_o^2-2\rho\rho_o\cos(\xi+2\pi pm)]^{\frac{1}{2}}\}, |\xi+2\pi pm| < \pi,$$

$$= 0, \qquad |\xi+2\pi pm| > \pi, \tag{1.19}$$

$$\omega_2(\rho,\xi) = \frac{-j}{8\pi}\int_{-\infty}^{\infty} \frac{\sin(jv+\frac{\pi}{m})\, H_o^{(2)}\{k[\rho^2+\rho_o^2+2\rho\rho_o\cosh(mv)]^{\frac{1}{2}}\}}{\cos(jv+\frac{\pi}{m}) - \cos(\frac{\xi}{m})}\, dv, \tag{1.20}$$

and p can take any integer value or zero.

At a large distance from the line source at (ρ_o,ψ), the incident cylindrical wave given in (1.13) appears as a plane wave, as evidenced by the asymptotic expansion of the Hankel function of the second kind[14],

$$H_\nu^{(2)}(z) \sim \sqrt{\frac{2j}{\pi z}}\, e^{-j(z-\frac{\nu\pi}{2})}, \quad z >> \nu. \tag{1.21}$$

After using the binomial theorem to expand the arguments of the Hankel functions in (1.13), (1.19), and (1.20) for $\rho_o >> \rho$, and multiplying the expressions in (1.13), (1.15), (1.19), and (1.20) by the normalization factor

$$4j\sqrt{\frac{\pi k\rho_o}{2j}}\, e^{jk\rho_o}, \tag{1.22}$$

it follows that when the field incident upon the wedge is the plane wave given in (1.6), the total field described in (1.15) becomes

$$U(\rho,\phi) = \nu \sum_{n=0}^{\infty} \varepsilon_n\, j^{n\nu} J_{n\nu}(k\rho)\, \{\cos[n\nu(\phi-\psi)] \pm \cos[n\nu(\phi+\psi)]\}, \tag{1.23}$$

and from (1.19) and (1.20),

$$\omega_1(\rho,\xi) = e^{jk\rho\cos(\xi+2\pi pm)}, \quad |\xi+2\pi pm| < \pi,$$

$$= 0, \quad |\xi+2\pi pm| > \pi, \tag{1.24}$$

$$\omega_2(\rho,\xi) = \frac{1}{2\pi}\int_{-\infty}^{\infty} \frac{\sin(jv+\frac{\pi}{m})\ e^{-jk\rho\cosh(mv)}}{\cos(jv+\frac{\pi}{m}) - \cos(\frac{\xi}{m})}\,dv. \tag{1.25}$$

When $k\rho$ is large, $\omega_2(\rho,\xi)$ can be evaluated by the method of stationary phase[15], which results in

$$\omega_2(\rho,\xi) = \frac{\sin(\frac{\pi}{m})\ e^{-jk\rho}}{\sqrt{j2\pi k\rho}\ m[\cos(\frac{\pi}{m})-\cos(\frac{\xi}{m})]}, \quad k\rho >> 1, \quad |\xi| \neq \pi. \tag{1.26}$$

Comparison of the expressions in (1.7) - (1.10), (1.12), with those given by (1.16), (1.18), (1.24) - (1.26), shows that corresponding expressions are identical except for that in (1.25). This expression is mathematically more tractable than either (1.10) or (1.11).

1.2(a) INTEGRAL EQUATION REPRESENTATION

Although rigorous explicit expressions describing the scattered field have been determined for only a few bodies, it is possible, by using an integral equation representation, to describe implicitly the field surrounding any scatterer. The integrand of the integral

equation is composed of two parts: a source distribution which describes the shape and composition of the scatterer, and the Greens function appropriate to those sources.

The body considered here is homogeneous and isotropic, has permeability μ_s, permittivity ε_s, conductivity σ, and occupies a volume V. It is surrounded by a homogeneous isotropic medium of permeability μ and permittivity ε in which exists a current source $\vec{J}$. Maxwell's equations in (1.1) enable the field at any point to be described by

$$\nabla^2 E - \frac{\ddot{\vec{E}}}{c^2} = (\mu_s \varepsilon_s - \frac{1}{c^2})\ddot{\vec{E}} + \mu\sigma\dot{\vec{E}} + \mu\dot{\vec{J}} + \nabla(\nabla\cdot\vec{E}) + \nabla\mu \times \vec{H}, \qquad (1.27)$$

$$\nabla^2 H - \frac{\ddot{\vec{H}}}{c^2} = (\mu_s \varepsilon_s - \frac{1}{c^2})\ddot{\vec{H}} + \mu\sigma\dot{\vec{H}} - \nabla \times \vec{J} + \dot{\vec{E}} \times \nabla\varepsilon + \vec{E} \times \nabla\sigma + \nabla(\nabla\cdot\vec{H}) \qquad (1.28)$$

where c is the velocity of electromagnetic propagation in the surrounding medium. By defining the scattered field $\vec{U}^s$ as

$$\vec{U}^s = \vec{U} - \vec{U}^i, \qquad (1.29)$$

where $\vec{U}^i$ is the field incident from the source distribution $\vec{J}$, and restricting the field to be monochromatic with angular frequency ω, the solutions to (1.27) and (1.28) are given by

$$\vec{E}^s(P) = \iiint_V \left[(\mu_r\varepsilon_r - 1)k^2\vec{E} - j\omega(\mu\sigma\vec{E} + \nabla\mu \times \vec{H})\right] G(kR)\, dv, \tag{1.30}$$

$$\vec{H}^s(P) = \iiint_V \left[(\mu_r\varepsilon_r - 1)k^2\vec{H} - \vec{E} \times \nabla\sigma - j\omega(\mu\sigma\vec{H} + \vec{E} \times \nabla\varepsilon)\right] G(kR)\, dv. \tag{1.31}$$

$\mu_s = \mu_r\mu$, $\varepsilon_s = \varepsilon_r\varepsilon$, k is the wavenumber appropriate to the surrounding medium, R is the distance from the elemental volume dv to the point P, and $G(kR) = e^{-jkR}/4\pi R$ is the three-dimensional Greens function.

When the surface S of the scatterer is perfectly conducting, the scattered field is given by

$$\vec{U}^s(P) = \{\mathbb{A}\}\iint_S \vec{K}(s)\, G(kR)\, ds, \tag{1.32}$$

where the surface current density $\vec{K}(s)$ on S is defined by

$$\vec{K}(s) = \hat{n} \times \vec{H}, \tag{1.33}$$

and $\hat{n}$ is the outward unit normal vector to S at s. The vector operator $\{\mathbb{A}\}$ is $\{-j\mu c^2(k^2 + \nabla\nabla\cdot)/\omega\}$ when $\vec{U}$ represents the electric field intensity $\vec{E}$, and is $\{\nabla \times\}$ when $\vec{U}$ represents the magnetic field intensity $\vec{H}$.

When the problem is two-dimensional, the volume integrals in (1.30) and (1.31) reduce to integrals over τ, the normal cross-section of the scatterer, and the surface integral in (1.32) reduces to a line integral along C, the perimeter of the scatterer. Thus, the expressions in (1.30), (1.31) and (1.32) reduce to

$$\vec{E}^s(P) = \iiint_\tau \left[(\mu_r\varepsilon_r - 1)k^2\vec{E} - j\omega(\mu\sigma\vec{E} + \nabla\mu \times \vec{H})\right] g(kR)\, ds, \qquad (1.34)$$

$$\vec{H}^s(P) = \iiint_\tau \left[(\mu_r\varepsilon_r - 1)k^2\vec{H} - \vec{E} \times \nabla\sigma - j\omega(\mu\sigma\vec{H} + \vec{E} \times \nabla\varepsilon)\right] g(kR)\, ds, \qquad (1.35)$$

$$\vec{U}^s(P) = \{\Lambda\} \int_c \vec{K}(c)\, g(kR)\, dc, \qquad (1.36)$$

where $\{\Lambda\}$ is $\{-j\omega\mu\}$ when $\vec{U}$ represents the electric field intensity $\vec{E}$, and is $\{\nabla \times\}$ when $\vec{U}$ represents the magnetic field intensity $\vec{H}$. $g(kR)$ is the two-dimensional Greens function obtained by integrating the three-dimensional Greens function along an infinite path in the z-direction:

$$g(kR) = \int_{-\infty}^{\infty} G\left[k(R^2 + z^2)^{\frac{1}{2}}\right] dz = \frac{-j}{4} H_o^{(2)}(kR). \qquad (1.37)$$

The first terms in the kernel of the integrals in (1.30), (1.31), (1.34), and (1.35) are often referred to as the "polarization current density".[16] The remaining terms in these kernels can also be regarded as polarization current densities.

1.2(b) MODAL EXPANSIONS

The integral equation representation of the scattered field discussed in section 1.2(a) is valid at all points inside, outside, and on the surface of the scatterer. Once the polarization current density or the surface current

density in the integrand of the integral equation is determined, the field at any point can be calculated. Techniques which represent the current density as a modal expansion and use numerical methods to evaluate the modal coefficients are known as Moment Methods.[17]

The simplest method of modally expanding the current density is the method of subsections. This involves subdividing the volume or surface of the scattering body into N parts, and approximating the current density in the n^{th} part by the unknown constant K_n. Alternatively, the electric or magnetic field intensity may be approximated by an unknown constant in the n^{th} part. The integral over the volume or surface is approximated by a summation over the N subsections. N simultaneous equations are derived by equating the two representations of the field or current density in each of the N subsections. These simultaneous equations can be derived for a perfectly conducting body by ensuring that the boundary conditions are satisfied at a point in each subsection. Care must be taken in dealing with the singularity which occurs in the Greens function when the effect of the sources on themselves is considered.

The position at which the boundary condition is enforced in each subsection of a perfectly conducting scatterer has been shown to affect the accuracy of the method

of subsections.[18] Hashimoto and Fujisawa conclude that the best position is the midpoint of each subsection.

The application of the method of subsections to a perfectly conducting body having a surface with edges or corners requires special consideration.[19] When the field is electrically polarized parallel to an edge, the surface current density is integrably infinite at the edge.[32] Kay and Nihen[33] studied the effect of decreasing the subsectional size near an edge, and also the effect of considering the edge to have a small but finite radius of curvature. They found that the forward scattered field is insensitive to the subsectional arrangement near the edge, except when the radius of curvature of the curve approximating the edge becomes too large.

Andreason[19] uses the method of subsections in conjunction with (1.36) to formulate the scattering from two-dimensional metallic cylinders as a matrix equation. He ensures that the boundary condition in (1.4) or (1.5) is satisfied at the midpoint of each of the N subsections. The problem of the singularity of the Greens function, which occurs in the n^{th} subsection while deriving the n^{th} simultaneous equation, is overcome by performing analytically the integration over this subsection.

Results are presented for various single and multiple cylindrical bodies.

Earlier, Mei and van Bladel had used the method of subsections to obtain the surface current density on perfectly conducting rectangular cylinders, and hence the scattered field.[20] Many of their results have since been experimentally verified.[21] However, the resonance phenomenon which appears in one of their results is incorrect.[22] Such resonances may arise during the course of a numerical solution if resonant field modes can exist in the interior of the scattering body.[23,24,25] However, these resonances can not exist if use is made of the extended boundary condition[25,26] in the formulation of the scattering algorithm.

The extended boundary condition requires not only the satisfaction of the boundary conditions in (1.4) or (1.5) on the surface of a perfectly conducting closed body, but also that the total field be zero in a region interior to the body. Analytic continuation arguments[4,25,29] ensure that if such a condition is met, the field is zero everywhere inside the body. Thus it is impossible for resonant field modes to exist in the interior of the scatterer and contribute to the surface current density. Although the use of the boundary conditions with the method of subsections is sufficient to ensure that a close approximation to the scattered field is obtained, it is necessary to use

the extended boundary conditions to be certain of obtaining accurate values for the surface current density on the body. A "Null field method" is a method which employs the extended boundary condition in the formulation of a scattering problem.

"Point-matching methods" rely on satisfying the boundary conditions at points on the surface of a scattering body in order to determine the field modal coefficients.[27] Fuller and Audeh[28] use the point-matching method to determine the cutoff frequencies of a nonsymmetric waveguide. They observe that the point-matching method becomes less accurate as the boundary contour of the waveguide becomes more complicated.

Bates[29] has recently critically appraised the point-matching method and calculated the cutoff frequencies of various modes in several waveguides. He shows that identical expressions are obtained for the cutoff frequencies of a waveguide whether the boundary conditions or the extended boundary conditions are invoked.

Richmond[16] uses the method of subsections to calculate the field scattered by an infinite dielectric cylinder when the incident field is electrically polarized. A matrix equation is derived by substituting $\nabla\mu = \sigma = 0$ into the expression in (1.34) and representing the total electric field intensity in the n^{th} subsection by the constant $\vec{E}_n$. A set of simultaneous equations is obtained by

equating $(\vec{E}_n - \vec{E}^i)$ at the midpoint of the n^{th} subsection to the expression on the right-hand side of (1.34). This latter expression is approximated by a summation over the N subsections. The singularity in the Greens function is overcome by integrating over a circular region of the same cross-sectional area as the n^{th} subsection. This integration is easier to perform than that over a rectangular subsection, and Richmond maintains that it introduces little error. Results are presented for dielectric shells, and homogeneous and inhomogeneous dielectric sheets.

When the field incident upon a homogeneous dielectric scatterer is magnetically polarized, and $\nabla\sigma = \sigma = 0$, $\mu_r = 1$, the integrand in (1.35) retains a term in $\vec{E} \times \nabla\varepsilon$. The best method of dealing with this polarization current density term, which exists only on the surface of the dielectric, is not immediately apparent.

Bates[30] uses the method of subsections to determine the scattering from a wedge covered with finite distributions of dielectric, when the field is magnetically polarized. He neglects the $\vec{E} \times \nabla\varepsilon$ polarization current density term in (1.35) and thereby implicitly assumes that for the narrow dielectric wedges studied, this term has the same magnitude but is in antiphase on either side of the wedges.

Richmond[31] avoids the problems associated with the integrand of (1.35). He evaluates the scattering from a

dielectric cylinder by expressing the magnetically polarized field in terms of the electric field intensity. The scattered field is evaluated by using the method of subsections and the expression in (1.34). Results are presented for cylindrical shells and dielectric slabs.

Because the method of subsections approximates the field or current density by a constant value in each subsection, the modal expansion of the method is discontinuous across each subsection boundary. However, by summing N continuous modal functions each weighted by an unknown coefficient, the field or current density can be represented in a continuous manner over the region of interest.

Bates[34] uses a Fourier series as the modal expansion of the surface current density on the perimeter of a perfectly conducting cylinder. The null field method is used to extract the Fourier coefficients of the incident and scattered fields. It is shown that fewer surface current density modes are required to calculate the scattered field than are required to calculate the surface current density to the same accuracy. This indicates that the scattered field is accurate to the second order when the surface current density is accurate to the first.[17,35] Results are presented for the scattering from a square cylinder.

Mullin et al[36] express the scattered field exterior to an infinite perfectly conducting cylinder of arbitrary cross-section as a sum of outward travelling waves. By enforcing the boundary condition in (1.4) or (1.5) at points on the boundary, the unknown coefficients of the scattered field modes are obtained. The results fail "for cylinders which are large perturbations from the circular".[36] By continuing the outward travelling representation of the scattered field back to the surface of the cylindrical scatterer, Mullin has invoked the Rayleigh hypothesis[37] which, during the course of a recent controversy[38-41] has been shown by Millar[38] to be incorrect in general, and in particular incorrect for elliptical scatterers of appreciable eccentricity. This explains the failure of some of Mullin's results.

The scattering for nose-on incidence from perfectly conducting cones with blunted tips is evaluated by Weiner and Borison[42] by representing the total field in a general eigenfunction expansion. After satisfying the boundary conditions and ensuring that the incident part of the total field is equal to the incident field, the eigenfunction coefficients are obtained.

Waterman[43] expresses the field as a sum of continuous mode functions in order to determine the scattering from

three-dimensional dielectric bodies. The fields inside and outside the body are written as modal expansions with unknown mode coefficients. By using the boundary conditions[44] to relate the expansions across the dielectric boundary a matrix is derived, which after inversion enables the modal coefficients to be obtained.

The determination of scattering by using a modal representation of the field or current density requires the inversion of a matrix in order to find the modal coefficients. The order of the matrix is dependent upon the number of modes used in the representation.[17,45] When using the method of subsections, the extent of each subsection must be less than half the wavelength of the highest spatial harmonic of interest in the field or current density.[19] Andreason[19] suggests between four and ten subsections per wavelength of the incident field is adequate in the case of metallic scatterers, and Richmond[16] suggests $5\sqrt{\varepsilon_r}$ subsections per wavelength for dielectric scatterers. It follows from these considerations that the size of scatterer which can be dealt with by moment methods is limited by the capacity of available computational facilities.[45] The limit on the circumference of metallic scatterers is about 25-40 wavelengths[19], although symmetry in the scattering problem enables this

limit to be increased significantly.

1.3(a) RAY-TRACING TECHNIQUES

Both the integral equation representation of the scattered field discussed in section 1.2(a), and the rigorous explicit solutions mentioned in section 1.1(a), describe exactly the total field surrounding a scattering body. The ray tracing techniques discussed in this section give an estimate of the field surrounding the scatterer. The accuracy of this estimate depends upon the nature and shape of the scatterer as well as the sophistication of the ray-tracing technique employed.

Ray-tracing techniques are based on the assumption that the field propagating from one point to another travels along ray paths joining the two points. Fermat's principle states that the rays between two points "are those curves along which the optical path length is stationary with respect to infinitesimal variations in path".[46] The intensity of the field predicted by ray theory is obtained by applying the principle of conservation of energy to a tube of rays.

The simplest ray-tracing theory is Geometrical Optics (G.O.). The field U_{go} predicted by geometrical optics in the vicinity of a scattering body is defined as

$$U_{go} = U^{i} + U^{r} + U_{r}, \tag{1.38}$$

where U^i is the incident field, U^r is the field reflected from the body, and U_r is the field refracted by the body. At a congruence of rays, called a caustic, the geometrical optics field is undefined. Geometrical optics is the leading term in the high-frequency asymptotic expansion of the field surrounding a scattering body[46], and therefore is useful for predicting the field scattered from a body whose surface has radii of curvature which are large compared with the wavelength of the field.

The expressions in (1.7) - (1.12) show that the high-frequency asymptotic expansion of the field in the vicinity of a perfectly conducting wedge illuminated by the plane wave given in (1.6), is

$$U(\rho,\phi) \approx V_1(\rho,\phi-\psi) \pm V_1(\rho,\phi+\psi), \qquad (1.39)$$

where $V_1(\rho,\xi)$ is given in (1.9). Examination of the existence condition $|\xi+2\pi pm| < \pi$ associated with $V_1(\rho,\xi)$ shows that when $\xi = \phi-\psi$, only $p=0$, $|\phi-\psi| < \pi$ satisfies this condition. When $\xi = \phi+\psi$, only $p=0$, $|\phi+\psi| < \pi$ and $p= -1$, $|\phi+\psi-2\pi m| < \pi$ satisfy the existence condition. Substitution of these three values of p into (1.9) results in three expressions which describe the incident field, the field reflected from the surface $\phi= 0$, and the field reflected from the surface $\phi = m\pi$ respectively. Thus the expression in (1.39) describes the geometrical optics field in the vicinity of the perfectly conducting wedge.

It can be seen from the preceeding discussion that geometrical optics predicts no field in the shadowed regions of an opaque body. The extension of geometrical optics which overcomes this limitation is called the Geometrical Theory of Diffraction (G.T.D.).[47] The field U_{gtd} predicted by the geometrical theory of diffraction in the vicinity of a scatterer is given by

$$U_{gtd} = U_{go} + U^d, \tag{1.40}$$

where U^d represents a diffracted field. This diffracted field is produced whenever a ray strikes an edge, corner, or vertex of a boundary surface, or grazes such a surface. The geometrical theory of diffraction assumes that the diffracted field in a given direction is dependent upon only the incident field and the local geometry of the diffracting surface. By using the explicit solution of a simple canonical problem which contains the appropriate type of surface discontinuity (such as the wedge for edge diffraction[47], and the circular cylinder and sphere for diffraction by a convex surface[48]), the relationship between incident and diffracted fields is deduced. The diffracted field is given by the term following the geometrical optics term in the high-frequency asymptotic expansion of the field appropriate to the canonical problem. Thus, the diffracted field from an edge when the incident field is given in (1.6), is found from (1.7), (1.8) and (1.12)

to be

$$U^d(\rho,\phi) = V_2(\rho,\phi-\psi) \pm V_2(\rho,\phi+\psi), \quad k\rho[1+\cos(\phi\pm\psi)] >> 1, \tag{1.41}$$

where the upper (lower) sign applies when the field is magnetically (electrically) polarized.

The field diffracted from a surface discontinuity in a two-dimensional problem can be written in the form[47]

$$U^d(\rho,\phi) = U^i\, d_m(\phi,\psi)\, \frac{e^{-jk\rho}}{\sqrt{\rho}}, \tag{1.42}$$

where $d_m(\phi,\psi)$ is the diffraction coefficient appropriate to the discontinuity. The edge diffraction coefficient for a perfectly conducting body is found from (1.12) (1.41) and (1.42) to be

$$d_m(\phi,\psi) = \frac{\sin(\frac{\pi}{m})}{m\sqrt{j2\pi k}} \left[\frac{1}{\cos(\frac{\pi}{m})-\cos(\frac{\phi-\psi}{m})} \pm \frac{1}{\cos(\frac{\pi}{m})-\cos(\frac{\phi+\psi}{m})} \right]. \tag{1.43}$$

Like the geometrical optics field, the diffracted field of the geometrical theory of diffraction travels along ray directions. For edge diffraction, the ray paths are defined by the modified Fermat's principle: "an edge diffracted ray from P to Q is a curve which has stationary length among all curves from P to Q having a point on the edge".[47] By considering the energy in a tube of rays,

Keller[47] modified the edge diffraction coefficient given in (1.43) to a coefficient appropriate to a curved edge. Tip diffraction coefficients have also been defined.[49] When an incident field grazes a smooth convex boundary surface, a surface ray is generated.[48] This surface ray travels along a geodesic arc of the surface and produces diffracted rays which leave the surface tangentially from each point on the arc.

The geometrical theory of diffraction has been used to estimate the fields scattered by many different bodies.[47-57] The use of the geometrical theory of diffraction is attractive because of the ease with which an estimate of the field surrounding a scatterer can be obtained. Although the ray approach to diffraction problems is an asymptotic high-frequency technique, it often gives accurate results when the characteristic dimension of the scatterer is of wavelength order.[47,50,52,54]

1.3(b) EDGE DIFFRACTION USING THE G.T.D.

The use of the geometrical theory of diffraction in problems involving edge diffraction is restricted by the constraints associated with (1.41). Pauli[10] maintains that the discontinuity associated with the geometrical optics field $V_1(\rho,\xi)$ and its derivatives on the shadow and reflection boundaries $|\phi \pm \psi| = \pi$, is matched exactly by the discontinuities associated with $V_2(\rho,\xi)$ in (1.10) and its derivatives on the reflection and shadow boundaries,

thereby ensuring that the total field given in (1.7) is continuous everywhere. The neglect of the higher order terms of (1.11) in the asymptotic expansion in (1.12) causes the discontinuity at $|\phi \pm \psi| = \pi$ in the diffracted field of the geometrical theory of diffraction given by (1.41).

Ahluwalia et al[58] overcome the problem of the discontinuities in the case of a plane screen by deriving a uniform asymptotic expansion for the diffracted field. Higher order terms of the expansion are obtained recursively.

Yee et al[54] use the geometrical theory of diffraction to obtain the reflection from the open end of a waveguide. The incident field mode is decomposed into two plane waves, and the diffraction from the terminating edges of the waveguide is calculated separately for each plane wave. Multiply diffracted fields, generated when the diffracted field from one edge strikes the other edge, are not predicted by the geometrical theory of diffraction for the waveguide because the direction of multiple diffraction coincides with the reflection boundary of the terminating edges. This difficulty is overcome by Yee et al by using a Fresnel integral formula for the diffraction coefficient and thereby providing a continuous transition of the diffracted field through the reflection boundary.

Hamid[59] suggests using correction factors with the diffraction coefficient in (1.43) not only to avoid the discontinuities across the shadow and reflection boundaries, but also to compensate to some extent for the asymptotic nature of the diffraction coefficient. The correction factors are functions of $k\rho, \phi,$ and ψ, and are obtained by comparison of the field predicted by the geometrical theory of diffraction with the exact solution.

Mohsen and Hamid[60] derive a diffraction coefficient for the scattering by a half plane by considering both the first and second terms in the asymptotic expansion of the exact solution given by Keller et al.[61] This improved diffraction coefficient results in a more accurate estimate of the field diffracted by a narrow slit, strip and circular aperture.[60,62]

Other attempts to overcome the asymptotic nature of the diffracted field given in (1.41) involve the use of the Pauli diffraction function given by the first term in the expression in (1.11).

Ryan and Rudduck[63] use the Pauli diffraction function to estimate the multiply diffracted field radiated from the edges of a parallel-plate waveguide. Improved results are obtained by Rudduck and Wu[64] who introduce a slope wave diffraction function derived by differentiating the Pauli diffraction function with respect to the angle of incidence. This technique is similar to that used by

other workers.[47,51]

Yu and Rudduck[65] use the Pauli diffraction function in representing the sum of the multiply diffracted fields from an edge of a perfectly conducting strip by a cylindrical wave. The strengths of the diffracted fields are found by a selfconsistent method similar to that used by Karp and Russek.[66]

However, most improvements[60,63,65,66] to the geometrical theory of diffraction do not predict a multiply diffracted field from a perfectly conducting body illuminated by a field electrically polarized parallel to the edges of the body. Expressions for such a multiply diffracted field are derived in Chapter 7 of this thesis.

The concept of representing the field diffracted by an edge as a cylindrical wave emanating from the edge is related to the use of fictitious edge currents to describe the diffraction. This technique is used by Millar[67-69] to find the field diffracted by circular and elliptic apertures, and more recently by Ryan and Peters[70] to find the diffraction from finite axially symmetric cone frustrums, a conically capped finite cylinder, and a stub mounted above a circular disc. Moullin and Phillips[71] use a similar

approximation to describe the presence of an edge.

A concise survey of the theory of diffraction of short waves by edges up to 1964 is given by Keller and Hansen.[72] Other survey and review papers are available.[6,73-75]

1.4(a) PHYSICAL OPTICS

Physical optics (P.O.) approximates the field scattered from a perfectly conducting body by the radiation from a surface current density $\vec{K}$ given by

$$\begin{aligned} \vec{K} &= 2\hat{n} \times \vec{H}^{i}, \quad \text{on a directly illuminated surface,} \\ &= 0, \qquad\quad \text{on a shadowed surface.} \end{aligned} \tag{1.44}$$

Comparison of the expression in (1.44) with the exact description of the surface current density given in (1.33) shows that physical optics approximates the tangential magnetic field intensity at the surface of the scatterer by twice the tangential component of the incident magnetic field intensity. The physical optics surface current density, which is due to the geometrical optics field, is therefore dependent only upon the incident field and the orientation of the surface at a point on a perfectly conducting body.

Because the physical optics surface current density exists only upon the directly illuminated surface of a scattering body, the interchange of transmitter and receiver will, in general, result in a different prediction for

the physical optics field. Thus, physical optics does not always satisfy the reciprocity theorem.[73,77] Unlike the geometrical theory of diffraction, physical optics fails to account for the polarization of the field in the backscattered direction.[53]

One advantage of the physical optics approximation is that it often enables the integrals in (1.32) and (1.36) to be evaluated analytically, resulting in simple algorithms suitable for numerical evaluation. Thus a quick check on other calculations is available.[70,76] Because physical optics approximates the surface current density, and errors in the estimate of the current density on a body do not contribute equivalent errors to the scattered field,[17,35] the physical optics estimate often accurately describes the scattered field. Physical optics is most useful in estimating the field scattered in the direction of specular reflection.[70] It is in this direction that the field predicted by the geometrical theory of diffraction is discontinuous.

However, although an iterative technique which starts with the physical optics estimate of the scattered field will converge to the exact solution for large smooth obstacles, it does not converge to the exact solution for the half-plane and the strip.[76] This is because the physical optics surface current density does not have the correct behaviour at an edge.[32,33] In the case of normal backscattering from the half-plane and strip, the physical

optics field does approach the exact backscattering because the radiation from the surface current density in the vicinity of the edge is masked.[76]

Fock[78,79] defines a transition region on the surface of a convex metallic scatterer between the illuminated surface and the surface on which the physical optics surface current density is zero. The surface current density in the transition region is approximated by a universal function which is the same for all bodies having the same local radius of curvature and illuminated by the same incident field. Thus, the Fock theory extends the physical optics current density into the shadow region of a smooth convex body.

In Chapter 7 of this thesis, a modification is suggested to the physical optics current density near the edge of a perfectly conducting body. This modification extends the physical optics current density onto a surface shadowed by an edge.

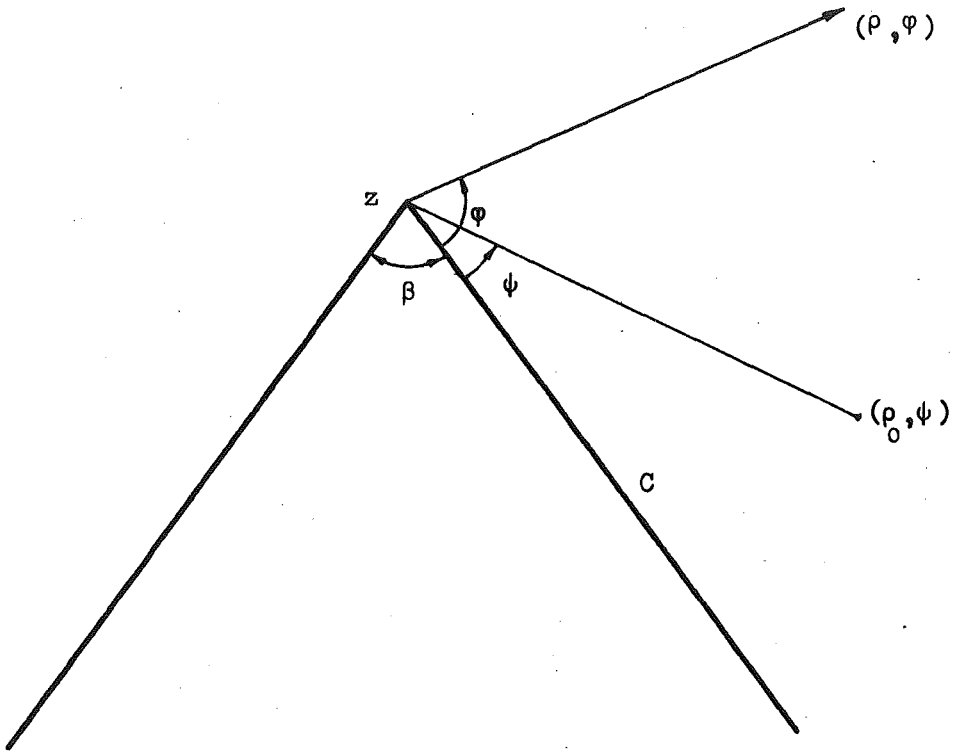

Figure 1.1 z axis perpendicular to the paper.

CHAPTER 2

This chapter contains the formulation of a current density replacement technique which can be used to determine the electromagnetic field surrounding a scattering body. When applied to non-metallic bodies the method is called the Polarization Current Replacement (P.C.R.) technique and when applied to metallic bodies it is called the Surface Current Replacement (S.C.R.) technique. The S.C.R. technique is used to determine the field scattered from a perfectly conducting deformed wedge in a form suitable for numerical evaluation.

It has been shown in Chapter 1 that the number of scattering problems for which an explicit solution can be obtained is very small. The size of scattering body which can be dealt with by numerical techniques (in conjunction with the integral equation representation of the scattered field), is limited by the available computational facilities. It is comparatively simple to use ray-tracing techniques to construct an expression describing the scattered field which requires little computational effort to evaluate. However, since these ray-tracing techniques use the leading terms of far field asymptotic expansions of the field, they become less accurate when the scatterer has dimensions of wavelength order.

To be able to evaluate the usefulness of any suggested improvement to existing ray-tracing techniques, it is desirable to have available accurate solutions to simple scattering problems involving dimensions of wavelength order. The technique introduced in this chapter enables such solutions to be obtained for the field scattered from a perfectly conducting deformed wedge. The deformation of the wedge apex has dimensions of wavelength order. Waterman[80,81], in considering the field around a perfectly conducting strip, uses similar reasoning to that in the following two sections, as does Plonsey.[82]

Some of the results of this chapter and the next have been published elsewhere.[2]

2.1(a) POLARIZATION CURRENT REPLACEMENT

Consider a homogeneous isotropic body of permeability μ, permittivity ε, and conductivity σ, occupying a volume V with surface S (Fig. 2.1), where

$$S = \beta \cup \gamma. \tag{2.1}$$

When the body is illuminated by an incident monochromatic field $\vec{U}^i$, (1.29) - (1.31) give the total field $\vec{U}_2$ at any point as

$$\vec{U}_2 = \vec{U}^i + \iiint_V \vec{P}_2(v)\, G(kR)\, dv \tag{2.2}$$

where $P_2(v)$ is the polarization current density in V and is given by (1.30) and (1.31) as

$$\vec{P}_2(v) = (\mu_r\varepsilon_r - 1)k^2\vec{E}_2 - j\omega(\mu\sigma\vec{E}_2 + \nabla\mu \times \vec{H}_2), \qquad (2.3)$$

when $\vec{U}$ represents the electric field intensity $\vec{E}$, and by

$$\vec{P}_2(v) = (\mu_r\varepsilon_r - 1)k^2\vec{H}_2 - \vec{E}_2 \times \nabla\sigma - j\omega(\mu\sigma\vec{H}_2 + \vec{E}_2 \times \nabla\varepsilon) \qquad (2.4)$$

when $\vec{U}$ represents the magnetic field intensity $\vec{H}$. Since the volume integration of (2.2) must include S, all terms of $\vec{P}_2(v)$ involving the vector gradient operator are included in the integrand.

The field $\vec{U}_2$ can be determined using the P.C.R. technique by first treating two other problems.

Problem (i)

Consider a body of permeability μ, permittivity ε, and conductivity σ occupying a volume V_1 with surface S_1 (Fig. 2.2), where

$$V_1 = V \cup \tau, \quad S_1 = \alpha \cup \gamma. \qquad (2.5)$$

When the body is illuminated by the incident field $\vec{U}^i$, the total field $\vec{U}_1$ is given by (1.29) - (1.31) as

$$\vec{U}_1 = \vec{U}^i + \iiint_{V_1} \vec{P}_1(v)\, G(kR)\, dv, \qquad (2.6)$$

where $\vec{P}_1(v)$ is the polarization current density in V_1.

Problem (ii)

Consider the body occupying volume V illuminated by the field radiated from sources of strength $[-\vec{P}_1(v)]$

situated throughout the volume τ (Fig. 2.3). The total field $\vec{U}$ at any point is

$$\vec{U} = - \iiint_{\tau} \vec{P}_1(v)\ G(kR)\,dv + \iiint_{V} \vec{P}(v)\ G(kR)\,dv, \quad (2.7)$$

$\vec{P}(v)$ being the polarization current density in V. Notice that the source distribution $[-\vec{P}_1(v)]$ contains no terms involving the vector gradient operator across the surface β.

Adding the expressions in (2.6) and (2.7), and using (2.5) gives

$$\vec{U}_1 + \vec{U} = \vec{U}^i + \iiint_{V} \vec{P}_3(v)\ G(kR)\,dv \quad (2.8)$$

where

$$\vec{P}_3(v) = \vec{P}(v) + \vec{P}_1(v). \quad (2.9)$$

Comparison of (2.8) with (2.2) shows that

$$\vec{U}_2 \equiv \vec{U}_1 + \vec{U},$$

$$\vec{P}_2(v) \equiv \vec{P}_3(v). \quad (2.10)$$

Thus the problem represented by the combination of Figs. 2.2 and 2.3 is identical to the problem represented by Fig. 2.1. The polarization current replacement technique is the method of determining the field $\vec{U}_2$ by adding together the fields $\vec{U}_1$ and $\vec{U}$.

The extension of this section to ansiotropic, inhomogeneous bodies is straightforward although the expression describing the polarization current density is more complicated.

2.1(b) SURFACE CURRENT REPLACEMENT

Consider a perfectly conducting closed body with surface S present in an incident monochromatic field $\vec{U}^i$ (Fig. 2.4). The total field $\vec{U}_2$ at any point is given by (1.29) and (1.32) as

$$\vec{U}_2 = \vec{U}^i + \{A\} \iint_S \vec{h}(s)\, G(kR)\, ds \tag{2.11}$$

where $\vec{h}(s)$, the surface current density on S, is defined from (1.33) as

$$\vec{h}(s) = \hat{n} \times \vec{H}, \tag{2.12}$$

and

$$S = \beta \cup \gamma . \tag{2.13}$$

In order to evaluate $\vec{U}_2$ using the S.C.R. technique, it is first necessary to treat two other problems.

Problem (i)

Consider a perfectly conducting closed body with surface S_1, such that

$$S_1 = \alpha \cup \gamma, \tag{2.14}$$

illuminated by the incident field $\vec{U}^i$ (Fig. 2.5). The total field $\vec{U}_1$ is given by (1.33) as

$$\vec{U}_1 = \vec{U}^i + \{A\} \iint_{S_1} \vec{I}(s)\, G(kR)\, ds, \tag{2.15}$$

where $\vec{I}(s)$ is the surface current density on S_1.

Problem (ii)

Consider the surface S illuminated by the field radiated by a surface current density $[-\vec{i}(s)]$ on α, which is external to S, as shown in Fig. 2.6. The total field $\vec{U}$ is given by

$$\vec{U} = - \{A\} \iint_{\alpha} \vec{i}(s)\ G(kR)\,ds + \{A\} \iint_{S} \vec{f}(s)\ G(kR)\,ds, \qquad (2.16)$$

where $\vec{f}(s)$ is the surface current density on S.

Adding (2.15) and (2.16), and using (2.14), gives

$$\vec{U}_1 + \vec{U} = \vec{U}^i + \{A\} \iint_{S} \vec{k}(s)\ G\ (kR)\,ds, \qquad (2.17)$$

where the surface current density $\vec{k}(s)$ is

$$\begin{aligned} \vec{k}(s) &= \vec{f}(s) + \vec{i}(s), \quad \text{on} \quad \gamma, \\ &= \vec{f}(s), \quad \text{on} \quad \beta. \end{aligned} \qquad (2.18)$$

Since both S and S_1 are perfectly conducting surfaces,

$$\begin{aligned} \vec{U} = \vec{U}_2 &= 0, \text{ inside S}, \\ \vec{U}_1 &= 0, \text{ inside } S_1. \end{aligned} \qquad (2.19)$$

Thus, the problem represented by Fig. 2.4 is identical to the problem represented by the combination of Figs. 2.5 and 2.6. Hence,

$$\vec{U}_2 \equiv \vec{U}_1 + \vec{U}, \qquad (2.20)$$

and from a comparison of (2.11) and (2.17)

$$\vec{h}(s) \equiv \vec{k}(s). \tag{2.21}$$

Since the S.C.R. technique requires the solution of two problems in order to find the solution to a third, it is, in general, a more protracted method of obtaining the field $\vec{U}_2$ than solving the third problem directly. However, if the solution $\vec{U}_1$ to Problem (i) is known explicitly, only Problem (ii) remains to be solved. Because Problem (ii) has sources only in close proximity to the scattering body, the total field external to an appropriate region can be completely described by a sum of outward travelling waves. The use of such an expansion to represent the field enables the scattering from large or even infinite bodies to be determined with only the size of the deformed surface being limited by available computational facilities.

To illustrate the use of the S.C.R. technique, it will be applied to the problem of determining the scattering from a perfectly conducting two-dimensional wedge with deformed apex, for both magnetic and electric polarizations of the incident field. Problem (i) corresponds to the problem of scattering from a perfectly conducting undeformed wedge, and Problem (ii) corresponds to the problem of determining the field scattered from the deformed wedge in the presence of sources situated on the replaced surface. The S.C.R. technique derived in this section

is formulated for a three-dimensional body. Since the deformed wedge to be considered in the next sections is two-dimensional, the vector operator $\{\mathbb{A}\}$ of section 2.1(b) becomes the vector operator $\{\Lambda\}$, and the three-dimensional Greens function G(kR) becomes the two-dimensional Greens function g(kR). These operators and Greens functions are defined in section 1.2(a).

Although the scattering from the deformed wedge is determined only for plane wave incidence, it should be remembered that any incident field can be represented by a superposition of plane waves.[83]

2.2(a) THE DEFORMED WEDGE (Electric Polarization)

Problem (i)

Consider the infinite perfectly conducting wedge in Fig. 2.7 occupying the region $|\phi| \leq \chi$ and illuminated by an electrically polarized plane wave. Use is made of the vector potential notation

$$\mu\vec{H} = \nabla \times \vec{A}, \qquad \vec{A} = \hat{z}A, \tag{2.22}$$

where $\hat{z}$ is the unit vector in the z direction. The symbol $\vec{U}$ used in section 2.1(b) is replaced in this section by $\vec{A}$, and the vector operator $\{\Lambda\}$ reduces to the scalar operator μ. The incident field, normalized so that the incident magnetic field intensity is of unit

strength, is given by

$$A^i = \frac{\mu}{k} e^{jk\rho\cos(\phi-\chi-\psi)}. \tag{2.23}$$

The field A_1 surrounding the wedge is given by (1.23) as

$$A_1 = \frac{4\mu\nu}{k} \sum_{n=1}^{\infty} j^{n\nu} J_{n\nu}(k\rho) \sin[n\nu(\phi-\chi)] \sin[n\nu\psi], \tag{2.24}$$

$$\nu = \frac{\pi}{2(\pi-\chi)}. \tag{2.25}$$

The symbol r is used to denote the distance from the apex of the wedge to a point on the wedge surface. The surface current density on the wedge can then be defined, by using the expressions in (2.22) and (1.33), as

$$\vec{I}(r) = \mp \frac{\hat{z}}{\mu r} \frac{\partial A_1}{\partial \phi}\Bigg|_{\phi=\frac{\chi}{2\pi-\chi}} \tag{2.26}$$

where the upper (lower) symbol refers to the wedge surface $\phi=\chi$ $(\phi = 2\pi - \chi)$.

Problem (ii)

Consider the perfectly conducting deformed wedge of cross-sectional contour C defined in the cylindrical polar co-ordinates (r,θ,z) (Fig. 2.7). Let the maximum value of r for $|\theta| < \chi$ be a. Then, without loss of

generality, it is possible to define the deformation C_3 as being the cross-sectional contour between $(a,-\chi)$ and (a,χ).

The surface current density on the surface $\phi=\chi$ will be distinguished by the subscript 1, that on $\phi= 2\pi - \chi$ by the subscript 2, and that on C_3 by the subscript 3.

The field incident upon the deformed wedge is radiated from the current distribution $[-\vec{I}(r)]$, $0 \leq r \leq a$ on $\phi = \chi$ and $\phi = 2\pi-\chi$. Writing

$$\vec{I}(r) = \hat{z}I(r), \tag{2.27}$$

and using (2.24) with (2.26), it is readily deduced that

$$I_m(r) = \mp \frac{4\nu}{kr} \sum_{n=1}^{\infty} (\pm 1)^n n\nu \; j^{n\nu} J_{n\nu}(kr) \sin(n\nu\psi), \; m = \frac{1}{2}. \tag{2.28}$$

The total field $A(\rho,\phi)$ surrounding the deformed wedge is found from (2.16) to be

$$A(\rho,\phi) = \frac{-j\mu}{4} \int_C F(c) \, H_o^{(2)}(kR)\, dc + \frac{j\mu}{4} \int_0^a [I_1(r) + I_2(r)] \, H_o^{(2)}(kR)\, dr, \tag{2.29}$$

where R is the distance from the elemental contour dc or dr to (ρ,ϕ), and $\vec{F}(c) = \hat{z}F(c)$ is the z-directed

surface current density on C.

The use of Graf's addition theorem for Bessel functions[14] enables the expression in (2.29) to be expanded as

$$A(b,\phi) = \frac{-j\mu}{4} \sum_{m=-\infty}^{\infty} \Bigg[J_m(kb) \int_b^{\infty} \{F_1(r)\cos[m(\phi-\chi)] + F_2(r)\cos[m(\phi+\chi)]\} H_m^{(2)}(kr)\, dr$$

$$+ H_m^{(2)}(kb) \Bigg[\int_a^b \{F_1(r)\cos[m(\phi-\chi)] + F_2(r)\cos[m(\phi+\chi)]\} J_m(kr)\, dr$$

$$- \int_o^a \{I_1(r)\cos[m(\phi-\chi)] + I_2(r)\cos[m(\phi+\chi)]\} J_m(kr)\, dr$$

$$+ \int_{C_3} F_3(c)\cos[m(\phi-\theta)] J_m(kr)\, dc \Bigg] \Bigg], \qquad b \geq a. \tag{2.30}$$

The representation of the total field given in (2.30) is valid for all ϕ, and may be written as a trigonometrical Fourier series on the circle $\rho = b$. Thus

$$A(b,\phi) = B_o^+ + 2 \sum_{p=1}^{\infty} [B_p^+ \cos(p\phi) + B_p^- \sin(p\phi)], \qquad b \geq a, \tag{2.31}$$

where the $B_p^{\pm}$ are functions of b. The $B_p^{\pm}$ are extracted from (2.31) by performing the integration

$$B_p^{\pm} = \frac{1}{2\pi} \int_0^{2\pi} A(b,\phi) \begin{matrix}\cos\\ \sin\end{matrix}(p\phi)\, d\phi. \qquad (2.32)$$

Using the property of any cylindrical Bessel function $C_m(z)$ that[14]

$$C_m(z) = (-1)^m C_{-m}(z) \qquad (2.33)$$

where m is any integer or zero, it follows from (2.30) and (2.32) that

$$B_p^{\pm} = \frac{-j\mu}{4} \left[\begin{matrix}\cos\\ \sin\end{matrix}(p\chi) \left[J_p(kb) \int_b^{\infty} [F_1(r) \pm F_2(r)] H_p^{(2)}(kr)\, dr \right.\right.$$

$$+ H_p^{(2)}(kb) \int_a^b [F_1(r) \pm F_2(r)] J_p(kr)\, dr$$

$$\left. - H_p^{(2)}(kb) \int_0^a [I_1(r) \pm I_2(r)] J_p(kr)\, dr \right]$$

$$\left. + H_p^{(2)}(kb) \int_{C_3} F_3(c) J_p(kr) \begin{matrix}\cos\\ \sin\end{matrix}(p\theta)\, dc \right]. \qquad (2.34)$$

The sources of the field $A(\rho,\phi)$ are contained within the circle $\rho = a$, and $A(\rho,\phi)$ is entirely outgoing

for $\rho > a$. A representation of the field which satisfies the radiation condition at infinity[84] and the boundary condition (1.5) on the wedge surface is

$$A(\rho,\phi) = \frac{\mu}{k} \sum_{n=1}^{\infty} a_n H_{n\nu}^{(2)}(k\rho) \sin[n\nu(\phi-\chi)], \qquad p > a,\ \chi \leq \phi \leq 2\pi-\chi, \tag{2.35}$$

where the complex coefficients a_n are yet to be determined.

The surface current density on the wedge surfaces $r > a$ can be described in terms of the a_n by using (2.35) with (2.22) and (1.33). Then

$$F_m(r) = \mp \frac{1}{kr} \sum_{n=1}^{\infty} (\pm 1)^n n\nu\, a_n H_{n\nu}^{(2)}(kr), \quad r > a,\ m = \frac{1}{2}. \tag{2.36}$$

Because the total field inside the deformed wedge is everywhere zero, the Fourier coefficients $B_p^{\pm}$ of the field on the circle $\rho = b$ are given by

$$B_p^{\pm} = \frac{1}{2\pi} \int_{\chi}^{2\pi-\chi} A(b,\phi) \begin{matrix}\cos\\ \sin\end{matrix}(p\phi)\, d\phi, \tag{2.37}$$

as an alternative to (2.32). Using (2.35) with (2.37) to obtain the $B_p^{\pm}$ in terms of the a_n results in

$$B_p^{\pm} = \frac{\mu}{\pi k} \begin{matrix}\cos\\ \sin\end{matrix}(p\chi) \sum_{n=1}^{\infty} \frac{t\nu\, a_t H_{t\nu}^{(2)}(kb)}{(t\nu)^2-p^2}, \quad t = \frac{2n-1}{2n}, \quad p \neq t\nu. \tag{2.38}$$

After noting from (2.28) and (2.36) that

$$I_1(r) \pm I_2(r) = \frac{-8\nu}{kr} \sum_{n=1}^{\infty} t\nu \, j^{t\nu} J_{t\nu}(kr) \sin(t\nu\psi), \quad t = \frac{2n-1}{2n} \tag{2.39}$$

$$F_1(r) \pm F_2(r) = \frac{-2}{kr} \sum_{n=1}^{\infty} t\nu \, a_t H^{(2)}_{t\nu}(kr), \quad t = \frac{2n-1}{2n}, \tag{2.40}$$

equating the two descriptions of the $B_p^{\pm}$ in (2.34) and (2.38) gives

$$\sum_{n=1}^{\infty} a_t \, D'_{t,p} + C'_{t,p} = Y'_{t,p}, \quad t = \frac{2n-1}{2n}, \tag{2.41}$$

where

$$D'_{t,p} = \frac{j^{t\nu}}{2k} q_t(p\chi) \left[J_p(kb) \int_b^{\infty} \frac{H^{(2)}_{t\nu}(kr) \, H^{(2)}_p(kr)\,dr}{r} + H^{(2)}_p(kb) \int_a^b \frac{H^{(2)}_{t\nu}(kr) \, J_p(kr)\,dr}{r} + \frac{2j \, H^{(2)}_{t\nu}(kb)}{\pi[(t\nu)^2 - p^2]} \right], \tag{2.42}$$

$$C'_{t,p} = \frac{-j}{4} H^{(2)}_p(kb) \int_{C_3} F_3(c) \, J_p(kr) \, q_t(p\theta)\,dc, \tag{2.43}$$

$$Y'_{t,p} = \frac{2j\nu}{k} H^{(2)}_p(kb) q_t(p\chi) \sum_{n=1}^{\infty} t\nu \, j^{t\nu} \sin(t\nu\psi) \int_o^a \frac{J_{t\nu}(kr) \, J_p(kr)}{r} dr, \tag{2.44}$$

and

$$q_{2n}(\xi) = \sin(\xi), \quad q_{2n-1}(\xi) = \cos(\xi). \tag{2.45}$$

Using the relationship[85]

$$\int_z C_\mu(kz)\ \tilde{C}_\nu(kz)\frac{dz}{z} = -kz\left\{\frac{C_{\mu+1}(kz)\ \tilde{C}_\nu(kz) - C_\mu(kz)\ \tilde{C}_{\nu+1}(kz)}{\mu^2 - \nu^2}\right\} + \frac{C_\mu(kz)\ \tilde{C}_\nu(kz)}{\mu + \nu}, \tag{2.46}$$

where $C_\mu(kz)$, $\tilde{C}_\nu(kz)$ are any two cylindrical Bessel functions, and simplifying (2.42) with the use of Appendix 1 allows the expression in (2.41) to be reduced to

$$\sum_{n=1}^{\infty} a_t\ D_{t,p} + C_{t,p} = Y_{t,p}, \quad t = \begin{matrix} 2n-1 \\ 2n \end{matrix}, \tag{2.47}$$

where

$$D_{t,p} = t\nu\ q_t(p\chi)\left[\frac{H^{(2)}_{t\nu}(ka)\ J_p(ka)}{t\nu + p}\right.$$

$$\left. - ka\ \frac{H^{(2)}_{t\nu+1}(ka)\ J_p(ka) - H^{(2)}_{t\nu}(ka)\ J_{p+1}(ka)}{(t\nu)^2 - p^2}\right], \tag{2.48}$$

$$C_{t,p} = \frac{k}{2}\int_{C_3} F_3(c)\ J_p(kr)\ q_t(p\theta)\,dc, \tag{2.49}$$

and

$$Y_{t,p} = 4\nu\ q_t(p\chi) \sum_{n=1}^{\infty} t\nu\ j^{t\nu} \sin(t\nu\psi)$$

$$\cdot \left[ka\ \frac{J_{t\nu+1}(ka)\ J_p(ka) - J_{t\nu}(ka)\ J_{p+1}(ka)}{(t\nu)^2 - p^2} \right.$$

$$\left. - \frac{J_{t\nu}(ka)\ J_p(ka)}{t\nu + p} \right] . \qquad (2.50)$$

The $q_t(\xi)$ are defined in (2.45), p is any positive integer or zero, and $t\nu \neq p$.

2.2(b) THE DEFORMED WEDGE (Magnetic Polarization)

Problem (i)

Consider the infinite perfectly conducting wedge in Fig. 2.7 occupying the region $|\phi| \leq \chi$ and illuminated by a magnetically polarized plane wave. The symbol $\vec{U}$ used in section 2.1(b) is replaced in this section by $\vec{H}$, the magnetic field intensity, and the vector operator $\{\Lambda\}$ becomes (∇X). The incident field is given by

$$\vec{H} = \hat{z}H, \qquad H^i = e^{jk\rho\cos(\phi-\chi-\psi)} . \qquad (2.51)$$

The field H_1 surrounding the wedge is given by (1.23) as

$$H_1 = 2\nu \sum_{n=0}^{\infty} \varepsilon_n\ j^{n\nu}\ J_{n\nu}(kp)\ \cos[n\nu(\phi-\chi)]\cos[n\nu\psi], \qquad (2.52)$$

where ν is defined in (2.25).

The symbol r is used to denote the distance from the apex of the wedge to a point on the wedge surface. The surface current density $\vec{I}(r)$ on the wedge is then defined from (1.33) as

$$\vec{I}(r) = \pm \hat{\rho} H \Big|_{\phi = \substack{\chi \\ 2\pi-\chi}}, \qquad (2.53)$$

where the upper (lower) symbol refers to the wedge surface $\phi=\chi$ ($\phi=2\pi-\chi$).

Problem (ii)

Consider the perfectly conducting deformed wedge of cross-sectional contour C defined by the cylindrical polar co-ordinates (r,θ,z) (Fig. 2.7). Let the maximum value of r for $|\theta| < \chi$ be a. Then, without loss of generality, it is possible to define the deformation C_3 as being the cross-sectional contour between $(a,-\chi)$ and (a,χ).

The surface current density on the surface $\phi=\chi$ will be distinguished by the subscript 1, that on $\phi= 2\pi-\chi$ by the subscript 2, and that on C_3 by the subscript 3. The unit vectors $\hat{r}_1$, $\hat{r}_2$, and $\hat{r}_3$ are defined by

$$\hat{r}_n = \hat{\rho}\cos(\eta_n) - \hat{\phi}\sin(\eta_n), \quad n=1,2,3, \qquad (2.54)$$

where

$$\eta_1 = \phi-\chi, \quad \eta_2 = \phi+\chi, \quad \eta_3 = \phi-\delta, \qquad (2.55)$$

and δ is defined in Fig. 2.7. Define

$$\xi_1 = \eta_1, \quad \xi_2 = \eta_2, \quad \xi_3 = \phi - \theta. \tag{2.56}$$

The field incident upon the deformed wedge is radiated by the current distribution $[-\vec{I}(r)]$, $0 \leq r \leq a$ on $\phi=\chi$ and $\phi= 2\pi - \chi$. After writing

$$\vec{I}_n(r) = \hat{r}_n \, I_n(r), \tag{2.57}$$

it follows from (2.52) and (2.53) that

$$I_m(r) = \pm 2\nu \sum_{n=0}^{\infty} \varepsilon_n (\pm 1)^n j^{n\nu} J_{n\nu}(kr) \cos(n\nu\psi), \quad m = \frac{1}{2}. \tag{2.58}$$

The total field $\vec{H}(\rho,\phi)$ surrounding the deformed wedge is found from (2.16) to be

$$\vec{H}(\rho,\phi) = \frac{-j}{4} \nabla X \int_C \vec{F}(c) \, H_o^{(2)}(kR)\, dc$$

$$+ \frac{j}{4} \nabla X \int_o^a [\vec{I}_1(r) + \vec{I}_2(r)] H_o^{(2)}(kR)\, dr, \tag{2.59}$$

where R is the distance from the elemental contour dc or dr to (ρ,ϕ), and $\vec{F}(c)$ is the surface current density on the wedge. Because the field is magnetically polarized $(\vec{H} = \hat{z}H)$, $\vec{F}(c)$ is directed along C in the (ρ,ϕ) plane.

Thus it is possible to write

$$\vec{F}_n(c) = \hat{r}_n F_n(c), \qquad (2.60)$$

where the $\hat{r}_n$ are defined in (2.54).

The use of Graf's addition theorem for Bessel functions,[14] and (2.57) and (2.60) enables (2.59) to be expanded into

$$\vec{H}(\rho,\phi) = \frac{\nabla}{\mu} \times \sum_{m=-\infty}^{\infty} \left(\frac{-j\mu}{4}\right) \Bigg[J_m(k\rho) \int_{\rho}^{\infty} [\hat{r}_1 F_1(r)\cos(m\xi_1) + \hat{r}_2 F_2(r)\cos(m\xi_2)] H_m^{(2)}(kr)\, dr + H_m^{(2)}(k\rho) \Bigg[\int_{a}^{\rho} [\hat{r}_1 F_1(r)\cos(m\xi_1) + \hat{r}_2 F_2(r)\cos(m\xi_2)] J_m(kr)\, dr - \int_{o}^{a} [\hat{r}_1 I_1(r)\cos(m\xi_1) + \hat{r}_2 I_2(r)\cos(m\xi_2)] J_m(kr)\, dr + \int_{C_3} \hat{r}_3 F_3(c)\cos(m\xi_3) J_m(kr)\, dc \Bigg] \Bigg], \quad \rho \geq a. \qquad (2.61)$$

The argument of the vector curl operator in (2.61) is the magnetic vector potential $\vec{A}(\rho,\phi)$. Examination of the expression in (2.54) shows that $\vec{A}(\rho,\phi)$ can be written as

$$\vec{A}(\rho,\phi) = \hat{\rho} A_\rho + \hat{\phi} A_\phi, \quad \frac{\partial \vec{A}}{\partial z} = 0, \qquad (2.62)$$

enabling $\vec{H}(\rho,\phi)$ to be written as

$$\vec{H}(\rho,\phi) = \hat{z}H(\rho,\phi), \quad H(\rho,\phi) = \frac{1}{\mu\rho}\left[\rho\frac{\partial A_\phi}{\partial \rho} + A_\phi - \frac{\partial A_\rho}{\partial \phi}\right]. \qquad (2.63)$$

The evaluation of the first term of (2.63) is accomplished after noting that

$$\frac{\partial}{\partial \rho}\left[f(\rho)\int_\rho^\infty h(x)\ g(x)dx + g(\rho)\int_a^\rho h(x)\ f(x)dx\right]$$

$$= f'(\rho)\int_\rho^\infty h(x)\ g(x)dx + g'(\rho)\int_a^\rho h(x)\ f(x)dx, \qquad (2.64)$$

where the prime denotes differentiation with respect to ρ. The second term on the right-hand side of the expression in (2.63) is cancelled by a part of the third, leaving the description of $H(\rho,\phi)$ in the form

$$H(\rho,\phi) = \frac{-j}{4\rho}\sum_{m=-\infty}^{\infty}\left[\int_\rho^\infty [S_1(\eta_1,\xi_1)\ F_1(r) + S_1(\eta_2,\xi_2)\ F_2(r)]H_m^{(2)}(kr)\,dr\right.$$

$$+ \int_a^\rho [S_2(\eta_1,\xi_1)\ F_1(r) + S_2(\eta_2,\xi_2)\ F_2(r)]J_m(kr)\ dr$$

$$- \int_o^a [S_2(\eta_1,\xi_1)\ I_1(r) + S_2(\eta_2,\xi_2)\ I_2(r)]J_m(kr)\ dr$$

$$\left. + \int_{C_3} S_2(\eta_3,\xi_3)\ F_3(c)J_m(kr)\ dr\right], \qquad (2.65)$$

where

$$S_1(\eta,\xi) = mJ_m(k\rho)\ \sin(m\xi)\cos\eta - k\rho\ J_m'(k\rho)\ \cos(m\xi)\sin\eta, \qquad (2.66)$$

$$S_2(\eta,\xi) = mH_m^{(2)}(k\rho)\ \sin(m\xi)\cos\eta - k\rho\ H_m^{(2)\prime}(k\rho)\ \cos(m\xi)\sin\eta, \qquad (2.67)$$

and the prime denotes differention with respect to the argument of the Bessel function. Use of the recurrence relations for Bessel functions[14] enables $S_1(\eta,\xi)$ and $S_2(\eta,\xi)$ to be simplified to

$$S_1(\eta,\xi) = \frac{k\rho}{2}\{J_{m-1}(k\rho)\sin(m\xi-\eta) + J_{m+1}(k\rho)\sin(m\xi+\eta)\}, \qquad (2.68)$$

$$S_2(\eta,\xi) = \frac{k\rho}{2}\{H_{m-1}^{(2)}(k\rho)\sin(m\xi-\eta) + H_{m+1}^{(2)}(k\rho)\sin(m\xi+\eta)\}. \qquad (2.69)$$

The representation of the total field given by (2.65) is valid for all ϕ, and may be written as a trigonometrical Fourier series on the circle $\rho = b$. Thus

$$H(b,\phi) = B_o^+ + 2\sum_{p=1}^{\infty}[B_p^+\cos(p\phi) + B_p^-\sin(p\phi)], \qquad (2.70)$$

the $B_p^{\pm}$ being functions of b. The $B_p^{\pm}$ are extracted from

(2.70) by performing the integration

$$B_p^{\pm} = \frac{1}{2\pi} \int_0^{2\pi} H(b,\phi) \begin{matrix}\cos\\ \sin\end{matrix}(p\phi)\, d\phi. \qquad (2.71)$$

Using (2.33) and Appendix 2, it is found from (2.65), (2.68) and (2.69) that

$$B_p^{\pm} = \frac{-j}{4} \left[p \begin{matrix}\sin\\ \cos\end{matrix}(p\chi) \left[J_p(kb) \int_b^{\infty} \frac{[F_2(r) \mp F_1(r)] H_p^{(2)}(kr)}{r}\, dr \right.\right.$$

$$+ H_p^{(2)}(kb) \int_a^b \frac{[F_2(r) \mp F_1(r)] J_p(kr)}{r}\, dr$$

$$\left.\left. - H_p^{(2)}(kb) \int_0^a \frac{[I_2(r) \mp I_1(r)] J_p(kr)}{r}\, dr \right] \right.$$

$$\mp \frac{k}{2} H_p^{(2)}(kb) \int_{C_3} F_3(c) \left[J_{p+1}(kr) \begin{matrix}\sin\\ \cos\end{matrix}\{(p+1)\theta - \delta\} \right.$$

$$\left. + J_{p-1}(kr) \begin{matrix}\sin\\ \cos\end{matrix}\{(p-1)\theta + \delta\} \right] dc \Bigg]. \qquad (2.72)$$

The sources of the field $H(\rho,\phi)$ are contained within the circle $\rho = a$, and $H(\rho,\phi)$ is entirely outgoing for $\rho > a$. A representation of the field which satisfies the radiation condition at infinity[84] and the boundary condition (1.4) on the wedge is

$$H(\rho,\phi) = \sum_{n=0}^{\infty} a_n H_{n\nu}^{(2)}(k\rho) \cos[n\nu(\phi-\chi)],$$

$$\rho > a, \quad \chi \leq \phi \leq 2\pi-\chi, \tag{2.73}$$

where the complex coefficients a_n are yet to be determined.

The surface current density on the surfaces r > a can be described in terms of the a_n by using (2.73) with (1.33). Thus, using (2.54) and (2.60),

$$F_m(r) = \pm \sum_{n=0}^{\infty} (\pm 1)^n a_n H_{n\nu}^{(2)}(kr), \quad m = \frac{1}{2}. \tag{2.74}$$

Because the total field inside the deformed wedge is everywhere zero, the Fourier coefficients $B_p^{\pm}$ of the field on the circle $\rho = b$ can be obtained from

$$B_p^{\pm} = \int_{\chi}^{2\pi-\chi} H(b,\phi) \begin{matrix}\cos\\ \sin\end{matrix}(p\phi)\, d\phi \tag{2.75}$$

as an alternative to (2.71). Using (2.73) with (2.75) to obtain the $B_p^{\pm}$ in terms of the a_n gives

$$B_p^{\pm} = \pm \frac{p}{\pi} \begin{matrix}\sin\\ \cos\end{matrix}(p\chi) \sum_{n=0}^{\infty} \frac{a_t H_{t\nu}^{(2)}(kb)}{(t\nu)^2 - p^2}, \quad t = \begin{matrix}2n\\ 2n+1\end{matrix}, \quad t\nu \neq p, \; p \neq 0, \tag{2.76}$$

$$B_o^{+} = \frac{a_o}{2\nu} H_o^{(2)}(kb). \tag{2.77}$$

After noting from (2.58) and (2.74) that

$$F_2(r) \mp F_1(r) = \mp 2 \sum_{n=0}^{\infty} a_t H_{t\nu}^{(2)}(kr), \quad t = \begin{matrix} 2n \\ 2n+1 \end{matrix}, \tag{2.78}$$

$$I_2(r) \mp I_1(r) = \mp 4\nu \sum_{n=0}^{\infty} \varepsilon_t j^{t\nu} J_{t\nu}(kr) \cos(t\nu\psi), \quad t = \begin{matrix} 2n \\ 2n+1 \end{matrix}, \tag{2.79}$$

equating the two descriptions in (2.72) and (2.76) of the $B_p^{\pm}$ gives

$$\sum_{n=0}^{\infty} a_t D'_{t,p} + C'_{t,p} = Y'_{t,p}, \quad t = \begin{matrix} 2n \\ 2n+1 \end{matrix}, \tag{2.80}$$

where

$$D'_{t,p} = \frac{jp}{2} q_t(p\chi) \left[J_p(kb) \int_b^{\infty} \frac{H_{t\nu}^{(2)}(kr)\, H_p^{(2)}(kr)}{r}\, dr \right.$$

$$\left. + H_p^{(2)}(kb) \int_a^b \frac{H_{t\nu}^{(2)}(kr)\, J_p(kr)}{r}\, dr + \frac{2j\, H_{t\nu}^{(2)}(kb)}{\pi\left[(t\nu)^2 - p^2\right]} \right], \quad D'_{o,o} = \frac{-H_o^{(2)}(kb)}{2\nu}, \tag{2.81}$$

$$C'_{t,p} = \frac{jk}{8} H_p^{(2)}(kb) \int_{C_3} F_3(c) \left[J_{p+1}(kr)\, q_t\{(p+1)\theta - \delta\} \right.$$

$$\left. + J_{p-1}(kr)\, q_t\{(p-1)\theta + \delta\} \right] dc, \tag{2.82}$$

$$Y'_{t,p} = jp\nu\, q_t(p\chi) H_p^{(2)}(kb) \sum_{n=0}^{\infty} \varepsilon_t\, j^{t\nu} \cos(t\nu\psi) \int_o^a \frac{J_{t\nu}(kr)\, J_p(kr)}{r} dr, \tag{2.83}$$

and the $q_t(\xi)$ are defined in (2.45).

Using (2.46) and Appendix 1 to simplify the expression in (2.81) enables (2.80) to be reduced to

$$\sum_{n=0}^{\infty} a_t\, D_{t,p} + C_{t,p} = Y_{t,p}, \quad t = \begin{matrix} 2n \\ 2n+1 \end{matrix}, \tag{2.84}$$

where

$$D_{t,p} = p\, q_t(p\chi) \left[\frac{ka}{(t\nu)^2 - p^2} \{ H_{t\nu+1}^{(2)}(ka)\, J_p(ka) - H_{t\nu}^{(2)}(ka)\, J_{p+1}(ka) \} \right.$$

$$\left. - \frac{H_{t\nu}^{(2)}(ka)\, J_p(ka)}{t\nu + p} \right], \quad D_{o,o} = \frac{j}{\nu}, \tag{2.85}$$

$$C_{t,p} = \frac{k}{4} \int_{C_3} F_3(c) [J_{p+1}(kr)\, q_t\{(p+1)\theta - \delta\}$$

$$+ J_{p-1}(kr)\, q_t\{(p-1)\theta + \delta\}] dc, \tag{2.86}$$

$$Y_{t,p} = 2p\nu \sum_{n=0}^{\infty} \varepsilon_t\, j^{t\nu}\, q_t(p\chi)\, \cos(t\nu\psi) \left[\frac{J_{t\nu}(ka)\, J_p(ka)}{t\nu + p} \right.$$

$$\left. - \frac{ka}{(t\nu)^2 - p^2} \{ J_{t\nu+1}(ka)\, J_p(ka) - J_{t\nu}(ka)\, J_{p+1}(ka) \} \right]. \tag{2.87}$$

p is any positive integer or zero, and $t\nu \neq p$.

2.2(c) COMMENTS ON THE RESULTS OF SECTION 2.2

As shown in section 2.1(b), the superposition of the field described in (2.35) and the field scattered from the undeformed perfectly conducting wedge (given in (2.24)), results in an exact description of the field scattered from the deformed wedge by the electrically polarized incident field in (2.23). Similarly, the superposition of the field described in (2.73) and the field scattered from the undeformed perfectly conducting wedge (given in (2.52)) results in an exact description of the field scattered from the deformed wedge by the magnetically polarized incident field in (2.51).

The exact values of the a_n modal coefficients in (2.35) or (2.73) are obtained by solving the expressions in (2.47) or (2.84) respectively. The a_n can be evaluated by using a moment method[17] to represent the surface current density $\vec{F}_3(c)$ and then forming a matrix equation by letting p take a number of values in (2.47) or (2.84). The matrix equation must be of finite order if the a_n are to be evaluated numerically.

The description of the fields in (2.35) and (2.73) is valid in the region $\rho \geq a$, $\chi \leq \phi \leq 2\pi-\chi$. By evaluating the a_n field coefficients and using analytic continuation techniques[25,29], the field in $\rho < a$, $\chi < \phi < 2\pi-\chi$ can be determined. However, to find the field in $\rho < r$, $|\phi| < \chi$, the fields given in (2.29) and (2.59)

must be evaluated and superimposed upon the fields given in (2.24) and (2.52) respectively.

In the derivation of the expressions in (2.47) and (2.84) two representations of the Fourier coefficients of the scattered field are equated on the circle $\rho = b$, $b \geq a$. One of these representations ensures that the field is zero for $\rho = b$, $|\phi| < \chi$. The expressions in (2.47) and (2.84) are independent of b. Not only does this confirm that the a_n are independent of ρ, but it also ensures that the field is zero for $\rho \geq a$, $|\phi| < \chi$. Analytic continuation arguments enable this region of zero field to be extended everywhere inside the deformed wedge. Hence the formulations in sections 2.2(a) and 2.2(b) satisfy the extended boundary condition.[25]

The expressions in (2.47) and (2.84) can each be regarded as a pair of equations coupled by the $C_{t,p}$ term. In Chapter 3 it is shown that when the wedge deformation is symmetric about $\phi = 0$, as are the rounded and symmetrically truncated wedges, the pair of equations in (2.47) or (2.84) can be decoupled.

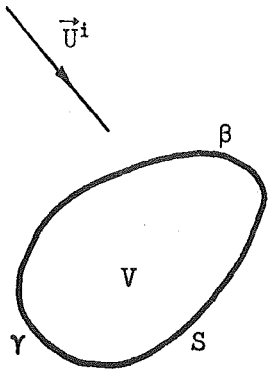

Figure 2.1

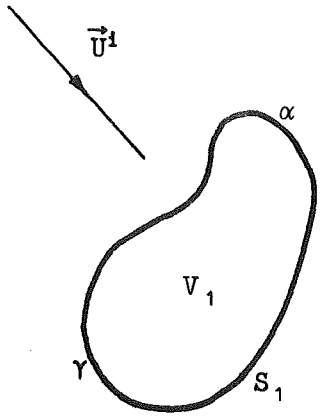

Figure 2.2

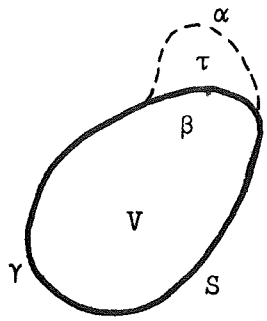

Figure 2.3

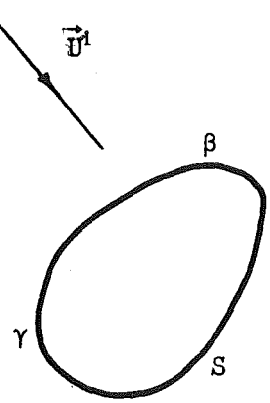

Figure 2.4

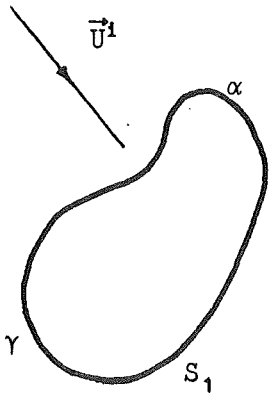

Figure 2.5

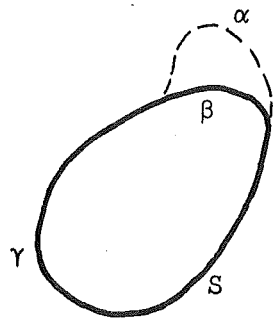

Figure 2.6

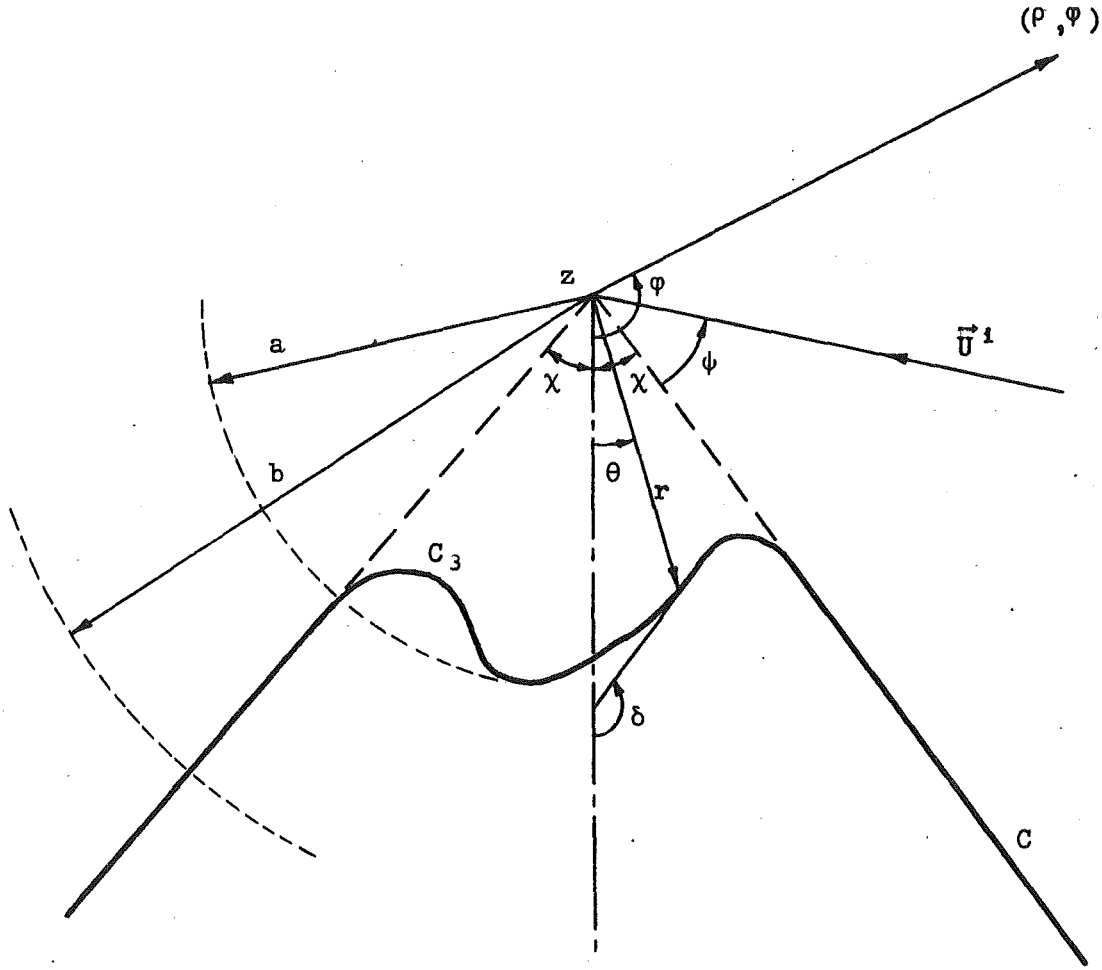

Figure 2.7 Deformed wedge. z axis perpendicular to the paper.

CHAPTER 3

In this chapter, the surface current density replacement technique is applied to the truncated and round-topped perfectly conducting wedges. The scattered field is determined for both electric and magnetic polarization of the incident field.

Equations which ensure the continuity of the surface current density at suitable points on the wedge surface are derived.

Results showing the convergence of the solutions are presented, and the factors affecting the rate of convergence are discussed.

3.1(a) TRUNCATED WEDGE. (Electric Polarization).

The primary concern in the application of the result in section 2.2(a) to the truncated wedge is to find a representation of $F_3(c)$ which adequately describes the behaviour of the surface current density on C_3. Once a suitable representation has been found, it can be used with (2.49) to enable the a_n coefficients in (2.47) to be determined.

Consider the perfectly conducting closed surface having the contour C in Fig. 3.1. The side C_1 is of length a, and the side C_2 is of length b, where $b < a$. The (ρ, ϕ, z) cylindrical co-ordinate system has its origin at the edge with internal angle β. A suitable representation will be found for $F_3(c)$ when the field is electrically

polarized by considering the form of the surface current density on C_1 and C_2.

A representation of the field $\vec{A}$ which satisfies the Helmholtz equation (1.2), the boundary condition (1.5) on C_1 and C_2, and the edge condition[84] at $\rho = 0$ is

$$\vec{A} = \hat{z}\mu \sum_{m=1}^{\infty} D_m J_{m\tau}(kp) \sin(m\tau\phi), \qquad \rho < b, \tag{3.1}$$

where $\tau = 1/(2-\beta/\pi)$, and the D_m are constants which depend upon the incident field and the shape of the contour C. By using (2.22) and (1.33) with (3.1), the surface current density $\vec{S}_1(x)$ on C_1 is found to be

$$\vec{S}_1(x) = -\hat{z} \sum_{m=1}^{\infty} D_m \, m\tau \, \frac{J_{m\tau}(kx)}{x}, \qquad x < b, \tag{3.2}$$

and the surface current density $\vec{S}_2(x)$ on C_2 is

$$\vec{S}_2(x) = \hat{z} \sum_{m=1}^{\infty} (-1)^m D_m \, m\tau \, \frac{J_{m\tau}(kx)}{x}, \tag{3.3}$$

where x is the distance from the edge $\rho = 0$ to a point on C_1 or C_2. Because the field is continuous everywhere outside C, and the contour C_1 has no discontinuities, the surface current density on C_1 is continuous. Thus, the expression in (3.2) is a valid representation of $\vec{S}_1(x)$ everywhere on C_1.

Notice that an integrable infinity exists in the surface current density at the edge of the body. This infinity restricts the accuracy which can be obtained by using the method of subsections to represent the surface current density near the edge.[17,33]

Consider the perfectly conducting truncated wedge in Fig. 3.2. The (ρ,ϕ,z) co-ordinate system has its origin at the apex of the undeformed wedge. The "truncation surface" of length 2b is the surface between edge 1 at $\rho = a_1, \phi = \chi$, and edge 2 at $\rho = a_2, \phi = 2\pi - \chi$, where $a_2 \geq a_1$. It is convenient to describe the deformed surface C_3 of the truncated wedge as the surface between $\rho = a$, $\phi = 2\pi-\chi$, and $\rho= a$, $\phi=\chi$, where

$$a = a_2+b. \tag{3.4}$$

When considered in conjunction with section 2.2(a), the definition of C_3 may be better understood by referring to Fig. 3.3. Then

$$\lim_{\varepsilon\to 0} C = C_3. \tag{3.5}$$

Define C_1 to be the contour of the surface $\rho \geq a$, $\phi = \chi$, and C_2 to be the contour of the surface $\rho \geq a$, $\phi = 2\pi-\chi$.

A representation of the surface current density $\vec{F}_3(c)$ on C_3 will now be constructed, and is later specialized for the case of the symmetrically truncated wedge, $a_1 = a_2$.

Define x to be the distance from edge 1 to a point on C_3. It follows from (3.2) and (3.3) that the surface

current density $\vec{S}_1(x)$ at a point on the surface $\phi=\chi$, and the surface current density $\vec{S}_3(x)$ at a point on the truncation surface can be represented by

$$\vec{S}_n(x) = \hat{z}\, S_n(x), \quad S_n(x) = \pm \sum_{m=1}^{\infty} (\pm 1)^m D_m \, m\tau \, \frac{J_{m\tau}(kx)}{x}, \quad n = \begin{matrix} 3 \\ 1 \end{matrix}, \tag{3.6}$$

where the D_m are constants, and

$$\tau = \frac{\pi}{2\pi - \beta}. \tag{3.7}$$

Define y to be the distance from edge 2 to a point on C_3. It follows from (3.2) and (3.3) that the surface current density $\vec{T}_2(y)$ on the surface $\phi = 2\pi - \chi$, and the surface current density $\vec{T}_3(y)$ on the truncation surface can be represented by

$$\vec{T}_n(y) = \hat{z}\, T_n(y), \quad T_n(y) = \pm \sum_{m=1}^{\infty} (\pm 1)^m E_m \, m\gamma \, \frac{J_{m\gamma}(ky)}{y}, \quad n = \begin{matrix} 3 \\ 2 \end{matrix}, \tag{3.8}$$

where the E_m are constants, and

$$\gamma = \frac{\pi}{2\pi - \alpha}. \tag{3.9}$$

The surface current density $F_3(c)$ of (2.49) is defined as

$$F_3(c) = T_2(y), \quad 0 \leq y \leq b, \quad \phi = 2\pi - \chi,$$

$$= T_3(y) \text{ or } S_3(x), \quad 0 \leq \begin{matrix} x \\ y \end{matrix} \leq 2b \text{ on the truncation surface,}$$

$$= S_1(x), \quad 0 \leq x \leq b, \quad \phi = \chi. \tag{3.10}$$

The limiting form of the Bessel function of the first kind when the order ν is fixed and the argument z tends to zero is[14]

$$J_\nu(z) \sim (\tfrac{z}{2})^\nu / \Gamma(\nu+1), \quad \nu \neq -1,-2,-3,\cdots, \quad z \to 0. \tag{3.11}$$

Therefore, the first terms in the series for $S_3(x)$ will adequately approximate the surface current density near edge 1, and the first terms in the series for $T_3(y)$ will adequately approximate the surface current density near edge 2.

Equation (3.10) indicates that either $S_3(x)$ or $T_3(y)$ is a suitable representation of $F_3(c)$ at all points on the truncation surface. However, when $x \approx 2b$, a large number of terms of the series given in (3.6) are required to approximate the infinite nature of the surface current density near edge 2. Similarly, when $y \approx 2b$, a large number of terms of the series in (3.8) are required to approximate the surface current density near edge 1. Since it is numerically impractical to deal with a large number of unknowns in (2.47), the use of either $S_3(x)$ or $T_3(y)$ to represent $F_3(c)$ everywhere on the truncation

surface would introduce a gross error in the approximation of the surface current density near either edge 2 or edge 1.

Instead, $T_3(y)$ is used to represent the current density for $0 \leq y \leq b$, and $S_3(x)$ is used for $0 \leq x \leq b$, giving

$$\begin{aligned} F_3(c) &= T_2(y), \quad 0 \leq y \leq b, \ \phi = 2\pi - \chi, \\ &= T_3(y), \quad 0 \leq y \leq b, \quad \text{on the truncation surface}, \\ &= S_3(x), \quad 0 \leq x \leq b, \quad \text{on the truncation surface}, \\ &= S_1(x), \quad 0 \leq x \leq b, \ \phi = \chi. \end{aligned} \tag{3.12}$$

Using (3.12), the expression in (2.49) becomes

$$\begin{aligned} C_{t,p} = \frac{k}{2} \Bigg[& \int_0^{a-a_2} T_2(y)\, J_p(kr)\, q_t(-p\chi)\, dy \\ & + \int_0^{b} T_3(y)\, J_p(kr)\, q_t(p\theta)\, dy \\ & + \int_0^{b} S_3(x)\, J_p(kr)\, q_t(p\theta)\, dx + \int_0^{a-a_1} S_1(x)\, J_p(kr)\, q_t(p\chi)\, dx \Bigg]. \end{aligned} \tag{3.13}$$

Substituting (3.6) and (3.8), and using Graf's addition theorem[14] with (3.13) gives

$$C_{t,p} = \frac{k}{2} \sum_{m=1}^{\infty} \sum_{\ell=-\infty}^{\infty} \Big[(-1)^{m+1} E_m \, m\gamma \, q_t[-p\chi] J_{p-\ell}(ka_2) \, f_{m\gamma,\ell}[k(a-a_2)]$$

$$+(-1)^{\ell} E_m \, m\gamma \, q_t[-(p\chi+\ell\alpha)] J_{p+\ell}(ka_2) \, f_{m\gamma,\ell}(kb)$$

$$+(-1)^{\ell} D_m \, m\tau \, q_t[p\chi + \ell\beta] J_{p+\ell}(ka_1) \, f_{m\tau,\ell}(kb)$$

$$+(-1)^{m+1} D_m \, m\tau \, q_t[p\chi] J_{p-\ell}(ka_1) \, f_{m\tau,\ell}[k(a-a_1)] \Big], \quad a_2 \geq a_1 > b, \tag{3.14}$$

where, from (2.46),

$$f_{\nu,\ell}(kz) = \int_0^z \frac{J_\nu(kz) \, J_\ell(kz)}{z} \, dz = \frac{J_\nu(kz) \, J_\ell(kz)}{\nu+\ell}$$

$$- \frac{kz}{\nu^2 - \ell^2} [J_{\nu+1}(kz) \, J_\ell(kz) - J_\nu(kz) \, J_{\ell+1}(kz)],$$

$$\nu > 0. \tag{3.15}$$

When the wedge is symmetrically truncated,

$$a_1 = a_2, \quad a - a_1 = a - a_2 = b, \quad \alpha = \beta, \; \gamma = \tau, \tag{3.16}$$

and $C_{t,p}$ reduces to

$$C_{t,p} = \frac{k}{2} \sum_{m=1}^{\infty} \sum_{\ell=-\infty}^{\infty} m\tau \, f_{m\tau,\ell}(kb) \Big[(-1)^{m+1} J_{p-\ell}(ka_1)$$

$$\cdot [q_t(-p\chi) E_m + q_t(p\chi) D_m]$$

$$+(-1)^{\ell}J_{p+\ell}(ka_1)[q_t(-p\chi-\ell\beta)E_m+q_t(p\chi+\ell\beta)D_m]\Bigg]. \qquad (3.17)$$

From (3.15)

$$f_{\nu,\ell}(kz) = (-1)^{\ell}f_{\nu,-\ell}(kz), \qquad (3.18)$$

which enables (3.17) to be separated into the two equations

$$C_{t,p} = \frac{k}{4}\sum_{\substack{m=1\\ \ell=0}}^{\infty} \varepsilon_{\ell}(D_m \pm E_m)m\tau\, f_{m\tau,\ell}(kb)\Bigg[(-1)^{m+1}q_t(p\chi)$$

$$\cdot[J_{p-\ell}(ka_1)+(-1)^{\ell}J_{p+\ell}(ka_1)] + (-1)^{\ell}[q_t(p\chi+\ell\beta)\, J_{p+\ell}(ka_1)$$

$$+(-1)^{\ell}q_t(p\chi-\ell\beta)\, J_{p-\ell}(ka_1)]\Bigg], \qquad t = \begin{matrix}2n-1\\2n\end{matrix}, \qquad (3.19)$$

where ε_{ℓ} is the Neumann factor, and n is an integer.

After defining the two infinite sets of complex constants Q_m and R_m by

$$Q_m = D_m + E_m, \quad R_m = D_m - E_m, \quad m=1,2,3,\text{---}, \qquad (3.20)$$

(2.47) specializes, in the case of the symmetrically truncated wedge,

$$\sum_{n=1}^{\infty} a_t\, D_{t,p} + \sum_{m=1}^{\infty} \begin{matrix}Q_m\\R_m\end{matrix} C_{t,p,m} = Y_{t,p}, \quad t = \begin{matrix}2n-1\\2n\end{matrix}, \qquad (3.21)$$

where, from (3.19) and (3.20),

$$C_{t,p,m} = \frac{km\tau}{4} \sum_{\ell=0}^{\infty} \varepsilon_\ell f_{m\tau,\ell}(kb) \Bigg[J_{p+\ell}(ka_1)(-1)^\ell [(-1)^{m+1} q_t(p\chi) + q_t(p\chi+\ell\beta)] + J_{p-\ell}(ka_1)[(-1)^{m+1} q_t(p\chi)+q_t(p\chi-\ell\beta)] \Bigg] , \tag{3.22}$$

and the $D_{t,p}$ and $Y_{t,p}$ are defined by (2.48) and (2.50) respectively. Thus, when applied to the symmetrically truncated wedge, the expression in (2.47) separates into the two independent equations in (3.21). As no approximations have been made during the derivation of (3.21), the solution to these equations describes exactly the field scattered from the truncated wedge.

3.1(b) SURFACE CURRENT CONTINUITY (Electric Polarization).

The unique description of the constants a_t, Q_m and R_m given in (3.21) is obtained by equating the Fourier coefficients of two representations of the field surrounding the truncated wedge (see Chapter 2). It is possible to obtain other relationships between these constants by ensuring the continuity of surface current density at points on the truncated wedge.

First, consider the continuity of the surface current density on the truncation surface of the wedge. From (3.10),

$$T_3(b - \delta) = S_3(b + \delta), \quad \forall\ |\delta| < b, \tag{3.23}$$

and moreover, since the truncation surface is absolutely continuous,

$$\frac{\partial^q}{\partial \delta^q}\left[T_3(b-\delta)\right] = \frac{\partial^q}{\partial \delta^q}\left[S_3(b+\delta)\right], \quad q = 0,1,2,\text{---}, \quad \forall \ |\delta| < b. \tag{3.24}$$

By using the recurrence relations[14] and the addition theorem with (3.6) and (3.8), the expression in (3.24) expands into

$$\sum_{\substack{m=1\\ \ell=0}}^{\infty} \varepsilon_\ell E_m \left[(m\gamma+\ell)J_{m\gamma+\ell}(kb) + (-1)^\ell (m\gamma-\ell)J_{m\gamma-\ell}(kb)\right] \frac{\partial^q}{\partial \delta^q} J_\ell(k\delta)$$

$$= \sum_{\substack{m=1\\ \ell=0}}^{\infty} \varepsilon_\ell D_m \left[(m\tau-\ell)J_{m\tau-\ell}(kb)+(-1)^\ell (m\tau+\ell)J_{m\tau+\ell}(kb)\right] \frac{\partial^q}{\partial \delta^q} J_\ell(k\delta), \quad \forall \ |\delta| < b. \tag{3.25}$$

It can be deduced from the recurrence relations for Bessel functions that provided

$$\xi(q-2n) = 0, \quad n=1,2,3,\text{---}\ q/2, \tag{3.26}$$

then (Appendix 3)

$$\xi(\ell)\frac{\partial^q}{\partial \delta^q} J_\ell(k\delta)\Big|_{\delta=0} = \begin{cases} 0, & \ell \neq q, \\ \left(\frac{k}{2}\right)^q \xi(q), & \ell = q, \end{cases} \tag{3.27}$$

where $\xi(\ell)$ is any function of ℓ; ℓ being a positive integer or zero.

Using (3.27) with (3.25) gives

$$\sum_{m=1}^{\infty} \{D_m - (-1)^q E_m\}[(m\tau-q)\ J_{m\tau-q}(kb) + (-1)^q (m\tau+q)\ J_{m\tau+q}(kb)] = 0, \tag{3.28}$$

when the symmetry conditions in (3.16) apply. The expression in (3.28) ensures the continuity of the q^{th} derivative of the surface current density about the midpoint of the truncation surface, provided that lower derivatives of the current density are continuous there.

Now consider the continuity of the surface current density across $\rho = a$ on C_1 and C_2. It can be seen from (2.28) and (2.36) that this current density can be expressed as

$$I_m(r) + F_m(r) = \mp \frac{1}{r} \sum_{n=1}^{\infty} (\pm 1)^n\ P_{n\ n\nu}\ L_{n\nu}(kr), \quad r > a, \ m = \frac{1}{2}, \tag{3.29}$$

$$P_{n\ n\nu}\ L_{n\nu}(kr) = \frac{4\nu_j^{\ n\nu}}{k}\ J_{n\nu}(kr)\ \sin(n\nu\psi) + \frac{a_n}{k} H^{(2)}_{n\nu}(kr). \tag{3.30}$$

Since $P_n L_{n\nu}(kr)$ is a linear combination of cylindrical Bessel functions, it can be manipulated as a cylindrical Bessel function.

Because the surface C_1 is absolutely continuous for $\rho > a_1$, the surface current density is absolutely continuous on C_1. Hence, the representations in (3.6) and (3.29) may be equated at any point on C_1, giving

$$\frac{\partial^q}{\partial\delta^q}\,[S_1(a-a_1+\delta)]=\frac{\partial^q}{\partial\delta^q}\,[I_1(a+\delta)+F_1(a+\delta)],\quad q=0,1,2,\cdots,$$

$$\delta > a_1 - a. \qquad (3.31)$$

By using the addition theorem for Bessel functions, the expression in (3.31) expands into

$$\sum_{\substack{m=1\\ \ell=0}}^{\infty} \varepsilon_\ell \frac{(-1)^m D_m}{a-a_1}\left[(m\tau-\ell)\,J_{m\tau-\ell}(k[a-a_1])+(-1)^\ell(m\tau+\ell)\right.$$

$$\left.\cdot J_{m\tau+\ell}(k[a-a_1])\right]\frac{\partial^q}{\partial\delta^q}\,J_\ell(k\delta) = \sum_{\substack{n=1\\ \ell=0}}^{\infty}\frac{\varepsilon_\ell P_n}{a}\left[(n\nu-\ell)\,L_{n\nu-\ell}(ka)\right.$$

$$\left.+(-1)^\ell(n\nu+\ell)\,L_{n\nu+\ell}(ka)\right]\frac{\partial^q}{\partial\delta^q}\,J_\ell(k\delta),\quad |\delta| < (a-a_1). \qquad (3.32)$$

The use of (3.27) enables the expression in (3.32) to be reduced to

$$\sum_{m=1}^{\infty}\frac{(-1)^m D_m}{a-a_1}\left[(m\tau-q)\,J_{m\tau-q}(k[a-a_1])+(-1)^q(m\tau+q)\,J_{m\tau+q}(k[a-a_1])\right]$$

$$=\sum_{n=1}^{\infty}\frac{P_n}{a}\left[(n\nu-q)\,L_{n\nu-q}(ka)+(-1)^\ell(n\nu+\ell)\,L_{n\nu+q}(ka)\right], \qquad (3.33)$$

thereby ensuring the continuity of the q^{th} derivative of the surface current density about $\rho=a$ on C_1, provided that lower derivatives of the current density are continuous there.

Similarly, the continuity of the q^{th} derivative of the

surface current density about $\rho=a$ on C_2 is ensured if

$$-\sum_{m=1}^{\infty}(-1)^m\frac{E_m}{b}\left[(m\gamma-q)\ J_{m\gamma-q}(kb)+(-1)^q(m\gamma+q)\ J_{m\gamma+q}(kb)\right]$$

$$=\sum_{n=1}^{\infty}(-1)^n\frac{P_n}{a}\left[(n\nu-q)\ L_{n\nu-q}(ka)+(-1)^q(n\nu+q)\ L_{n\nu+q}(ka)\right],\quad (3.34)$$

provided that lower derivatives of the surface current density are continuous there.

When the wedge is symmetrically truncated, the addition and subtraction of the expressions in (3.33) and (3.34) gives the two equations

$$\sum_{m=1}^{\infty}\frac{(D_m\pm E_m)}{b}(-1)^m[(m\tau-q)\ J_{m\tau-q}(kb)+(-1)^q(m\tau+q)\ J_{m\tau+q}(kb)]$$

$$=\sum_{n=1}^{\infty}\frac{2P_t}{a}[(t\nu-q)\ L_{t\nu-q}(ka)+(-1)^q(t\nu+q)\ L_{t\nu+q}(ka)],\ t=\frac{2n-1}{2n}.$$

(3.35)

Substituting (3.20) and (3.30) into (3.35) results in

$$\frac{-2}{ka}\sum_{n=1}^{\infty}a_t\left[(t\nu-q)\ H^{(2)}_{t\nu-q}(ka)+(-1)^q(t\nu+q)\ H^{(2)}_{t\nu+q}(ka)\right]$$

$$+\sum_{m=1}^{\infty}\frac{(-1)^m}{b}\frac{Q_m}{R_m}\left[(m\tau-q)J_{m\tau-q}(kb)+(-1)^q(m\tau+q)J_{m\tau+q}(kb)\right]$$

$$=\frac{8\nu}{ka}\sum_{n=1}^{\infty}j^{t\nu}\sin(t\nu\psi)\left[(t\nu-q)\ J_{t\nu-q}(ka)+(-1)^q(t\nu+q)\ J_{t\nu+q}(ka)\right],$$

$$t=\frac{2n-1}{2n},\qquad (3.36)$$

which are valid if derivatives of the surface current density below the q^{th} are continuous about $\rho=a$.

3.1(c) TRUNCATED WEDGE. (Magnetic Polarization).

To determine a representation of the surface current density $\vec{F}_3(c)$ on the surface C_3 of the truncated wedge when the field is magnetically polarized, consider the perfectly conducting closed surface C in Fig. 3.1. The geometry of this figure is described in section 3.1(a).

A representation of the field $\vec{H}$ which satisfies the Helmholtz equation (1.2), the boundary condition (1.4) on C_1 and C_2, and the edge condition at $\rho = 0$, is

$$\vec{H} = \hat{z} \sum_{m=0}^{\infty} D_m J_{m\tau}(k\rho) \cos(m\tau\phi), \qquad \rho < b, \tag{3.37}$$

where τ is defined in (3.7), and the D_m are constants which depend upon the incident field and the shape of the contour C. By using (3.37) with (1.33), the surface current density $\vec{S}_1(x)$ on C_1 is found to be

$$\vec{S}_1(x) = \hat{r}_1 \sum_{m=0}^{\infty} D_m J_{m\tau}(kx), \qquad x < b, \tag{3.38}$$

and the surface current density $\vec{S}_2(x)$ on C_2 is

$$\vec{S}_2(x) = -\hat{r}_2 \sum_{m=0}^{\infty} (-1)^m D_m J_{m\tau}(kx), \tag{3.39}$$

where

$$\hat{r}_1 = \hat{\rho}\cos\phi - \hat{\phi}\sin\phi, \qquad \hat{r}_2 = \hat{\rho}\cos(\phi+\beta) - \hat{\phi}\sin(\phi+\beta), \tag{3.40}$$

and x is the distance from $\rho=0$ to a point on C_1 or C_2. Because the field is continuous everywhere outside C, and the contour C_1 has no discontinuities, the current density on C_1 is continuous. Thus, the expression in (3.38) is a valid representation of $\vec{S}_1(x)$ everywhere on C_1.

Consider the perfectly conducting truncated wedge in Fig. 3.2. The description of this figure, and the definition of the deformed surface C_3 is given in section 3.1(a). It follows from (3.38) and (3.39) that the surface current density $\vec{S}_1(x)$ at a point on the surface $\phi=\chi$, and the surface current density $\vec{S}_3(x)$ at a point on the truncation surface can be represented by

$$\vec{S}_n(x) = \hat{r}_n S_n(x), \quad S_n(x) = -\sum_{m=0}^{\infty} (\pm 1)^m D_m J_{m\tau}(kx), \quad n = \begin{matrix} 3 \\ 1 \end{matrix}, \tag{3.41}$$

where the D_m are constants, and the unit vectors $\hat{r}_1$ and $\hat{r}_3$ are defined in (2.54) as

$$\hat{r}_1 = \hat{\rho}\cos(\phi-\chi) - \hat{\phi}\sin(\phi-\chi), \quad \hat{r}_3 = \hat{\rho}\cos(\phi-\delta) - \hat{\phi}\sin(\phi-\delta). \tag{3.42}$$

Similarly, the surface current density $\vec{T}_2(y)$ on the surface $\phi = 2\pi-\chi$, and the surface current density $\vec{T}_3(y)$ on the truncation surface can be represented by

$$\vec{T}_n(y) = \hat{r}_n T_n(y), \quad T_n(y) = \sum_{m=0}^{\infty} (\pm 1)^m E_m J_{m\gamma}(ky), \quad n = \begin{matrix} 3 \\ 2 \end{matrix}, \tag{3.43}$$

where the E_m are constants, the unit vector $\hat{r}_2$ is defined in (2.54), and γ is defined in (3.9). The surface current density $F_3(c)$ of (2.86) is given by

$$\begin{aligned} F_3(c) &= T_2(y), \quad 0 \leq y \leq b, \ \phi = 2\pi-\chi, \\ &= T_3(y), \quad 0 \leq y \leq b, \ \text{on the truncation surface}, \\ &= S_3(x), \quad 0 \leq x \leq b, \ \text{on the truncation surface}, \\ &= S_1(x), \quad 0 \leq x \leq b, \ \phi = \chi \ . \end{aligned} \tag{3.44}$$

Substituting (3.44) into (2.86) gives

$$\begin{aligned} C_{t,p} = \frac{k}{4}\Bigg[&\int_o^b T_2(y)\left[J_{p+1}(kr)\ q_t(-p\chi-\pi) + J_{p-1}(kr)\ q_t(-p\chi+\pi)\right]dy \\ &+\int_o^b T_3(y)\left[J_{p+1}(kr)\ q_t([p+1]\theta-\tfrac{\pi}{2})+J_{p-1}(kr)\ q_t([p-1]\theta+\tfrac{\pi}{2})\right]dy \\ &+\int_o^b S_3(x)\left[J_{p+1}(kr)\ q_t([p+1]\theta-\tfrac{\pi}{2})+J_{p-1}(kr)\ q_t([p-1]\theta+\tfrac{\pi}{2})\right]dx \\ &+\int_o^{a-a_1} S_1(x)[J_{p+1}(kr) + J_{p-1}(kr)]\ q_t(p\chi)\,dx\Bigg]. \end{aligned} \tag{3.45}$$

From (2.45),

$$q_t(-p\chi\pm\pi) = (-1)^t\, q_t(p\chi), \quad q_t([p+1]\theta\pm\tfrac{\pi}{2}) = \pm(-1)^t\, q_{t+1}([p+1]\theta). \tag{3.46}$$

Using the recurrence relations for Bessel functions, and substituting (3.41), (3.43), and (3.46) into (3.45) results in

$$C_{t,p} = \frac{k}{4} \sum_{m=0}^{\infty} \left[(-1)^{m+t} E_m 2p\, q_t(p\chi) \int_o^b \frac{J_p(k[a_2+y])\, J_{m\gamma}(ky)}{k(a_2+y)}\, dy \right.$$

$$+(-1)^{t+1} E_m \int_o^b \left[J_{p+1}(kr)\, q_{t+1}([p+1]\theta) - J_{p-1}(kr)\, q_{t+1}([p-1]\theta) \right]$$

$$\cdot J_{m\gamma}(ky)\, dy + (-1)^t D_m \int_o^b \left[J_{p+1}(kr)\, q_{t+1}([p+1]\theta) - J_{p-1}(kr) \right.$$

$$\left. \left. \cdot q_{t+1}([p-1]\theta) \right] J_{m\tau}(kx)\, dx + (-1)^{m+1} D_m\, 2p\, q_t(p\chi) \right.$$

$$\left. \cdot \int_o^{a-a_1} \frac{J_p(k[a_1+x])\, J_{m\tau}(kx)}{k(a_1+x)}\, dx \right], \quad a_2 \geq a_1 > b. \qquad (3.47)$$

When the truncated wedge exhibits the symmetry defined in (3.16), $C_{t,p}$ simplifies to

$$C_{t,p} = \frac{k}{4} \sum_{m=0}^{\infty} (D_m \mp E_m) \int_o^b \left[(-1)^{m+1} \frac{2p\, J_p(k[a_1+x])}{k(a_1+x)} q_t(p\chi) \right.$$

$$\left. \pm \{J_{p+1}(kr)\, q_{t+1}([p+1]\theta) - J_{p-1}(kr)\, q_{t+1}([p-1]\theta)\} \right] J_{m\tau}(kx)\, dx,$$

$$t = \begin{matrix} 2n \\ 2n+1 \end{matrix}, \qquad (3.48)$$

where

$$\theta = \sin^{-1}\left[\frac{b-x}{r}\right], \quad r = (a_1^2 + x^2 - 2bx)^{\frac{1}{2}}. \qquad (3.49)$$

Using the definition in (3.20) extended to include m=0, (2.84) can be specialized for the symmetrically truncated wedge to

$$\sum_{n=0}^{\infty} a_t D_{t,p} + \sum_{m=0}^{\infty} \begin{matrix} R_m \\ Q_m \end{matrix} C_{t,p,m} = Y_{t,p}, \qquad t = \begin{matrix} 2n \\ 2n+1 \end{matrix}, \qquad (3.50)$$

where the $D_{t,p}$ and $Y_{t,p}$ are given by (2.85) and (2.87) respectively, and from (3.48)

$$C_{t,p,m} = \frac{k}{4} \int_o^b \left[(-1)^{m+1}\, 2p\, \frac{J_p(k[a_1+x])}{k(a_1+x)} q_t(p\chi) \right.$$

$$\left. + (-1)^t \{J_{p+1}(kr)\, q_{t+1}([p+1]\theta) - J_{p-1}(kr)\, q_{t+1}([p-1]\theta)\} \right] J_{m\tau}(kx)\, dx.$$

(3.51)

3.1(d) SURFACE CURRENT CONTINUITY. (Magnetic Polarization).

In a similar manner to that of section 3.1(b), the equations which explicitly ensure the continuity of the current density on the truncated wedge are derived in this section for magnetic polarization of the field. First, consider the continuity of the surface current density about the midpoint of the truncation surface. Using the addition theorem for Bessel functions[14] to expand (3.41) and (3.43) enables the expression in (3.24) to be expanded into

$$\sum_{\substack{m=0\\ \ell=0}}^{\infty} \varepsilon_\ell E_m \left[J_{m\gamma+\ell}(kb) + (-1)^\ell J_{m\gamma-\ell}(kb) \right] \frac{\partial^q}{\partial \delta^q} J_\ell(k\delta)$$

$$= - \sum_{\substack{m=0\\ \ell=0}}^{\infty} \varepsilon_\ell D_m \left[J_{m\tau-\ell}(kb) + (-1)^\ell J_{m\tau+\ell}(kb) \right] \frac{\partial^q}{\partial \delta^q} J_\ell(k\delta), \quad \forall |\delta| < b. \tag{3.52}$$

When the wedge is symmetrically truncated as defined in (3.16), the expression in (3.52) is reduced, by using (3.27), to

$$\sum_{m=0}^{\infty} \{D_m + (-1)^q E_m\} \left[J_{m\tau-q}(kb) + (-1)^q J_{m\tau+q}(kb) \right] = 0, \tag{3.53}$$

which ensures the continuity of the q^{th} derivative of the surface current density about the midpoint of the truncation surface, provided that lower derivatives of the current density are continuous there.

Now consider the continuity of the surface current density across $\rho = a$ on C_1 and C_2. It can be seen from (2.58) and (2.74) that this current density can be expressed as

$$I_m(r) + F_m(r) = \pm \sum_{n=0}^{\infty} (\pm 1)^n P_n L_{n\nu}(kr), \quad r > a, \; m = \frac{1}{2}, \tag{3.54}$$

$$P_n L_{n\nu}(kr) = 2\nu \varepsilon_n j^{n\nu} J_{n\nu}(kr) \cos(n\nu\psi) + a_n H^{(2)}_{n\nu}(kr), \tag{3.55}$$

where the function $P_n L_{n\nu}(kr)$ can be manipulated as a cylindrical Bessel function.

Because the surface C_1 is absolutely continuous for $\rho > a_1$, the surface current density is absolutely continuous on C_1. Hence, the representations in (3.41) and (3.54) can be equated as in (3.31). By using the addition theorem for Bessel functions, the expression in (3.31) expands into

$$\sum_{\substack{m=0\\ \ell=0}}^{\infty} \varepsilon_\ell (-1)^{m+1} D_m \left[J_{m\tau-\ell}(k[a-a_1]) + (-1)^\ell J_{m\tau+\ell}(k[a-a_1]) \right] \frac{\partial^q}{\partial \delta^q} J_\ell(k\delta)$$

$$= \sum_{\substack{n=0\\ \ell=0}}^{\infty} \varepsilon_\ell P_n \left[L_{n\nu-\ell}(ka) + (-1)^\ell L_{n\nu+\ell}(ka) \right] \frac{\partial^q}{\partial \delta^q} J_\ell(k\delta), \quad |\delta| < (a-a_1). \tag{3.56}$$

The use of (3.27) enables the expression in (3.56) to be reduced to

$$\sum_{m=0}^{\infty} (-1)^{m+1} D_m \left[J_{m\tau-q}(k[a-a_1]) + (-1)^q J_{m\tau+q}(k[a-a_1]) \right]$$

$$= \sum_{n=0}^{\infty} P_n \left[L_{n\nu-q}(ka) + (-1)^q L_{n\nu+q}(ka) \right], \tag{3.57}$$

thereby ensuring the continuity of the q^{th} derivative of the surface current density about $\rho = a$ on C_1, provided that lower derivatives of the current density are continuous there.

Similarly, the continuity of the q^{th} derivative of the surface current density about $\rho = a$ on C_2 is ensured if

$$\sum_{m=0}^{\infty} (-1)^m E_m\left[J_{m\gamma-q}(k[a-a_2])+(-1)^q J_{m\gamma+q}(k[a-a_2])\right]$$

$$= \sum_{n=0}^{\infty} (-1)^n P_n\left[L_{n\nu-q}(ka) + (-1)^q L_{n\nu+q}(ka)\right], \qquad (3.58)$$

provided that lower derivatives of the surface current density are continuous there.

When the wedge is symmetrically truncated as in (3.16), the addition and subtraction of the expressions in (3.57) and (3.58) gives the two equations

$$\sum_{m=0}^{\infty} (D_m \tilde{+} E_m)(-1)^m[J_{m\tau-q}(kb)+(-1)^q J_{m\tau+q}(kb)]$$

$$= -2 \sum_{n=0}^{\infty} P_t[L_{t\nu-q}(ka)+(-1)^q L_{t\nu+q}(ka)], \quad t = \begin{matrix}2n\\2n+1\end{matrix}. \qquad (3.59)$$

Substituting (3.20) and (3.55) into (3.59) gives

$$2 \sum_{n=0}^{\infty} a_t[H^{(2)}_{t\nu-q}(ka)+(-1)^q H^{(2)}_{t\nu+q}(ka)]+ \sum_{m=0}^{\infty} \frac{R_m}{Q_m}(-1)^m$$

$$\cdot[J_{m\tau-q}(kb)+(-1)^q J_{m\tau+q}(kb)] = -4\nu \sum_{n=0}^{\infty} \varepsilon_t j^{t\nu} \cos(t\nu\psi)$$

$$\cdot[J_{t\nu-q}(ka)+(-1)^q J_{t\nu+q}(ka)], \quad t = \begin{matrix}2n\\2n+1\end{matrix}, \qquad (3.60)$$

which are valid if derivatives of the surface current density below the q^{th} are continuous about $\rho = a$.

3.2(a) ROUNDED WEDGE. (Electric Polarization)

The specialation of the results of section 2.2(a) to the rounded wedge is studied in this section. As in previous sections of this chapter, the representation of the surface current density $\vec{F}_3(c)$ over the wedge deformation is of primary interest.

Consider the perfectly conducting rounded wedge in Fig. 3.4. The (ρ,ϕ,z) co-ordinate system has its origin at the apex of the undeformed wedge. The deformation contour C_3 is the arc of a circle centred on $\phi = 0$ such that the surfaces $\phi = \chi$ and $\phi = 2\pi - \chi$ are tangents to the arc at $\rho = a, \phi = \pm\chi$. Let x be the distance measured along the surface in a clockwise direction from the mid-point of C_3 to a point on the surface. The maximum value of x on C_3 is X. The incident field is electrically polarized in the z-direction.

A representation of $\vec{F}_3(c)$ which acknowledges *à priori* that any oscillations in the surface current density are likely to have a period close to that of the field in the surrounding medium is

$$\vec{F}_3(c) = \hat{z}\, F_3(x), \qquad F_3(x) = \sum_{m=0}^{\infty} b_m J_m(kx), \qquad (3.61)$$

where the b_m are constants. Substituting this representation into (2.49) gives

$$C_{t,p} = \frac{k}{2} \sum_{m=0}^{\infty} b_m \int_{-X}^{X} J_m(kx)\ J_p(kr)\ q_t(p\theta)\,dx. \qquad (3.62)$$

Since, from (2.45)

$$q_t(\xi) = (-1)^{t+1}\ q_t(-\xi), \qquad (3.63)$$

and r is an even function of x, $C_{t,p}$ is simplified by using (2.33), to

$$C_{t,p} = k \sum_{m=0}^{\infty} b_s \int_{o}^{X} J_s(kx)\ J_p(kr)\ q_t(p\theta)\ dx,\ s = \frac{2m}{2m+1},\ t=\frac{2n-1}{2n}. \qquad (3.64)$$

Thus, in the case of the rounded wedge, the expression in (2.47) becomes

$$\sum_{n=1}^{\infty} a_t\ D_{t,p} + \sum_{m=0}^{\infty} b_s\ C_{t,p,s} = Y_{t,p},\ t = \frac{2n-1}{2n},\ s = \frac{2m}{2m+1}, \qquad (3.65)$$

where the $D_{t,p}$ and $Y_{t,p}$ are defined in (2.48) and (2.50) respectively, and from (3.64),

$$C_{t,p,s} = k \int_{o}^{X} J_s(kx)\ J_p(kr)\ q_t(p\theta)\ dx. \qquad (3.66)$$

The surface current density on C_1 and C_2 when the field is electrically polarized is given by (3.29) and (3.30). The q^{th} derivative of the surface current density across $x = X$ is continuous if

$$\frac{\partial^q}{\partial \delta^q}\left[F_3(X+\delta)\right]\Big|_{\delta=0} = \frac{\partial^q}{\partial \delta^q}\left[I_1(a+\delta)+F_1(a+\delta)\right]\Big|_{\delta=0}, \tag{3.67}$$

and is continuous across $x = -X$ if

$$\frac{\partial^q}{\partial \delta^q}\left[F_3(-X-\delta)\right]\Big|_{\delta=0} = \frac{\partial^q}{\partial \delta^q}\left[I_2(a+\delta)+F_2(a+\delta)\right]\Big|_{\delta=0}. \tag{3.68}$$

Substitution of (3.29) and (3.61) and the use of the addition theorem for Bessel functions[14] enables the expression in (3.67) to be expanded as

$$\sum_{\substack{m=0\\ \ell=0}}^{\infty} \varepsilon_\ell\, b_m\left[J_{m-\ell}(kX)+(-1)^\ell J_{m+\ell}(kX)\right]\frac{\partial^q}{\partial \delta^q}J_\ell(k\delta)\Big|_{\delta=0}$$

$$= -\sum_{\substack{n=1\\ \ell=0}}^{\infty} \frac{\varepsilon_\ell P_n}{a}\left[(n\nu-\ell)\, L_{n\nu-\ell}(ka)+(-1)^\ell(n\nu+\ell)\, L_{n\nu+\ell}(ka)\right]\frac{\partial^q}{\partial \delta^q}J_\ell(k\delta)\Big|_{\delta=0}, \tag{3.69}$$

which, with the use of (3.27), reduces to

$$\sum_{m=0}^{\infty} b_m\left[J_{m-q}(kX)+(-1)^q J_{m+q}(kX)\right] = -\sum_{n=1}^{\infty}\frac{P_n}{a}\left[(n\nu-q)\ L_{n\nu-q}(ka)\right.$$

$$\left.+(-1)^q\ (n\nu+q)\ L_{n\nu+q}(ka)\right]. \qquad (3.70)$$

The expression in (3.70) ensures the continuity of the q^{th} derivative of the current density across x = X provided that derivatives of lower order are continuous there. Similarly, if

$$\sum_{m=0}^{\infty}(-1)^m b_m\left[J_{m-q}(kX)+(-1)^q J_{m+q}(kX)\right]=\sum_{n=1}^{\infty}(-1)^n\frac{P_n}{a}$$

$$\cdot\left[(n\nu-q)\ L_{n\nu-q}(ka)+(-1)^q(n\nu+q)\ L_{n\nu+q}(ka)\right], \qquad (3.71)$$

the q^{th} derivative of the surface current density across x=-X is continuous, provided that derivatives of lower order are continuous there. Adding and subtracting the expressions in (3.70) and (3.71) gives

$$\sum_{m=0}^{\infty} b_s\left[J_{s-q}(kX)+(-1)^q J_{s+q}(kX)\right]$$

$$= -\sum_{n=1}^{\infty}\frac{P_t}{a}\left[(t\nu-q)\ L_{t\nu-q}(ka)+(-1)^q(t\nu+q)\ L_{t\nu+q}(ka)\right],$$

$$s = \begin{matrix}2m\\2m+1\end{matrix},\ t=\begin{matrix}2n-1\\2n\end{matrix}. \qquad (3.72)$$

Substitution of (3.30) into (3.72) gives

$$\sum_{n=1}^{\infty} \frac{a_t}{ka} \left[(t\nu-q)\ H^{(2)}_{t\nu-q}(ka) + (-1)^q\ (t\nu+q)\ H^{(2)}_{t\nu+q}(ka) \right]$$

$$+ \sum_{m=0}^{\infty} b_s \left[J_{s-q}(kX) + (-1)^q\ J_{s+q}(kX) \right]$$

$$= \frac{-4\nu}{ka} \sum_{n=1}^{\infty} j^{t\nu} \sin(t\nu\psi) \left[(t\nu-q)\ J_{t\nu-q}(ka) + (-1)^q (t\nu+q)\ J_{t\nu+q}(ka) \right],$$

$$s = \begin{matrix} 2m \\ 2m+1 \end{matrix}, \quad t = \begin{matrix} 2n-1 \\ 2n \end{matrix}, \qquad (3.73)$$

which is valid if derivatives of surface current density below the q^{th} are continuous across both $x = X$ and $x = -X$.

3.2(b) ROUNDED WEDGE. (Magnetic Polarization).

Consider the perfectly conducting rounded wedge in Fig. 3.4 illuminated by a magnetically polarized field. The geometry of the figure is described in section 3.2(a). For the reason given in that section, the form of $\vec{F}_3(c)$ used to represent the surface current density on C_3 is

$$\vec{F}_3(c) = \hat{r}_3\ F_3(x), \quad F_3(x) = \sum_{m=0}^{\infty} b_m\ J_m(kx), \qquad (3.74)$$

where the b_m are constants. The unit vector $\hat{r}_3$ is defined in (2.54) and (2.55) with

$$\eta_3 = \phi - \theta - \frac{\pi}{2} + \Gamma, \quad \Gamma = \sin^{-1}\left[\frac{\sin\theta}{\sin\chi}\right] . \tag{3.75}$$

Substituting the expression in (3.74) into (2.86) gives

$$C_{t,p} = \frac{k}{4} \sum_{m=0}^{\infty} b_m \int_{-X}^{X} J_m(kx) \left[J_{p+1}(kr)\ q_t(p\theta+\Gamma-\tfrac{\pi}{2}) \right.$$

$$\left. + J_{p-1}(kr)\ q_t(p\theta-\Gamma+\tfrac{\pi}{2}) \right] dx. \tag{3.76}$$

Since r is an even function of x, while θ and Γ are both odd functions of x, $C_{t,p}$ can be simplified by using (3.46), (3.63) and (2.33), to

$$C_{t,p} = \frac{k}{2} \sum_{m=0}^{\infty} (-1)^{s+1} b_s \int_{o}^{X} J_s(kx) \left[J_{p+1}(kr)\ q_{t+1}(p\theta+\Gamma) \right.$$

$$\left. - J_{p-1}(kr)\ q_{t+1}(p\theta-\Gamma) \right] dx, \qquad s = \begin{matrix} 2m \\ 2m+1 \end{matrix}, \quad t = \begin{matrix} 2n \\ 2n+1 \end{matrix}. \tag{3.77}$$

The expression in (2.84) are specialized, in the case of the rounded wedge, to

$$\sum_{n=0}^{\infty} a_t\ D_{t,p} + \sum_{m=0}^{\infty} b_s\ C_{t,p,s} = Y_{t,p}, \quad t = \begin{matrix} 2n \\ 2n+1 \end{matrix}, \quad s = \begin{matrix} 2m \\ 2m+1 \end{matrix}, \tag{3.78}$$

where the $D_{t,p}$ and $Y_{t,p}$ are given in (2.85) and (2.87) respect-

ively, and from (3.77)

$$C_{t,p,s} = (-1)^{s+1} \frac{k}{2} \int_0^X J_s(kx) \left[J_{p+1}(kr)\ q_{t+1}(p\theta+\Gamma) \right.$$

$$\left. - J_{p-1}(kr)\ q_{t+1}(p\theta-\Gamma) \right] dx. \qquad (3.79)$$

The surface current density on C_1 and C_2 when the field is magnetically polarized is given by (3.54) and (3.55). The q^{th} derivative of the surface current density across $x = X$ is continuous if the expression in (3.67) holds, and the q^{th} derivative of the surface current density across $x = -X$ is continuous if the expression in (3.68) holds. Using the addition theorem for Bessel functions to expand (3.54), and substituting into (3.67) gives

$$\sum_{\substack{m=0 \\ \ell=0}}^{\infty} \varepsilon_\ell b_m \left[J_{m-\ell}(kX) + (-1)^\ell J_{m+\ell}(kX) \right] \frac{\partial^q}{\partial \delta^q} J_\ell(k\delta) \Big|_{\delta=0}$$

$$= \sum_{n=0}^{\infty} \varepsilon_\ell P_n \left[L_{n\nu-\ell}(ka) + (-1)^\ell L_{n\nu+\ell}(ka) \right] \frac{\partial^q}{\partial \delta^q} J_\ell(k\delta) \Big|_{\delta=0}, \qquad (3.80)$$

which, with the use of (3.27) reduces to

$$\sum_{m=0}^{\infty} b_m \left[J_{m-q}(kX)+(-1)^q J_{m+q}(kX)\right]$$

$$= \sum_{n=0}^{\infty} P_n \left[L_{n\nu-q}(ka) +(-1)^q L_{n\nu+q}(ka)\right]. \qquad (3.81)$$

The expression in (3.81) ensures the continuity of the q^{th} derivative of the current density across $x = X$, provided that derivatives of lower order are continuous there. Similarly, if

$$\sum_{m=0}^{\infty} (-1)^m b_m \left[J_{m-q}(kX)+(-1)^q J_{m+q}(kX)\right] = \sum_{n=0}^{\infty} (-1)^n P_n$$

$$\cdot\left[L_{n\nu-q}(ka)+(-1)^q L_{n\nu+q}(ka)\right], \qquad (3.82)$$

the q^{th} derivative of the surface current density across $x = -X$ is continuous, provided that derivatives of lower order are continuous there. Adding and subtracting the expressions in (3.81) and (3.82) gives

$$\sum_{m=0}^{\infty} b_s \left[J_{s-q}(kX)+(-1)^q J_{s+q}(kX)\right]$$

$$= \sum_{n=0}^{\infty} P_t \left[L_{t\nu-q}(ka)+(-1)^q L_{t\nu+q}(ka)\right], \quad t = \begin{matrix}2n\\2n+1\end{matrix}, \; s = \begin{matrix}2m\\2m+1\end{matrix},$$

$$(3.83)$$

which, after substituting (3.55), gives

$$-\sum_{n=0}^{\infty} a_t\left[H^{(2)}_{t\nu-q}(ka)+(-1)^q H^{(2)}_{t\nu+q}\right] + \sum_{m=0}^{\infty} b_s\left[J_{s-q}(kX)+(-1)^q\right.$$

$$\left.J_{s+q}(kX)\right] = 2\nu \sum_{n=0}^{\infty} \varepsilon_t\, j^{t\nu} \cos(t\nu\psi)\left[J_{t\nu-q}(ka)+(-1)^q J_{t\nu+q}(ka)\right],$$

$$t = \begin{matrix}2n\\2n+1\end{matrix}, \quad s = \begin{matrix}2m\\2m+1\end{matrix}, \qquad (3.84)$$

where ε_ℓ is the Neumann factor. The expressions in (3.84) ensure the continuity of the q^{th} derivative of the surface current density across $x = \pm X$ provided that lower derivatives of the current density are continuous there.

3.3(a) NUMERICAL CONSIDERATIONS

The four expressions in (3.21), (3.50), (3.65), and (3.78) are specializations of the expressions in (2.47) and (2.84) for the cases of a symmetrically truncated wedge and a rounded wedge in either an electrically or a magnetically polarized field. Each of the four expressions consists of two independent equations with an infinite number of unknowns.

The independence of these two equations arizes from the symmetry of the wedge deformation about $\phi = 0$. As

a result of this symmetry, half of the unknown field modal coefficients (the a_n) and half of the unknown surface current density modal coefficients (the Q_m and R_m, or b_m) appear in one equation, and the remainder appear in the other. The coefficients separate into exactly the same groups in the equations derived from surface current density continuity considerations.

Because similar methods are used to obtain the unknown modal coefficients from either (3.21), (3.50), (3.65) or (3.78), only the expressions relating to the truncated wedge in an electrically polarized field will be discussed.

By letting p take all positive integer values and zero, the equations of (3.21) may be written as two independent matrix equations of infinite order. Because there has been no approximation made during the derivation of (3.21), the solution to these matrix equations enables an exact description of the field scattered from a truncated wedge to be obtained. However, in order to numerically determine the unknown modal coefficients in these matrix equations, it is necessary to limit the number of a_n to a finite number N, and the number of Q_m or R_m to a finite number M. The maximum values of N and M are limited by available computational facilities.

Thus, from (3.21)

$$\sum_{n=1}^{N} a_t D_{t,p} + \sum_{m=1}^{M} \begin{matrix} Q_m \\ R_m \end{matrix} C_{t,p,m} = Y_{t,p}, \quad t = \begin{matrix} 2n-1 \\ 2n \end{matrix}, \tag{3.85}$$

and by letting p take a suitable number of values, these equations can each be expressed in matrix form as

$$[A][x] = [y]. \tag{3.86}$$

The elements of [A] are the $D_{t,p}$ and the $C_{t,p,m}$; while [x], the vector of unknowns, contains the a_t and Q_m or R_m. It can be seen from (2.50) that the characteristics of the incident field are contained in the elements $Y_{t,p}$ of the known vector [y]. Thus, having determined the inverse $[A]^{-1}$ of the matrix [A], the modal coefficients may be obtained for any incident field by post-multiplication of $[A]^{-1}$ by the appropriate vector [y].

Define T to be the order of the matrix [A] in (3.86). The matrix elements are obtained by letting p (the field Fourier component harmonic number) take the first T zero and positive integer values to give T algebraic equations. It follows that an increase in N or M resulting in an increase in T means that a greater number of Fourier field components must be considered.

The inclusion of Q equations from both (3.28) and (3.36) in the matrix equation (3.86) explicitly ensures

the continuity of the surface current density up to the $(Q-1)^{th}$ derivative. These equations are obtained by letting q take all positive integer values between zero and (Q-1) inclusive. This requires that the range of p be reduced by Q in a matrix of order T. Thus for a given matrix order, the inclusion of current density continuity equations results in the neglect of higher order field Fourier components.

The separation of the matrix equation in (2.47) into the two matrix equations in (3.85) when the wedge truncation is symmetric, enables considerable savings to be made in both computational time and storage. Since the time required to numerically invert a matrix of order 2T is proportional to $8T^{3}$,[86] the separation of (2.47) into two equations of approximately equal order T enables the inversions to be completed in a time proportional to $2T^{3}$. The storage requirement for a matrix of order 2T is $4T^{2}$ locations, while that for two matrices of order T is only $2T^{2}$ locations.

The limiting of the matrices to finite order is justified only if the neglected terms and equations have negligible influence on the values obtained for the modal coefficients. The convergence of the modal coefficients to constant values as N and M increase indicates that these coefficients are adequately defined in the matrix equations of finite order.

3.3(b) PROGRAMMING

Simpson's Rule[87] was used to evaluate the contour integrals of (3.51), (3.66), and (3.79) to obtain respectively the $C_{t,p,m}$ for the symmetrically truncated wedge in a magnetically polarized field, and the rounded wedge in an electrically or magnetically polarized field.

By dividing the range of integration into (L-1) equal subdivisions, where L is an odd integer, the expression in (3.51) can be approximated by

$$C_{t,p,m} = \frac{kh}{6}\left[(-1)^{m+1}\, pq_t(p\chi)\sum_{\ell=1}^{L} e_\ell \frac{J_p[k(a_1+x_\ell)]}{k(a_1+x_\ell)} J_{m\tau}(kx_\ell)\right.$$

$$\left. + \frac{(-1)^t}{2}\sum_{\ell=1}^{L} e_\ell\left[J_{p+1}(kr_\ell)\, q_{t+1}([p+1]\theta_\ell) - J_{p-1}(kr_\ell)\, q_{t+1}([p-1]\theta_\ell)\right] \cdot J_{m\tau}(kx_\ell)\right], \tag{3.87}$$

where

$$h = \frac{b}{L-1}, \quad x_\ell = (\ell-1)h, \tag{3.88}$$

and from (3.49)

$$\theta_\ell = \sin^{-1}\left\{\frac{b-x_\ell}{r_\ell}\right\}, \quad r_\ell = (a_1^2 + x_\ell^2 - 2bx_\ell)^{\frac{1}{2}}. \tag{3.89}$$

The weighting factor e_ℓ is defined by

$$\begin{aligned} e_\ell &= 1, \quad \ell = 1, L, \\ &= 2, \quad \ell = 2n-1, \ \ell \neq 1, L, \\ &= 4, \quad \ell = 2n, \end{aligned} \tag{3.90}$$

where n is an integer.

In a similar manner, (3.66) was approximated by

$$C_{t,p,s} = \frac{kh}{3} \sum_{\ell=1}^{L} e_\ell \, J_s(kx_\ell) \, J_p(kr_\ell) \, q_t(p\theta_\ell), \tag{3.91}$$

where

$$h = \frac{X}{L-1}, \quad x_\ell = (\ell-1)h, \tag{3.92}$$

and X is defined in terms of the radius R of the round top by

$$X = R(\tfrac{\pi}{2} - \chi). \tag{3.93}$$

Then,

$$r_\ell = [R^2 + a_1^2 \sec^2\chi - 2Ra_1 \sec\chi \cos(x_\ell/R)]^{\frac{1}{2}},$$

$$\theta_\ell = \sin^{-1}\left[\frac{R}{r_\ell}\sin\left(\frac{x_\ell}{R}\right)\right]. \tag{3.94}$$

Similarly, (3.79) was approximated by

$$C_{t,p,s} = (-1)^{s+1} \frac{kh}{6} \sum_{\ell=1}^{L} J_s(kx_\ell)\Big[J_{p+1}(kr_\ell) \, q_{t+1}(p\theta_\ell + \Gamma_\ell)$$

$$- J_{p-1}(kr_\ell) \, q_{t+1}(p\theta_\ell - \Gamma_\ell)\Big], \tag{3.95}$$

where the definitions in (3.92)-(3.94) hold, and from (3.75),

$$\Gamma_\ell = \sin^{-1}\left[\frac{\sin\theta_\ell}{\sin\chi}\right]. \tag{3.96}$$

The subroutine which was written to evaluate the Bessel function of the first kind uses the formula[14]

$$J_\nu(z) = \left(\frac{z}{2}\right)^\nu \sum_{k=0}^{\infty} \frac{\left(-\frac{z^2}{4}\right)^k}{k!\ \Gamma(\nu+k+1)}, \qquad (3.97)$$

where $\Gamma(z)$ is the Gamma function. Using the recurrence formula

$$\Gamma(z+1) = z\,\Gamma(z), \qquad (3.98)$$

$J_\nu(z)$ can be expressed as

$$J_\nu(z) = \left(\frac{z}{2}\right)^\nu \sum_{k=0}^{K} T_k, \quad K(K!)^2 >> \left(\frac{z}{2}\right)^{2K}, \qquad (3.99)$$

where

$$T_o = \frac{1}{\Gamma(\nu+1)}; \quad T_k = \frac{-z^2\, T_{k-1}}{4k(\nu+k)}, \quad k > 0. \qquad (3.100)$$

Because the summation in (3.99) involves the subtraction of large similar terms, the algorithm is unsuitable for large z. However, it was suitable for the range of orders and arguments which arose during the construction of the matrices discussed in section 3.3(a). When ν was not an integer, Hankel functions of the second kind were calculated from a subroutine using the formula[14]

$$H_\nu^{(2)}(z) = J_\nu(z) - j\,\frac{J_\nu(z)\cos(\nu\pi) - J_{-\nu}(z)}{\sin(\nu\pi)}. \qquad (3.101)$$

When ν was an integer, the formula used was

$$H_n^{(2)}(z) = J_n(z) - j\left[-\frac{1}{\pi}\left(\frac{2}{z}\right)^n \sum_{k=0}^{n=1} \frac{(n-k-1)!}{k!}\left(\frac{z}{2}\right)^{2k} + \frac{2}{\pi}\log\left(\frac{z}{2}\right) J_n(z)\right.$$

$$\left. - \frac{1}{\pi}\left(\frac{z}{2}\right)^n \sum_{k=0}^{\infty} \{\psi(k+1) + \psi(n+k+1)\} \frac{\left(-\frac{z}{4}^2\right)^k}{k!\ (n+k)!}\right], \qquad (3.102)$$

where

$$\psi(1) = -\gamma; \quad \psi(k) = -\gamma + \sum_{n=1}^{k-1} n^{-1}, \quad k \geqslant 2, \qquad (3.103)$$

and γ is the Euler constant.

3.3(c) RESULTS

For the purposes of this discussion, a modal coefficient is said to have converged if its modulus remains constant to at least three significant figures as N is increased. The convergence is said to be fast if the modal coefficient converges when N is small, and is said to be slow if the coefficient converges when N is large.

Define w = 2b for the truncated wedge, and w = 2asinχ (the chord length of C_3) for the rounded wedge.

Some results obtained by numerically evaluating the a_n coefficients in (3.21), (3.50), (3.65) or (3.78) are presented in Figs. 3.5 - 3.11. The legend for Figs. 3.6 - 3.11 follows Fig. 3.7. These representative curves have been included in this chapter to indicate how certain factors affect the convergence of the field modal coefficients.

A summary of these factors and their effects, which have been deduced from many curves such as those in Figs. 3.5-3.11, is given at the end of this section.

Figs. 3.5 and 3.6 show the convergence of three a_n when the rounded wedge is illuminated by an electrically polarized wave. (Equations (3.65) and (3.73)). Fig. 3.5 shows the effect of M on the convergence of the a_n field coefficients. With M=1 convergence appears to be occurring, but only slowly. Convergence is faster with M=5 than with M=7. This indicates that there is an optimum value of M for which convergence of the a_n is fastest. The use of a greater or lesser number of surface current density modes then the optimum hinders the convergence of the field mode coefficients. Fig. 3.6 illustrates the faster convergence which is achieved by explicitly matching the two representations of the surface current density across $x = \pm X$ (Q=1), and by matching the two representations of the surface current density and their first derivative across $x = \pm X$ (Q=2). Six modes (M=5) of the current density representation in (3.61) are used.

Fig. 3.7 is plotted for the rounded wedge in the presence of a magnetically polarized field. (Equations (3.78) and (3.84)). This figure illustrates the faster convergence of the field coefficients which is obtained by including the expression in (3.84) with the matrix equation

derived from (3.78), and thereby ensuring the continuity of the surface current density across $x = \pm X$.

Figs. 3.8 and 3.9 both show the convergence of some a_n when a symmetrically truncated wedge is illuminated by an electrically polarized field. (Equations (3.21), (3.28), (3.36)). Fig. 3.8 is plotted for M=5 with Q=0,2,4. It is evident that the convergence of the a_n is faster when Q=2 than when Q=0. However, the convergence becomes slower with a further increase in Q to Q=4. Fig. 3.9 is plotted for M=7 with Q=0,2,4. In this case, each higher value of Q brings faster convergence of the a_n. Figs. 3.8 and 3.9 indicate that for fastest convergence of the a_n, there is an optimum value of Q which is dependent upon M.

Fig. 3.10 shows the faster convergence of the a_n when the representations of the surface current density and their derivatives are matched at suitable points.

The curves in Fig. 3.11 are plotted for the symmetrically truncated wedge illuminated by a magnetically polarized field. (Equations (3.50), (3.53), (3.60)). This figure indicates that convergence of the a_n may not occur below a large value of N unless current density matching equations are included with the matrix equation derived from (3.50).

From the study of Figs. 3.5 - 3.11 and other similar results obtained for $0.1\lambda \leq w \leq 2\lambda$, the following trends have been noticed:

(a) Convergent solutions can be obtained by limiting the

the summations of (3.21), (3.50), (3.65), and (3.78) to a finite number of terms.

(b) The value of N at which the a_n converges becomes larger with an increase in w.

(c) There is an optimum value M_o of M for fastest convergence of the a_n for a given problem. This optimum value becomes larger as w increases.

(d) The inclusion of surface current density matching equations in the matrix formulation of the scattering problem often results in much faster convergence of the a_n.

(e) If $M < M_o$ convergence of the a_n may be very slow. Inclusion of any surface current density matching equations in the matrix formulation can result in instability of the a_n with N.

(f) If $M > M_o$ it is often necessary to use the surface current matching equations to obtain convergence of the a_n at some reasonable value of N.

(g) If the number of current density matching equations Q is increased to near M, instability of the a_n with N occurs.

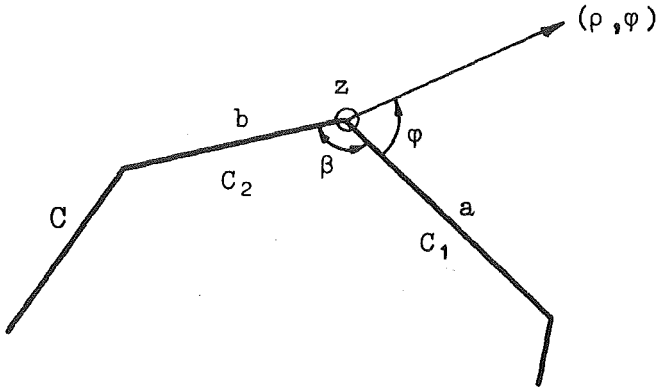

Figure 3.1

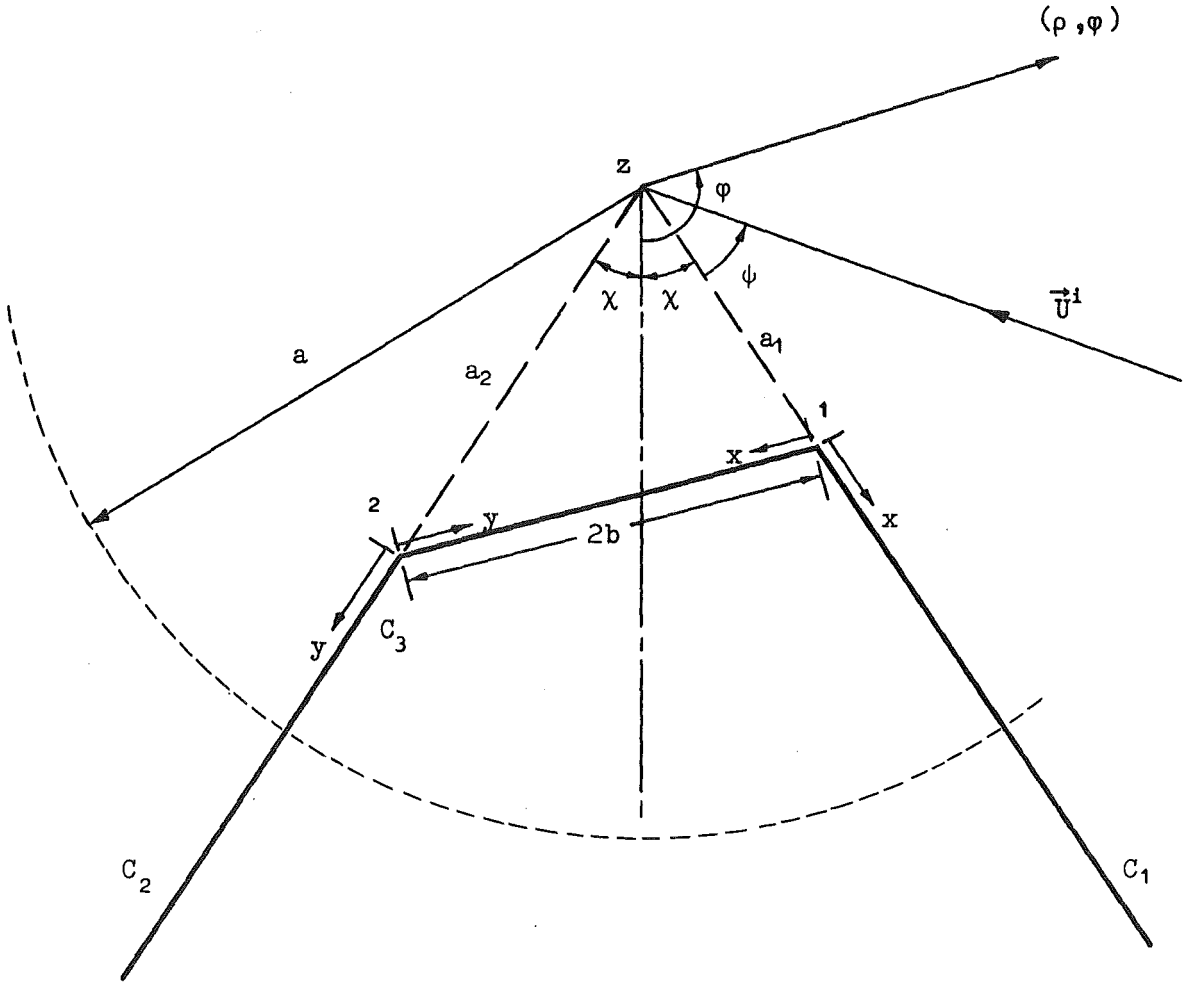

Figure 3.2 z axis perpendicular to the paper.

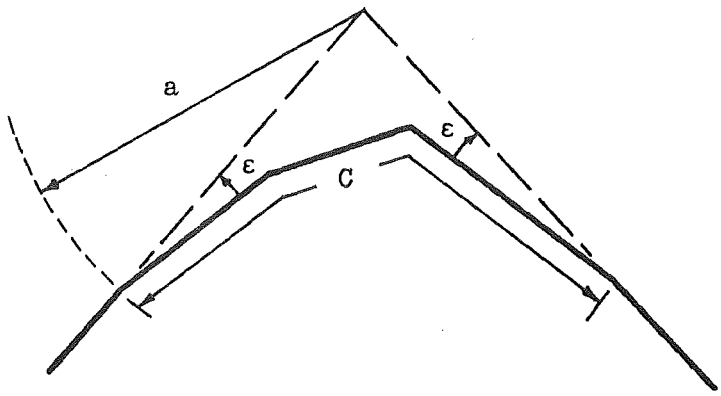

Figure 3.3

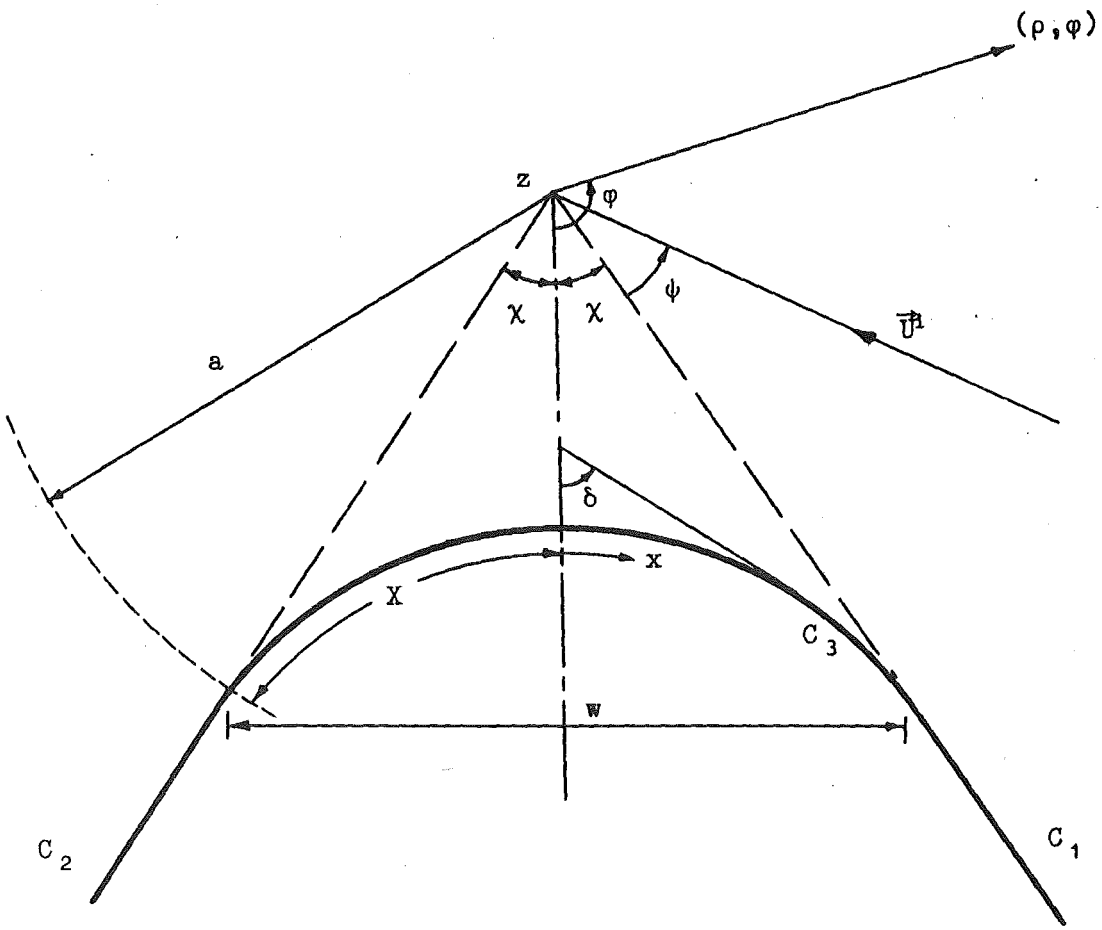

Figure 3.4 z axis perpendicular to the paper.

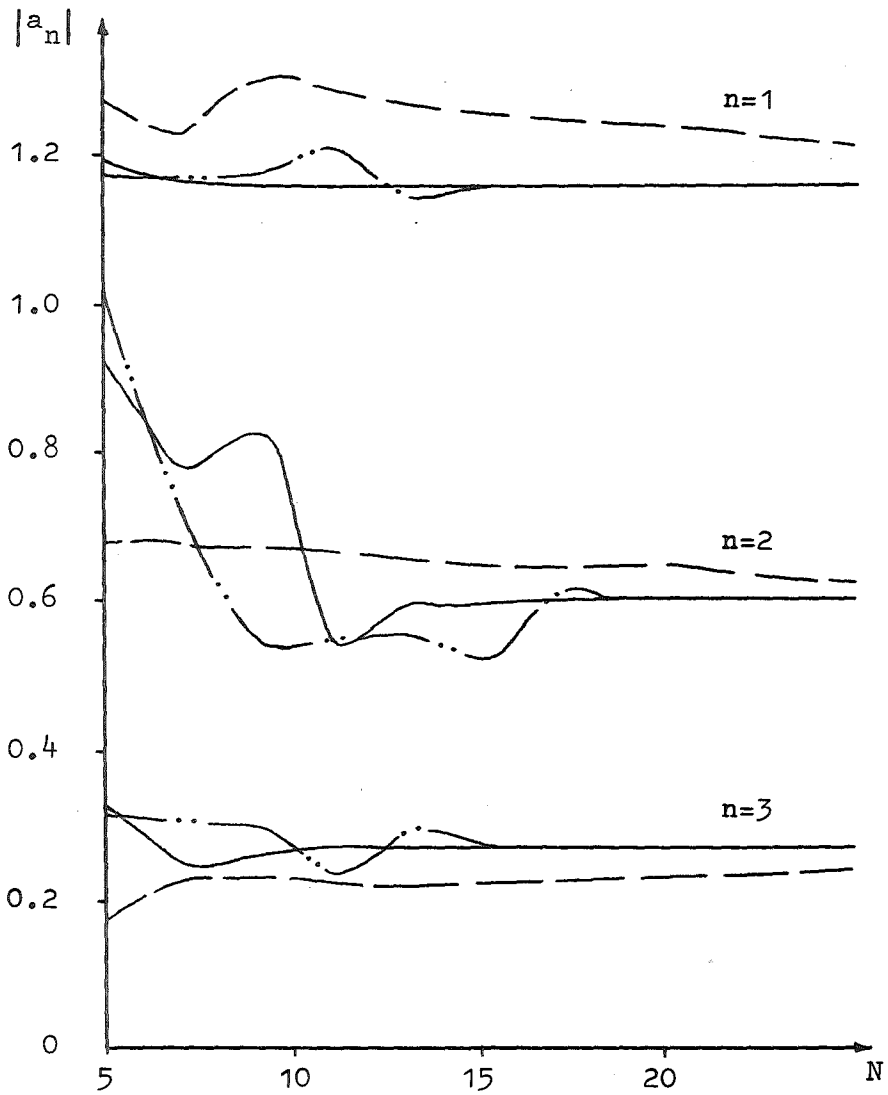

Figure 3.5 —— —— M=1, ———— M=5, —·—·—M=7.
Rounded Wedge. Electric Polarization. ($2\chi=94^0$, $\psi=60^0$, $w=1.0\lambda$)

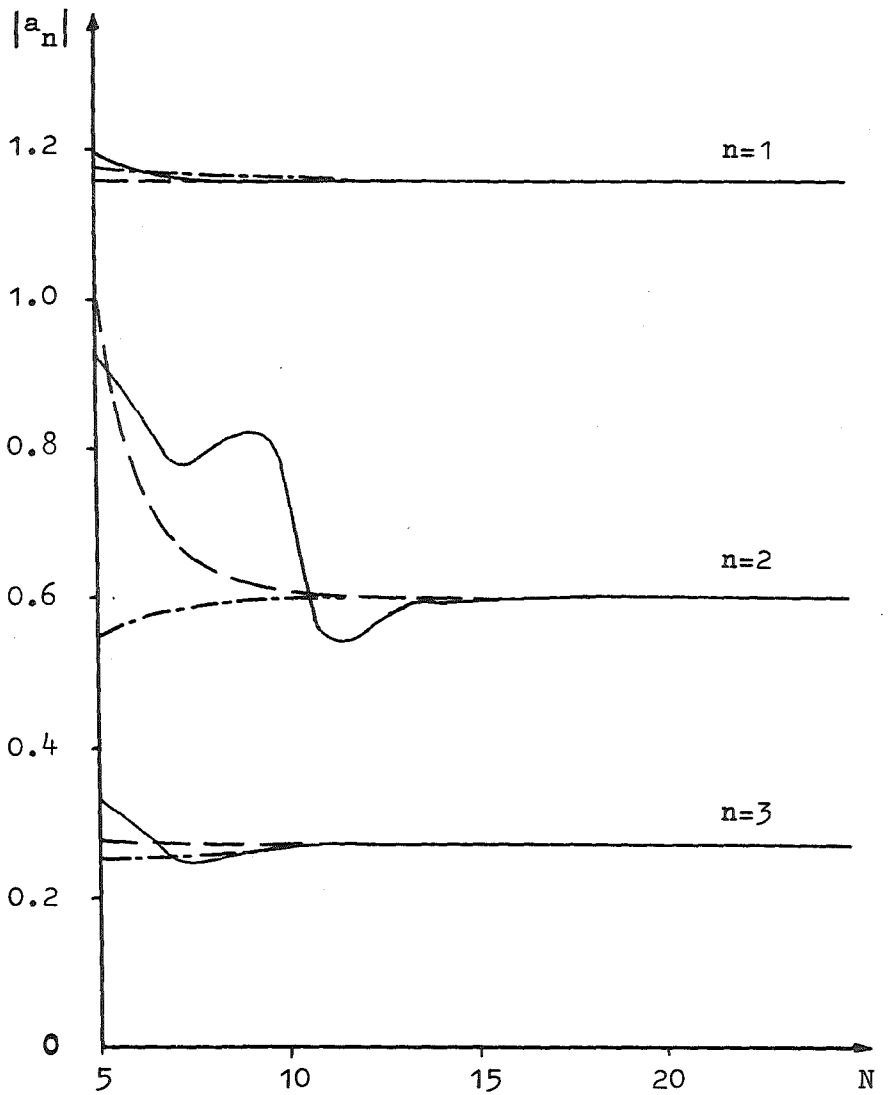

Figure 3.6 M=5. Legend on p110.

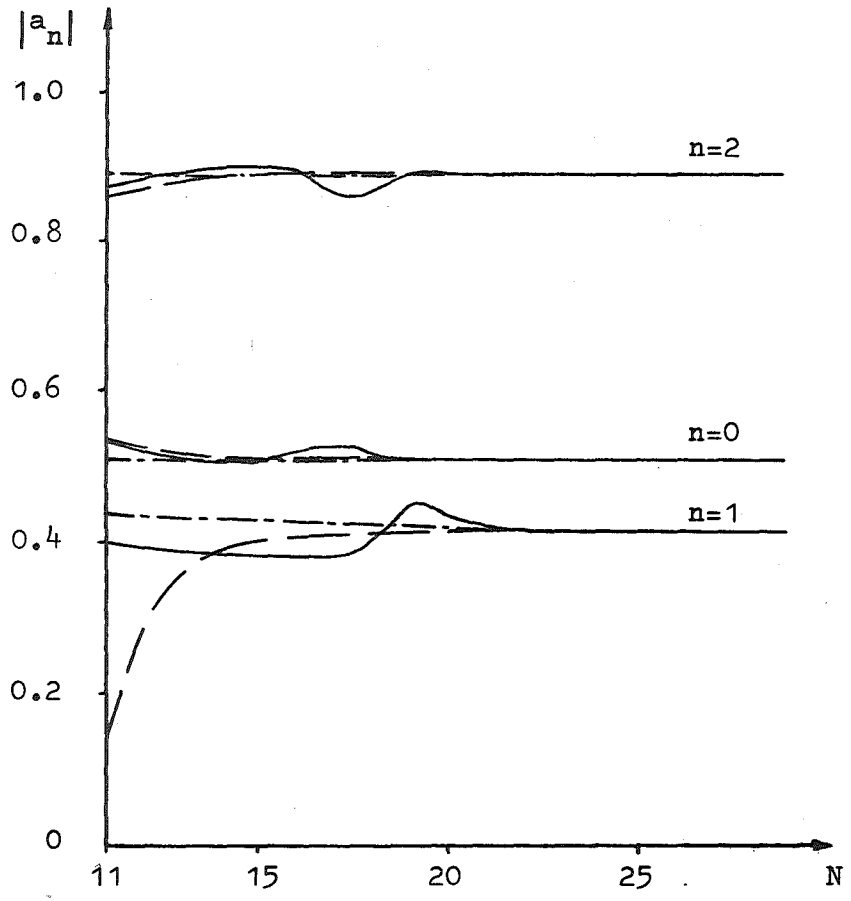

Figure 3.7 M=7. ($2\chi=94^0$, $\psi=60^0$, $w=1.0\lambda$)
Rounded Wedge. Magnetic Polarization.

LEGEND FOR FIGURES 3.6-3.11

Q=0 ——————————

Q=1 — — — — —

Q=2 —·—·—·—·

Q=3 —·—·—·—·

Q=4 —··—··—··—··

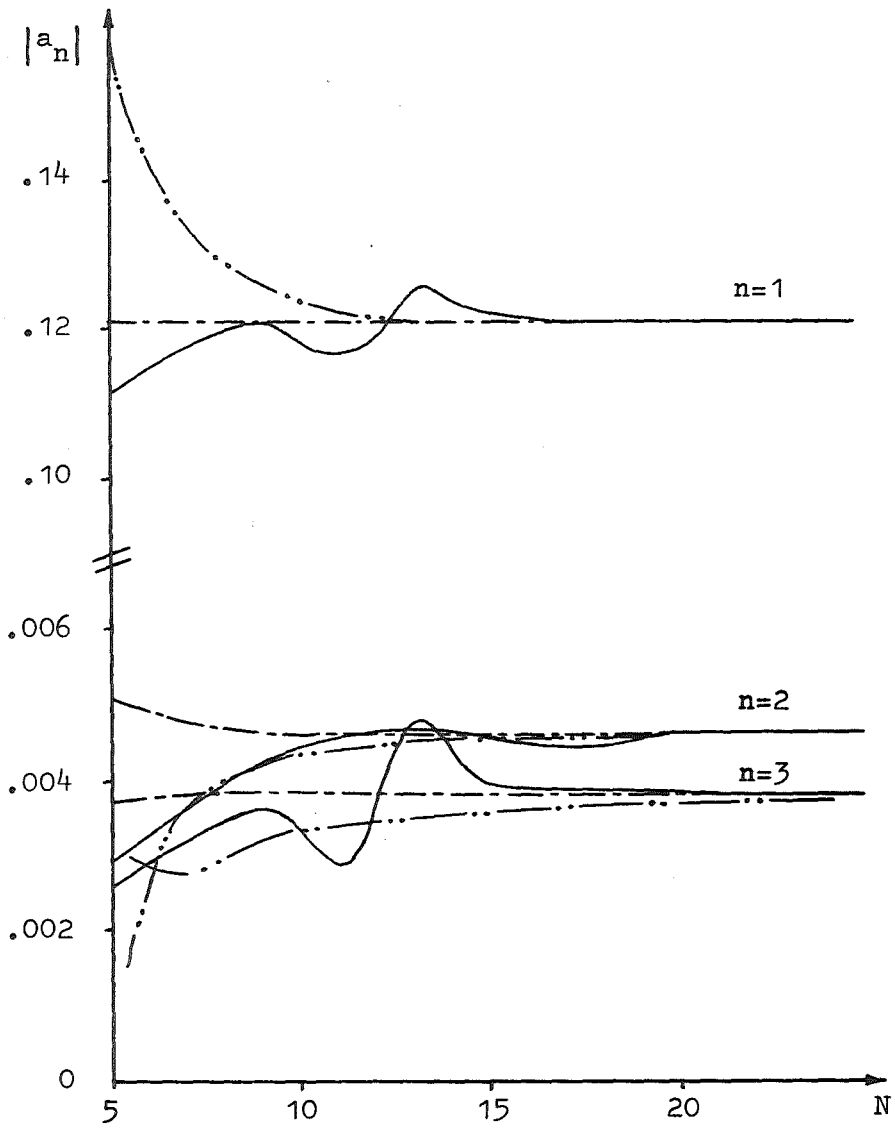

Figure 3.8 M=5. Legend on p110.

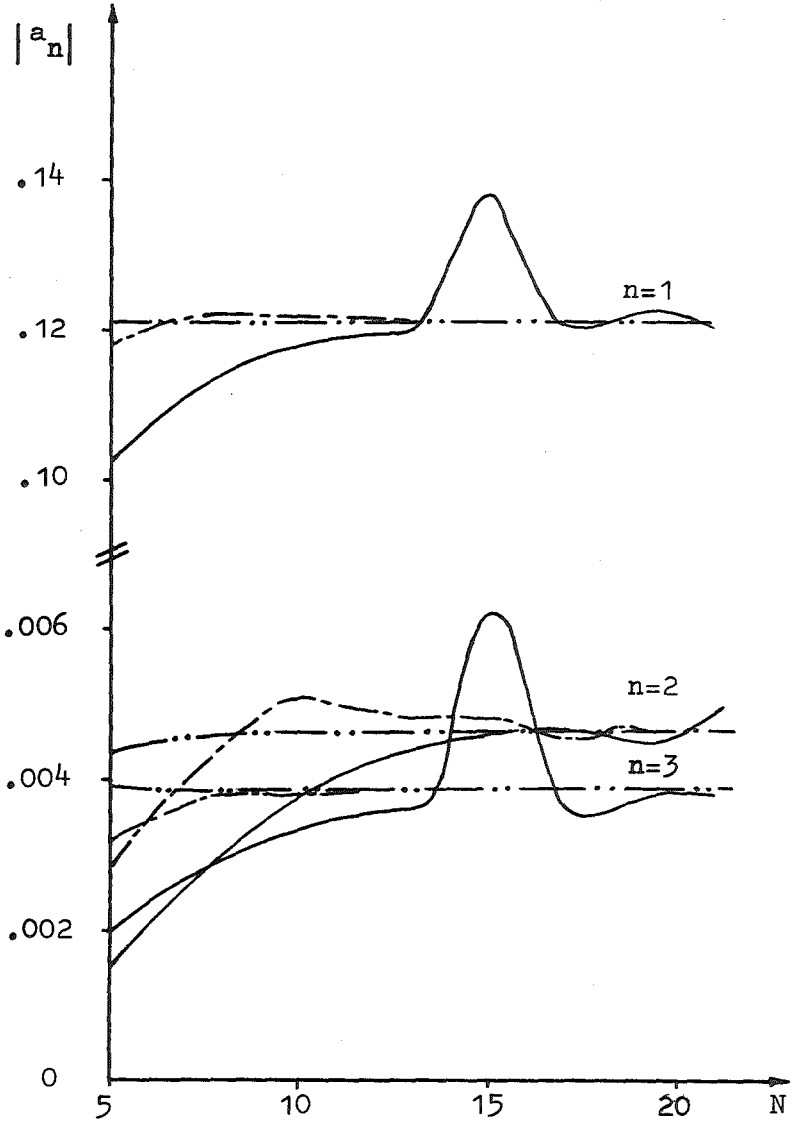

Figure 3.9 M=7. Legend on p110.

Symmetrically Truncated Wedge. Electric Polarization. ($2\chi=94^0$, $\psi=60^0$, $w=0.1\lambda$)

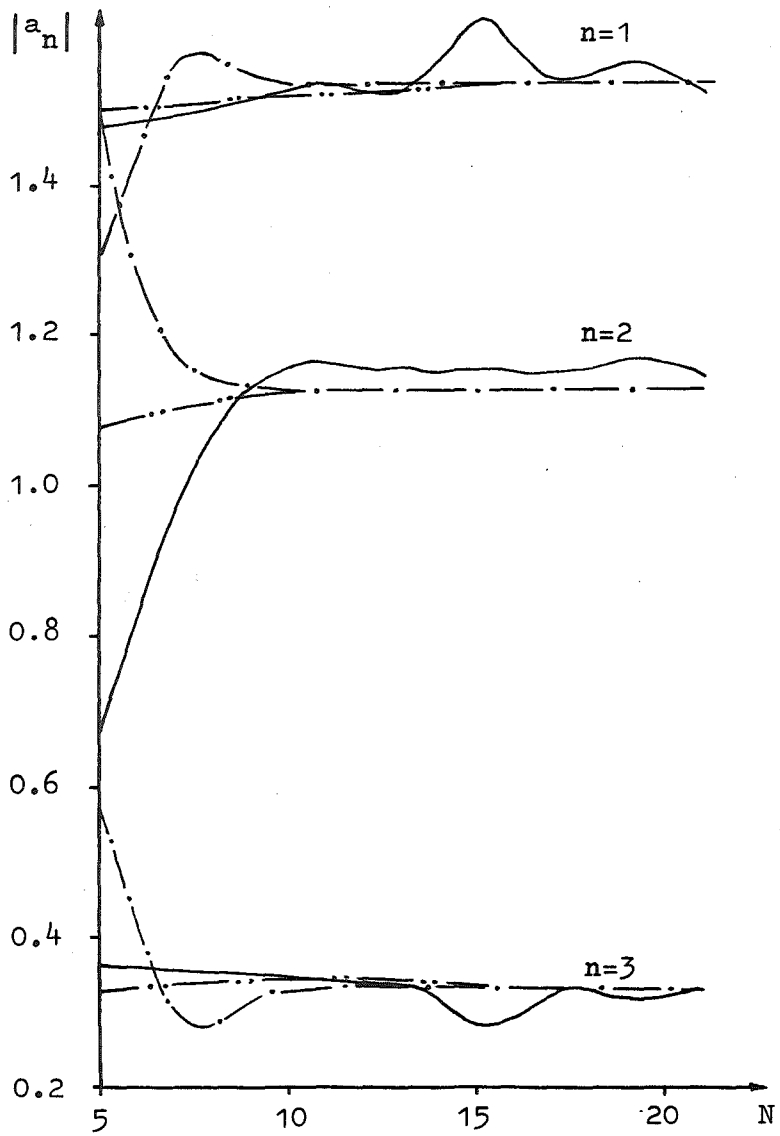

Figure 3.10 M=7 ($2\chi=94^0$, $\psi=60^0$, $w=1.0\lambda$)
Electric Polarization.
Symmetrically Truncated Wedge.

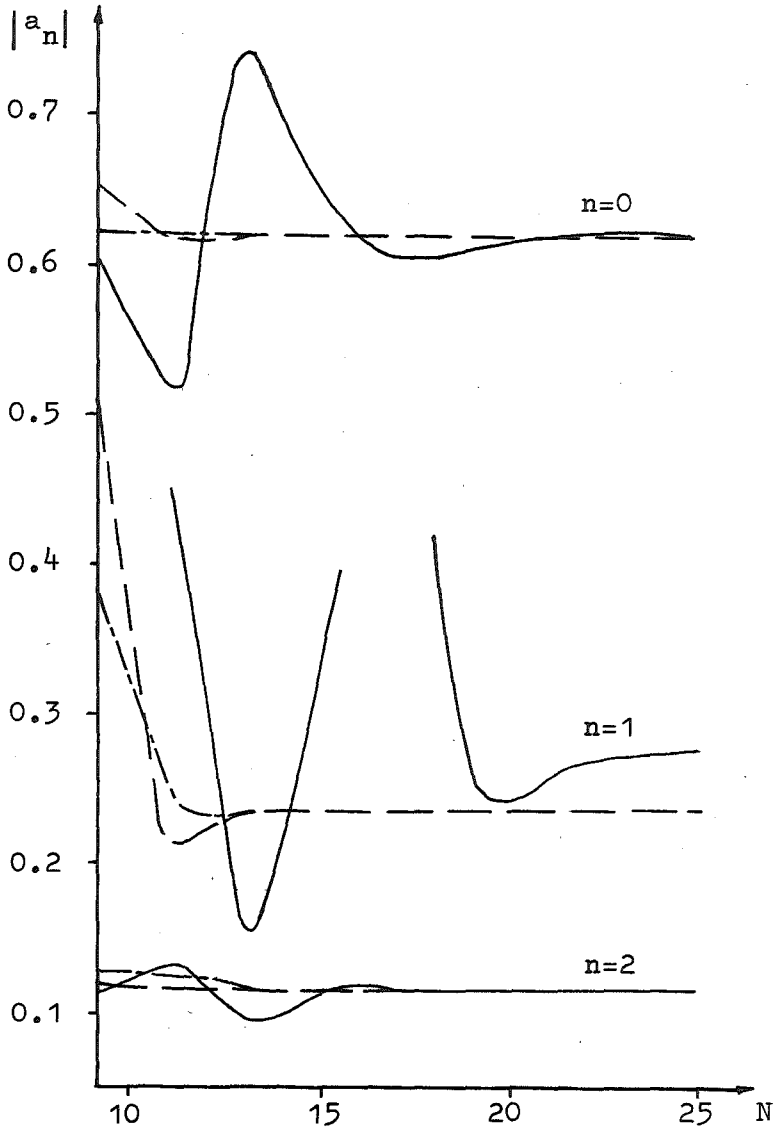

Figure 3.11 M=5 ($2\chi=114^0$, $\psi=60^0$, $w=1.0\lambda$)
Magnetic Polarization.
Legend on p110.

CHAPTER 4

The geometrical theory of diffraction and the physical optics approximation are used to predict the field scattered from truncated and rounded wedges when the incident field is electrically or magnetically polarized. These predictions are compared with the results of Chapter 3, which were obtained by using the surface current density replacement technique.

4.1(a) INTRODUCTION

The fields to be compared in this chapter are those which can be normalized with respect to ρ by removal of the factor

$$\sqrt{\frac{2j}{\pi k\rho}}\ e^{-jk\rho}\ , \qquad (4.1)$$

where ρ is the distance from the apex of the undeformed wedge to some point in the far field. The comparison is between the diffracted fields predicted by the geometrical theory of diffraction, the surface current density replacement technique, and physical optics. The reflected field from the rounded surface of the rounded wedge can be normalized by (4.1), and hence this field is included in the prediction of the geometrical theory of diffraction.

Throughout this chapter, the incident magnetic vector potential $\vec{A}^i$ or the incident magnetic field strength $\vec{H}^i$ is defined by

$$\vec{U}^i = \hat{z}U^i, \quad U^i = e^{jk\rho \cos(\phi-\psi)}, \tag{4.2}$$

in the cylindrical polar co-ordinate system shown in Fig. 4.1. The field expressions compared in this chapter are represented by $\vec{U}_{gtd}$, $\vec{U}_{scr}$, $\vec{U}_{po}$, with the subscripts indicating the method used to derive the expression. Since we are concerned with only the leading diffraction term of the geometrical theory of diffraction, secondary diffraction coefficients, such as those derived by Burke and Keller[91], are not considered here.

The field $\vec{U}_{scr}$ surrounding the deformed wedge is given by (2.20) as

$$\vec{U} = \hat{z}U, \quad U_{scr} = U + U_1, \tag{4.3}$$

where U is the diffracted field surrounding the undeformed wedge, and U_1 is the extra diffracted field caused by the deformation. U is defined in (1.42), and after normalization by the factor in (4.1) becomes

$$U = \sqrt{\frac{\pi k}{2j}} \quad d_m(\phi,\psi), \qquad m\pi = 2\pi-2\chi, \tag{4.4}$$

with $d_m(\phi,\psi)$ defined in (1.43).

When the field is electrically polarized, A_1 is defined by (2.35) suitably modified for the incident field

gnetically polarized field, H_1 is defined

g the asymptotic form of the Hankel

(1.21) for large ρ, the normalized

nd H_{scr} may be written as

$$\sqrt{\frac{\pi k}{2j}}\ d_m(\phi,\psi) + \sum_{n=1}^{\infty} a_n\, e^{j\frac{n\nu\pi}{2}} \sin[n\nu\phi], \qquad (4.5)$$

$$H_{scr} = \sqrt{\frac{\pi k}{2j}}\ d_m(\phi,\psi) + \sum_{n=0}^{\infty} a_n\, e^{j\frac{n\nu\pi}{2}} \cos[n\nu\phi], \qquad (4.6)$$

where

$$\nu = 1/m, \qquad (4.7)$$

and the negative (positive) sign is used in the definition in (1.43) of $d_m(\phi,\psi)$ when the field is electrically (magnetically) polarized.

4.2(a) G.T.D. DIFFRACTED FIELD. TRUNCATED WEDGE. (Electric Polarization).

Consider the perfectly conducting truncated wedge in Fig. 4.1. Edge 1 is at $(a_1,0,z)$ in the (ρ,ϕ,z) co-ordinate system and has internal angle β. Edge 2 is at $(a_2,m\pi,z)$ and has internal angle α. m is defined in (4.4), and

$$\tau\pi = 2\pi-\beta, \qquad \gamma\pi = 2\pi-\alpha. \qquad (4.8)$$

The length of the "truncation surface" between edge 1 and edge 2 is w. The cylindrical polar co-ordinate systems (r,ξ,z) and (s,δ,z) have their origins at edge 1 and edge 2 respectively.

The field A_1^i incident upon edge 1, and the field A_2^i incident upon edge 2 are, from (4.2),

$$A_1^i = e^{jka_1\cos\psi}, \quad 0 < \psi < \tau\pi,$$
$$= 0, \quad \tau\pi < \psi,$$

$$A_2^i = e^{jka_2\cos(m\pi-\psi)}, \quad \pi-\beta < \psi < m\pi,$$
$$= 0, \quad \psi < \pi-\beta. \tag{4.9}$$

The primary diffracted field $\vec{A}$ of the geometrical theory of diffraction is given by (1.42) and (1.43) as

$$\vec{A} = \hat{z}A, \quad A = A_1^i \varepsilon_1 d_\tau(\xi,\psi) \frac{e^{-jkr}}{\sqrt{r}} + A_2^i \varepsilon_2 d_\gamma(\delta,\psi+\beta-\pi) \frac{e^{-jks}}{\sqrt{s}},$$

where (4.10)

$$\varepsilon_1 = 1, \quad 0 < \xi < \tau\pi, \qquad \varepsilon_2 = 1, \quad 0 < \delta < \gamma\pi,$$
$$= 0, \quad \tau\pi < \xi < 2\pi, \qquad = 0, \quad \gamma\pi < \delta < 2\pi. \tag{4.11}$$

The existence conditions imposed in (4.11) are necessary to ensure that the diffracted rays from an edge do not directly illuminate a shadowed region.

A secondary diffracted field is generated by a primary diffracted ray travelling along the truncation surface of the wedge and striking an edge. However, since

$$d_\tau(\tau\pi,\psi) = d_\gamma(0,\psi+\beta-\pi) = 0, \tag{4.12}$$

no rays exist on the surface of the wedge when the field is electrically polarized. Therefore, the expression in (4.10) represents the total diffracted field of the geometrical theory of diffraction.

When ρ is large,

$$r \approx \rho - a_1\cos\phi, \quad s \approx \rho - a_2\cos(m\pi-\phi), \quad \xi \approx \phi, \quad \delta \approx \phi+\beta-\pi. \tag{4.13}$$

The field A_{gtd} is found by using (4.13) with (4.10) and normalizing by the factor in (4.1). Thus,

$$A_{gtd} = \sqrt{\frac{\pi k}{2j}} \left[A_1^i \varepsilon_1 d_\tau(\phi,\psi) e^{jka_1\cos\phi} + A_2^i \varepsilon_2 \cdot d_\gamma(\phi+\beta-\pi, \psi+\beta-\pi) e^{jka_2\cos(m\pi-\phi)} \right]. \tag{4.14}$$

It can be seen from (1.43) that in the directions of specular reflection $\phi = \pi-\psi$ or $\phi = (2\tau-1)\pi-\psi$, $d_\tau(\phi,\psi)$ becomes infinite. However, in the direction of reflection $\phi = (2\tau-1)\pi-\psi$ from the truncation surface of a symmetrically truncated wedge, careful manipulation of the expression in (4.14) results in a finite value for A_{gtd} given by

$$A_{gtd} = \frac{-j}{2} e^{jka_1\sin(\beta+\psi)} \sin\beta \left[\frac{2\sin(\frac{\pi}{\tau})}{\tau\left[\cos(\frac{\pi}{\tau}) - \cos(\frac{\pi+2\psi}{\tau})\right]} + \frac{\cot(\frac{\pi}{\tau})}{\tau} + jkw\sin(\beta+\psi) \right], \quad \phi = (2\tau-1)\pi-\psi, \quad a_1 = a_2. \tag{4.15}$$

4.2(b) G.T.D. DIFFRACTED FIELD. TRUNCATED WEDGE. (Magnetic Polarization).

Consider the truncated wedge in Fig. 4.1. Edges 1 and 2 are illuminated by the fields given in (4.9), with the symbol A replaced by H. The geometry of the figure is described in section 4.2(a).

The field diffracted from the truncated wedge is composed of an infinite number of multiply diffracted fields. Unlike the electrically polarized case, rays exist on the wedge surface when the field is magnetically polarized, and travel from edge to edge. Each time a ray strikes an edge a diffracted field is produced. Define H_1^n (H_2^n) to be the field diffracted when edge 1 (edge 2) is struck by a ray which has previously undergone modification at (n-1) edges. Before generating a diffracted field H_1^n or H_2^n, the ray has made (n-1) passes along the "truncation surface" of length w. The total diffracted field $\vec{H}$ is described by

$$\vec{H} = \hat{z}H, \qquad H = \sum_{n=1}^{\infty} (H_1^n + H_2^n). \tag{4.16}$$

The primary diffracted fields are given by (1.42) and (1.43) as

$$H_1^1 = H_1^i \, \varepsilon_1 \, d_\tau(\xi,\psi) \frac{e^{-jkr}}{\sqrt{r}}, \qquad H_2^1 = H_2^i \, \varepsilon_2 \, d_\gamma(\delta,\psi+\beta-\pi) \frac{e^{-jks}}{\sqrt{s}}, \tag{4.17}$$

where ε_1 and ε_2 are defined in (4.11). The secondary diffracted field is produced when a ray diffracted from edge 1 and of strength[51]

$$H_1^i \, d_\tau(\tau\pi,\psi) \, \frac{e^{-jkw}}{2\sqrt{w}} \, , \tag{4.18}$$

strikes edge 2, and a ray diffracted from edge 2 and of strength

$$H_2^i \, d_\gamma(0,\psi+\beta-\pi) \, \frac{e^{-jkw}}{2\sqrt{w}} \, , \tag{4.19}$$

strikes edge 1. Thus,

$$H_2^2 = \varepsilon_2 \, H_1^i \, d_\tau(\tau\pi,\psi) \, \frac{e^{-jkw}}{2\sqrt{w}} \quad d_\gamma(\delta,0) \, \frac{e^{-jks}}{\sqrt{s}} \, , \tag{4.20}$$

$$H_1^2 = \varepsilon_1 \, H_2^i \, d_\gamma(0,\psi+\beta-\pi) \, \frac{e^{-jkw}}{2\sqrt{w}} \, d_\tau(\xi,\tau\pi) \, \frac{e^{-jkr}}{\sqrt{r}} \, , \tag{4.21}$$

and similarly,

$$H_1^3 = \varepsilon_1 \, H_1^i \, d_\tau(\tau\pi,\psi) \left[\frac{e^{-jkw}}{2\sqrt{w}}\right]^2 d_\gamma(0,0) \, d_\tau(\xi,\tau\pi) \, \frac{e^{-jkr}}{\sqrt{r}} \, , \tag{4.22}$$

$$H_2^3 = \varepsilon_2 \, H_2^i \, d_\gamma(0,\psi+\beta-\pi) \left[\frac{e^{-jkw}}{2\sqrt{w}}\right]^2 d_\tau(\tau\pi,\tau\pi) \, d_\gamma(\delta,0) \, \frac{e^{-jks}}{\sqrt{s}} \, . \tag{4.23}$$

After writing a sufficient number of the higher order diffraction expressions in the above manner, it becomes clear that the expression in (4.16) can be expanded as

$$H = \frac{e^{-jkr}}{\sqrt{r}}\left[\varepsilon_1 H_1^i \left[d_\tau(\xi,\psi) + \sigma\left[\frac{e^{-jkw}}{2\sqrt{w}}\right]^2 d_\tau(\tau\pi,\psi)\, d_\gamma(0,0)\, d_\tau(\xi,\tau\pi)\right]\right.$$

$$\left. + \varepsilon_2 H_2^i \sigma \frac{e^{-jkw}}{2\sqrt{w}} d_\gamma(0,\psi+\beta-\pi)\, d_\tau(\xi,\tau\pi)\right] + \frac{e^{-jks}}{\sqrt{s}}\left[\varepsilon_2 H_2^i\left[d_\gamma(\delta,\psi+\beta-\pi)\right.\right.$$

$$\left.+\sigma\left[\frac{e^{-jkw}}{2\sqrt{w}}\right]^2 d_\gamma(0,\psi+\beta-\pi)\, d_\tau(\tau\pi,\tau\pi)\, d_\gamma(\delta,0)\right]$$

$$\left. + \varepsilon_1 H_1^i \sigma \frac{e^{-jkw}}{2\sqrt{w}}\, d_\tau(\tau\pi,\psi)\, d_\gamma(\delta,0)\right], \qquad (4.24)$$

where

$$\sigma = \sum_{n=0}^{\infty} C^n, \quad C = \left[\frac{e^{-jkw}}{2\sqrt{w}}\right]^2 d_\gamma(0,0)\, d_\tau(\tau\pi,\tau\pi). \qquad (4.25)$$

By using the expressions in (4.13) and normalizing with the factor in (4.1), H reduces to H_{gtd}, where

$$H_{gtd} = \sqrt{\frac{\pi k}{2j}}\left[e^{jka_1\cos\phi}\left[\varepsilon_1 H_1^i\, d_\tau(\phi,\psi)\right.\right.$$

$$\left.+\sigma\, d_\tau(\phi,\tau\pi)\, \frac{e^{-jkw}}{2\sqrt{w}}\left[\varepsilon_2 H_2^i\, d_\gamma(0,\psi+\beta-\pi)\right.\right.$$

$$+ \varepsilon_1 H_1^i \, d_\tau(\tau\pi,\psi) \, d_\gamma(0,0) \, \frac{e^{-jkw}}{2\sqrt{w}} \Bigg] \Bigg]$$

$$+ e^{jka_2\cos(m\pi-\phi)} \Bigg[\varepsilon_2 H_2^i \, d_\gamma(\delta,\psi+\beta-\pi)$$

$$+\sigma \, d_\gamma(\delta,0) \, \frac{e^{-jkw}}{2\sqrt{w}} \Bigg[\varepsilon_1 H_1^i \, d_\tau(2\pi-\beta,\psi) + \varepsilon_2 H_2^i \, d_\gamma(0,\psi+\beta-\pi)$$

$$\cdot d_\tau(2\pi-\beta,2\pi-\beta) \, \frac{e^{-jkw}}{2\sqrt{w}} \Bigg] \Bigg] \Bigg] . \qquad (4.26)$$

For H_{gtd} to describe a diffracted field of finite magnitude, σ must converge to a constant value in the summation of the geometric progression in (4.25) as $n \to \infty$. This requires $|C| < 1$, and then

$$\sigma = \frac{1}{1-C}, \qquad |C| < 1. \qquad (4.27)$$

The restriction $|C| < 1$ imposes a minimum value on the separation w of edge 1 from edge 2. It follows from (4.25) and (1.43) that this restriction is

$$w > \left| \frac{\cot(\frac{\pi}{2\tau}) \, \cot(\frac{\pi}{2\gamma})}{4\pi^2 \tau\gamma} \right|, \qquad (4.28)$$

where w is measured in wavelengths.

Curves showing the minimum value of w for various α and β are given in Fig. 4.2. This minimum value is very much less than the edge separations for which the plane wave

diffraction coefficients would normally be used to approximate the diffracted field.

The expressions in (4.25) and (4.26) are similar to those derived by Russo et al[90], who used the more accurate Pauli diffraction function in formulating the diffraction by a thick edge.

The primary diffracted field $(H_1^1 + H_2^1)$ is, in general, infinite in a direction of specular reflection. However, in the direction of reflection $\phi = (2\tau-1)\pi-\psi$ from the truncation surface of a symmetrically truncated wedge, a finite value for the primary diffracted field H^p_{gtd} is obtained as

$$H^p_{gtd} = \frac{-j}{2} e^{jka_1\sin(\beta+\psi)} \sin\beta \left[\frac{2\sin(\frac{\pi}{\tau})}{\tau[\cos(\frac{\pi}{\tau})-\cos(\frac{\pi+2\psi}{\tau})]} - \frac{\cot(\frac{\pi}{\tau})}{\tau} \right.$$

$$\left. - jkw \sin(\beta+\psi) \right] , \phi = (2\tau-1)\pi-\psi, \quad a_1 = a_2. \qquad (4.29)$$

4.2(c) G.T.D. DIFFRACTED FIELD. ROUNDED WEDGE.

Consider the perfectly conducting rounded wedge in Fig. 4.3. The (ρ,ϕ,z) cylindrical co-ordinate system has its origin at the apex of the undeformed wedge of angle 2χ. The incident field $\vec{U}^i$ given in (4.2) makes an angle ξ with the normal to the rounded surface at a point T. The radius of curvature of the rounded surface is R.

Levy and Keller[48] give the diffracted field $\vec{U}$ of the geometrical theory of diffraction as

$$\vec{U} = \hat{z}U, \quad U = U^i(Q)\,\frac{e^{-jks}}{\sqrt{s}} \sum_m D_m\, e^{(-jk-\alpha_m)t},$$

$$\pi + \psi < \phi < m\pi, \tag{4.30}$$

where m is defined in (4.4). $U^i(Q)$ is the field incident at a point Q given by $\xi = \pi/2$ on the rounded surface. The diffracted field is produced when an incident ray, grazing the surface at Q, travels a distance t along a geodesic arc of the surface and leaves the surface tangentially at P. The distance s is measured from P to the point (ρ, ϕ) at which U is observed, and if s is large,

$$t = R(\phi - \psi - \pi). \tag{4.31}$$

The α_m and D_m of (4.30) are defined in Table 4.1 for both electric and magnetic polarization of the field.

POLARIZATION	$\alpha_m = e^{j\frac{\pi}{6}} \left(\frac{k}{6R^2}\right)^{\frac{1}{3}} q_m$	$e^{j\frac{5\pi}{4}} \left(\frac{k}{2\pi}\right)^{\frac{1}{2}} D_m$
Electric	$Ai(q_m) = 0$	$\frac{\pi}{6}\, e^{-j\frac{5\pi}{6}} \left(\frac{kR}{6}\right)^{\frac{1}{3}} \frac{1}{[Ai'(q_m)]^2}$
Magnetic	$Ai'(q_m) = 0$	$\frac{\pi}{2}\, e^{-j\frac{5\pi}{6}} \left(\frac{kR}{6}\right)^{\frac{1}{3}} \frac{1}{Ai^2(q_m)}$

TABLE 4.1

The prime denotes differentiation of the Airy function Ai(x) with respect to the argument x, where

$$Ai(x) = \int_0^\infty \cos(\tau^3 - x\tau)\, d\tau. \qquad (4.32)$$

The field reflected from the rounded surface is described in Appendix 4 by

$$U = \pm U^i(T) \sqrt{\frac{R\cos\xi}{2r}}\; e^{-jkr}, \qquad \pi-\psi < \phi < \pi+\psi, \qquad (4.33)$$

where r is the distance from T to the point (ρ, ϕ) at which U is observed, and the negative (positive) sign in (4.33) is used when the field is electrically (magnetically) polarized.

From the geometry of Fig. 4.3, and from (4.2)

$$\xi = \frac{\phi-\psi}{2}, \qquad U^i(T) = e^{jkR\left[\cos(\psi+\chi)/\sin\chi + \cos\left(\frac{\phi-\psi}{2}\right)\right]}, \qquad (4.34)$$

and thus

$$U^i(Q) = e^{jkR\cos(\psi+\chi)/\sin\chi}. \qquad (4.35)$$

When ρ is large,

$$r \approx \rho - R\left[\cos(\phi+\chi)/\sin\chi + \cos\left(\frac{\phi-\psi}{2}\right)\right], \quad s \approx \rho + R\cos(\phi+\chi)/\sin\chi. \qquad (4.36)$$

The use of (4.34), (4.35) and (4.36) with (4.30) and (4.33), and normalization by the factor in (4.1) results in

$$U_{gtd} = \sqrt{\frac{\pi k}{2j}}\ e^{jkR\left[\cos(\psi+\chi)+\cos(\phi+\psi)\right]}/\sin\chi$$

$$\cdot\left[\pm\ \varepsilon_r\sqrt{\frac{R}{2}\cos\left(\frac{\phi-\psi}{2}\right)}\ e^{j2kR\cos\left(\frac{\phi-\psi}{2}\right)} + \varepsilon_d \sum_m D_m\, e^{(-jk-\alpha_m)t}\right], \quad (4.37)$$

where

$$\varepsilon_r = 1, \quad \pi-\psi < \phi < \pi+\psi, \qquad \varepsilon_d = 1, \quad \pi+\psi < \phi < m\pi,$$
$$= 0, \quad \phi < \pi-\psi, \ \phi > \pi+\psi, \qquad = 0, \quad 0 < \phi < \pi+\psi. \quad (4.38)$$

4.3(a) PHYSICAL OPTICS FIELD. (Electric Polarization)

Consider the perfectly conducting deformed wedge in Fig. 4.4. The origin of the (ρ,ϕ,z) co-ordinate system is at the apex of the undeformed wedge of angle 2χ, and m is defined in (4.4).

In this section, the field radiated by the physical optics surface current density on the surfaces $\rho \geq a_1$, $\phi = 0$ and $\rho \geq a_2$, $\phi = m\pi$ of the deformed wedge is calculated for electric polarization of the incident field. The field radiated by the physical optics surface current density existing on the deformed surface of the wedge is calculated in later sections.

The incident field is given by (4.2) with $\vec{U}$ replaced by the symbol $\vec{A}$ for the magnetic vector potential. The physical optics surface current density $\vec{K}_1(r)$ at $\rho = r$

on the surface $\phi = 0$ of the wedge is given by (1.44) and (2.22) as

$$\vec{K}_1(r) = 2\hat{n} \times \vec{H}^i = \frac{2\hat{\phi}}{\mu} \times (\nabla \times \vec{A}^i) = \frac{-\hat{z}2}{\mu r} \frac{\partial A^i}{\partial \phi} \Bigg|_{\phi = 0}, \qquad (4.39)$$

which, after writing

$$\vec{K}_1(r) = \hat{z}\, K_1(r),$$

and using (4.2), reduces to

$$K_1(r) = -\varepsilon_1 \frac{2jk}{\mu} \sin\psi\, e^{jkr\cos\psi}, \quad \varepsilon_1 = 1, \quad 0 < \psi < \pi,$$
$$= 0, \quad \pi < \psi < m\pi. \qquad (4.40)$$

Similarly, the physical optics current density $\vec{K}_2(r)$ at $\rho = r$ on the surface $\phi = m\pi$ is

$$\vec{K}_2(r) = \hat{z}\, K_2(r), \quad K_2(r) = -\varepsilon_2 \frac{2jk}{\mu} \sin(m\pi - \psi)\, e^{jkr\cos(m\pi - \psi)}, \qquad (4.41)$$

where

$$\varepsilon_2 = 1, \quad (m-1)\pi < \psi < m\pi,$$
$$= 0, \quad 0 < \psi < (m-1)\pi. \qquad (4.42)$$

The field $\vec{A}$ radiated from the current distributions $\vec{K}_1(r)$ and $\vec{K}_2(r)$ on the deformed wedge is determined from (1.36) and (1.37) with the vector operator $\{\Lambda\}$ replaced by the scalar μ. Then,

$$\vec{A} = \hat{z}A, \quad A = \frac{-j\mu}{4} \left[\int_{a_1}^{\infty} K_1(r)\, H_o^{(2)}(kR_1)\, dr + \int_{a_2}^{\infty} K_2(r)\, H_o^{(2)}(kR_2)\, dr \right]. \qquad (4.43)$$

where R_1 and R_2 are the distances from the elemental contours dr to (ρ,ϕ). When ρ is large,

$$R_1 \sim \rho - r\cos\phi, \quad R_2 \sim \rho - r\cos(m\pi-\phi), \quad \rho >> r. \tag{4.44}$$

By using the asymptotic form of the Hankel function in (1.21) with (4.44), and substituting the expressions in (4.40) and (4.41) into (4.43), the physical optics field A^1_{po} which can be normalized by the factor in (4.1) is given by

$$A^1_{po} = \frac{-k}{2}\sqrt{\frac{2j}{\pi k\rho}}\, e^{-jk\rho}\left[\varepsilon_1 \sin\psi \int_{a_1}^{\infty} e^{jkr(\cos\psi+\cos\phi)}\, dr \right.$$

$$\left. + \varepsilon_2 \sin(m\pi-\psi) \int_{a_2}^{\infty} e^{jkr[\cos(m\pi-\psi)+\cos(m\pi-\phi)]}\, dr\right]. \tag{4.45}$$

When k has a vanishingly small negative imaginary part, it is readily shown that

$$\int_a^{\infty} e^{-jkx}\, dx = \frac{-je^{-jka}}{k}. \tag{4.46}$$

Performing the integrations in (4.45) and normalizing by the factor in (4.1) gives

$$A^1_{po} = \frac{-j}{2}\left[\frac{\varepsilon_1 \sin\psi\, e^{jka_1[\cos\psi+\cos\phi]}}{\cos\phi+\cos\psi}\right.$$

$$\left. + \frac{\varepsilon_2 \sin(m\pi-\psi)\, e^{jka_2[\cos(m\pi-\psi)+\cos(m\pi-\phi)]}}{\cos(m\pi-\psi)+\cos(m\pi-\phi)}\right]. \tag{4.47}$$

4.3(b) P.O. FIELD. TRUNCATED WEDGE. (Electric Polarization).

Consider the perfectly conducting truncated wedge in Fig. 4.5. The "truncation surface" C_3 of length w is defined in terms of the cylindrical polar co-ordinate system (r,θ,z) whose origin is at the apex of the undeformed wedge. The line $\theta = 0$ is perpendicular to C_3 and x is the distance from $\theta = 0$ to a point on C_3.

The physical optics current density $\vec{K}_3(c)$ on C_3 is given by (1.44) and (2.22) as

$$\vec{K}_3(c) = \frac{2\hat{n}}{\mu} \times \left[\frac{1}{\rho} \frac{\partial A^i}{\partial \phi} \hat{\rho} - \frac{\partial A^i}{\partial \rho} \hat{\phi} \right]. \tag{4.48}$$

where the electrically polarized incident field A^i is given in (4.2). The unit normal vector $\hat{n}$ to C_3 is

$$\hat{n} = -\hat{\rho} \sin(\phi+\beta) - \hat{\phi} \cos(\phi+\beta). \tag{4.49}$$

Using (4.49) and (4.2) with (4.48) results in

$$\vec{K}_3(c) = \hat{z}\, K_3(c), \quad K_3(c) = \varepsilon_3 \frac{2jk}{\mu} \sin(\beta+\psi)\, e^{jkr\sin(\beta+\psi-\theta)}, \tag{4.50}$$

where

$$\varepsilon_3 = 1, \ \pi - \beta < \psi < 2\pi - \beta,$$
$$= 0, \ \psi < \pi-\beta, \ \psi > 2\pi-\beta. \tag{4.51}$$

The field $\vec{A}$ radiated by $\vec{K}_3(c)$ is given by (1.36) with the operator $\{\Lambda\}$ replaced by μ. When ρ is large, the distance R from the elemental contour dx of C_3 to (ρ,ϕ) is

$$R \sim \rho - r \sin(\beta+\phi-\theta), \qquad \rho >> r. \tag{4.52}$$

After using (4.52) with (1.21) to asymptotically expand the Hankel function in (1.36)

$$\vec{A} = \hat{z}A, \quad A_{po}^2 = \varepsilon_3 \frac{k}{2} \sin(\beta+\psi) \int_{a_2 \cos\alpha}^{-a_1 \cos\beta} e^{jkr[\sin(\beta+\psi-\theta)+\sin(\beta+\phi-\theta)]} dx, \tag{4.53}$$

where the normalization factor in (4.1) has been removed. By writing the integrand in terms of x using the relationship

$$r \sin\theta = x, \quad r \cos\theta = a_1 \sin\beta, \tag{4.54}$$

A_{po}^2 is evaluated as

$$A_{po}^2 = \varepsilon_3 \frac{j \sin(\beta+\psi)}{2 P(\beta)} e^{jka_1 Q(\beta) \sin\beta} \left[e^{jka_1 P(\beta)\cos\beta} - e^{-jka_2 P(\beta)\cos\alpha} \right], \tag{4.55}$$

$Q(\beta) = \sin(\beta+\psi)+\sin(\beta+\phi)$, $P(\beta) = \cos(\beta+\psi)+\cos(\beta+\phi)$.

When the wedge is symmetrically truncated ($a_1 = a_2$), the expression for A_{po}^2 simplifies to

$$A_{po}^2 = \varepsilon_3 \frac{\cos(\psi+\chi)}{Q(\chi)} \sin[\tfrac{kw}{2} Q(\chi)] e^{jkaP(\chi)\cos\chi}, \quad a_1 = a_2 = a. \tag{4.56}$$

The field A_{po} radiated by the physical optics current density on the truncated wedge is given by (4.47) and (4.55) as

$$A_{po} = A_{po}^1 + A_{po}^2. \tag{4.57}$$

For normal backscattering from the truncation surface ($\phi=\psi=\pi-\chi$), the expression for A_{po} in (4.57) reduces to

$$A_{po} = \frac{-j}{2} e^{-jka \sin\beta} [-\tan(\chi)-jkw]. \qquad (4.58)$$

Notice the similarity between this expression for the physical optics backscattered field and that of the geometrical theory of diffraction given in (4.15) with $\psi = (\tau-\frac{1}{2})\pi$.

4.3(c) P.O. FIELD. ROUNDED WEDGE. (Electric Polarization).

Consider the perfectly conducting rounded wedge in Fig. 4.6. The radius of curvature of the rounded surface C_3 is R, and the centre of curvature is at Q. P is the point at which C_3 joins the wedge surface $\phi = 0$. C_3 is defined in terms of the cylindrical polar co-ordinates (r,θ) whose origin is at $\rho = 0$, which is the apex of the undeformed wedge. The angle τ is measured in an anticlockwise direction from QP, and the distance x along C_3 is given by $x = R\tau$.

The electrically polarized incident field $\vec{A}^i$ is given in (4.2). Without loss of generality, ψ is restricted such that

$$0 \leqslant \psi \leqslant \pi. \qquad (4.59)$$

From the geometry of Fig. 4.6, the arc length δ of C_3 which is illuminated by the incident field is

$$\delta = R\psi_1, \quad \psi_1 = \psi, \quad \psi \leqslant \pi - 2\chi,$$
$$= \pi - 2\chi, \quad \psi > \pi - 2\chi. \qquad (4.60)$$

The physical optics current density $\vec{K}_3(c)$ on C_3 is found from (4.48) with the unit vector $\hat{n}$ normal to C_3 defined by

$$\hat{n} = \hat{\rho}\sin(\phi-\tau) + \hat{\phi}\cos(\phi-\tau). \tag{4.61}$$

Using (4.2) and (4.61) with (4.48), $\vec{K}_3(c)$ reduces to

$$\vec{K}_3(c) = \hat{z}\, K_3(c), \quad K_3(c) = \frac{2jk}{\mu}\sin(\tau-\psi)\, e^{jkr\cos(\theta-\chi-\psi)}, \quad 0 < \tau < \psi_1, \tag{4.62}$$

$$= 0, \quad \tau > \psi_1.$$

The field $\vec{A}$ radiated by the current distribution $\vec{K}_3(c)$ is given by (1.36), in which the Hankel function can be expanded when ρ is large by using (1.21) and

$$R_1 \sim \rho - r\cos(\theta-\phi-\chi). \tag{4.63}$$

R_1 is the distance from the elemental contour dx to the point (ρ,ϕ) at which the field is observed. Then,

$$\vec{A} = \hat{z}A, \quad A_{po}^2 = \frac{kR}{2}\int_0^{\psi_1} \sin(\tau-\psi)\, e^{jkr[\cos(\theta-\psi-\chi)+\cos(\theta-\phi-\chi)]}\, d\tau, \tag{4.64}$$

where the normalization factor (4.1) has been removed. Since

$$r\cos\theta = R[\sin(\tau+\chi)-\operatorname{cosec}(\chi)], \quad r\sin\theta = R\cos(\tau+\chi), \tag{4.65}$$

the expression for A_{po}^2 reduces to

$$A_{po}^2 = \frac{kR}{2} e^{jkR\ P(\chi)}/\sin\chi \int_0^{\psi_1} \sin(\tau-\psi)\ e^{-jkR\ Q(\pi-\tau)}\ d\tau, \quad (4.66)$$

where $P(\beta)$ and $Q(\beta)$ are defined in (4.55). The field A_{po} radiated by the physical optics current density on the rounded wedge is obtained by substituting the expressions in (4.47) and (4.66) into (4.57).

4.4(a) PHYSICAL OPTICS FIELD. (Magnetic Polarization).

Consider the perfectly conducting deformed wedge in Fig. 4.4. The geometry of the figure is discussed in section 4.3(a).

In this section, the field radiated by the physical optics current density on the surfaces $\rho \geq a_1$, $\phi = 0$ and $\rho \geq a_2$, $\phi = m\pi$ of the deformed wedge is calculated for magnetic polarization of the incident field. The field radiated by the physical optics current density existing on the deformed surface of the wedge is calculated in subsequent sections.

The incident field is given by (4.2) with $\vec{U}$ replaced by $\vec{H}$. The physical optics surface current density $\vec{K}_1(r)$ at $\rho = r$ on the surface $\phi = 0$ is given by (1.44) and (4.2) as

$$\vec{K}_1(r) = 2\hat{n} \times \vec{H}^i\Big|_{\phi = 0} = \hat{r}_1\ \varepsilon_1\ 2e^{jkr\ \cos\psi}, \quad (4.67)$$

where

$$\hat{r}_1 = \hat{\rho}\cos\phi \quad -\hat{\phi}\sin\phi, \tag{4.68}$$

and ε_1 is defined in (4.40). Similarly, the physical optics current density $\vec{K}_2(r)$ at $\rho = r$ on the surface $\phi = m\pi$ is

$$\vec{K}_2(r) = -\hat{r}_2\ \varepsilon_2\ 2e^{jkr\cos(m\pi-\psi)}, \quad \hat{r}_2 = \hat{\rho}\cos(m\pi-\phi) + \hat{\phi}\sin(m\pi-\phi), \tag{4.69}$$

where ε_2 is defined in (4.42).

The field $\vec{H}$ radiated from the current distributions $\vec{K}_1(r)$ and $\vec{K}_2(r)$ on the deformed wedge is given by (1.36) and (1.37) as

$$\vec{H} = \frac{-j}{4}\nabla \times \left[\int_{a_1}^{\infty} \vec{K}_1(r)\ H_o^{(2)}(kR_1)\ dr + \int_{a_2}^{\infty} \vec{K}_2(r)\ H_o^{(2)}(kR_2)\ dr\right], \tag{4.70}$$

where R_1 and R_2 are defined in (4.44) for $\rho >> r$. When the asymptotic form of the Hankel function (1.21) is used with (4.44), the physical optics field H_{po}^1 which can be normalized by the factor in (4.1) is given by

$$H_{po}^1 = \frac{-j}{2}\nabla \times \sqrt{\frac{2j}{\pi k\rho}}\ e^{-jk\rho}\left[\hat{r}_1 \int_{a_1}^{\infty} \varepsilon_1\ e^{jkr[\cos\psi + \cos\phi]}dr\right.$$

$$\left. - \hat{r}_2 \int_{a_2}^{\infty} \varepsilon_2\ e^{jkr[\cos(m\pi-\psi)+\cos(m\pi-\phi)]}\ dr\right], \tag{4.71}$$

where the expressions in (4.67) and (4.69) have been substituted for $\vec{K}_1(r)$ and $\vec{K}_2(r)$ respectively. The vector curl operation in (4.71) is of the form

$$\nabla \times (\hat{\rho}\, F_\rho + \hat{\phi}\, F_\phi) = \frac{\hat{z}}{\rho}\left[\frac{\partial(\rho F_\phi)}{\partial \rho} - \frac{\partial F_\rho}{\partial \phi}\right], \quad \frac{\partial F_\rho}{\partial z} = \frac{\partial F_\phi}{\partial z} = 0. \qquad (4.72)$$

Using (4.46) and (4.72), the expression in (4.71) reduces to[76]

$$\vec{H}^1_{po} = \hat{z}\, H^1_{po}, \quad H^1_{po} = \frac{j}{2}\left[\frac{\varepsilon_1 \sin\phi\; e^{jka_1[\cos\psi+\cos\phi]}}{\cos\psi+\cos\phi}\right.$$

$$\left. + \frac{\varepsilon_2 \sin(m\pi-\phi)\; e^{jka_2[\cos(m\pi-\psi)+\cos(m\pi-\phi)]}}{\cos(m\pi-\psi)+\cos(m\pi-\phi)}\right], \qquad (4.73)$$

when ρ is large. The expression in (4.73) is normalized by the factor in (4.1).

4.4(b) P.O. FIELD. TRUNCATED WEDGE. (Magnetic Polarization).

Consider the perfectly conducting truncated wedge in Fig. 4.5. The geometry of the figure is described in section 4.3(b). The incident field $\vec{H}^i$ is given in (4.2).

The physical optics surface current density $\vec{K}_3(c)$ on C_3 is given by (1.44) and (4.2) as

$$\vec{K}_3(c) = 2\hat{n} \times \vec{H}^i = [\hat{\phi}\sin(\phi+\beta) - \hat{\rho}\cos(\phi+\beta)]\varepsilon_3\, 2e^{jkr\sin(\beta+\psi-\theta)}, \qquad (4.74)$$

since $\hat{n}$ is defined in (4.49). ε_3 is defined in (4.51).

The field $\vec{H}$ radiated by the current distribution $\vec{K}_3(c)$ is given by (1.36) and (1.37) as

$$\vec{H} = \frac{-j}{4} \nabla \times \int_{a_2 \cos\alpha}^{-a_1 \cos\beta} \vec{K}_3(c)\, H_o^{(2)}(kR)\, dx, \qquad (4.75)$$

where R is the distance from the elemental contour dx to (ρ,ϕ). When ρ is large, R is approximated by the expression in (4.52), and the Hankel function in (4.75) can be expanded using (1.21). Thus, substituting the expression for $\vec{K}_3(c)$ into (4.75) when $\rho >> r$,

$$\vec{H} = \frac{-j\varepsilon_3}{2} \nabla \times [\hat{\phi} \sin(\phi+\beta) - \hat{\rho} \cos(\phi+\beta)] \sqrt{\frac{2j}{\pi k\rho}}\, e^{-jk\rho}$$

$$\cdot \int_{a_2 \cos\alpha}^{-a_1 \cos\beta} e^{jkr[\sin(\beta+\psi-\theta)+\sin(\beta+\phi-\theta)]} dx. \qquad (4.76)$$

The vector curl operation in (4.76) is of the form given in (4.72). By neglecting terms of order lower than $\rho^{-\frac{1}{2}}$, and using the relations given in (4.54), it follows from (4.76) that

$$\vec{H}^2_{po} = \hat{z}\, H^2_{po}, \quad H^2_{po} = \frac{-j\varepsilon_3 \sin(\beta+\phi)}{2\ P(\beta)}\, e^{jka_1 Q(\beta)\ \sin\beta}$$

$$\cdot\left[e^{jka_1 P(\beta)\ \cos\beta} \quad -e^{-jka_2 P(\beta)\ \cos\alpha}\right], \tag{4.77}$$

where $P(\beta)$ and $Q(\beta)$ are defined in (4.55). When the wedge is symmetrically truncated ($a_1 = a_2$), the expression for H^2_{po} simplifies to

$$H^2_{po} = -\varepsilon_3 \frac{\cos(\phi+\chi)}{Q(\chi)} \sin\left[\frac{kw}{2} Q(\chi)\right] e^{jka\ P(\chi)\cos\chi}, \tag{4.78}$$

$$a_1 = a_2 = a.$$

The field H_{po} radiated by the physical optics surface current density on the truncated wedge is given by (4.73) and (4.78) as

$$H_{po} = H^1_{po} + H^2_{po}. \tag{4.79}$$

Notice that $|H_{po}|$ in (4.79) equals $|A_{po}|$ in (4.57) when $\phi = \psi$, illustrating that physical optics predicts a polarization insensitive backscattered field.

For normal backscattering from the truncation surface ($\phi=\psi=\pi-\chi$), the expression for H_{po} in (4.79) reduces to

$$H_{po} = \frac{-j}{2} e^{-jka\ \sin\beta}\ [\tan(\chi)+jkw]. \tag{4.80}$$

Notice the similarity between this expression for the physical optics backscattered field, and that of the geometrical theory of diffraction given in (4.29) with $\psi=(\tau-\frac{1}{2})\pi$.

4.4(c) PHYSICAL OPTICS. ROUNDED WEDGE. (Magnetic Polarization).

Consider the perfectly conducting rounded wedge in Fig. 4.6. The geometry of the figure is described in section 4.3(c). The magnetically polarized incident field $\vec{H}^i$ is given in (4.2) subject to the restriction in (4.59). The physical optics current density $\vec{K}_3(c)$ on C_3 is defined in (1.44), $\hat{n}$ is defined in (4.61), and ψ_1 is defined in (4.60). Thus

$$\vec{K}_3(c) = [\hat{\rho}\cos(\phi-\tau)-\hat{\phi}\sin(\phi-\tau)]\ 2e^{jkr\cos(\theta-\psi-\chi)}, \quad 0<\tau<\psi_1,$$
$$= 0, \quad \tau>\psi_1. \tag{4.81}$$

The field $\vec{H}$ radiated by the current distribution $\vec{K}_3(c)$ is given in (1.36). Using (4.63) with (1.21) to expand the Hankel function when $\rho >> r$ enables $\vec{H}$ to be described by

$$\vec{H} = \frac{-jR}{2}\ \nabla \times \sqrt{\frac{2j}{\pi k\rho}}\ e^{-jk\rho}$$
$$\cdot\int_0^{\psi_1} [\hat{\rho}\cos(\phi-\tau)-\hat{\phi}\sin(\phi-\tau)\ e^{jkr[\cos(\theta-\psi-\chi)+\cos(\theta-\phi-\chi)]}\ d\tau. \tag{4.82}$$

The vector curl operation in (4.82) is of the form given in (4.72). By neglecting terms of order lower than $\rho^{-\frac{1}{2}}$, $\vec{H}^2_{po}$ is given from (4.82) as

$$\vec{H}^2_{po} = \hat{z}\, H^2_{po},$$

$$H^2_{po} = \frac{-kR}{2} \int_0^{\psi_1} \sin(\tau-\phi)\; e^{jkr[\cos(\theta-\psi-\chi)+\cos(\theta-\phi-\chi)]}\, d\tau. \tag{4.83}$$

The relations given in (4.65) enable H^2_{po} to be simplified to

$$H^2_{po} = \frac{-kR}{2}\; e^{jkR\, P(\chi)/\sin\chi} \int_0^{\psi_1} \sin(\tau-\phi)\; e^{-jkR\, Q(\pi-\tau)}\, d\tau, \tag{4.84}$$

where $P(\beta)$ and $Q(\beta)$ are defined in (4.55).

The field H_{po} radiated by the physical optics current density on the rounded wedge is obtained by substituting the expressions in (4.73) and (4.84) into (4.79). Notice that, as in the case of the truncated wedge, physical optics predicts a polarization insensitive backscattered field.

4.5(a) NUMERICAL CONSIDERATIONS

Table 4.2 indicates which expressions in this chapter have been numerically evaluated for purposes of comparison.

WEDGE DEFORMATION	POLARIZATION	DERIVATION		
		S.C.R.	G.T.D	P.O.
Truncated	Electric	(4.5) [(1.42)+(2.35)]	(4.14)	(4.57) [(4.47)+(4.55)]
	Magnetic	(4.6) [(1.42)+(2.73)]	(4.26)	(4.79) [(4.73)+(4.78)]
Rounded	Electric	(4.5) [(1.42)+(2.35)]	(4.37)	(4.57) [(4.47)+(4.66)]
	Magnetic	(4.6) [(1.42)+(2.73)]	(4.37)	(4.79) [(4.73)+(4.84)]

TABLE 4.2

The a_n modal coefficients in (2.35) must be obtained before the electrically polarized diffracted field surrounding the deformed wedge (and given in (4.5)) can be calculated. Similarly, before evaluating the magnetically polarized

diffracted field given in (4.6), the a_n coefficients of (2.73) must be obtained. Because of the restriction on the size of matrix which can be inverted by a computer, only a finite number of the a_n can be obtained. Thus the summations in (4.5) and (4.6) are limited to a finite number of terms. This number N was chosen such that

$$|a_p| < 10^{-3} |a_1|, \qquad p \geq N. \tag{4.85}$$

When w is small (w ~ 0.1λ), it was found that $3 \leq N \leq 5$, but when w is larger (w ~ 1.0λ) it was found that $9 \leq N \leq 20$. (In the case of the rounded wedge w is defined to be the chord length of the rounded surface C_3 in Fig. 4.6). The condition in (4.85) was met with all the coefficients a_n, $n \leq N$ convergent to the third decimal place.

As well as evaluating the expression in (4.26) for the G.T.D. field diffracted from the truncated wedge, the primary diffracted field H^p_{gtd} was calculated. This field is given by (4.17) as

$$H^p_{gtd} = \sqrt{\frac{\pi k}{2j}} \left[e^{jka_1\cos\phi} \varepsilon_1 H_1^i \, d_\tau(\phi,\psi) \right.$$

$$\left. + e^{jka_2\cos(m\pi-\phi)} \varepsilon_2 H_2^i \, d_\gamma(\delta,\psi+\beta-\pi) \right]. \tag{4.86}$$

A comparison of H^p_{gtd} and H_{gtd} enables the effect of including the higher order diffracted fields in the geometrical theory of diffraction to be studied.

The evaluation of the expression in (4.37) requires the zeros of the Airy function and its derivative to be calculated. It can be seen from (4.37) that the number of these zeros which must be calculated before the summation has converged with a given accuracy is dependent upon t, the length of arc of the rounded surface along which the grazing ray travels. The evaluation of (4.37) takes more time when t is small ($\phi \approx \pi+\psi$), than when t is large.

The integrations of (4.66) and (4.84) were performed numerically using Simpson's rule integration[87] with at least ten subdivisions per wavelength.

4.5(b) RESULTS.

The curves plotted in Figures 4.7 - 4.18 all pertain to the rounded wedge. Figs. 4.7 - 4.11 show the diffracted field surrounding the rounded wedge when the incident field is electrically or magnetically polarized. The physical optics estimate, the geometrical theory of diffraction prediction, and the field diffracted from an undeformed wedge are all plotted, as well as the accurate diffracted field. The two directions in which the field becomes large correspond respectively to the direction of reflection from the illuminated wedge surface, and the forward scattering direction which is a shadow boundary.

Figs. 4.7 - 4.9 are plotted for three rounded wedges with $2\chi = 94^{o}$ illuminated by similar fields electrically polarized in the z-direction. The rounded wedges are characterized by $w = 0.1\lambda$, $w = 0.5\lambda$, and $w = 1.0\lambda$ respectively. When $w = 0.1\lambda$ the rounded wedge diffracts a field little different from that diffracted by an undeformed wedge. As w increases (Figs. 4.8 and 4.9), so does the difference between the diffracted field and that diffracted by an undeformed wedge. However, in no case is the field in the region $\phi > \pi+\psi$ significantly different to that diffracted by the undeformed wedge. The physical optics estimate of the field increases in accuracy as w increases, particularly in the region $\phi < \pi-\psi$ where the geometrical theory of diffraction predicts no scattered field. Over the region $\pi-\psi < \phi < \pi+\psi$, the geometrical theory of diffraction field, given by the reflection of the incident field from the rounded surface, is less accurate than physical optics.

Similar comments apply to the curves in Figs. 4.10 and 4.11 which are plotted for two rounded wedges with $2\chi = 94^{o}$, illuminated by magnetically polarized fields.

Figs. 4.12 - 4.17 show the field backscattered from rounded wedges which are illuminated by a field normally incident upon the rounded surface in the direction $\psi=(\pi-\chi)$.

The backscattered field is plotted against w for the three cases $2\chi = 54^{o}$, $2\chi = 94^{o}$, and $2\chi = 134^{o}$ when the incident field is electrically polarized in the z-direction. The accurate values were obtained by using the S.C.R. technique described in Chapters 2 and 3, and the accurate value at $w = 0$ is the field backscattered from the undeformed wedge. Also plotted in these figures is the physical optics estimate of the backscattered field, and the geometrical theory of diffraction approximation. This latter estimate is wholly due to the reflection of the incident field from the rounded surface and is directly proportional to $\sqrt{w}$ as can be deduced from (4.33). The physical optics estimate increases in accuracy as w increases. However, for $w < 0.15\lambda$ it can be seen that in general the most accurate estimate of the backscattered field is that from the undeformed wedge.

When w is small, physical optics underestimates the strength of the normally backscattered electrically polarized field, but overestimates the strength of the normally backscattered magnetically polarized field.

Fig. 4.18 shows the manner in which the surface current density on the surface $\rho > a$, $\phi = 0$ of the rounded wedge differs from that on the undeformed wedge for $w = 1.0\lambda$, $2\chi = 94^{o}$, $\psi = 60^{o}$, when the incident field is electrically polarized. Notice the faster rate of decay of the oscillations in the surface current density of the rounded wedge.

This suggests that the rounded surface of the wedge causes less disturbance to the physical optics current density on the surface $\phi = 0$ than does the apex of the undeformed wedge.

From Figs. 4.7 - 4.18 and other curves unpublished here, the following trends relating to the field diffracted by a perfectly conducting rounded wedge have been noticed:
(i) The field diffracted by an undeformed wedge is, in general, a more accurate estimate of the field diffracted by a rounded wedge with $w < .15\lambda$ than either the estimate of physical optics or the geometrical theory of diffraction.
(ii) The increase in accuracy of the physical optics approximation with w is particularly noticeable in the region $\phi < \pi-\psi$, and the backscattering region.
(iii) Unlike physical optics, the geometrical theory of diffraction does not predict the form of the ϕ-variation of the field in the region $\pi-\psi < \phi < \pi+\psi$, and gives no estimate of the field in the region $\phi < \pi-\psi$.

The curves plotted in Figs. 4.19 - 4.30 pertain to symmetrically truncated wedges. In Figs. 4.19 and 4.20 are curves of the difference between the field diffracted from an undeformed wedge and the field diffracted from a truncated wedge. A similar electrically polarized incident field illuminates the wedges. Notice the increased accuracy of the geometrical theory of diffraction when w is larger.

The curves in Fig. 4.21 show the field diffracted from a symmetrically truncated wedge as calculated by the S.C.R. method, and estimated by physical optics and the geometrical theory of diffraction. Also plotted is the field diffracted from the undeformed wedge of angle $2\chi = 94^{o}$. The incident field is electrically polarized. The curves in Fig. 4.21 can be compared with those in Fig. 4.7 for the rounded wedge similarly illuminated. It can be seen that when $w = 0.1\lambda$, there is little difference between the fields diffracted by a rounded or a symmetrically truncated wedge. This conclusion is similar to that reached by Jones[88] who considered the effect of the shape of the end of a thick semi-infinite plate.

Fig. 4.22 shows the field diffracted from a symmetrically truncated wedge ($2\chi = 114^{o}$, $w = 1.0\lambda$) when the incident field is magnetically polarized in the z-direction. In addition to the field of the geometrical theory of diffraction and the field surrounding the undeformed wedge, the primary diffracted field of the geometrical theory of diffraction is plotted. Notice that for much of the scattering region, this primary diffracted field is a better estimate of the diffracted field than is the complete G.T.D. approximation which includes the multiply diffracted fields.

Figs. 4.23 and 4.24 show the fields diffracted by symmetrically truncated wedges illuminated normal to the truncation surface by similar electrically polarized fields

($\psi = \pi-\chi$). The two truncated wedges are characterized by $2\chi = 94^{o}$ with $w = 0.1\lambda$ and $w = 1.0\lambda$ respectively. The formulae in (4.15) and (4.58) were used to evaluate the G.T.D. and P.O. backscattered fields respectively. Because of the symmetry about $\phi = (\pi-\chi)$, the fields are plotted only in the region $0 < \phi \leqslant (\pi-\chi)$. For both wedges, the diffracted field in the region $\phi < (\pi-\psi)$ is little different from that diffracted by the undeformed wedge. However, in the backscattering direction there is an appreciable difference which is larger for the larger value of w. The physical optics estimate is more accurate for $w = 1.0\lambda$ than for $w = 0.1\lambda$, particularly in the backscattering region, but the geometrical theory of diffraction closely approximates the diffracted field for all values of ϕ for both truncated wedges.

Figs. 4.25 - 4.30 show the field backscattered from symmetrically truncated wedges illuminated by a field normally incident upon the truncation surface ($\phi = \psi = \pi - \chi$). The backscattered field is plotted against w for the three cases $2\chi = 54^{o}$, $2\chi = 94^{o}$, and $2\chi = 134^{o}$ when the incident field is electrically polarized in the z-direction; and for $2\chi = 74^{o}$, $2\chi = 114^{o}$, and $2\chi = 154^{o}$ when the field is magnetically polarized in the z-direction.

As well as the accurate value of the backscattered field, the physical optics and geometrical theory of diffraction estimates are also plotted in Figs. 4.25 - 4.27.

The expressions for the G.T.D. and P.O. backscattered fields are given in (4.15) and (4.58) respectively. Each of the three figures shows that the G.T.D. approximation is more accurate than the physical optics estimate which underestimates the electrically polarized backscattered field.

Figs. 4.25- 4.27 may be compared with Figs. 4.12 - 4.14 for the rounded wedge. The strength of the backscattered field increases more rapidly with w for the truncated wedge than for the rounded wedge.

The primary, the sum of the primary and secondary, and the complete G.T.D. backscattered fields have been calculated for the three truncated wedges of Figs. 4.28 - 4.30 when the incident field is magnetically polarized in the z-direction. Each of these diffracted fields was more accurate than the physical optics approximation, but the most consistently accurate was the sum of the primary and secondary G.T.D. diffracted fields. This result confirms the suggestion in section 4.2(b) that the inclusion of all the multiply diffracted fields is not always the best estimate of the G.T.D. Consequently, the sum of the primary and secondary diffracted fields of the G.T.D. is plotted in Figs. 4.28 - 4.30, and also the physical optics approximation and the accurate value obtained from using the S.C.R. technique. The expressions for the primary G.T.D. and P.O. backscattered fields are given in (4.29) and (4.80) respectively. Each of

the figures shows that P.O. overestimates these magnetically polarized backscattered fields when w is small.

From the curves in Figs. 4.19 - 4.30 and others, the following trends relating to the field diffracted by a perfectly conducting truncated wedge have been noticed:

(i) Both the physical optics and the geometrical theory of diffraction approximations to the scattered field increase in accuracy as w increases.

(ii) For the truncated wedges studied ($0.05\lambda \leqslant w \leqslant 1.0\lambda$), physical optics is not as accurate as the geometrical theory of diffraction. In general, the sum of the primary and secondary diffracted fields is a better estimate of the magnetically polarized diffracted field than the complete G.T.D. prediction.

(iii) The normally backscattered field ($\phi = \psi = \pi - \chi$) from a truncated wedge is stronger than that from a rounded wedge having the same values of 2χ and w.

(iv) The P.O. and G.T.D. estimates of the normally backscattered field given in (4.15), (4.29), (4.58), and (4.80), tend asymptotically towards the exact value of the backscattered field when w is large. For a given w, the G.T.D. approximation increases in accuracy as 2χ increases.

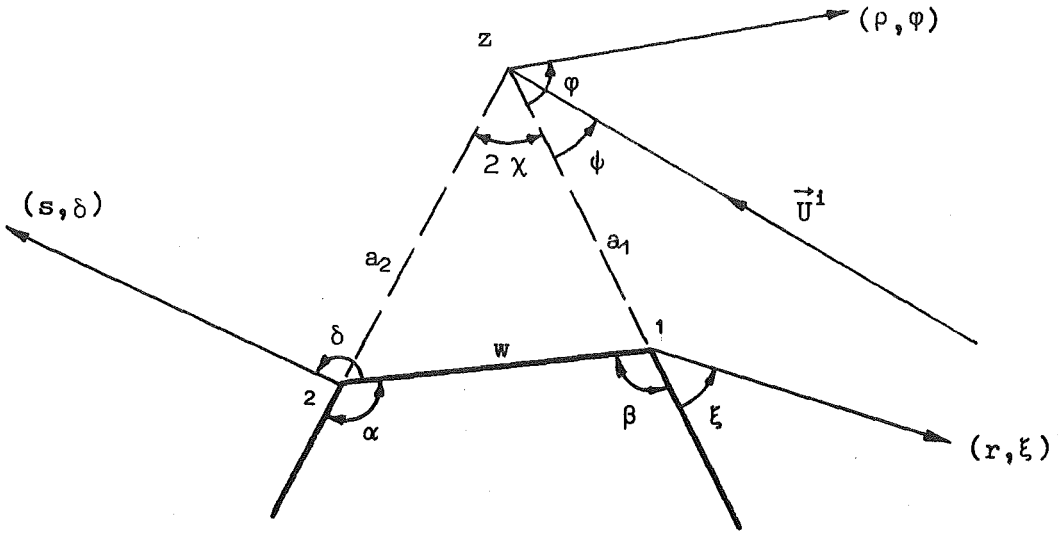

Figure 4.1 z axis perpendicular to the paper.

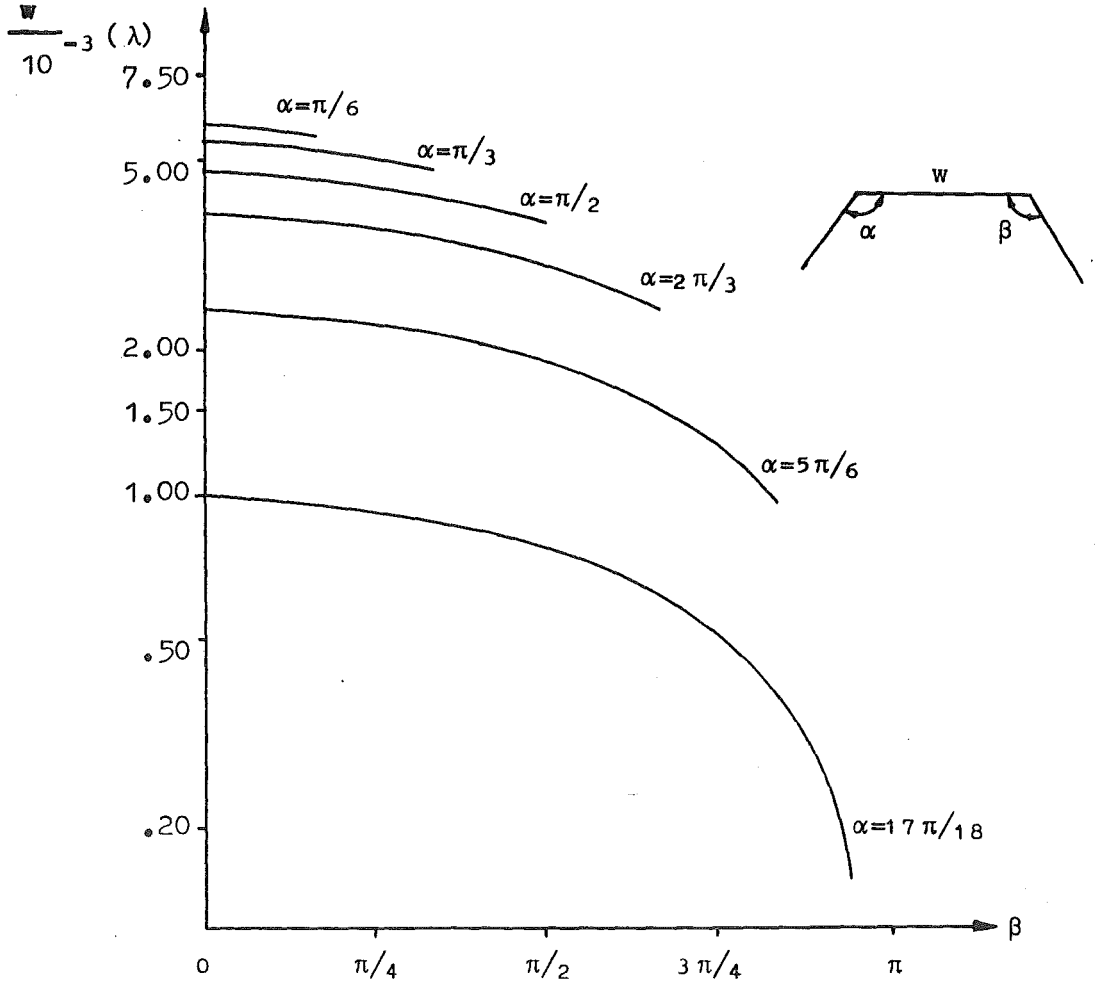

Figure 4.2

Minimum w for which the sum of the higher diffracted fields remains finite. From equation (4.28).

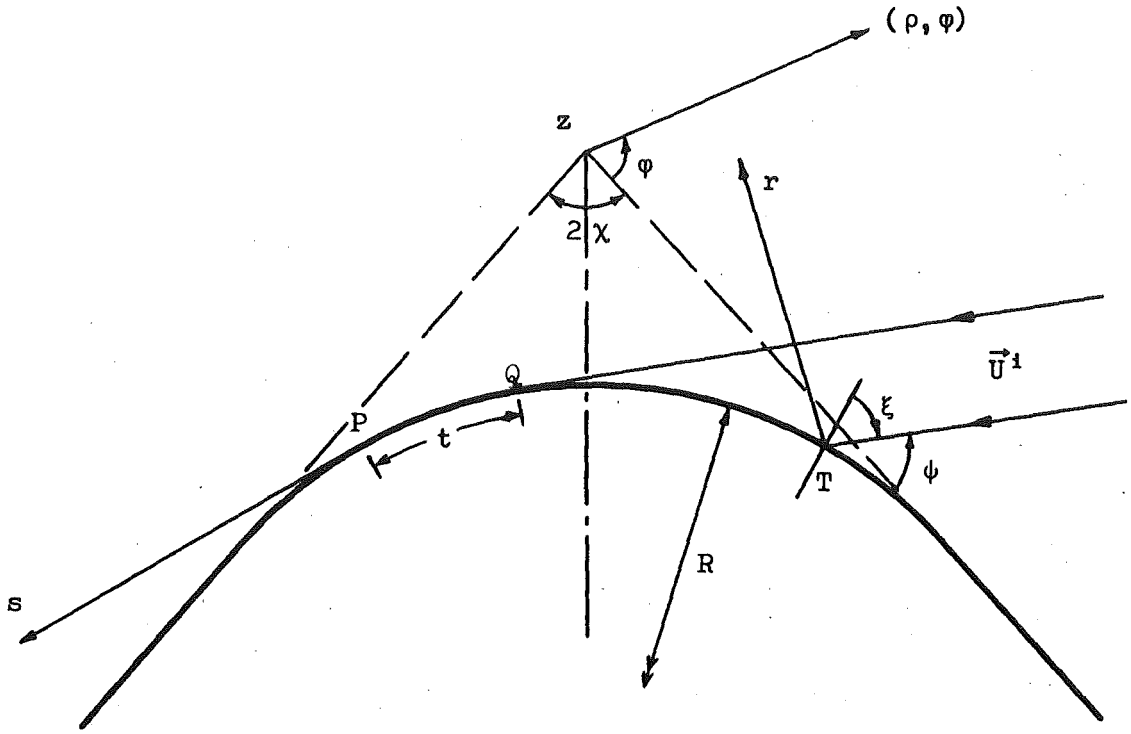

Figure 4.3 z axis perpendicular to the paper.

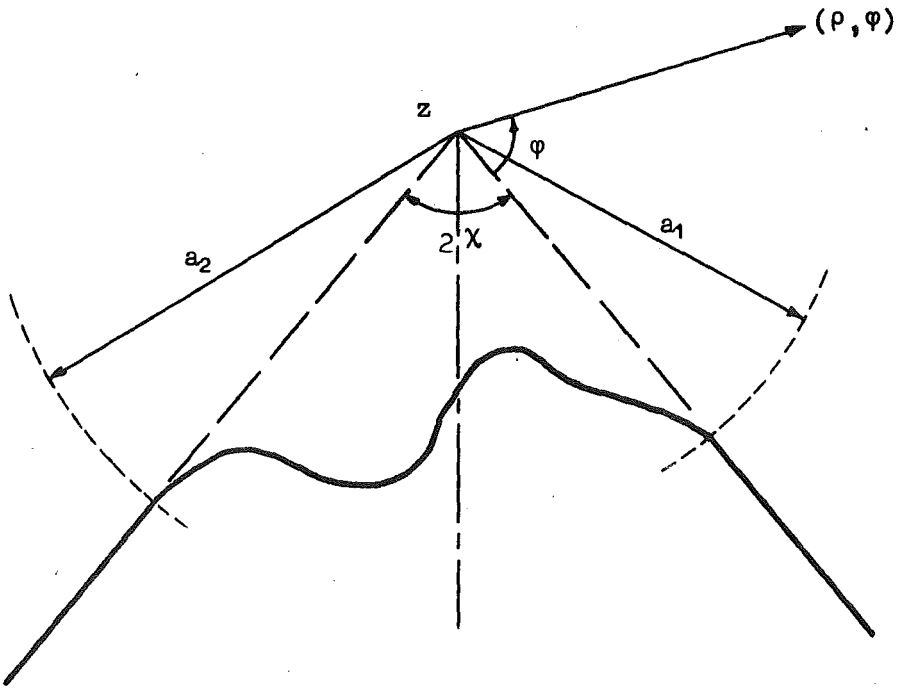

Figure 4.4 z axis perpendicular to the paper.

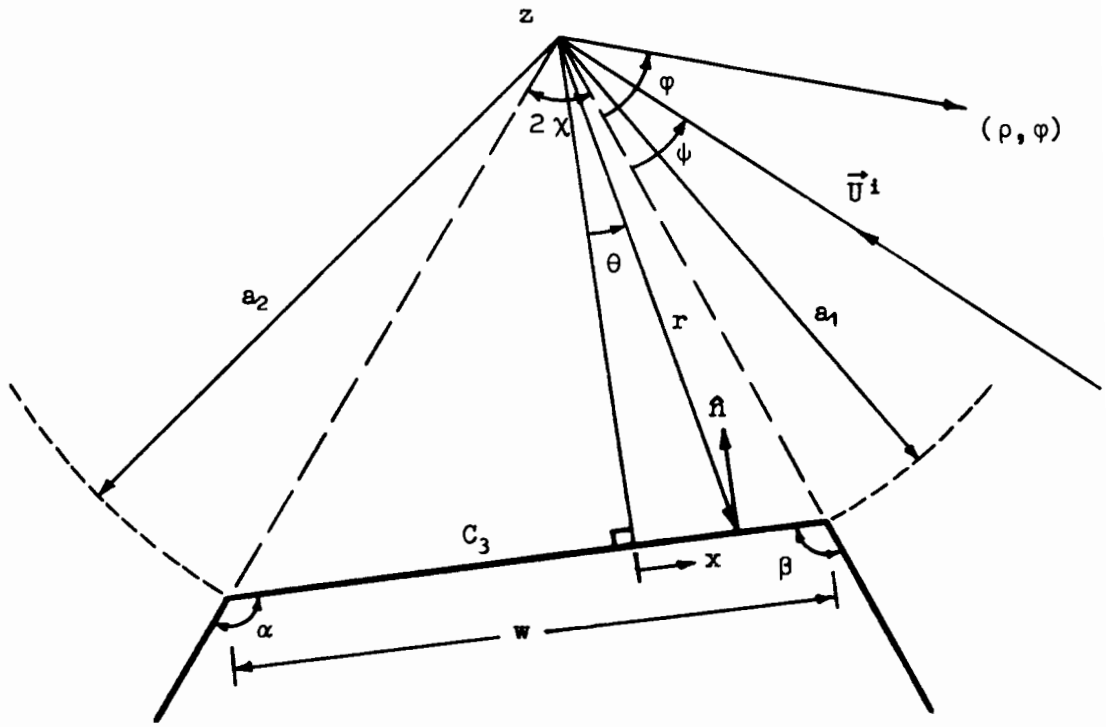

Figure 4.5 z axis perpendicular to the paper.

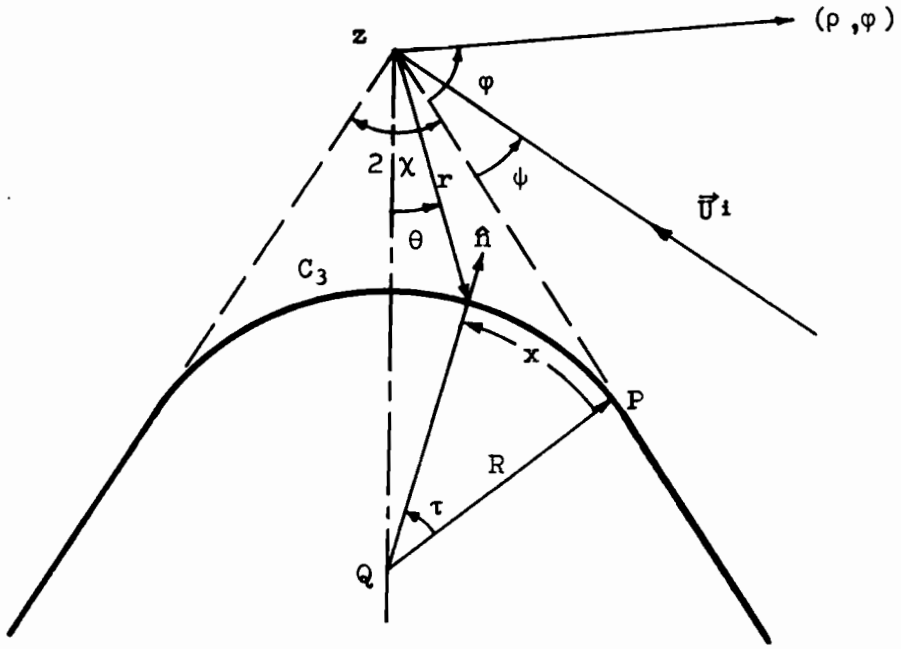

Figure 4.6 z axis perpendicular to the paper.

LEGEND FOR FIGURES 4.7-4.30

——————— from S.C.R. technique

— — — — — — from Physical Optics

— △ —— △ — from the undeformed wedge

— ○ —— ○ — G.T.D. diffracted field

— □ —— □ — G.T.D. primary diffracted field

— × —— × — G.T.D. sum of primary and secondary diffracted fields

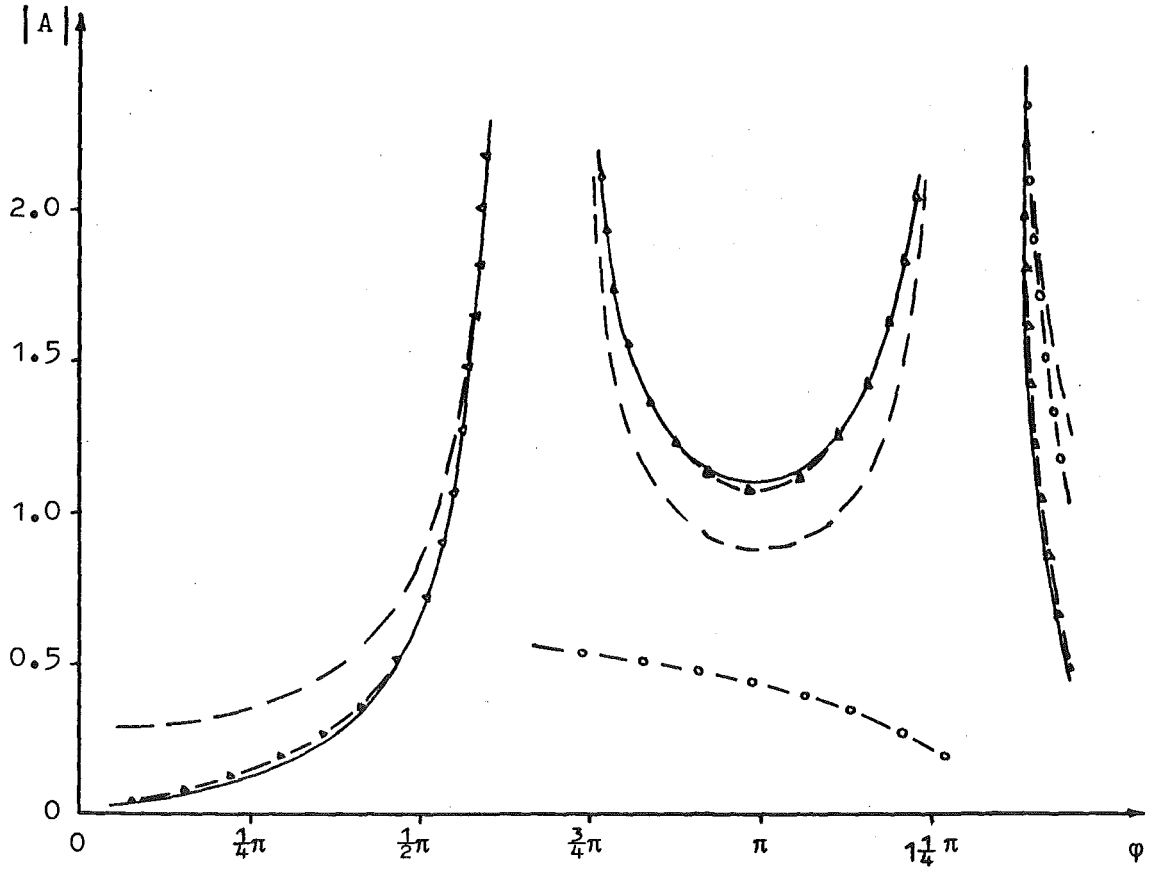

Figure 4.7 ($2\chi=94^{0}$, $\psi=60^{0}$, $w=0.1\lambda$)

Rounded Wedge. Electric Polarization.

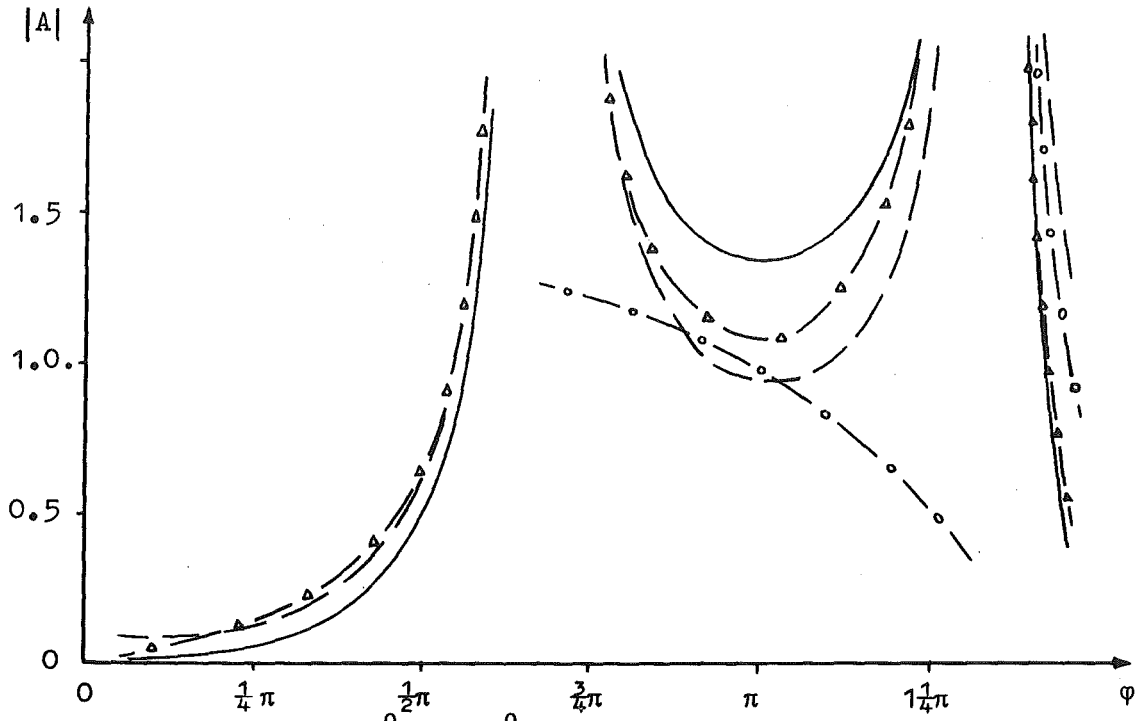

Figure 4.8 ($2\chi=94^0$, $\psi=60^0$, $w=0.5\lambda$) Legend on p 152.
Rounded Wedge. Electric Polarization.

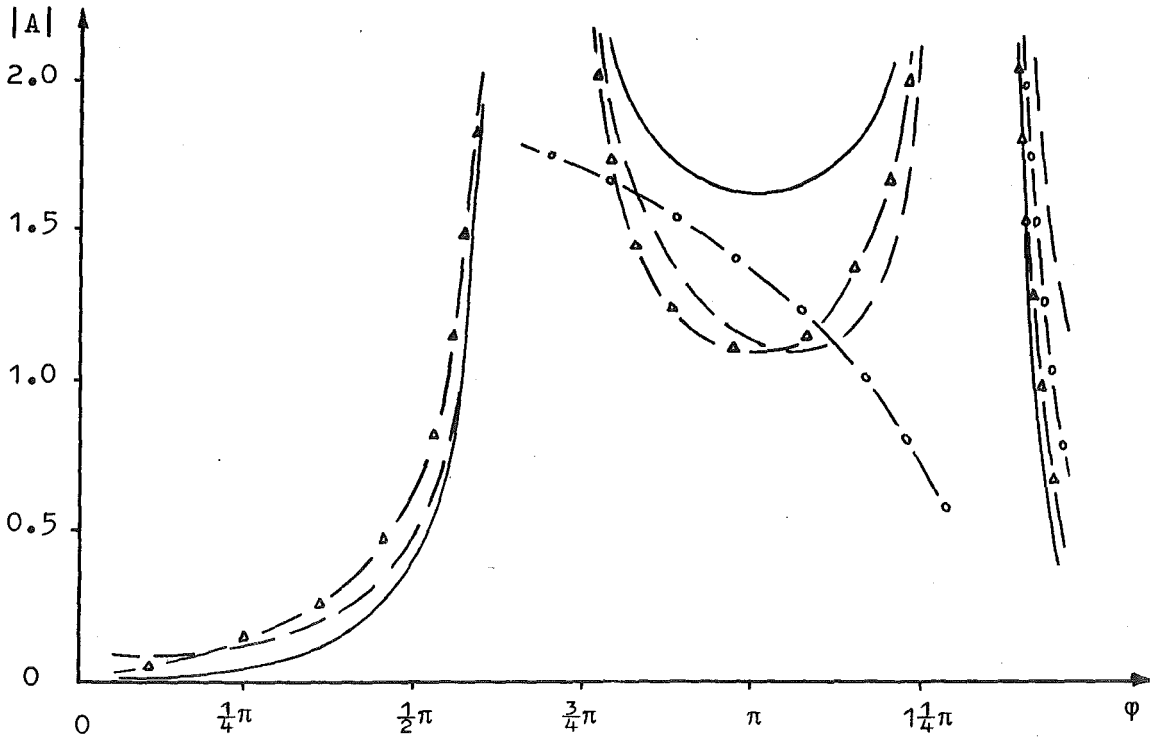

Figure 4.9 ($2\chi=94^0$, $\psi=60^0$, $w=1.0\lambda$) Legend on p 152.
Rounded Wedge. Electric Polarization.

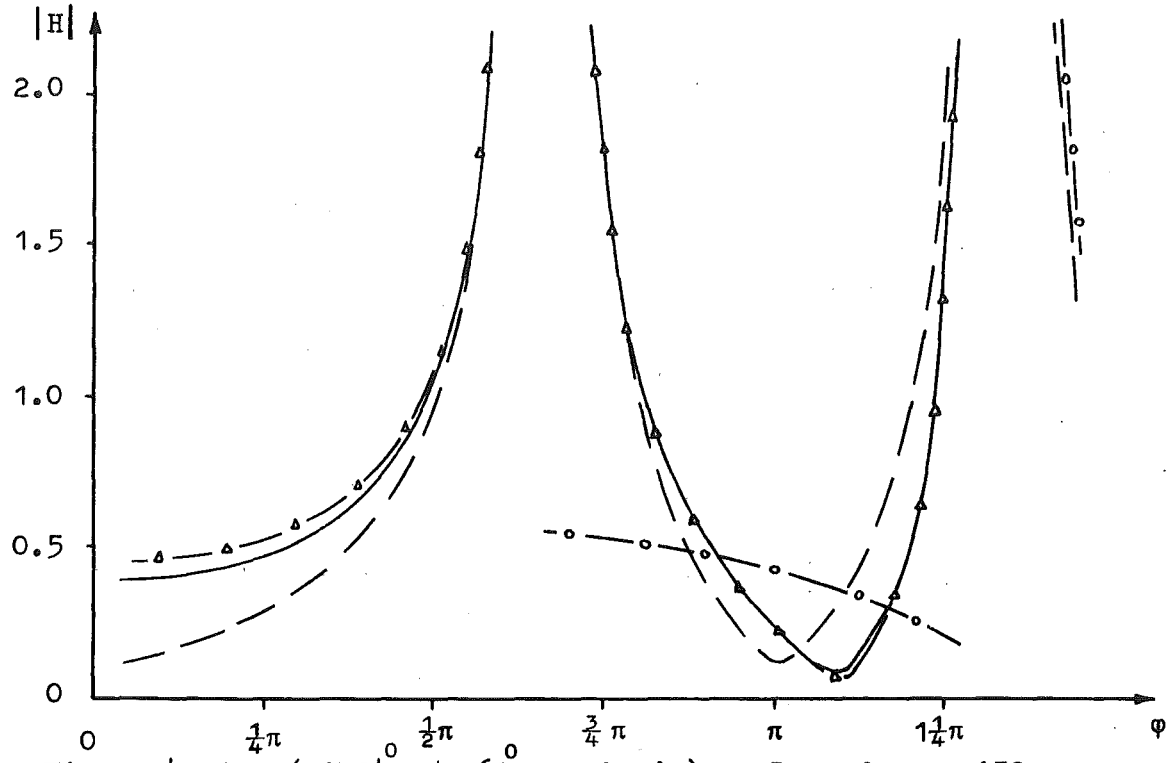

Figure 4.10 ($2\chi=94^0$, $\psi=60^0$, $w=0.1\lambda$) Legend on p 152.

Rounded Wedge. Magnetic Polarization.

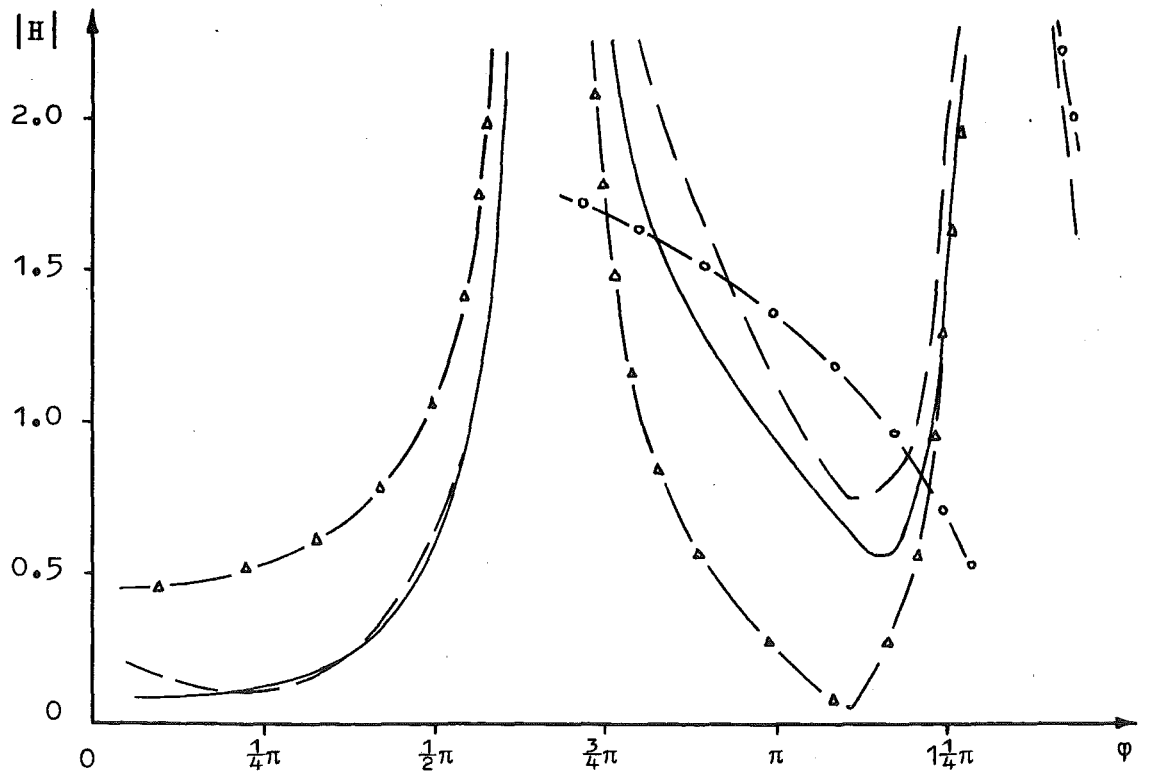

Figure 4.11 ($2\chi=94^0$, $\psi=60^0$, $w=1.0\lambda$) Legend on p 152.

Rounded Wedge. Magnetic Polarization.

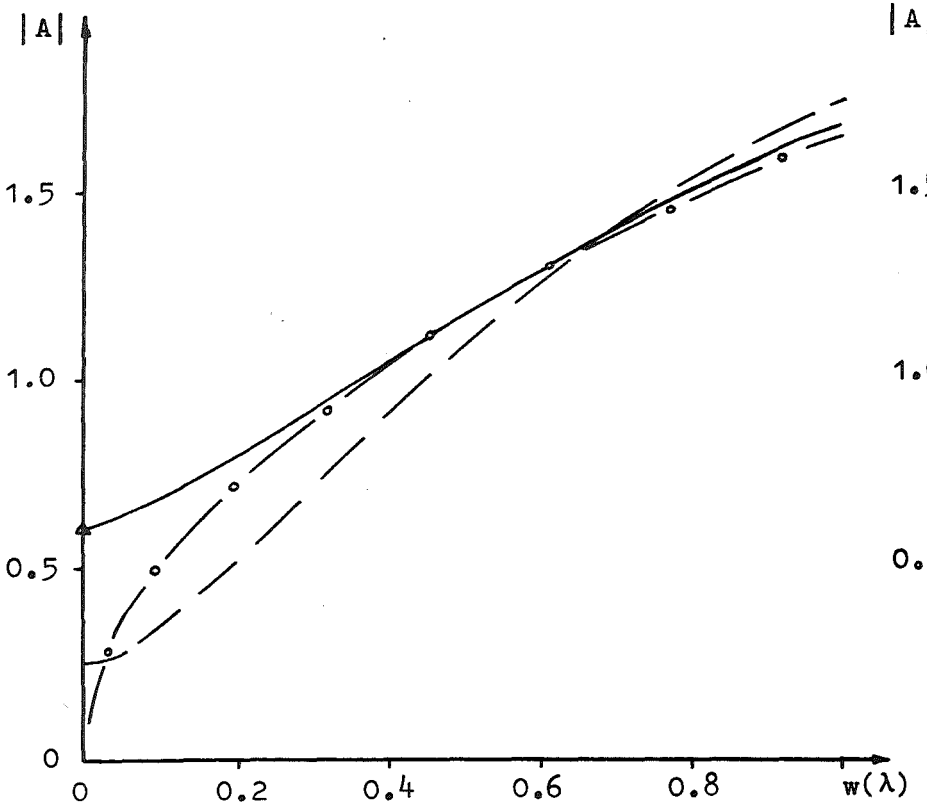

Figure 4.12 ($2\chi=54^0$, $\varphi=\psi=153^0$)

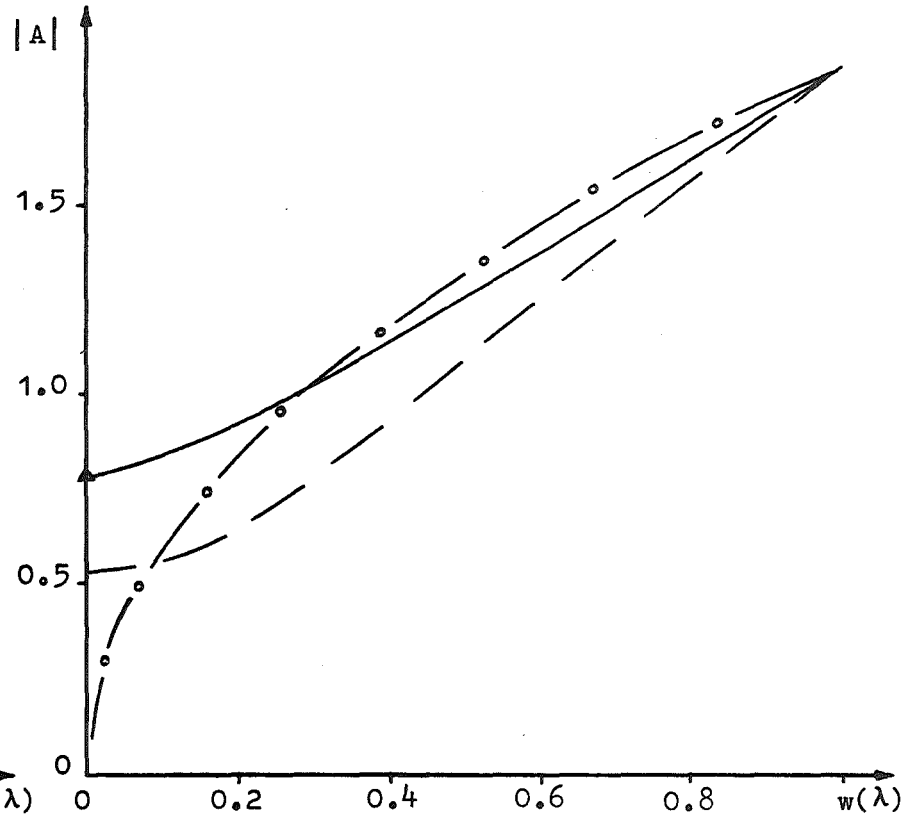

Figure 4.13 ($2\chi=94^0$, $\varphi=\psi=133^0$)

Rounded Wedge. Electric Polarization. Legend on p 152.

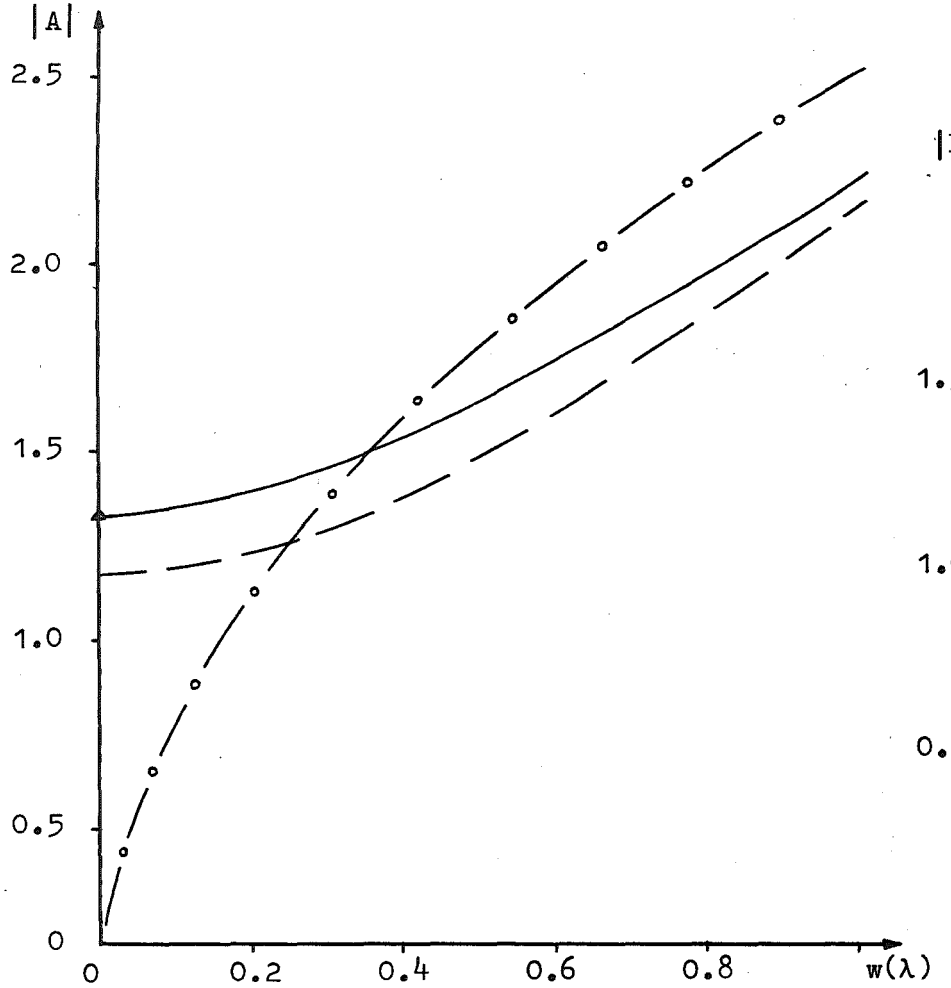

Figure 4.14 ($2\chi=134^{0}$, $\varphi=\psi=113^{0}$)
Electric Polarization

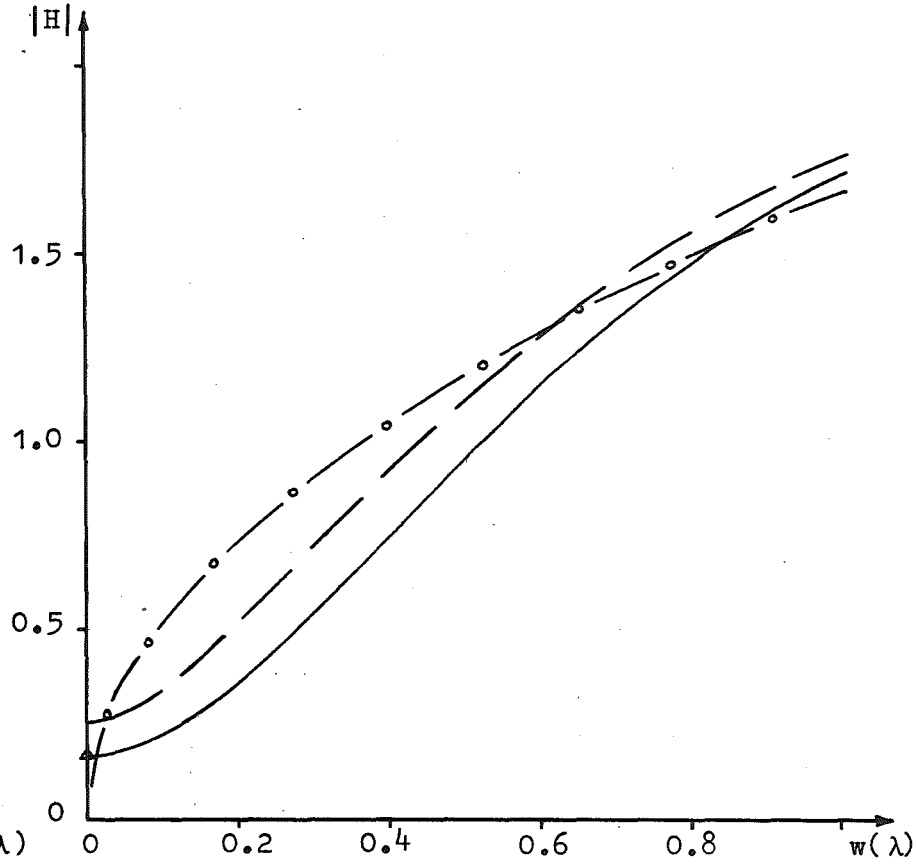

Figure 4.15 ($2\chi=54^{0}$, $\varphi=\psi=153^{0}$)
Magnetic Polarization

Rounded Wedge. Legend on p 152.

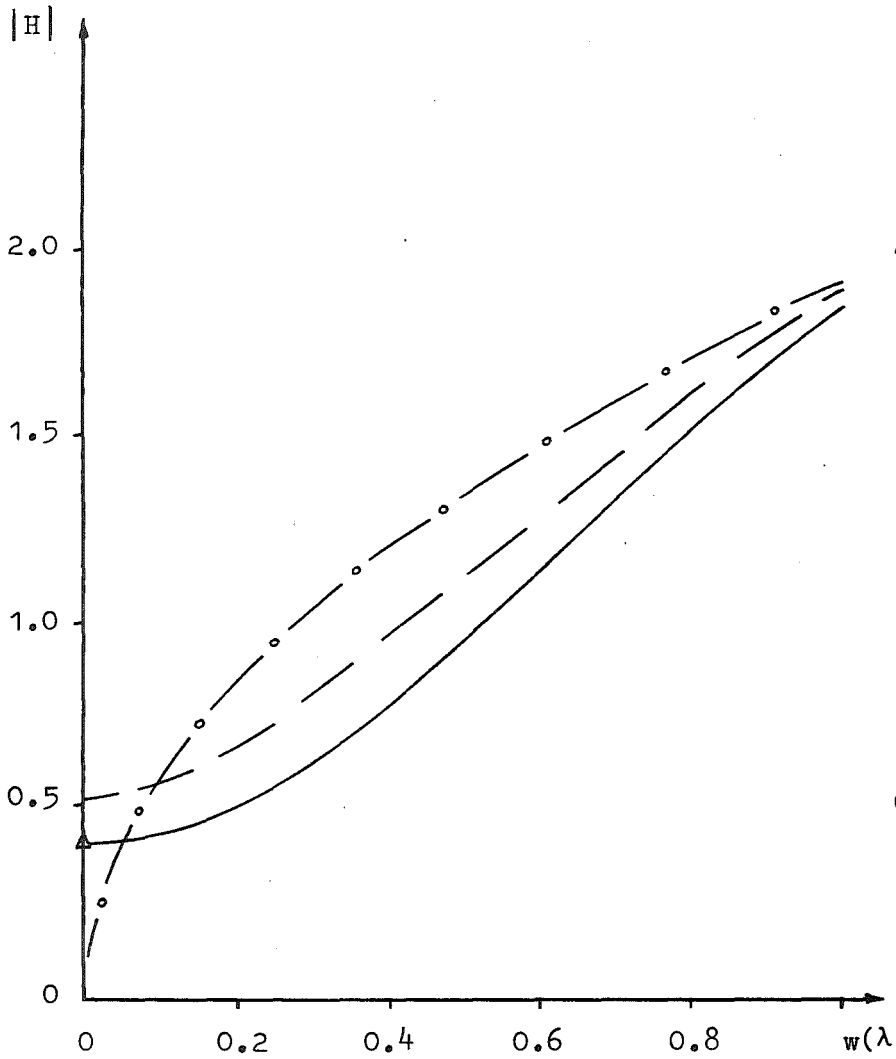

Figure 4.16 ($2\chi=94^0$, $\varphi=\psi=133^0$)

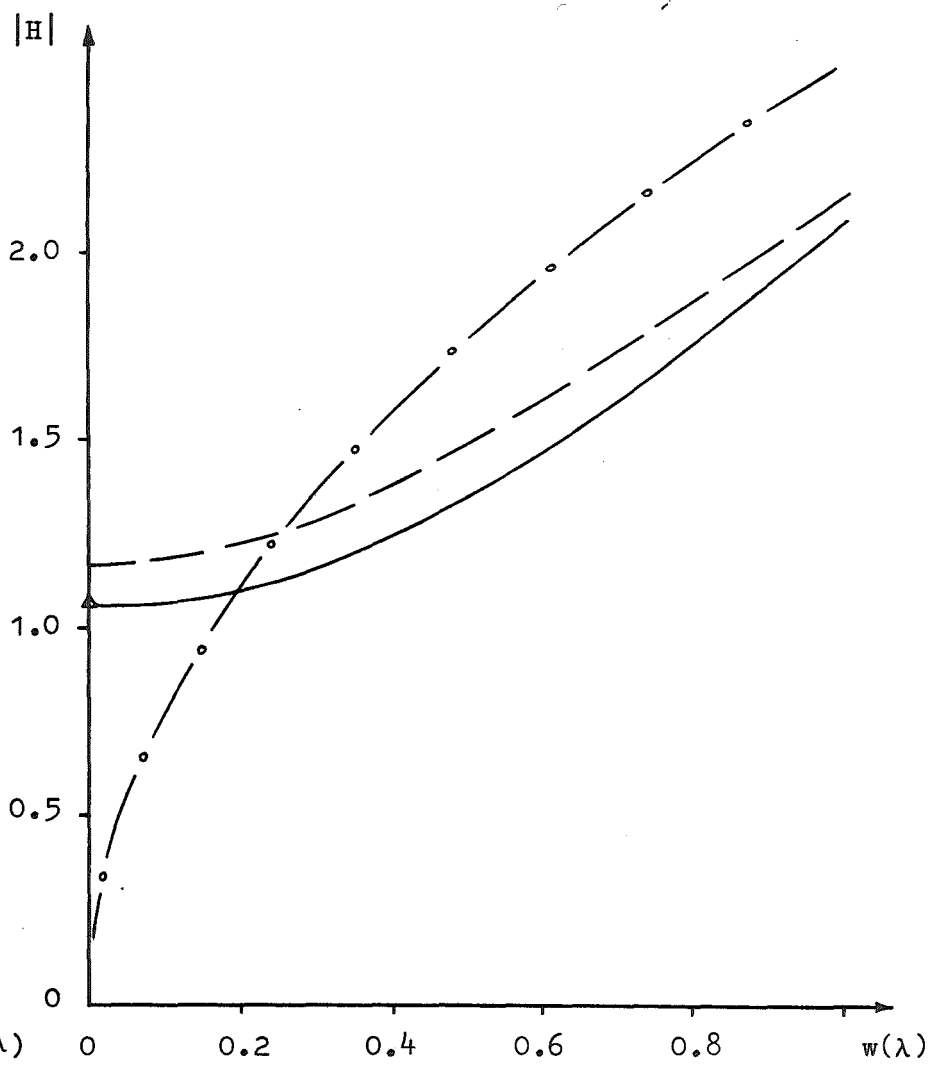

Figure 4.17 ($2\chi=134^0$, $\varphi=\psi=113^0$)

Rounded Wedge. Magnetic Polarization. Legend on p 152.

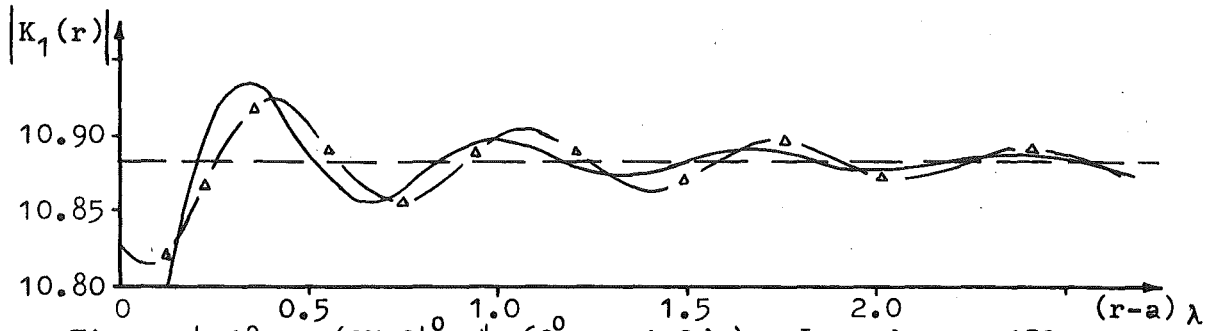

Figure 4.18 ($2\chi=94^0$, $\psi=60^0$, $w=1.0\lambda$) Legend on p 152.

Rounded Wedge. Electric Polarization.

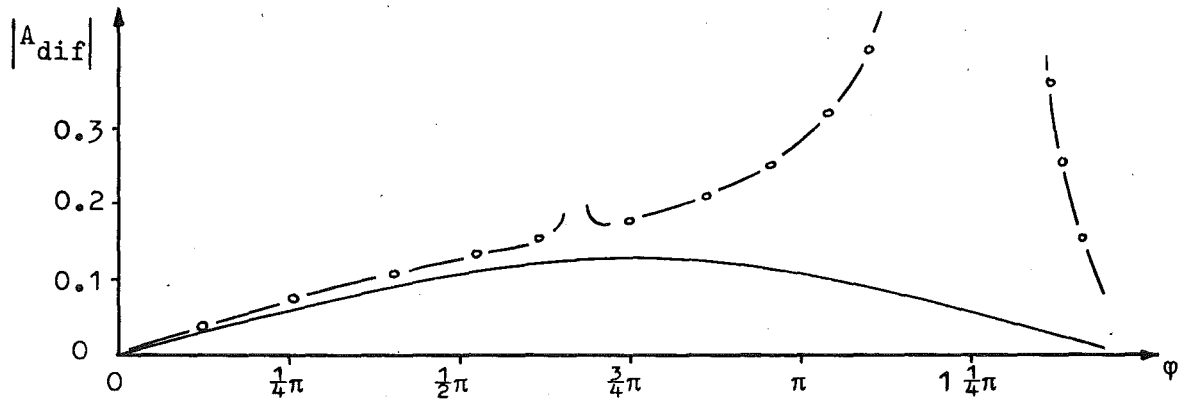

Figure 4.19 ($2\chi=94^0$, $\psi=60^0$, $w=0.1\lambda$) Legend on p 152.

Symmetrically Truncated Wedge. Electric Polarization.

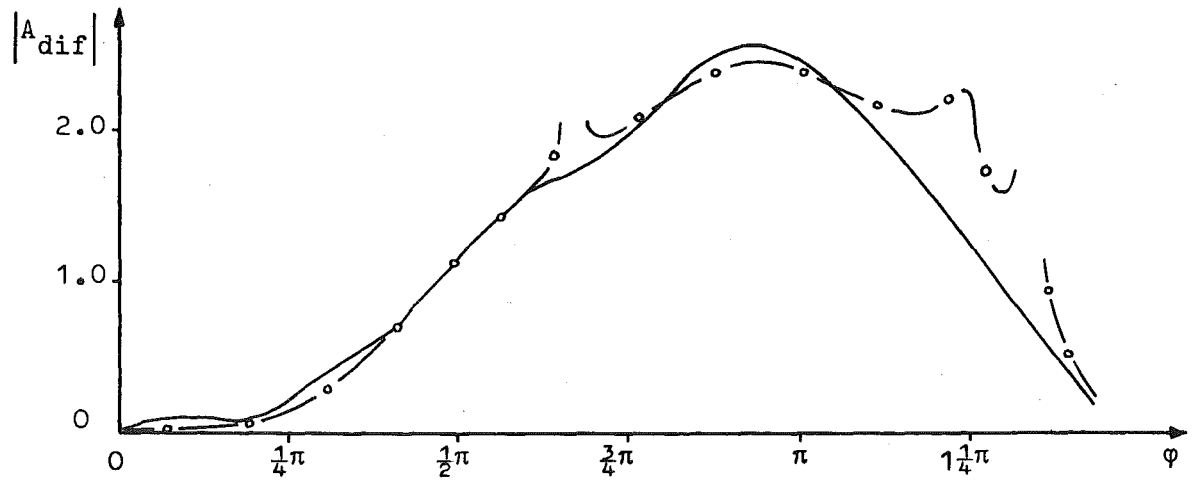

Figure 4.20 ($2\chi=94^0$, $\psi=60^0$, $w=1.0\lambda$) Legend on p 152.

Symmetrically Truncated Wedge. Electric Polarization.

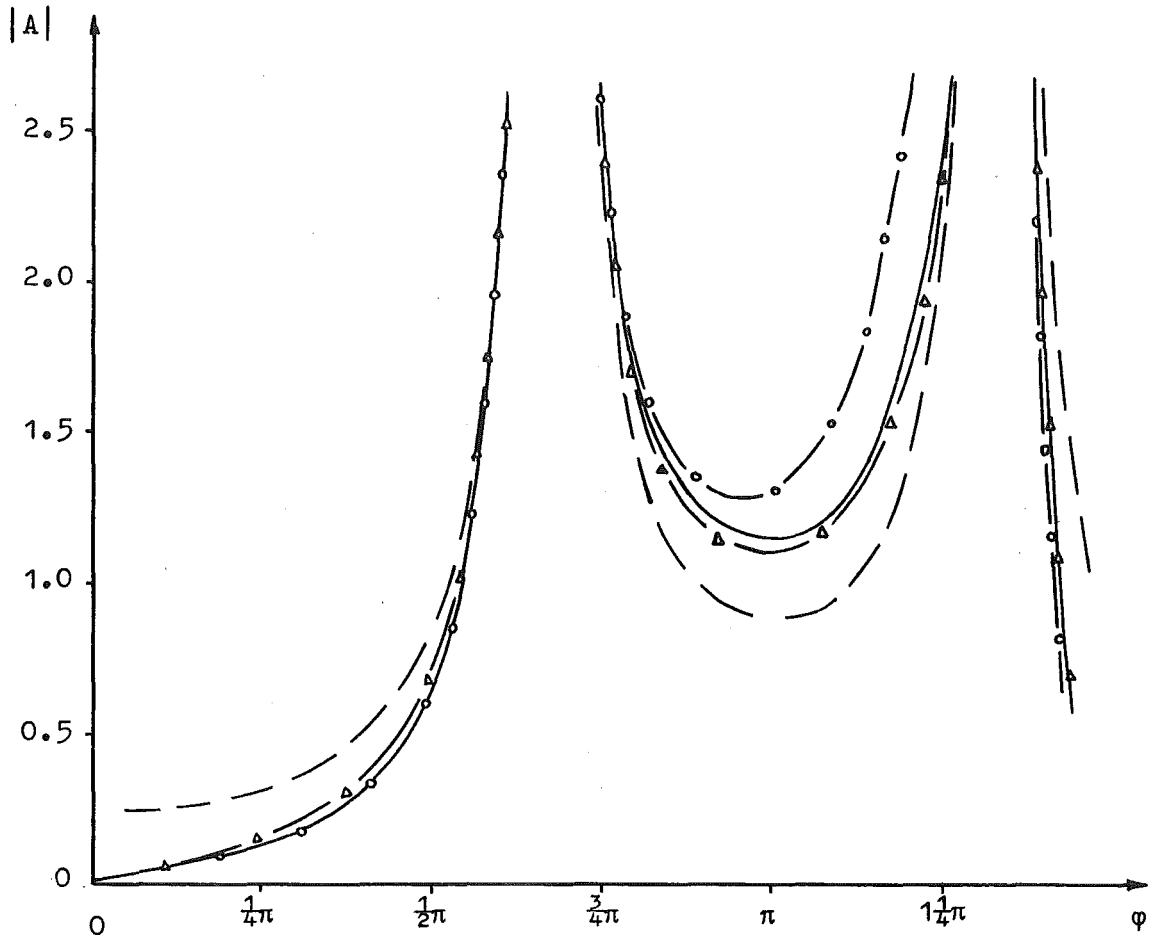

Figure 4.21 ($2\chi=94^0$, $\psi=60^0$, $w=0.1\lambda$) Legend on p 152.
Symmetrically Truncated Wedge. Electric Polarization.

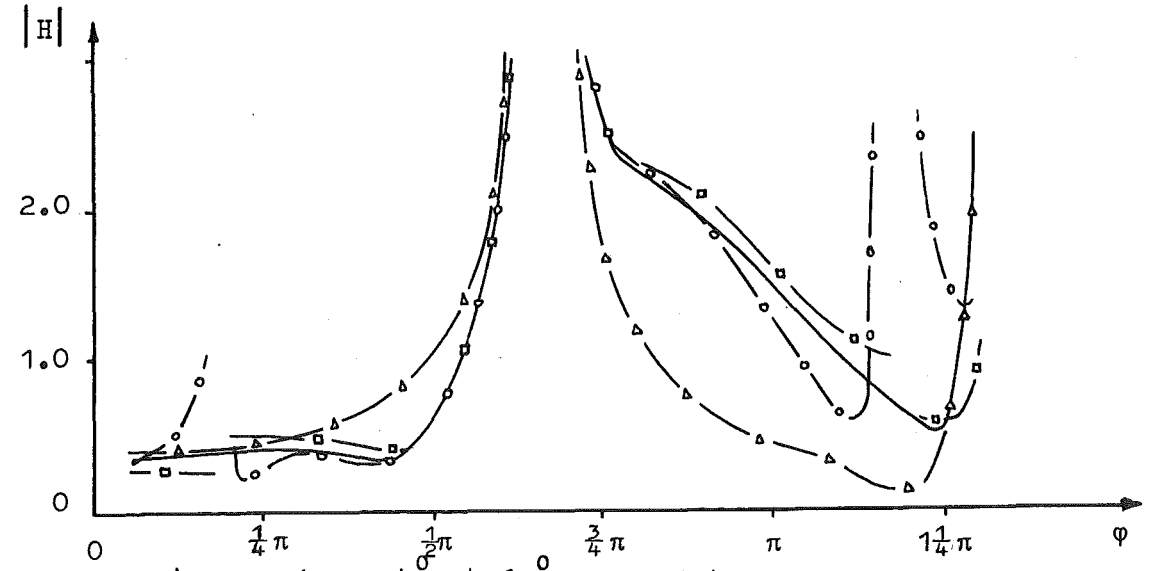

Figure 4.22 ($2\chi=114^0$, $\psi=60^0$, $w=0.1\lambda$) Legend on p 152.
Symmetrically Truncated Wedge. Magnetic Polarization.

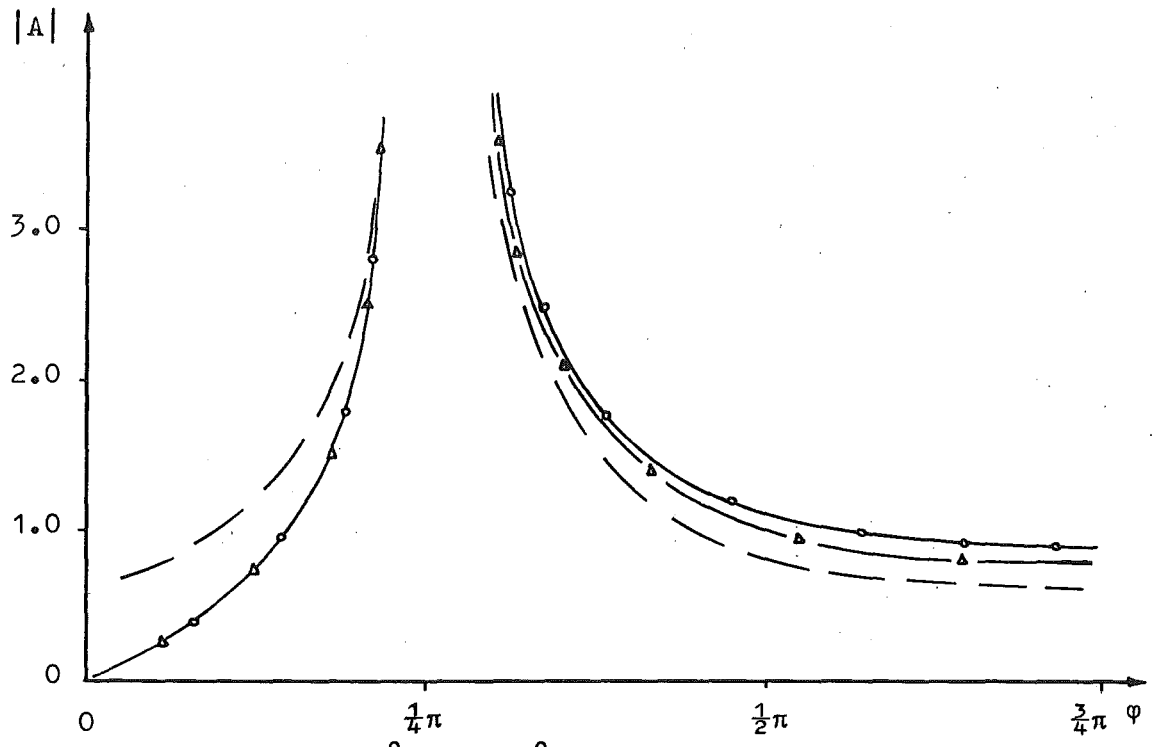

Figure 4.23 ($2\chi=94^0$, $\psi=133^0$, $w=0.1\lambda$) Legend on p 152.
Symmetrically Truncated Wedge. Electric Polarization.

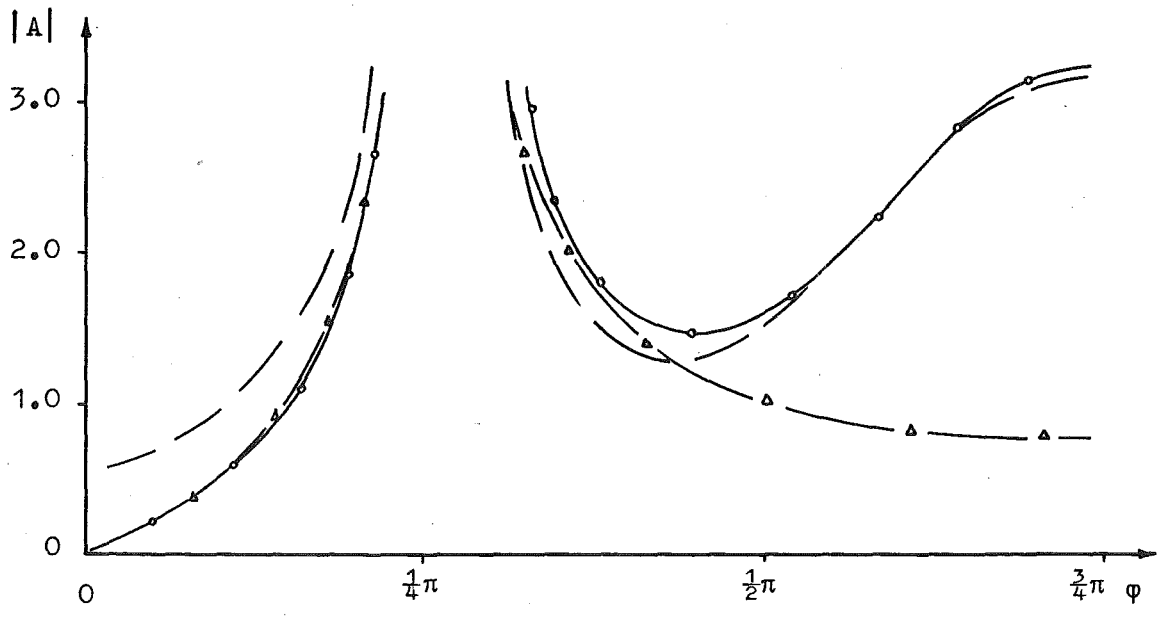

Figure 4.24 ($2\chi=94^0$, $\psi=133^0$, $w=1.0\lambda$) Legend on p 152.
Symmetrically Truncated Wedge. Electric Polarization.

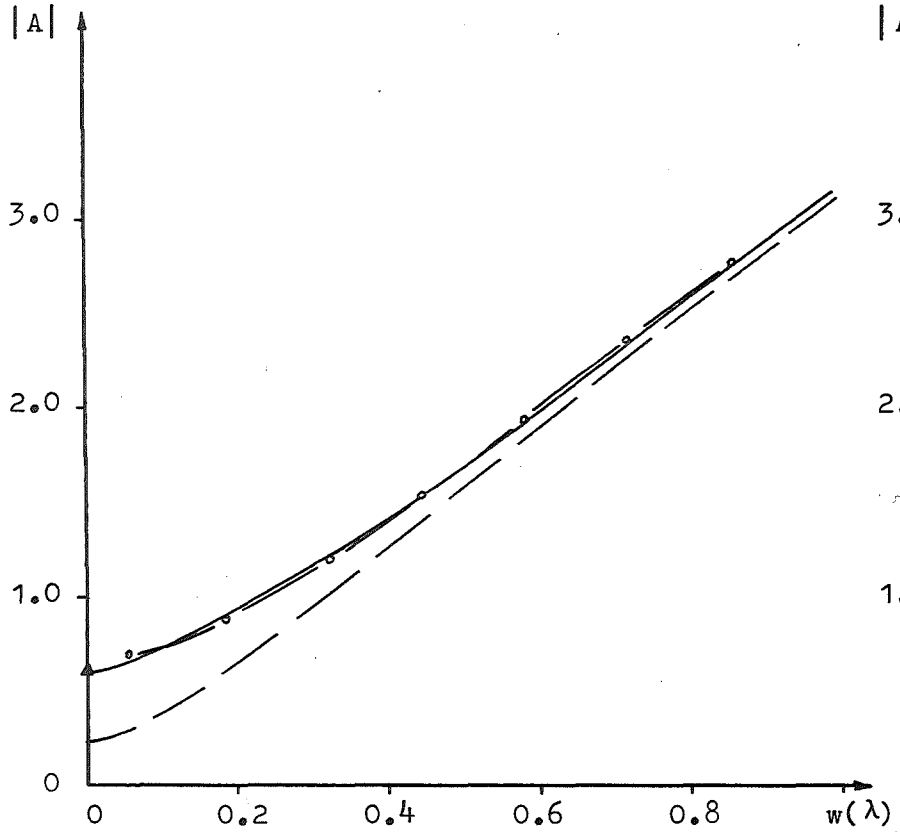

Figure 4.25 ($2\chi=54^0$, $\varphi=\psi=153^0$)

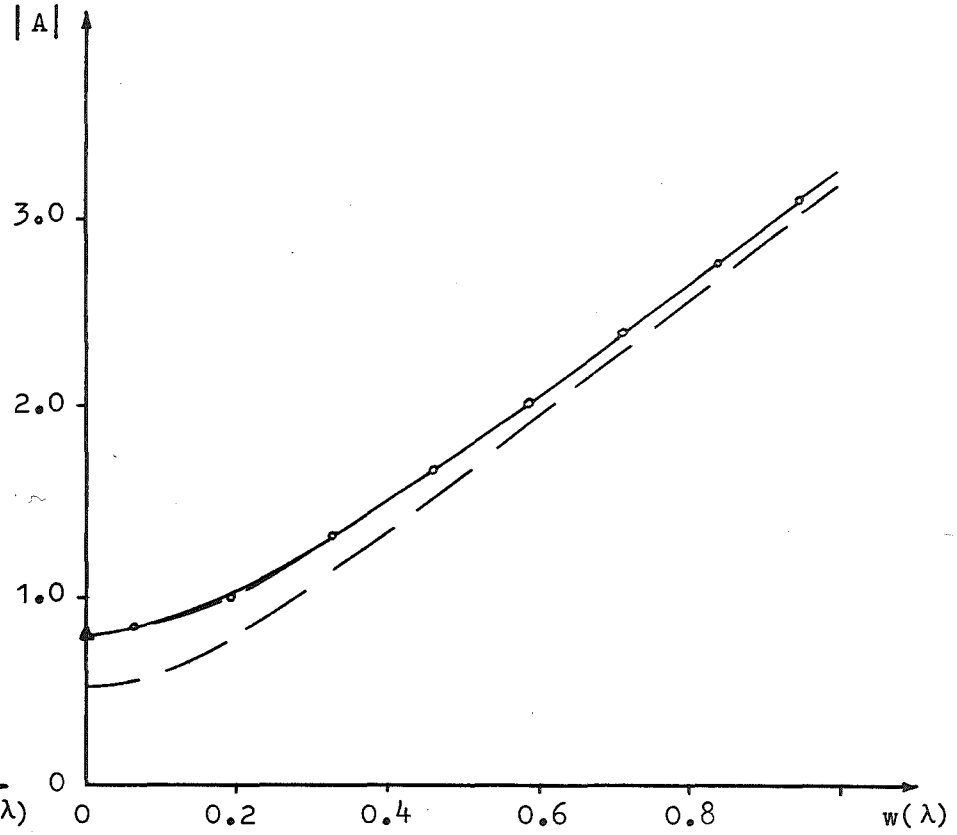

Figure 4.26 ($2\chi=94^0$, $\varphi=\psi=133^0$)

Symmetrically Truncated Wedge. Electric Polarization. Legend on p 152.

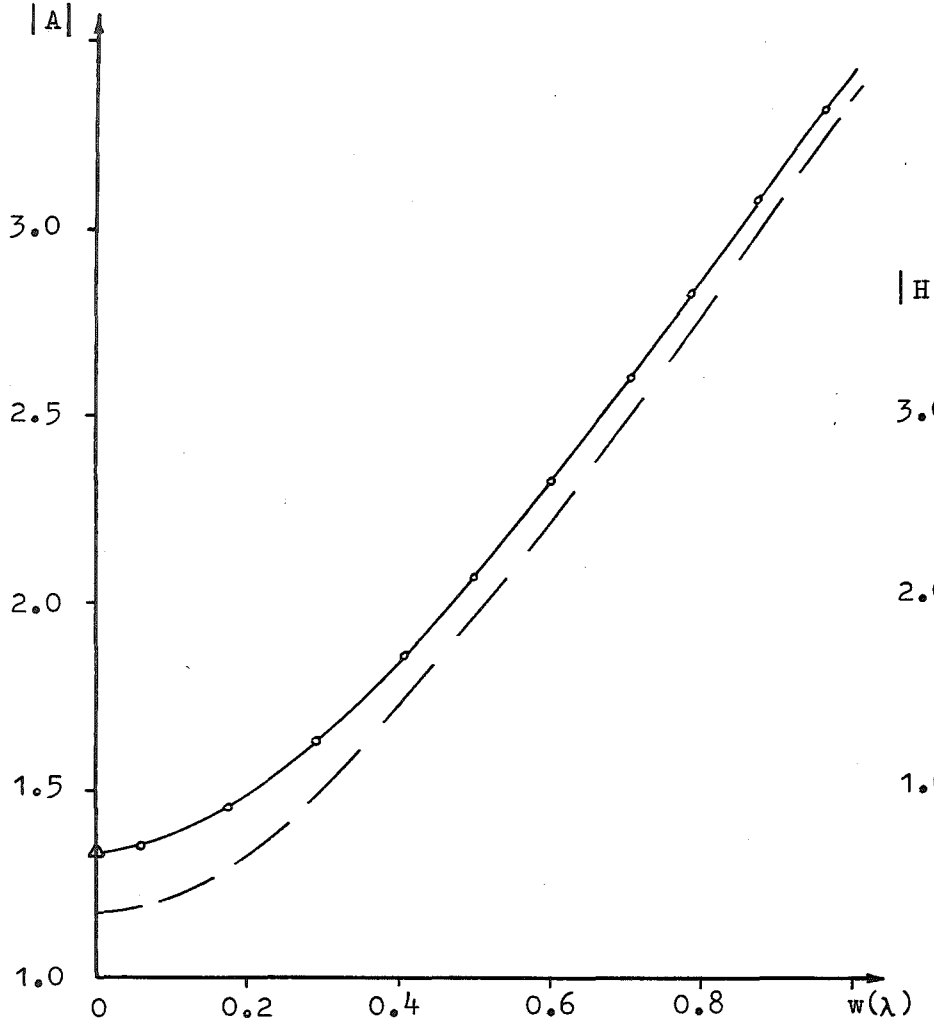

Figure 4.27 ($2\chi=134^0$, $\varphi=\psi=113^0$)

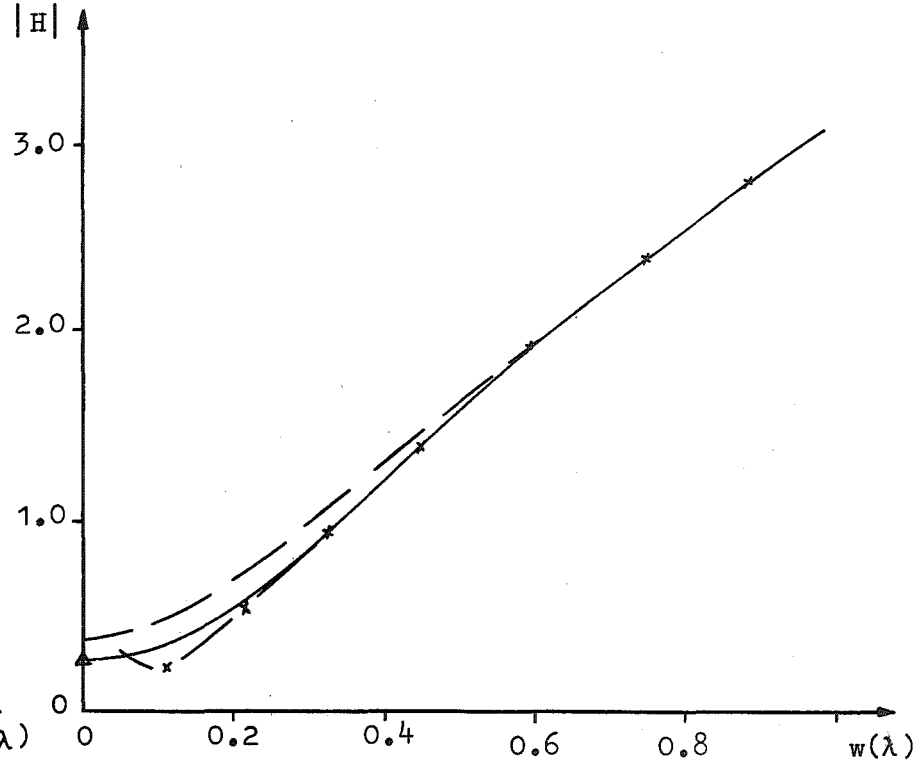

Figure 4.28 ($2\chi=74^0$, $\varphi=\psi=143^0$)

Symmetrically Truncated Wedge. Magnetic Polarization. Legend on p 152.

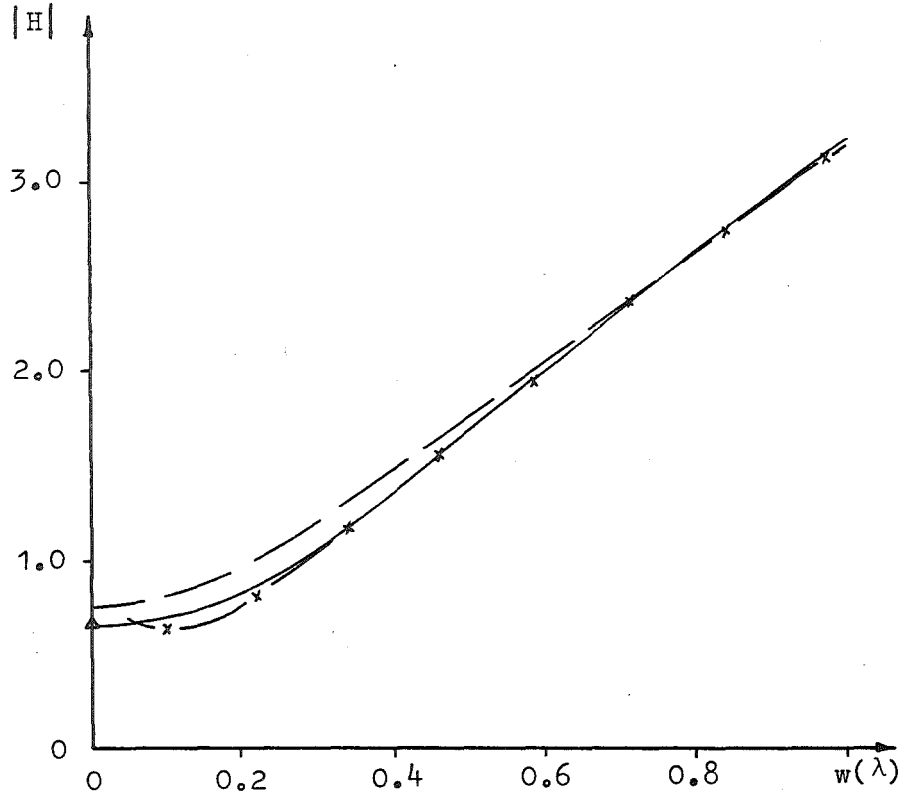

Figure 4.29 ($2\chi=114^{0}$, $\varphi=\psi=123^{0}$)

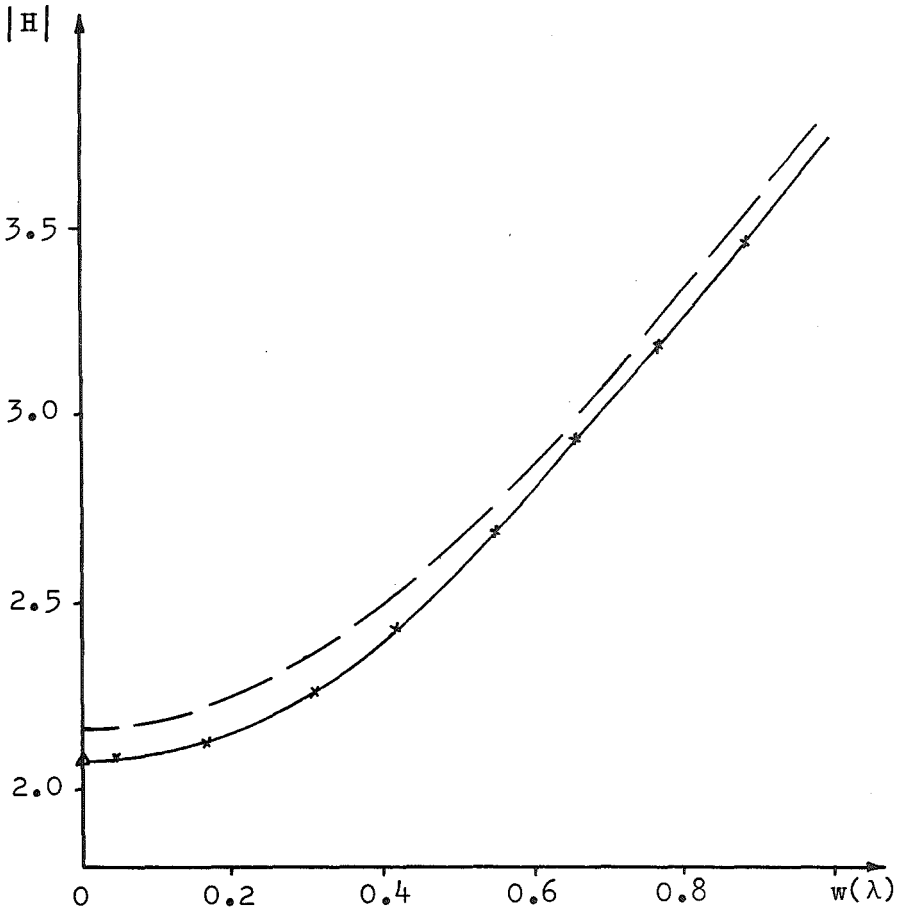

Figure 4.30 ($2\chi=154^{0}$, $\varphi=\psi=103^{0}$)

Symmetrically Truncated Wedge. Magnetic Polarization. Legend on p 152.

CHAPTER 5

The exact description of the field scattered from a perfectly conducting infinite wedge is obtained when the wedge is excited by line sources polarized in the plane normal to the wedge axis. The solutions for both electric and magnetic line sources are given. The results of this chapter are used in Chapter 6.

5.1(a) INTRODUCTION

Jones[13] derives the equations (1.16) - (1.20) describing the field surrounding a perfectly conducting wedge when the excitation is an electric or magnetic line source polarized parallel to the wedge axis. In Chapter 6 of this thesis, the description of the field surrounding a perfectly conducting wedge is required when the excitation is an electric line source polarized in the plane normal to the wedge axis. That description, and the one appropriate to a magnetic line source polarized in the plane normal to the wedge axis, are derived in this chapter. The expressions are presented in the same form as (1.16) - (1.20). The results of this chapter have been published elsewhere.[3]

5.2(a) TRANSVERSELY POLARIZED ELECTRIC LINE SOURCE.

Consider the perfectly conducting wedge in Fig. 5.1. The z axis is perpendicular to the paper. In terms of the cylindrical polar coordinates (ρ, ϕ), the line source

is at (ρ_o, ψ) and the wedge occupies the region $2\pi-\beta \leqslant \phi \leqslant 2\pi$. Rectangular co-ordinates (x,y) and polar co-ordinates (r,θ) are set up with origin at (ρ_o, ψ). The x axis is parallel to the direction $\phi = 0$.

The wedge is excited by the field from the transversely polarized electric line source $\vec{J}$ given by

$$\vec{J} = [\hat{x}\cos\theta_o + \hat{y}\sin\theta_o] \frac{\delta(\rho-\rho_o)\ \delta(\phi-\psi)}{\rho_o}, \tag{5.1}$$

where $\delta(\xi)$ is the Dirac delta function, and $\hat{x}$ and $\hat{y}$ are the unit vectors in the x and y directions respectively. $\vec{J}$ can also be written as

$$\vec{J} = \hat{x}\, J_x + \hat{y}\, J_y. \tag{5.2}$$

Since

$$\nabla \times \vec{J} = \hat{z}\,(\frac{\partial J_y}{\partial x} - \frac{\partial J_x}{\partial y}), \tag{5.3}$$

it follows from (1.28) that the source distribution $\vec{J}$ generates a magnetically polarized field. However, because of the curl of the delta function on the right-hand side of the expression in (1.28), it is not clear how to determine $\vec{H}$ by using the Kontorowich-Lebedev transform.

In order to overcome this difficulty, consider $\vec{J}$ to be a continuous source distribution with a Gaussian form centred on (ρ_o, ψ). Thus

$$\vec{J} = [\hat{x}\cos\theta_o + \hat{y}\sin\theta_o] \frac{e^{(\frac{-r^2}{2b^2})}}{2\pi b^2}, \quad r^2 = x^2 + y^2, \tag{5.4}$$

where b is a constant. Since

$$\lim_{b\to 0}\left[\frac{e^{\left(\frac{-x^2}{2b^2}\right)}}{\sqrt{2\pi}\ b}\right] = \delta(x), \tag{5.5}$$

the expressions in (5.4) and (5.1) are identical in the limit $b \to 0$.

By using the expressions in (5.4) with those in (5.2) and (5.3), and noting that

$$x = r\cos\theta, \quad y = r\sin\theta, \tag{5.6}$$

$\nabla \times \vec{J}$ can be described by

$$\nabla \times \vec{J} = \hat{z}\, S(r,\theta), \quad S(r,\theta) = \frac{r\, e^{\left(\frac{-r^2}{2b^2}\right)}}{2\pi b^4}\sin(\theta-\theta_o). \tag{5.7}$$

A solution $\vec{H}(\rho,\phi)$ is now required such that

$$\vec{H} = \hat{z}H, \quad \nabla^2 H + k^2 H = -S(r,\theta), \tag{5.8}$$

subject to the boundary conditions in (1.4), that

$$\left.\frac{\partial H}{\partial n}\right|_{\phi=\begin{matrix}0\\ m\pi\end{matrix}} = 0, \quad m\pi = 2\pi-\beta. \tag{5.9}$$

The solution $U(\rho,\phi)$ of (1.14) subject to the boundary condition (1.4) is given by (1.16) and (1.17). That solution is the Greens function for an infinite z-directed magnetic line source. The solution of (5.8) can therefore

be written as

$$H(\rho,\phi) = \int_0^{\infty}\int_0^{2\pi} S(r,\theta)\ U(\rho,\phi)\ r\ d\theta\ dr, \qquad (5.10)$$

where

$$U(\rho,\phi) = \Omega(\rho,\phi-\phi_1) + \Omega(\rho,\phi+\phi_1), \qquad (5.11)$$

$$\Omega(\rho,\xi) = -\frac{1}{8\pi}\int_{\infty-j\frac{\pi}{m}}^{\infty+j\frac{\pi}{m}} \frac{H_o^{(2)}\{k[\rho^2-\rho_1^2-2\rho\rho_1\cosh(mv)]^{\frac{1}{2}}\}\sinh v\ dv}{\cosh v - \cos(\frac{\xi}{m})} \qquad (5.12)$$

Consider the term of $H(\rho,\phi)$ given by

$$H_1(\rho,\phi) = \int_0^{\infty}\int_0^{2\pi} S(r,\theta)\ \Omega(\rho,\phi-\phi_1)\ r\ d\theta\ dr. \qquad (5.13)$$

It can be seen from (5.4) that as b tends to zero, all important contributions to the integral in (5.10) will come from the neighbourhood of $r = 0$. In this region,

$$\rho_1 \approx \rho_o + r\cos(\theta-\psi),\ \cos(\frac{\phi-\phi_1}{m}) \approx \cos(\frac{\phi-\psi}{m}) + \frac{r}{\rho_o m}\sin(\theta-\psi)\sin(\frac{\phi-\psi}{m}), \qquad (5.14)$$

enabling the denominator of $\Omega(\rho,\phi-\phi_1)$ to be written, with the use of the binomial theorem, as

$$\cosh v - \cos\left(\frac{\phi-\phi_1}{m}\right) = C_1\,[1-C_2\, r\,\sin(\theta-\psi)] \approx \frac{C_1}{1+C_2 r\sin(\theta-\psi)}\,, \tag{5.15}$$

where

$$C_1 = \cosh v-\cos\left(\frac{\phi-\psi}{m}\right), \qquad C_2 = \frac{\sin\left(\frac{\theta-\psi}{m}\right)}{\rho_o m C_1}. \tag{5.16}$$

The Hankel function in the integrand of (5.12) is

$$H_o^{(2)}(kz) = H_o^{(2)}\{k[\rho^2-\rho_1^2-2\rho\rho_1\cosh(mv)]^{\frac{1}{2}}\}. \tag{5.17}$$

The distance z is represented by the side AC of the triangle ABC in Fig. 5.2. The line AD of length y is constructed such that the length of BD is ρ_o. Then, using the addition theorem[14] and (5.14) with (5.17),

$$H_o^{(2)}(kz) = \sum_{n=-\infty}^{\infty} H_n^{(2)}(ky)\; J_n[kr\,\cos(\theta-\psi)]\cos(n\alpha), \tag{5.18}$$

where, from the geometry of Fig. 5.2,

$$y = [\rho^2+\rho_o^2-2\rho\rho_o\cosh(mv)]^{\frac{1}{2}}, \quad \cos\alpha = \frac{\rho\cosh(mv) - \rho_o}{y}. \tag{5.19}$$

When kr is small, the use of the limiting form of the Bessel function of small argument in (3.11) gives

$$J_n[kr\,\cos(\theta-\psi)] \approx \frac{\left[\frac{kr\,\cos(\theta-\psi)}{2}\right]^n}{\Gamma(n+1)}, \qquad n \geq 0. \tag{5.20}$$

Substitution of (5.20) into (5.18), and the use of (2.33), results in

$$H_o^{(2)}(kz) = \sum_{n=0}^{\infty} \varepsilon_n \frac{H_n^{(2)}(ky)\cos(n\alpha)}{\Gamma(n+1)} \left[\frac{kr\cos(\theta-\psi)}{2}\right]^n, \quad (5.21)$$

where ε_n is the Neumann factor defined in (1.15).

By substituting the expressions in (5.7) and (5.12) with those in (5.15) and (5.21) into (5.13), the first term of $H(\rho,\phi)$ can be described by

$$H_1(\rho,\phi) = \frac{-1}{16\pi^2 b^4} \int_{\infty-j\frac{\pi}{m}}^{\infty+j\frac{\pi}{m}} \int_0^{\infty} \int_0^{2\pi} \sum_{n=0}^{\infty} \frac{1}{C_1} \left[\frac{\varepsilon_n H_n^{(2)}(ky)}{\Gamma(n+1)}\cos(n\alpha)\right.$$

$$\left. \cdot \sinh v \sin(\theta-\theta_o) \left[\frac{kr\cos(\theta-\psi)}{2}\right]^n [1+C_2 r\sin(\theta-\psi)] r^2 e^{\left(\frac{-r^2}{2b^2}\right)}\right] d\theta dr\, dv. \quad (5.22)$$

Notice that C_1, C_2, y and α are all independent of θ and r. Since

$$\int_0^{2\pi} \sin(\theta-\theta_o)\,d\theta = 0, \quad \int_0^{2\pi} \sin(\theta-\psi)\sin(\theta-\theta_o)\,d\theta = \pi\cos(\psi-\theta_o),$$

$$\int_0^{2\pi} \cos(\theta-\psi)\sin(\theta-\theta_o)\,d\theta = \pi\sin(\psi-\theta_o), \quad (5.23)$$

the integration with respect to θ in (5.22) can be performed, giving

$$H_1(\rho,\phi) = \frac{-1}{16\pi^2 b^4} \int_{\infty-j\frac{\pi}{m}}^{\infty+j\frac{\pi}{m}} \int_0^{\infty} \frac{1}{C_1} \Bigg[\pi r^3 \, e^{\left(\frac{-r^2}{2b^2}\right)} \sinh v$$

$$\cdot \Bigg[C_2 \, H_o^{(2)}(ky) \cos(\psi-\theta_o) + k \, H_1^{(2)}(ky) \cos\alpha \sin(\psi-\theta_o)$$

$$\cdot \Bigg[1 + C_2 \, r \int_0^{2\pi} \cos(\theta-\psi) \sin(\theta-\theta_o) \sin(\theta-\psi) d\theta \Bigg] \Bigg]$$

$$+2 \int_0^{2\pi} \sum_{n=2}^{\infty} \frac{H_n^{(2)}(ky) \cos(n\alpha) \sinh v \sin(\theta-\theta_o)}{\Gamma(n+1)}$$

$$\cdot \left[\frac{kr \cos(\theta-\psi)}{2} \right]^n r^2 \, e^{\left(\frac{-r^2}{2b^2}\right)} [1 + C_2 \, r \sin(\theta-\psi)] d\theta \Bigg] dr dv . \quad (5.24)$$

Now,

$$\lim_{b\to 0} \int_0^{\infty} \frac{r^n}{b^4} \, e^{\left(\frac{-r^2}{2b^2}\right)} dr \quad = 2, \quad n = 3,$$

$$= 0, \quad n > 3. \quad (5.25)$$

Therefore, performing the integration with respect to r in (5.24) as b tends to zero, results in

$$H_1(\rho,\phi) = \frac{-1}{8\pi}\int_{\infty-j\frac{\pi}{m}}^{\infty+j\frac{\pi}{m}}\left[C_2\, H_o^{(2)}(ky)\,\cos(\psi-\theta_o)+k\, H_1^{(2)}(ky)\,\cos\alpha\right.$$

$$\left.\cdot\sin(\psi-\theta_o)\right]\frac{\sinh v\, dv}{C_1}\,. \qquad (5.26)$$

After substitution of the expressions for C_1 and C_2 in (5.16) into (5.26), $H_1(\rho,\phi)$ is given by

$$H_1(\rho,\phi) = \eta(\rho,\phi-\psi), \qquad (5.27)$$

where

$$\eta(\rho,\xi) = \frac{-1}{8\pi}\int_{\infty-j\frac{\pi}{m}}^{\infty+j\frac{\pi}{m}}\left[\frac{\sin(\frac{\xi}{m})\, H_o^{(2)}(ky)\,\cos(\psi-\theta_o)}{\rho_o m\{\cosh v-\cos(\frac{\xi}{m})\}^2}\right.$$

$$\left.+\ \frac{k\, H_1^{(2)}(ky)\,\cos\alpha\,\sin(\psi-\theta_o)}{\cosh v-\cos(\frac{\xi}{m})}\right]\sinh v\, dv. \qquad (5.28)$$

Consider now the second term in (5.10) given by

$$H_2(\rho,\phi) = \int_0^{\infty}\int_0^{2\pi} S(r,\theta)\ \ \Omega(\rho,\phi+\phi_1)\, r\, d\theta\, dr. \qquad (5.29)$$

In the neighbourhood of $r = 0$,

$$\rho_1 \approx \rho_o + r\cos(\theta-\psi),\quad \cos(\frac{\phi+\phi_1}{m}) \approx \cos(\frac{\phi+\psi}{m}) - \frac{r}{\rho_o m}$$

$$\cdot\sin(\theta-\psi)\,\sin(\frac{\phi+\psi}{m}), \qquad (5.30)$$

enabling the denominator of $\Omega(\rho,\phi+\phi_1)$ to be written, by using the binomial theorem, as

$$\cosh v - \cos\left(\frac{\phi+\phi_1}{m}\right) = C_3[1 - C_4\, r\, \sin(\theta-\psi)] \approx \frac{C_3}{1+C_4 r\, \sin(\theta-\psi)}, \tag{5.31}$$

where

$$C_3 = \cosh v - \cos\left(\frac{\phi+\psi}{m}\right), \quad C_4 = \frac{-\sin\left(\frac{\phi+\psi}{m}\right)}{\rho_o m C_3}. \tag{5.32}$$

C_3 and C_4, like C_1 and C_2, are independent of θ and r. The development from (5.17) to (5.26) with C_1 and C_2 replaced by C_3 and C_4 respectively, enables the expression for $H_2(\rho,\phi)$ in (5.29) to be reduced to

$$H_2(\rho,\phi) = \frac{-1}{8\pi} \int_{\infty-j\frac{\pi}{m}}^{\infty+j\frac{\pi}{m}} [C_4 H_o^{(2)}(ky)\, \cos(\psi-\theta_o) + k\, H_1^{(2)}(ky)\, \cos\alpha \cdot \sin(\psi-\theta_o)]\, \frac{\sinh v\, dv}{C_3}. \tag{5.33}$$

After substituting the expressions in (5.32) into (5.33), $H_2(\rho,\phi)$ is given by

$$H_2(\rho,\phi) = \eta(\rho,-\phi,-\psi), \tag{5.34}$$

where $\eta(\rho,\xi)$ is given in (5.28). The solution $H(\rho,\phi)$ to (5.8) subject to the condition in (5.9) is given by (5.27) and (5.34) as

$$H(\rho,\phi) = \eta(\rho,\phi-\psi) + \eta(\rho,-\phi-\psi). \tag{5.35}$$

5.2(b) TRANSVERSELY POLARIZED MAGNETIC LINE SOURCE.

Consider the perfectly conducting wedge in Fig. 5.1. The co-ordinate systems in the figure are described in section 5.2(a).

The wedge is excited by the field from a transversely polarized magnetic line source $\vec{M}$ given by

$$\vec{M} = [\hat{x}\cos\theta_o + \hat{y}\sin\theta_o] \frac{\delta(\rho-\rho_o)\ \delta(\phi-\psi)}{\rho_o} . \tag{5.36}$$

The extended Maxwell equation

$$\nabla \times \vec{E} = \vec{M} - \dot{\vec{B}} \tag{5.37}$$

gives rise to the wave equation

$$\nabla^2 \vec{E} + k^2\vec{E} = -\nabla \times \vec{M} \tag{5.38}$$

in a homogeneous isotropic time-invariant medium free from electric current sources. Since

$$\nabla \times \vec{M} = \hat{z}\left(\frac{\partial M_y}{\partial x} - \frac{\partial M_x}{\partial y}\right), \quad \vec{M} = \hat{x}M_x + \hat{y}M_y, \tag{5.39}$$

it follows from (5.38) that the source distribution $\vec{M}$ will generate an electrically polarized field. Because of the curl of the delta function appearing on the right-hand side of the expression in (5.38), it is not clear how to determine the field $\vec{E}$ surrounding the wedge by using the Kontorowich-Lebedev transform. However, by considering $\vec{M}$ to be a continuous source distribution with the Gaussian form as given by the right-hand side of (5.4), it follows that

$$\nabla \times \vec{M} = \hat{z}\,S(r,\theta), \tag{5.40}$$

where $S(r,\theta)$ is defined in (5.7).

A solution is now required to

$$\vec{E} = \hat{z}E, \quad \nabla^2 E + k^2 E = -S(r,\theta), \tag{5.41}$$

subject to the boundary conditions (1.5)

$$E\Big|_{\phi = \begin{matrix} 0 \\ m\pi \end{matrix}} = 0, \quad m\pi = 2\pi - \beta. \tag{5.42}$$

The Greens function for an infinite z-directed electric line source when the field is subject to the boundary conditions in (5.42), is given by (1.16) and (1.17). Thus,

$$E(\rho,\phi) = \int_0^{\infty} \int_0^{2\pi} S(r,\theta) \quad V(\rho,\phi)\ r\ d\theta dr, \tag{5.43}$$

where

$$V(\rho,\phi) = \Omega(\rho,\phi-\phi_1) - \Omega(\rho,\phi+\phi_1), \tag{5.44}$$

and $\Omega(\rho,\xi)$ is defined in (5.12).

The two terms of (5.43) have been evaluated in section 5.2(a). Hence, from (5.27) and (5.34),

$$E(\rho,\phi) = \eta(\rho,\phi-\psi) - \eta(\rho,-\phi-\psi), \tag{5.45}$$

where $\eta(\rho,\xi)$ is defined in (5.28).

5.3(a) MANIPULATION OF $\eta(\rho,\xi)$

In this section $\eta(\rho,\xi)$ is manipulated into the same form as $\Omega(\rho,\xi)$ of (1.18), thus enabling the reflected and

diffracted field components to be readily identified.

Consider the first term of $\eta(\rho,\xi)$ in (5.28) with y defined by (5.19). Integration by parts shows that

$$\int_{\infty-j\frac{\pi}{m}}^{\infty+j\frac{\pi}{m}} \frac{H_o^{(2)}(ky)\ \sinh v\ dv}{[\cosh v-\cos(\frac{\xi}{m})]^2} = \left[\frac{-H_o^{(2)}(ky)}{\cosh v-\cos(\frac{\xi}{m})}\right]_{\infty-j\frac{\pi}{m}}^{\infty+j\frac{\pi}{m}}$$

$$+\int_{\infty-j\frac{\pi}{m}}^{\infty+j\frac{\pi}{m}} \frac{m\rho_o\ H_1^{(2)}(ky)\ k\rho\ \sinh(mv)\ dv.}{y[\cosh v-\cos(\frac{\xi}{m})]} \qquad (5.46)$$

On substituting the limits, the first term on the right-hand side of (5.46) becomes zero. $\eta(\rho,\xi)$ reduces to

$$\eta(\rho,\xi) = \frac{-1}{8\pi}\int_{\infty-j\frac{\pi}{m}}^{\infty+j\frac{\pi}{m}} \frac{k\ H_1^{(2)}(ky)}{y[\cosh v-\cos(\frac{\xi}{m})]}\Big[\rho\sin(\tfrac{\xi}{m})\ \cos(\psi-\theta_o)\ \sinh(mv)$$

$$+[\rho\ \cosh(mv)-\rho_o]\sin(\psi-\theta_o)\ \sinh v\Big]\,dv, \qquad (5.47)$$

where the expression for $\cos\alpha$ given by (5.19) has been substituted.

The contour of integration in (5.47) will be deformed

into the contour used by Jones[13] to derive (1.18) from (1.17). This contour is shown in Fig. 5.3. Using abbreviated notation,

$$\eta(\rho,\xi) = \int_{\infty-j\frac{\pi}{m}}^{\infty+j\frac{\pi}{m}} f(v)\ dv = \int_{C_1} = \int_{C_2} + \int_{C_3} + \int_{C_4} + \sigma, \tag{5.48}$$

where the definition of f(v) follows from (5.47), and σ is the sum of the residues evaluated at the included poles.

The variable of integration v can be defined along C_2 in terms of a real variable x given by

$$v = -x - j\frac{\pi}{m} . \tag{5.49}$$

Then

$$\int_{C_2} = \int_{\infty-j\frac{\pi}{m}}^{-j\frac{\pi}{m}} f(v)\ dv = -\int_{-\infty}^{0} f(-x-j\tfrac{\pi}{m})\ dx. \tag{5.50}$$

Along C_4, v can be defined in terms of x by

$$v = x + j\frac{\pi}{m} , \tag{5.51}$$

giving

$$\int_{C_4} = \int_{j\frac{\pi}{m}}^{\infty+j\frac{\pi}{m}} f(v)\ dv = \int_{0}^{\infty} f(x+j\tfrac{\pi}{m})\ dx. \tag{5.52}$$

Examination of (5.47) shows that f(v) is an odd function of v, and therefore

$$\int_{C_3} = \int_{-j\frac{\pi}{m}}^{j\frac{\pi}{m}} f(v)\ dv = 0, \tag{5.53}$$

and from (5.50) and (5.52)

$$\int_{C_2} + \int_{C_4} = \int_{-\infty}^{\infty} f(x+j\tfrac{\pi}{m})\ dx. \tag{5.54}$$

The poles of the integrand of (5.47) occur when v takes the values

$$v = \pm j(\tfrac{\xi}{m} + 2p\pi), \tag{5.55}$$

where p is any integer or zero. The contour C_3 of Fig. 5.3 must be deformed in a semicircle about each pole located on the imaginary axis within $|\xi+2p\pi m| < \pi$. The sum of the residues is given by

$$\sigma = \sum_p j\pi\left[g(j[\tfrac{\xi}{m}+2p\pi]) + g(-j[\tfrac{\xi}{m}+2p\pi])\right], \quad \forall\ |\xi+2p\pi m| < \pi, \tag{5.56}$$

where

$$g(v) = f(v)\ \frac{[\cosh v - \cos(\frac{\xi}{m})]}{\sinh v}. \tag{5.57}$$

Since g(v) is en even function of v,

$$\sigma = \sum_p 2\pi j\ g(j[\tfrac{\xi}{m} + 2p\pi]), \quad \forall \quad |\xi + 2p\pi m| < \pi. \tag{5.58}$$

By using (5.53), (5.54) and (5.58) with (5.48), $\eta(\rho,\xi)$ may

be expressed as

$$\eta(\rho,\xi) = h_1(\rho,\xi) + h_2(\rho,\xi), \tag{5.59}$$

$$h_1(\rho,\xi) = \frac{-jk}{4a} H_1^{(2)}(ka)\left[\rho\sin(\xi+\psi-\theta_o+2p\pi m)-\rho_o\sin(\psi-\theta_o)\right], \quad |\xi+2p\pi m| < \pi,$$

$$= 0, \qquad |\xi+2p\pi m| > \pi, \tag{5.60}$$

$$h_2(\rho,\xi) = \frac{-k}{8\pi}\int_{-\infty}^{\infty} \frac{H_1^{(2)}(kb)}{b[\cos(jv+\frac{\pi}{m})-\cos(\frac{\xi}{m})]}\left[\rho\sin(\tfrac{\xi}{m})\cos(\psi-\theta_o)\sinh(mv)\right.$$

$$\left.-j[\rho\cosh(mv)+\rho_o]\sin(\psi-\theta_o)\sin(jv+\tfrac{\pi}{m})\right] dv, \tag{5.61}$$

where

$$a = [\rho^2+\rho_o^2-2\rho\rho_o\cos(\xi+2p\pi m)]^{\frac{1}{2}}, \quad b = [\rho^2+\rho_o^2+2\rho\rho_o\cosh(mv)]^{\frac{1}{2}}. \tag{5.62}$$

The $h_1(\rho,\xi)$ term represents the cylindrical waves radiated directly by the line source, and those reflected by the faces of the wedge. The condition $|\xi+2p\pi m)| < \pi$ on the existence of these waves is the same as in (1.19). As discussed in section 1.3(a), when $\xi = (\phi-\psi)$ only $p=0$, $|\phi-\psi| < \pi$ satisfies the condition. When $\xi = (-\phi-\psi)$ however, $p=0$, $|\phi+\psi| < \pi$ and $p=1$, $|\phi+\psi-2\pi m| < \pi$ satisfy the condition. These three cases correspond respectively to the regions

of existence of the incident field, the field reflected by the surface $\phi = 0$, and the field reflected by the surface $\phi = m\pi$.

The $h_2(\rho,\xi)$ term represents the waves diffracted by the wedge apex. The detailed form of $h_2(\rho,\xi)$ is appreciably more complicated than $\omega_2(\rho,\xi)$ of (1.20) which is the corresponding expression for z-polarized line sources. However, when the transversely polarized line source is a great distance from the apex of the wedge such that $\rho_o >> \rho$, the use of (1.21) enables $h_1(\rho,\xi)$ and $h_2(\rho,\xi)$ to be expressed as

$$h_1(\rho,\xi) = -jk \sin(\psi-\theta_o)\, e^{jk\rho\cos(\xi+2p\pi m)}, \quad |\xi+2p\pi m| < \pi,$$
$$= 0, \quad |\xi+2p\pi m| > \pi, \tag{5.63}$$

$$h_2(\rho,\xi) = \frac{-jk}{2\pi} \sin(\psi-\theta_o) \int_{-\infty}^{\infty} \frac{\sin(jv+\frac{\pi}{m})\, e^{-jk\rho\cosh(mv)}}{\cos(jv+\frac{\pi}{m}) - \cos(\frac{\xi}{m})}\, dv, \tag{5.64}$$

where the normalization factor (1.22) has been removed.

Examination of the expressions in (5.63) and (5.64) shows that they are identical to the corresponding expressions (1.24) and (1.25) for the z-polarized line source, multiplied by the factor $[-jk\sin(\psi-\theta_o)]$. This factor describes the far field radiation pattern of the transversely polarized line source. Consequently, when the line sources are transversely polarized, the appropriate far field diffraction coefficients of the geometrical theory of diffraction are

the same as those used when the line sources are z-polarized.

The reason why $\eta(\rho,\xi)$ is not reciprocal in ρ and ρ_o is that when the source of the field is a transversely polarized electric current element, $\eta(\rho,\xi)$ is proportional to H_z, which implies that the field is being observed with a z-polarized magnetic current receiving element.

When the point (ρ,ϕ) at which the field is observed is a large distance from the wedge apex, the asymptotic form of the Hankel function (1.21) can be used to expand $H_1^{(2)}(ka)$ and $H_1^{(2)}(kb)$. Thus, from (5.60) - (5.62),

$$a \sim \rho - \rho_o \cos(\xi+2p\pi m), \quad b \sim \rho + \rho_o \cosh(mv), \quad \rho >> \rho_o, \tag{5.65}$$

$$H_1^{(2)}(ka) \sim \sqrt{\frac{2}{\pi k\rho}}\, e^{-j[k\rho - k\rho_o \cos(\xi+2p\pi m) - \frac{3\pi}{4}]}, \quad \rho >> \rho_o, \tag{5.66}$$

$$H_1^{(2)}(kb) \sim \sqrt{\frac{2}{\pi k\rho}}\, e^{-j[k\rho + k\rho_o \cosh(mv) - \frac{3\pi}{4}]}, \quad \rho >> \rho_o. \tag{5.67}$$

After normalization by the factor (4.1), $h_1(\rho,\xi)$ and $h_2(\rho,\xi)$ reduce to

$$h_1(\rho,\xi) = \frac{k}{4} \sin(\xi+\psi-\theta_o+2p\pi m)\, e^{jk\rho_o \cos(\xi+2p\pi m)}, \quad |\xi+2p\pi m| < \pi,$$

$$= 0, \quad |\xi+2p\pi m| > \pi, \tag{5.68}$$

$$h_2(\rho,\xi) = \frac{-jk}{8\pi} \int_{-\infty}^{\infty} \frac{e^{-jk\rho_o \cosh(mv)}}{\cos(jv+\frac{\pi}{m}) - \cos(\frac{\xi}{m})} \left[\sin(\tfrac{\xi}{m})\, \cos(\psi-\theta_o)\, \sinh(mv) - j\cosh(mv)\, \sin(\psi-\theta_o)\, \sin(jv+\tfrac{\pi}{m})\right] dv. \tag{5.69}$$

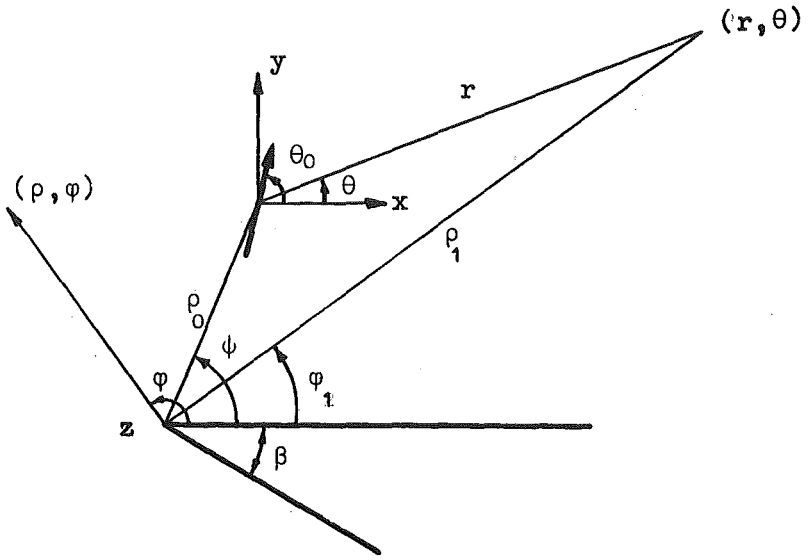

Figure 5.1 Wedge in the presence of a transversely polarized line source. z axis is perpendicular to the paper.

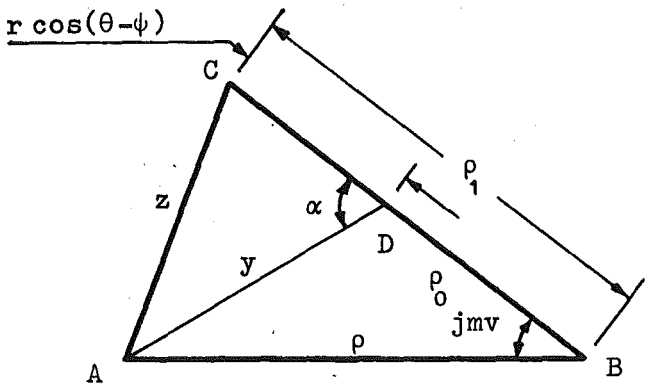

Figure 5.2

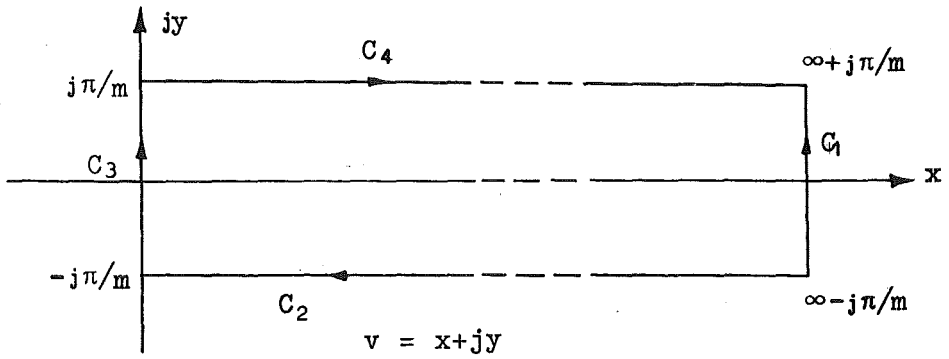

Figure 5.3

CHAPTER 6

The iterative surface current density replacement technique is introduced and applied to the problem of determining the scattering from a perfectly conducting truncated wedge when the field is electrically or magnetically polarized. The results of this Chapter are used in Chapter 7 to derive new edge diffraction coefficients.

6.1(a) THE I.R. TECHNIQUE.

In the iterative surface current density replacement (I.R.) technique the expression for the field is derived by summing an infinite number of field terms. Each term (other than the first) is directly dependent upon the preceeding term. It is postulated that the result of the summation is an exact description of the field surrounding the scattering body. However, it must be emphasized that the convergence of the series has not been proved, even though the application of the I.R. technique to determine the scattering from a truncated wedge suggests that the first terms in the series dominate the remainder.

The I.R. technique can be formulated for any body which is the intersection (in the set theory sense) of two perfectly conducting bodies from which the scattering is known explicitly. Some two-dimensional examples are the truncated wedge of Fig. 6.5 which can be regarded as the intersection of two infinite wedges; and

the cylinders of Fig. 6.6, which can be regarded as the intersection of two circular cylinders, and a circular cylinder and an infinite wedge respectively.

The I.R. technique will be described by applying it to the truncated wedge problem.

Consider the perfectly conducting wedge in Fig. 6.1 illuminated by an incident field $\vec{U}^i$. The wedge surfaces are defined by $\phi = 0$ and $\phi = 2\pi-\beta$ in the (ρ, ϕ, z) cylindrical polar co-ordinate system whose origin is at the wedge apex. $\vec{K}_1(r)$ is defined to be the induced surface current density at a distance r from the wedge apex on the surface $\phi = 2\pi-\beta$. The total field $\vec{U}_1$ is zero everywhere inside the wedge.

Now consider the perfectly conducting wedge in Fig. 6.2. The wedge surfaces are defined by $\theta = 0$ and $\theta = 2\pi-\alpha$ in the (s, θ, z) cylindrical polar co-ordinate system whose origin is at the wedge apex. The wedge is illuminated by the field radiated from a source distribution $[-\vec{K}_1(s+w)]$, $s \geq 0$ on $\theta = \pi$. The induced surface current density at a distance t from the wedge apex on the surface $\theta = 0$ is defined to be $\vec{K}_2(t)$. The total field $\vec{U}_2$ is zero everywhere inside the wedge.

Consider the wedge in Fig. 6.1 illuminated by the field radiated from a source distribution $[-\vec{K}_2(\rho+w)]$, $\rho \geq 0$ on $\phi=\pi-\beta$ as shown in Fig. 6.3. The induced surface current density on the surface $\phi = 2\pi-\beta$ is defined to be $\vec{K}_3(r)$.

In general, define $\vec{U}_{2n}$, $n \geq 1$ to be the field surrounding the wedge in Fig. 6.2 when the incident field is radiated by the source distribution $[-\vec{K}_{2n-1}(s+w)]$, $s \geq 0$ on $\theta=\pi$. $\vec{U}_{2n}$ is zero everywhere inside the wedge in Fig. 6.2. Define $\vec{U}_{2n+1}$, $n \geq 1$ to be the field surrounding the wedge in Fig. 6.3 when the incident field is radiated by the source distribution $[-\vec{K}_{2n}(\rho+w)]$, $\rho \geq 0$ on $\phi=\pi-\beta$. $\vec{U}_{2n+1}$ is zero everywhere inside the wedge in Fig. 6.3. The surface current densities $\vec{K}_n$ are defined from (1.33) as

$$\vec{K}_{2n}(t) = \hat{\theta} \times \vec{H}_{2n}\Big|_{\theta = 0} , \quad \vec{K}_{2n-1}(r) = -\hat{\phi} \times \vec{H}_{2n-1}\Big|_{\phi = 2\pi-\beta} , \tag{6.1}$$

where $\hat{\theta}$ and $\hat{\phi}$ are unit vectors in the θ and ϕ directions respectively.

Now consider the truncated wedge in Fig. 6.4 illuminated by an incident field $\vec{U}^i$. The cylindrical polar co-ordinate systems (ρ,ϕ,z) and (s,θ,z) have their origins at the edges with internal angles β and α respectively. The I.R. technique postulates that the total field $\vec{U}^t$ surrounding the truncated wedge is given by

$$\vec{U}^t = \sum_{n=1}^{\infty} \vec{U}_n , \tag{6.2}$$

where the fields $\vec{U}_n$ have been defined above; and that $\vec{U}^t$ is approximated with a finite error by $\vec{U}^t_N$, where

$$\vec{U}^t_N = \sum_{n=1}^{N} \vec{U}_n , \tag{6.3}$$

N being a finite positive integer. The expression in (6.2) states that the problem illustrated in Fig. 6.4 is equivalent to the superposition of the problem illustrated in Fig. 6.1 and the infinite number of problems each illustrated by either Fig. 6.2 or Fig. 6.3. Notice that $\vec{U}^t$ is zero everywhere inside the truncated wedge as required. The convergence of the series in (6.2) and the validity of the approximation in (6.3) have not been proved.

6.2(a) TRUNCATED WEDGE. (Electric Polarization).

The I.R. technique is used in this section to determine the approximation $\vec{A}_2^t$ to the electrically polarized field scattered by the perfectly conducting truncated wedge in Fig. 6.4. The notation used in this section follows that of section 6.1(a).

Three main steps are required to determine $\vec{A}_2^t$. Firstly the field $\vec{A}_1$ surrounding the wedge of Fig. 6.1 is determined. Then the surface current density $\vec{K}_1(r)$ is calculated, and finally an expression for the field $\vec{A}_2$ surrounding the wedge in Fig. 6.2 is obtained.

Consider the wedge in Fig. 6.1 illuminated by an electrically polarized plane wave. The incident magnetic vector potential $\vec{A}^i$ is given by

$$\vec{A} = \hat{z}\, A, \qquad A^i = e^{jk\rho\cos(\phi-\psi)}. \tag{6.4}$$

The total field A_1 surrounding the wedge is given in (1.16) as

$$A_1(\rho,\phi) = \Omega(\rho,\phi-\psi) - \Omega(\rho,\phi+\Psi), \tag{6.5}$$

where

$$\Omega(\rho,\xi) = \omega_1(\rho,\xi) + \omega_2(\rho,\xi), \tag{6.6}$$

and $\omega_1(\rho,\xi)$ and $\omega_2(\rho,\xi)$ are defined in (1.24) and (1.25) respectively.

The surface current density $\vec{K}_1(r)$ on the surface $\phi = 2\pi-\beta$ is calculated using (6.1) and (2.22) as

$$\vec{K}_1(r) = -\frac{\hat{\phi}}{\mu} \times (\nabla \times \vec{A}_1)\Big|_{\phi = m\pi}, \quad m\pi = 2\pi-\beta, \tag{6.7}$$

which reduces to

$$\vec{K}_1(r) = \hat{z}\, K_1(r), \quad K_1(r) = \frac{1}{\mu r} \frac{\partial A_1}{\partial \phi}\Big|_{\phi = m\pi}. \tag{6.8}$$

Defining

$$\frac{\partial}{\partial \xi}[\omega(\rho,\xi)]\Big|_{\xi=\chi} = \omega'(\rho,\chi), \tag{6.9}$$

enables $K_1(r)$ to be expressed as

$$K_1(r) = \frac{1}{\mu r}\left[\omega_1'(r,m\pi-\psi)+\omega_2'(r,m\pi-\psi)\right.$$

$$\left.-\omega_1'(r,m\pi+\psi) - \omega_2'(r,m\pi+\psi)\right]. \qquad (6.10)$$

From (1.24)

$$\omega_1'(r,\xi) = jkr\,\sin(\xi+2\pi pm)e^{jkr\cos(\xi+2\pi pm)}, \quad |\xi+2\pi pm| < \pi,$$
$$= 0, \qquad |\xi+2\pi pm| > \pi, \qquad (6.11)$$

and from (1.25),

$$\omega_2'(r,\xi) = \frac{-\sin(\frac{\xi}{m})}{2\pi m}\int_{-\infty}^{\infty}\frac{\sin(jv+\frac{\pi}{m})\ e^{-jkr\cosh(mv)}}{[\cos(jv+\frac{\pi}{m})-\cos(\frac{\xi}{m})]^2}\,dv. \qquad (6.12)$$

Performing the integration in (6.12) by parts gives

$$\omega_2'(r,\xi) = \frac{-kr}{2\pi}\sin(\frac{\xi}{m})\int_{-\infty}^{\infty}\frac{\sinh(mv)e^{-jkr\ \cosh(mv)}}{\cos(jv+\frac{\pi}{m})-\cos(\frac{\xi}{m})}\,dv, \qquad (6.13)$$

from which it is deduced that

$$\omega_2'(r,m\pi-\psi) = -\omega_2'(r,m\pi+\psi). \qquad (6.14)$$

The condition associated with the expression in (6.11) demands that $\omega_1'(r,m\pi-\psi)$ be zero unless $p=0$, $\pi-\beta < \psi < m\pi$; and that $\omega_1'(r,m\pi+\psi)$ be zero unless $p=-1$, $\pi-\beta < \psi < m\pi$. From (6.11),

$$\omega_1'(r,m\pi-\psi)\Big|_{p=0} = -\omega_1'(r,m\pi+\psi)\Big|_{p=-1}. \qquad (6.15)$$

Using (6.14) and (6.15) enables the expression in (6.10) to be reduced to

$$K_1(r) = \frac{2}{\mu r}[\varepsilon_2\ \omega_1'(r,m\pi-\psi)\Big|_{p=0} + \omega_2'(r,m\pi-\psi)],$$

$$\varepsilon_2 = 1, \quad \pi-\beta < \psi < m\pi,$$
$$= 0, \quad \psi < \pi-\beta, \quad \psi > m\pi, \tag{6.16}$$

where, from (6.11) and (6.13),

$$\frac{2}{\mu r}\ \omega_1'(r,m\pi-\psi)\Big|_{p=0} = \frac{-2jk}{\mu}\sin(m\pi-\psi)\ e^{jkr\cos(m\pi-\psi)}, \tag{6.17}$$

$$\frac{2}{\mu r}\ \omega_2'(r,m\pi-\psi) = \frac{-k}{\mu\pi}\sin(\tfrac{\psi}{m})\int_{-\infty}^{\infty}\frac{\sinh(mv)\ e^{-jkr\cosh(mv)}}{\cos(jv+\frac{\pi}{m})+\cos(\frac{\psi}{m})}\,dv. \tag{6.18}$$

Now consider the wedge in Fig. 6.2. The source distribution on $\theta=\pi$ is $[-\vec{K}_1(s_o+w)]$, $s_o \geq 0$, where s_o is the distance from the wedge apex to a point on $\theta=\pi$. The total field $\vec{A}_2$ surrounding the wedge is the sum of the fields due to all the elemental sources. Thus,

$$A_2(s,\theta) = -\mu\int_0^{\infty} K_1(s_o+w)\ A(s,\theta)\ ds_o, \tag{6.19}$$

where from (1.16),

$$A(s,\theta) = \Omega(s,\theta-\pi)-\Omega(s,\theta+\pi), \tag{6.20}$$

and $\Omega(s,\xi)$ is defined by (1.18). Let $s >> s_o$ for all important contributions from the source distribution $[-K_1(s_o+w)]$. Then $\omega_1(s,\xi)$ and $\omega_2(s,\xi)$ of (1.19) and (1.20)

can be expanded by using the asymptotic form of the Hankel function in (1.21), and after normalizing by the factor

$$\sqrt{\frac{2j}{\pi ks}}\ e^{-jks} \tag{6.21}$$

become

$$\omega_1(s,\xi) = \frac{-j}{4}\, e^{jks_o\cos(\xi+2\pi pn)}, \qquad |\xi+2\pi pn| < \pi, \quad s >> s_o,$$

$$= 0, \qquad |\xi+2\pi pn| > \pi, \tag{6.22}$$

and

$$\omega_2(s,\xi) = \frac{-j}{8\pi}\int_{-\infty}^{\infty} \frac{\sin(j\omega+\frac{\pi}{n})\ e^{-jks_o\cosh(n\omega)}}{\cos(j\omega+\frac{\pi}{n}) - \cos(\frac{\xi}{n})}\, d\omega, \quad s >> s_o, \tag{6.23}$$

where

$$n\pi = 2\pi-\alpha. \tag{6.24}$$

The condition associated with the expression in (6.22) demands that $\omega_1(s,\theta-\pi)$ be zero unless $p=0$; and that $\omega_1(s,\theta+\pi)$ be zero unless $p=-1$, $2\pi-2\alpha < \theta \leqslant n\pi$. Thus,

$$\omega_1(s,\theta-\pi) = \frac{-j}{4}\, e^{-jks_o\cos\theta}, \tag{6.25}$$

$$\omega_1(s,\theta+\pi) = \frac{-\varepsilon_o j}{4}\, e^{-jks_o\cos(\theta+2\alpha)}, \quad \varepsilon_o = 1, \ 2\pi-2\alpha < \theta \leqslant n\pi,$$

$$= 0, \ 0 < \theta < 2\pi-2\alpha, \tag{6.26}$$

and $A(s,\theta)$ is given from (6.20) - (6.26) by

$$A(s,\theta) = \frac{-j}{4}\left[e^{-jks_o\cos\theta} - \varepsilon_o\, e^{-jks_o\cos(\theta+2\alpha)}\right.$$

$$+ \frac{1}{2\pi}\int_{-\infty}^{\infty} \sin(j\omega+\tfrac{\pi}{n})\, e^{-jks_o\cosh(n\omega)}\left[\left[\cos(j\omega+\tfrac{\pi}{n}) - \cos(\tfrac{\theta-\pi}{n})\right]^{-1}\right.$$

$$\left.\left. - \left[\cos(j\omega+\tfrac{\pi}{n}) - \cos(\tfrac{\theta+\pi}{n})\right]^{-1}\right] d\omega\right]. \qquad (6.27)$$

Substituting (6.17) and (6.18) into (6.19) gives

$$A_2(s,\theta) = k\int_0^{\infty}\left[\varepsilon_2\; 2j\sin(m\pi-\psi)\; e^{jk(s_o+w)\cos(m\pi-\psi)}\right.$$

$$\left. + \frac{\sin(\frac{\psi}{m})}{\pi}\int_{-\infty}^{\infty} \frac{\sinh(mv)\, e^{-jk(s_o+w)\cosh(mv)}}{\cos(jv+\frac{\pi}{n}) + \cos(\frac{\psi}{n})}\, dv\right] A(s,\theta)\, ds_o. \qquad (6.28)$$

Using the expression in (4.46) to perform the integration with respect to s_o results in

$$A_2(s,\theta) = \tfrac{1}{2}\left[\varepsilon_2\; j\,\sin(\beta+\psi)\, e^{jkw\cos(\beta+\psi)}\, F(\beta+\psi)\right.$$

$$\left. - \frac{\sin(\frac{\psi}{m})}{2\pi}\int_{-\infty}^{\infty} \frac{\sinh(mv)\, e^{-jkw\cosh(mv)}}{\cos(jv+\frac{\pi}{m}) + \cos(\frac{\psi}{m})}\, F(jmv+\pi)\, dv\right], \qquad (6.29)$$

where

$$F(\xi) = [\cos\theta-\cos\xi]^{-1} - \varepsilon_o[\cos(\theta+2\alpha) - \cos\xi]^{-1}$$

$$+ \frac{1}{2\pi}\int_{-\infty}^{\infty} \frac{\sin(j\omega+\frac{\pi}{n})}{\cosh(n\omega)-\cos\xi}\left[[\cos(j\omega+\frac{\pi}{n})-\cos(\frac{\theta-\pi}{n})]^{-1}\right.$$

$$\left. - [\cos(j\omega+\frac{\pi}{n})-\cos(\frac{\theta+\pi}{n})]^{-1}\right] d\omega \ . \qquad (6.30)$$

Since $0 \leqslant (\beta+\psi) \leqslant 2\pi$, the substitution of $x = j(\beta+\psi-\pi)$ in Appendix 5 is valid. Hence,

$$F(\beta+\psi) = \frac{-\sin(\frac{\beta+\psi-\pi}{n})}{n\ \sin(\beta+\psi)}\left[[\cos(\frac{\beta+\psi-\pi}{n})-\cos(\frac{\theta-\pi}{n})]^{-1}\right.$$

$$\left.-[\cos(\frac{\beta+\psi-\pi}{n})-\cos(\frac{\theta+\pi}{n})]^{-1}\right], \qquad (6.31)$$

and also from Appendix 5,

$$F(jmv+\pi) = \frac{\sinh(\frac{mv}{n})}{n\ \sinh(mv)}\left[[\cosh(\frac{mv}{n})-\cos(\frac{\theta-\pi}{n})]^{-1}\right.$$

$$\left.-[\cosh(\frac{mv}{n}) - \cos(\frac{\theta+\pi}{n})]^{-1}\right]. \qquad (6.32)$$

The substitution of (6.31) and (6.32) into (6.29) results in

$$A_2(s,\theta) = \frac{-j\varepsilon 2}{2n} \sin\left(\frac{\beta+\psi-\pi}{n}\right) e^{jkw\cos(\beta+\psi)} \left[\left[\cos\left(\frac{\beta+\psi-\pi}{n}\right) - \cos\left(\frac{\theta-\pi}{n}\right)\right]^{-1} \right.$$

$$\left. - \left[\cos\left(\frac{\beta+\psi-\pi}{n}\right) - \cos\left(\frac{\theta+\pi}{n}\right)\right]^{-1} \right]$$

$$\frac{-\sin\left(\frac{\psi}{m}\right)}{4\pi n} \int_{-\infty}^{\infty} \frac{\sinh\left(\frac{mv}{n}\right) e^{-jkw\cosh(mv)}}{\cos\left(jv+\frac{\pi}{m}\right) + \cos\left(\frac{\psi}{m}\right)} \left[\left[\cosh\left(\frac{mv}{n}\right) - \cos\left(\frac{\theta-\pi}{n}\right)\right]^{-1} \right.$$

$$\left. - \left[\cosh\left(\frac{mv}{n}\right) - \cos\left(\frac{\theta+\pi}{n}\right)\right]^{-1} \right] dv. \qquad (6.33)$$

Notice that $A_2(s,\theta)$ as given in (6.33) is independent of ε_o, which in (6.26) defines the reflection boundary of the field radiated by the source distribution on $\theta = \pi$.

The field $\vec{A}_2^t$, defined with N=2 in (6.3), is given as

$$\vec{A}_2^t = \hat{z}\,(A_1 + A_2), \qquad (6.34)$$

where A_1 is given in (6.5), and A_2 is obtained by multiplying the expression in (6.33) by the normalization factor in (6.21).

6.2(b) TRUNCATED WEDGE. (Magnetic Polarization).

The I.R. technique is used to determine the approximation $\vec{H}_2^t$ to the magnetically polarized field scattered by the perfectly conducting truncated wedge in Fig. 6.4. The notation used in this section follows that of section 6.1(a).

Three main steps are required to determine $\vec{H}_2^t$. Firstly, the field $\vec{H}_1$ surrounding the wedge of Fig. 6.1 is determined. Then the surface current density $\vec{K}_1(r)$ is calculated, and finally an expression for the field $\vec{H}_2$ surrounding the wedge in Fig. 6.2 is obtained.

Consider the wedge in Fig. 6.1 illuminated by a magnetically polarized plane wave. The incident magnetic field intensity $\vec{H}^i$ is given by

$$\vec{H} = \hat{z}\, H, \quad H^i = e^{jk\rho\cos(\phi-\psi)}. \tag{6.35}$$

The total field H_1 surrounding the wedge is given in (1.16) as

$$H_1(\rho,\phi) = \Omega(\rho,\phi-\psi) + \Omega(\rho,\phi+\psi), \tag{6.36}$$

where

$$\Omega(\rho,\xi) = \omega_1(\rho,\xi) + \omega_2(\rho,\xi), \tag{6.37}$$

and $\omega_1(\rho,\xi)$ and $\omega_2(\rho,\xi)$ are defined in (1.24) and (1.25) respectively.

The surface current density $\vec{K}_1(r)$ on the surface $\phi = 2\pi-\beta$ is calculated from (6.1) as

$$\vec{K}_1(r) = -\hat{\phi} \times \vec{H}_1 \Big|_{\phi = 2\pi-\beta}. \tag{6.38}$$

After substituting the expressions in (6.35) and (6.36) into (6.38), and using the definition of $m\pi$ in (6.7), $\vec{K}_1(r)$ is described by

$$\vec{K}_1(r) = -\hat{r}\,[\Omega(r,m\pi-\psi)+\Omega(r,m\pi+\psi)], \qquad (6.39)$$

where

$$\hat{r} = \hat{\rho}\cos(\phi+\beta)-\hat{\phi}\sin(\phi+\beta). \qquad (6.40)$$

The condition associated with the expression in (1.24) demands that $\omega_1(r,m\pi-\psi)$ be zero unless $p=0$, $\pi-\beta < \psi < m\pi$; and that $\omega_1(r,m\pi+\psi)$ be zero unless $p=-1$, $\pi-\beta < \psi < m\pi$. Since, from (1.24) and (1.25)

$$\omega_1(r,m\pi-\psi)\Big|_{p=0} = \omega_1(r,m\pi+\psi)\Big|_{p=-1}, \qquad (6.41)$$

and

$$\omega_2(r,m\pi-\psi) = \omega_2(r,m\pi+\psi), \qquad (6.42)$$

the surface current density $\vec{K}_1(r)$ in (6.39) is given by

$$\vec{K}_1(r) = -2\hat{r}\left[\varepsilon_2 e^{jkr\cos(\psi+\beta)} + \frac{1}{2\pi}\int_{-\infty}^{\infty} \frac{\sin(jv+\frac{\pi}{m})\; e^{-jkr\cosh(mv)}}{\cos(jv+\frac{\pi}{m}) + \cos(\frac{\psi}{m})}\, dv\right], \qquad (6.43)$$

where ε_2 is defined in (6.16).

Now consider the wedge in Fig. 6.2. The source distribution on $\theta=\pi$ is $[-\vec{K}_1(s_o+w)]$, $s_o \geq 0$, where s_o is the distance from the wedge apex to a point on $\theta=\pi$. In the (s,θ,z) co-ordinate system $\hat{r}$ is defined by

$$\hat{r} = -\hat{s}\cos\theta + \hat{\theta}\sin\theta. \qquad (6.44)$$

The Greens function for the field surrounding a perfectly conducting wedge in the presence of a transversely polarized line source is derived in section 5.2(a). Let $s >> s_o$ for all important contributions from the source distribution $[-\vec{K}_1(s_o+w)]$. Then the Greens function $\vec{H}(s,\theta)$ is given by (5.35) as

$$\vec{H}(s,\theta) = \hat{z}\, H(s,\theta), \quad H(s,\theta) = \eta(s,\theta-\pi) + \eta(s,-\theta-\pi), \tag{6.45}$$

$$\eta(s,\xi) = h_1(s,\xi) + h_2(s,\xi), \tag{6.46}$$

where, from (5.68) and (5.69) after normalization by the factor in (6.21),

$$h_1(s,\xi) = \frac{k}{4}\sin(\xi+\pi-\theta_o+2p\pi n)\, e^{jks_o\cos(\xi+2p\pi n)}, \quad |\xi+2p\pi n| < \pi,$$
$$= 0, \qquad |\xi+2p\pi n| > \pi, \tag{6.47}$$

$$h_2(s,\xi) = \frac{jk}{8\pi}\int_{-\infty}^{\infty} \frac{e^{-jks_o\cosh(n\omega)}}{\cos(j\omega+\frac{\pi}{n})-\cos(\frac{\xi}{n})}\left[\sin(\tfrac{\xi}{n})\cos\theta_o\sinh(n\omega)\right.$$
$$\left. +j\cosh(n\omega)\sin\theta_o\sin(j\omega+\tfrac{\pi}{n})\right]d\omega. \tag{6.48}$$

The condition associated with the expression in (6.47) demands that $h_1(s,\theta-\pi)$ be zero unless $p=0$; and that $h_1(s,-\theta-\pi)$ be zero unless $p=1$, $2\pi-2\alpha < \theta \leq n\pi$. Thus

$$h_1(s,\theta-\pi) = \frac{k}{4}\sin(\theta-\theta_o)e^{-jks_o\cos\theta} \tag{6.49}$$

$$h_1(s,-\theta-\pi) = -\varepsilon_o\,\frac{k}{4}\sin(\theta+\theta_o+2\alpha)e^{-jks_o\cos(\theta+2\alpha)}, \tag{6.50}$$

where ε_o is defined in (6.26).

By defining

$$\vec{K}_1(s_o+w) = \hat{r}\, K_1(s_o+w), \tag{6.51}$$

the polarization angle θ_o becomes (see Fig. 5.1)

$$\theta_o = \pi. \tag{6.52}$$

Using (6.47) - (6.52), $H(s,\theta)$ defined in (6.45) reduces to

$$H(s,\theta) = -\frac{k}{4}\left[\sin\theta\; e^{-jks_o\cos\theta} - \varepsilon_o \sin(\theta+2\alpha)\; e^{-jks_o\cos(\theta+2\alpha)}\right.$$

$$+ \frac{j}{2\pi}\int_{-\infty}^{\infty} \sinh(n\omega)\; e^{-jks_o\cosh(n\omega)}\left[\frac{\sin(\frac{\theta-\pi}{n})}{\cos(j\omega+\frac{\pi}{n})-\cos(\frac{\theta-\pi}{n})}\right.$$

$$\left.\left. - \frac{\sin(\frac{\theta+\pi}{n})}{\cos(j\omega+\frac{\pi}{n})-\cos(\frac{\theta+\pi}{n})}\right]\, d\omega\right]. \tag{6.53}$$

The total field $\vec{H}_2$ surrounding the wedge is the sum of the fields due to all the elemental line sources in the distribution $[-\vec{K}_1(s_o+w)]$. Thus,

$$H_2(s,\theta) = -\int_o^{\infty} K_1(s_o+w)\; H(s,\theta)\; ds_o, \tag{6.54}$$

which becomes, after substituting the expressions in (6.43) and (6.51),

$$H_2(s,\theta) = 2\int_0^{\infty}\left[\varepsilon_2\, e^{jk(s_o+w)\cos(\psi+\beta)}\right.$$

$$\left. + \frac{1}{2\pi}\int_{-\infty}^{\infty}\frac{\sin(jv+\frac{\pi}{m})\, e^{-jk(s_o+w)\cosh(mv)}}{\cos(jv+\frac{\pi}{m}) + \cos(\frac{\psi}{m})}\, dv\right] H(s,\theta)\, ds_o. \qquad (6.55)$$

Using the result in (4.46) to perform the integration with respect to s_o gives

$$H_2(s,\theta) = \frac{j}{2}\left[\varepsilon_2 e^{jkw\cos(\psi+\beta)} F(\beta+\psi)\right.$$

$$\left. + \frac{1}{2\pi}\int_{-\infty}^{\infty}\frac{\sin(jv+\frac{\pi}{m})\, e^{-jkw\cosh(mv)}}{\cos(jv+\frac{\pi}{m}) + \cos(\frac{\psi}{m})}\, F(jmv+\pi)\, dv\right], \qquad (6.56)$$

where

$$F(\xi) = \frac{\sin\theta}{\cos\theta-\cos\xi} - \frac{\varepsilon_o \sin(\theta+2\alpha)}{\cos(\theta+2\alpha)-\cos\xi}$$

$$+ \frac{j}{2\pi}\int_{-\infty}^{\infty}\frac{\sinh(n\omega)}{\cosh(n\omega)-\cos\xi}\left[\frac{\sin(\frac{\theta-\pi}{n})}{\cos(j\omega+\frac{\pi}{n})-\cos(\frac{\theta-\pi}{n})}\right.$$

$$\left. - \frac{\sin(\frac{\theta+\pi}{n})}{\cos(j\omega+\frac{\pi}{n})-\cos(\frac{\theta+\pi}{n})}\right] d\omega. \qquad (6.57)$$

Since $0 \leq (\beta+\psi) \leq 2\pi$, the substitution of $x = j(\beta+\psi-\pi)$ in Appendix 6 is valid. Hence,

$$F(\beta+\psi) = \frac{-1}{n}\left[\frac{\sin(\frac{\theta-\pi}{n})}{\cos(\frac{\beta+\psi-\pi}{n})-\cos(\frac{\theta-\pi}{n})} - \frac{\sin(\frac{\theta+\pi}{n})}{\cos(\frac{\beta+\psi-\pi}{n})-\cos(\frac{\theta+\pi}{n})}\right], \quad (6.58)$$

and also from Appendix 6,

$$F(jmv+\pi) = \frac{-1}{n}\left[\frac{\sin(\frac{\theta-\pi}{n})}{\cosh(\frac{mv}{n})-\cos(\frac{\theta-\pi}{n})} - \frac{\sin(\frac{\theta+\pi}{n})}{\cosh(\frac{mv}{n})-\cos(\frac{\theta+\pi}{n})}\right]. \quad (6.59)$$

The substitution of the expressions in (6.58) and (6.59) into (6.56) gives

$$H_2(s,\theta) = \frac{-\varepsilon_2 j}{2n} e^{jkw\cos(\psi+\beta)}\left[\frac{\sin(\frac{\theta-\pi}{n})}{\cos(\frac{\beta+\psi-\pi}{n})-\cos(\frac{\theta-\pi}{n})}\right.$$

$$\left. - \frac{\sin(\frac{\theta+\pi}{n})}{\cos(\frac{\beta+\psi-\pi}{n})-\cos(\frac{\theta+\pi}{n})}\right]$$

$$\frac{-j}{4\pi n}\int_{-\infty}^{\infty} \frac{\sin(jv+\frac{\pi}{m})e^{-jkw\cosh(mv)}}{\cos(jv+\frac{\pi}{m})+\cos(\frac{\psi}{m})}\left[\frac{\sin(\frac{\theta-\pi}{n})}{\cosh(\frac{mv}{n})-\cos(\frac{\theta-\pi}{n})}\right.$$

$$\left. - \frac{\sin(\frac{\theta+\pi}{n})}{\cosh(\frac{mv}{n})-\cos(\frac{\theta+\pi}{n})}\right] dv. \quad (6.60)$$

Notice that $H_2(s,\theta)$ as given in (6.60) is independent of ε_o which defines the reflection boundary of the field radiated by the source distribution on $\theta=\pi$.

The field $\vec{H}_2^t$, defined with N=2 in (6.3), is given as

$$\vec{H}_2^t = \hat{z}\ (H_1 + H_2), \quad (6.61)$$

where H_1 is given in (6.36), and H_2 is obtained by multiplying the expression in (6.60) by the normalization factor in (6.21).

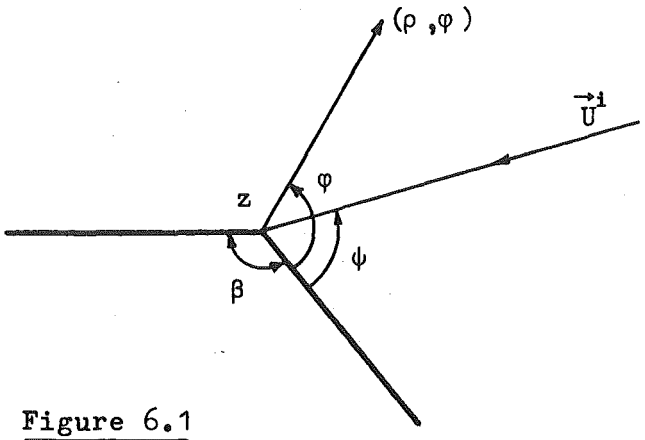

Figure 6.1

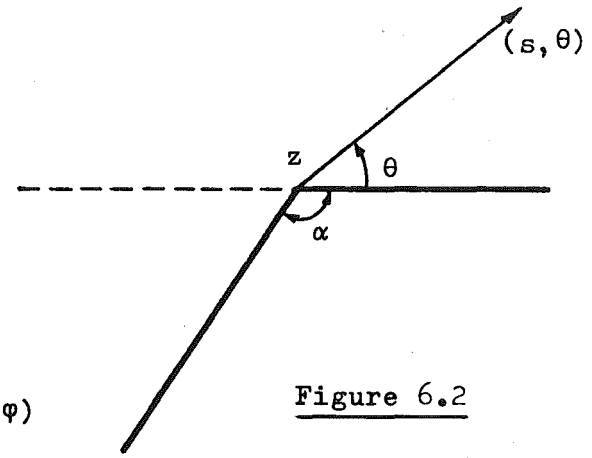

Figure 6.2

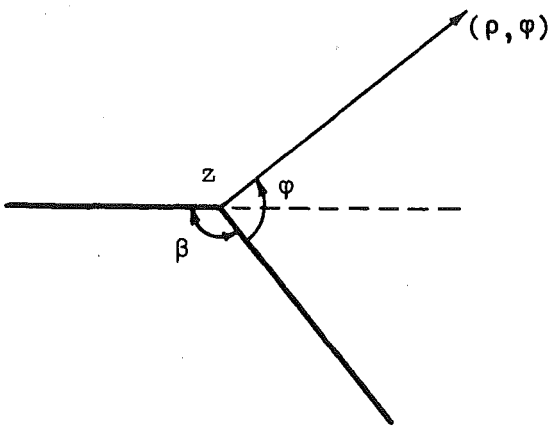

Figure 6.3

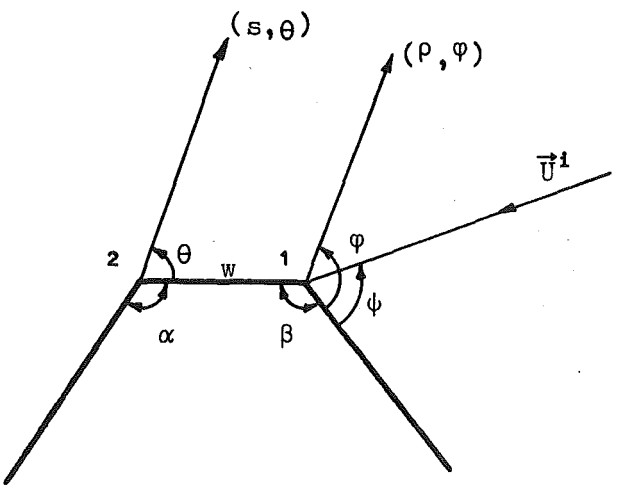

Figure 6.4

z axis perpendicular to the paper

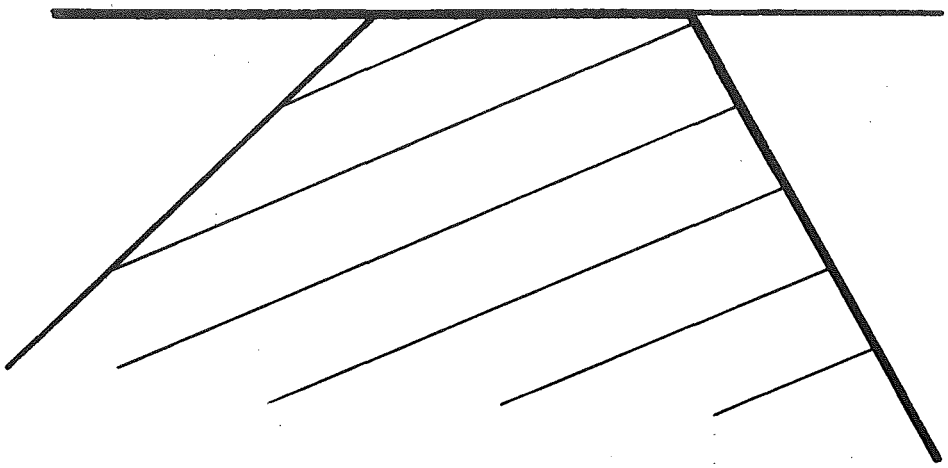

Figure 6.5

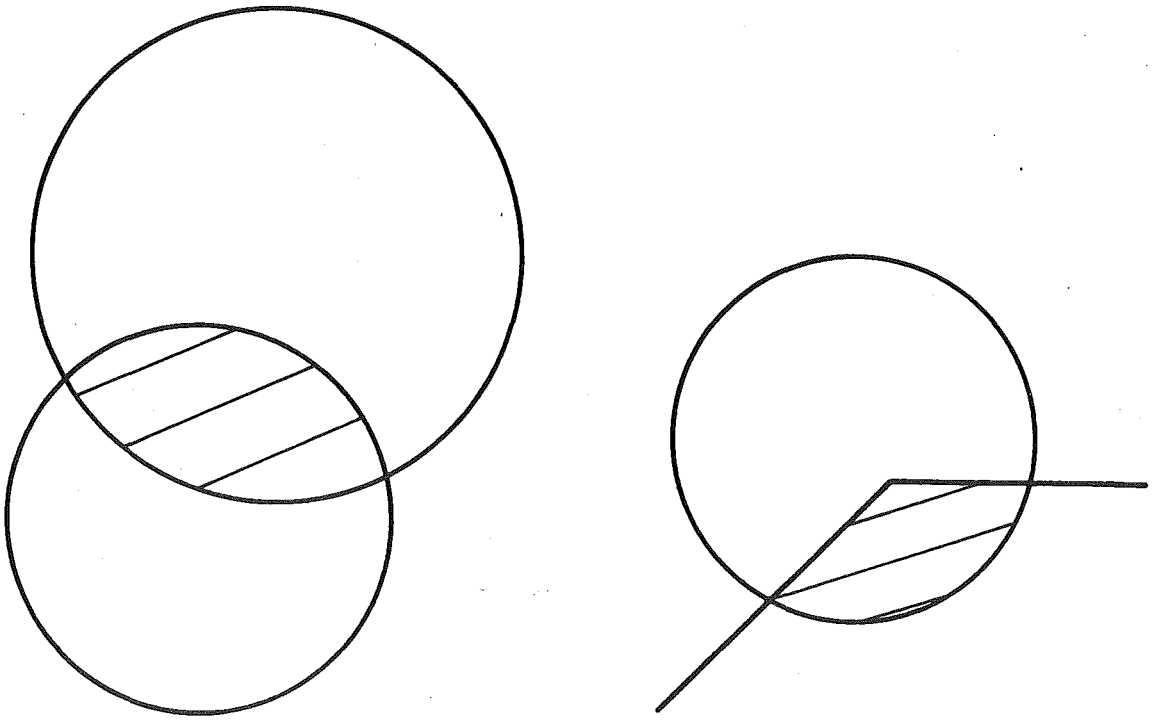

Figure 6.6

CHAPTER 7.

The I.R. technique is compared with the geometrical theory of diffraction. An I.R. secondary diffraction coefficient is derived which is valid when the distance between the edges of a scatterer is small, and is equal to the geometrical theory of diffraction coefficient when the distance between the edges is large. Results are presented which show the diffraction from a truncated wedge and a strip.

A modification to the physical optics current density on a body with edges is suggested, and results are presented which show the effect of this modification when applied to a truncated wedge.

Results are compared with the accurate values obtained from using the S.C.R. technique.

Areas of further research are suggested.

7.1(a) COMPARISON OF G.T.D. AND I.R. TECHNIQUE.

The I.R. technique and the geometrical theory of diffraction use similar methods to construct an expression for the diffracted field around a perfectly conducting truncated wedge. Consider the truncated wedge shown in Fig. 6.4. The incident field is $\vec{U}^i$, where

$$\vec{U}^i = \hat{z}\, U^i. \tag{7.1}$$

The I.R. technique expresses the total field surrounding the truncated wedge as

$$\vec{U} = \hat{z}\, U, \quad U = \sum_{n=1}^{\infty} U_n, \tag{7.2}$$

and postulates that the summation converges in the limit $n \to \infty$. Each term in this summation, which is discussed in section 6.1(a), is valid for all values of w.

The geometrical theory of diffraction field V surrounding the truncated wedge can be written in the form

$$\vec{V} = \hat{z}\, V, \quad V = \sum_{n=1}^{\infty} V_n, \tag{7.3}$$

which is assumed to approximate the exact field in the limit $n \to \infty$. Each of the higher order diffracted fields represented by the higher order terms in (7.3) is derived from (1.42) on the assumption that w is very much larger than the wavelength of the field. Higher order asymptotic terms of the expression in (1.25) are neglected.

Both U_n and V_n represent fields surrounding a perfectly conducting wedge. U_1 is the total field surrounding the wedge in Fig. 6.1 when the incident field is U^i. U_1 is zero in $2\pi-\beta < \phi < 2\pi$, and in general is non-zero in $0 \leqslant \phi \leqslant 2\pi-\beta$. The G.T.D. field V_1 surrounding the wedge in Fig. 6.1 is given in (1.40) as

$$V_1 = V_{go} + V^d, \tag{7.4}$$

where V_{go} is the geometrical optics field, and V^d is defined in (1.42). V_1 is zero in $2\pi-\beta < \phi < 2\pi$, and in general is non-zero in $0 \leqslant \phi \leqslant 2\pi-\beta$. The manner in which the expressions for V_{go} and V^d are derived in Chapter 1 ensures that at a large distance from the wedge apex,

$$V_1 \equiv U_1, \quad k\rho >> 1. \tag{7.5}$$

The parameters α and w of the truncated wedge enter the field formulations in the derivation of U_2 and V_2. U_2 is the total field surrounding the wedge in Fig. 6.2 when the incident field is due to a source distribution derived directly from U_1 and dependent upon w. U_2 is zero in $2\pi-\alpha < \theta < 2\pi$, and in general is non-zero in $0 \leqslant \theta \leqslant 2\pi-\alpha$. V_2 is the G.T.D. field scattered from the wedge in Fig. 6.2 when the incident field is U^i plus a ray of the field V_1 originating at (s=w, θ=0) and travelling along the surface towards the wedge apex. V_2 is zero in $2\pi-\alpha < \theta < 2\pi$, and in general is non-zero in $0 \leqslant \theta \leqslant 2\pi-\alpha$.

Each term U_{n+1} $(n \geqslant 1)$ in the summation in (7.2) is directly dependent upon U_n, and each term V_{n+1} $(n \geqslant 2)$ in the summation in (7.3) is directly dependent upon V_n. Thus, the higher order terms in each summation depend upon only the preceeding term and the shape of one of the perfectly conducting wedges in Figs 6.1 or 6.2. U_n and V_n both exist in the same region and are zero inside the wedge.

The boundary condition in (1.5) and the form of the expression in (1.43) show that no electrically polarized edge diffracted rays can travel along a perfectly conducting flat surface adjacent to the edge. Therefore, when the incident field is electrically polarized,

$$V_n = 0, \qquad n \geqslant 3, \tag{7.6}$$

in the summation in (7.3). No similar condition is associated with the U_n.

7.2(a) TRUNCATED WEDGE. (Electric Polarization).

In this section, the expression for the fields A_1 and A_2 are examined and the relationship between them and V_1 and V_2 is established. The notation of the previous section is used.

Because of the mathematical complexity of the terms following the second in the series in (6.2), only A_1 and A_2 are evaluated in section 6.2(a). The expressions for A_1 and A_2 are given in (6.5) and (6.33) respectively, and are derived for the truncated wedge of Fig. 6.4, illuminated by the incident field given in (6.4). These expressions are appropriate when the point at which the field is observed is a large distance from the truncated wedge. The normalization factor is given in (6.21).

First, consider A_1 given in (6.5). From (7.5),

$$A_1 \equiv V_1, \qquad k\rho >> 1. \tag{7.7}$$

$A_2(s,\theta)$, given in (6.33), can be written as

$$A_2(s,\theta) = \frac{-j\varepsilon_2 \sin(\frac{\beta+\psi-\pi}{n})\ \sin(\frac{\theta}{n})\ \sin(\frac{\pi}{n})\ e^{jkw\cos(\beta+\psi)}}{n[\cos(\frac{\beta+\psi-\pi}{n})-\cos(\frac{\theta-\pi}{n})][\cos(\frac{\beta+\psi-\pi}{n})-\cos(\frac{\theta+\pi}{n})]} + P, \tag{7.8}$$

where

$$P=\frac{-\sin(\frac{\psi}{m})}{4\pi n}\int_{-\infty}^{\infty} \frac{\sinh(\frac{mv}{n})\ e^{-jkw\cosh(mv)}}{\cos(jv+\frac{\pi}{m})+\cos(\frac{\psi}{m})}$$

$$\cdot\left[[\cosh(\frac{mv}{n})-\cos(\frac{\theta-\pi}{n})]^{-1} - [\cosh(\frac{mv}{n})-\cos(\frac{\theta+\pi}{n})]^{-1}\right] dv. \tag{7.9}$$

The trigonometrical identity

$$[\cos(a)-\cos(b-c)][\cos(a)-\cos(b+c)]$$

$$= [\cos(c)-\cos(a-b)][\cos(c)-\cos(a+b)], \qquad (7.10)$$

enables the expression in (7.8) to be rearranged as

$$A_2(s,\theta) = \frac{-j\varepsilon_2}{2n}\sin(\tfrac{\pi}{n})\, e^{jkw\cos(\beta+\psi)}\left[\left[\cos(\tfrac{\pi}{n})-\cos(\tfrac{\beta+\psi-\pi-\theta}{n})\right]^{-1}\right.$$

$$\left.-\left[\cos(\tfrac{\pi}{n})-\cos(\tfrac{\beta+\psi-\pi+\theta}{n})\right]^{-1}\right] + P. \qquad (7.11)$$

The field given by the first two terms of $A_2(s,\theta)$ in (7.11) is identical to the primary diffracted field from edge 2 predicted by the geometrical theory of diffraction. As mentioned in section 7.1(a), there is no secondary diffracted field predicted by the geometrical theory of diffraction for the truncated wedge when the incident field is electrically polarized. Thus,

$$A_2 = V_2 + P, \qquad ks >> 1. \qquad (7.12)$$

It is readily deduced from (7.9) by using the method of stationary phase[15] that

$$P \tilde{} 0, \quad kw >> 1. \qquad (7.13)$$

Hence, from (7.7), (7.12) and (7.13),

$$A_1 + A_2 = V_1 + V_2, \quad ks \gg 1, \quad kw \gg 1. \qquad (7.14)$$

This relationship shows that when the geometrical theory of diffraction approximations are valid, the diffracted fields given by the first two terms of the series in (7.2) and (7.3) are identical.

From the discussion in section 7.1(a) and the expressions in (7.12) - (7.14), it follows that the field described by P in (7.12) may be regarded as a correction to the G.T.D. field V_2 when w is small. It is evident that if the construction of the summation in (7.2) was such that the field U_1 was that diffracted by the wedge of Fig. 6.2 illuminated by U^i, and U_2 was the field diffracted by the wedge of Fig. 6.3, a similar correction for the G.T.D. field V_1 would result.

It is now possible to define the I.R. secondary diffraction coefficient $P_{m,n}(\theta,\psi,w)$ appropriate to a perfectly conducting body as in Fig. 7.1, illuminated by a field electrically polarized parallel to the edges. The fields $\vec{A}^i_\beta$ and $\vec{A}^i_\gamma$ are incident at angles ψ_β and ψ_γ on the edges having internal angles β and γ respectively, and

$$\vec{A}^i = \hat{z}\, A^i. \qquad (7.15)$$

The cylindrical polar co-ordinate system (s,θ,z) has its origin at the edge having internal angle α. The field $\vec{A}$ diffracted from this edge will be approximated by

$$\vec{A} = \hat{z}\, A, \quad A = A_{gtd} + \sqrt{\frac{2j}{\pi ks}}\; e^{-jks} \left[A^i_\beta\, P_{m,n}(\theta,\psi_\beta,a) + A^i_\gamma\, P_{\ell,n}(n\pi-\theta,\psi_\gamma,b) \right], \quad ks \gg 1, \qquad (7.16)$$

where A_{gtd} is the G.T.D. field diffracted from the edge, a and b are the separations of the edges as shown in the figure, and from (7.9) and (7.10),

$$P_{m,n}(\theta,\psi,w) = \varepsilon_n(\theta)\ \frac{j\sin(\frac{\pi}{n})\sin(\frac{\psi}{m})}{4\pi n}\int_{-\infty}^{\infty} \frac{e^{-jkw\cosh(mv)}}{\cos(jv+\frac{\pi}{m})+\cos(\frac{\psi}{m})}$$

$$\left[\left[\cos(\tfrac{\pi}{n})-\cos(\tfrac{jmv-\theta}{n})\right]^{-1} - \left[\cos(\tfrac{\pi}{n})-\cos(\tfrac{jmv+\theta}{n})\right]^{-1}\right]dv, \qquad (7.17)$$

$$m\pi = 2\pi-\beta, \quad n\pi = 2\pi-\alpha, \quad \ell\pi = 2\pi-\gamma, \qquad (7.18)$$

$$\varepsilon_n(\theta) = 1, \quad 0 \leqslant \theta \leqslant n\pi,$$

$$= 0, \quad n\pi < \theta < 2\pi. \qquad (7.19)$$

When a and b are large, it follows from (7.13) that the expression in (7.16) reduces to the G.T.D. estimate of the field diffracted by the edge at s=0.

7.2(b) TRUNCATED WEDGE. (Magnetic Polarization).

The expressions for the fields H_1 and H_2 given in (6.36) and (6.60) respectively are examined in this section, and the relationship between them and V_1 and V_2 is established. The notation of section 7.1(a) is used.

The fields H_1 and H_2 are derived for the truncated wedge of Fig. 6.4 illuminated by the magnetically polarized incident field in (6.35). Terms higher than the second in the series in (6.2) are not evaluated in section 6.2(b) because of their mathematical complexity. The expressions for H_1 and H_2 are appropriate when the point at which the field is observed is a large distance from the truncated wedge. The normalization factor for the expressions is given in (6.21).

From (7.5), it follows that

$$H_1 \equiv V_1, \qquad k\rho \gg 1. \tag{7.20}$$

$H_2(s,\theta)$, given in (6.60), can be written as

$$H_2(s,\theta) = \frac{-j\varepsilon_2}{n} e^{jkw\cos(\psi+\beta)} \sin\left(\frac{\pi}{n}\right)$$

$$\cdot \frac{\cos\left(\frac{\pi}{n}\right) - \cos\left(\frac{\theta}{n}\right)\cos\left(\frac{\beta+\psi-\pi}{n}\right)}{\left[\cos\left(\frac{\beta+\psi-\pi}{n}\right)-\cos\left(\frac{\theta-\pi}{n}\right)\right]\left[\cos\left(\frac{\beta+\psi-\pi}{n}\right)-\cos\left(\frac{\theta+\pi}{n}\right)\right]} + Q, \tag{7.21}$$

where

$$Q = \frac{-j}{4\pi n}\int_{-\infty}^{\infty} \frac{\sin\left(jv+\frac{\pi}{m}\right)e^{-jkw\cosh(mv)}}{\cos\left(jv+\frac{\pi}{m}\right)+\cos\left(\frac{\psi}{m}\right)} \left[\frac{\sin\left(\frac{\theta-\pi}{n}\right)}{\cosh\left(\frac{mv}{n}\right)-\cos\left(\frac{\theta-\pi}{n}\right)}\right.$$

$$\left. - \frac{\sin\left(\frac{\theta+\pi}{n}\right)}{\cosh\left(\frac{mv}{n}\right)-\cos\left(\frac{\theta+\pi}{n}\right)}\right] dv. \tag{7.22}$$

Using (7.10) to rearrange the expression in (7.21) results in

$$H_2(s,\theta) = \frac{-j\varepsilon_2}{2n}\sin\left(\frac{\pi}{n}\right)e^{jkw\cos(\psi+\beta)}\left[\left[\cos\left(\frac{\pi}{n}\right)-\cos\left(\frac{\beta+\psi-\pi\div\theta}{n}\right)\right]^{-1}\right.$$

$$\left. +\left[\cos\left(\frac{\pi}{n}\right)-\cos\left(\frac{\beta+\psi-\pi+\theta}{n}\right)\right]^{-1}\right] + Q. \tag{7.23}$$

The field given by the first two terms in (7.23) is identical to the primary diffracted field from edge 2 predicted by the geometrical theory of diffraction. By using the method

of stationary phase[15] when kw is large, the expression in (7.22) becomes

$$Q \approx \frac{e^{-j(kw-\frac{\pi}{4})} \sin(\frac{\pi}{m}) \sin(\frac{\pi}{n}) [\cos(\frac{\theta}{n})-\cos(\frac{\pi}{n})]}{nm\sqrt{2\pi kw}\,[\cos(\frac{\pi}{m})+\cos(\frac{\psi}{m})]\,[1-\cos(\frac{\theta-\pi}{n})][1-\cos(\frac{\theta+\pi}{n})]}, \quad kw >> 1. \tag{7.24}$$

The use of the identity in (7.10) enables this expression for Q to be reduced to

$$Q \approx \frac{-e^{-j(kw-\frac{\pi}{4})} \sin(\frac{\pi}{m}) \sin(\frac{\pi}{n})}{nm\sqrt{2\pi kw}\,[\cos(\frac{\pi}{m})+\cos(\frac{\psi}{m})][\cos(\frac{\pi}{n})-\cos(\frac{\theta}{n})]}, \quad kw >> 1. \tag{7.25}$$

A comparison of the field given in (7.25) with the field H_2^2 given in (4.20) shows that the expression for Q is identical to the normalized G.T.D. secondary diffracted field from edge 2. Thus,

$$H_1 + H_2 = V_1 + V_2, \quad ks >> 1, \quad kw >> 1. \tag{7.26}$$

From the discussion in section 7.1(a) and the expressions in (7.21)-(7.26) it follows that the field described by Q in (7.22) may be regarded as a corrected form of the secondary G.T.D. field when w is small.

In a similar manner to that in section 7.2(a), it is now possible to define the I.R. secondary diffraction coefficient $Q_{m,n}(\theta,\psi,w)$ appropriate to a perfectly conducting body, such as that of Fig. 7.1, when the incident field is magnetically polarized parallel to the edges. The fields

H^i_β and H^i_γ are incident at angles ψ_β and ψ_γ on the edges having internal angles β and γ respectively, and

$$\vec{H}^i = \hat{z}\, H^i. \tag{7.27}$$

The field $\vec{H}$ diffracted from the edge at s=0 is approximated by

$$\vec{H} = \hat{z}\, H, \quad H = H^p_{gtd} + \sqrt{\frac{2j}{\pi ks}}\, e^{-jks} \left[H^i_\beta \; Q_{m,n}(\theta,\psi_\beta,a) + H^i_\gamma \, Q_{\ell,n}(n\pi-\theta,\psi_\gamma,b) \right], \quad ks >> 1, \tag{7.28}$$

where H^p_{gtd} is the primary G.T.D. field diffracted from the edge, a and b are the separations of the edges as shown in the figure, and from (7.22) and (7.10),

$$Q_{m,n}(\theta,\psi,w) = -\varepsilon_n(\theta)\, \frac{j \sin(\frac{\pi}{n})}{4\pi n} \int_{-\infty}^{\infty} \frac{\sin(jv+\frac{\pi}{m})\; e^{-jkw\cosh(mv)}}{\cos(jv+\frac{\pi}{m})+\cos(\frac{\psi}{m})} \cdot \left[[\cos(\tfrac{\pi}{n})-\cos(\tfrac{jmv-\theta}{n})]^{-1} + [\cos(\tfrac{\pi}{n})-\cos(\tfrac{jmv+\theta}{n})]^{-1} \right] dv. \tag{7.29}$$

m,n and ℓ are defined in (7.18), and $\varepsilon_n(\theta)$ is defined in (7.19). When a and b are large, it follows from (7.25) that the expression in (7.28) reduces to the sum of the primary and secondary G.T.D. fields diffracted by the edge at s=0.

7.3(a) THE I.R. DIFFRACTION COEFFICIENT APPLIED TO A TRUNCATED WEDGE.

The I.R. secondary diffraction coefficient $P_{m,n}(\theta,\psi,w)$

in (7.17) or $Q_{m,n}(\theta,\psi,w)$ in (7.29) is applied to the problem of approximating the scattering from the truncated wedge of Fig. 4.1 when the incident field is electrically or magnetically polarized. The notation used in this section is that of Chapter 4.

Consider the perfectly conducting truncated wedge of Fig. 4.1 illuminated by the electrically polarized magnetic vector potential defined in (4.2). The fields A_1^i and A_2^i defined in (4.9) are incident upon edges 1 and 2 respectively. The normalized field A_{gtd} in (4.14) is the G.T.D. diffracted field surrounding the truncated wedge. By including with A_{gtd} the I.R. secondary diffracted fields defined in (7.16), a new estimate A of the diffracted field is obtained as

$$A = A_{gtd} + A_1^i\, e^{jka_2\cos(m\pi-\phi)}\; P_{\tau,\gamma}(\phi+\beta-\pi,\psi,w)$$

$$+ A_2^i\, e^{jka_1\cos\phi}\; P_{\gamma,\tau}(\tau\pi-\phi,\gamma\pi+\pi-\psi-\beta,w), \qquad (7.30)$$

where the normalization factor in (4.1) has been removed.

Consider the truncated wedge when the magnetically polarized incident fields H_1^i and H_2^i upon edges 1 and 2 respectively are given by (4.9) with the symbol A replaced by H. The primary field H^p_{gtd} diffracted by the truncated wedge is given from (4.17) as $(H_1^1 + H_2^1)$. By including with H^p_{gtd} the I.R. secondary diffracted field defined in (7.28), a new estimate H of the diffracted field is obtained as

$$H = H^{p}_{gtd} + H^{i}_{1}\, e^{jka_2\cos(m\pi-\phi)}\; Q_{\tau,\gamma}(\phi+\beta-\pi,\psi,w)$$

$$+ H^{i}_{2}\, e^{jka_1\cos\phi}\, Q_{\gamma,\tau}(\tau\pi-\phi,\gamma\pi+\pi-\psi-\beta,w)\,, \qquad (7.31)$$

where the normalization factor in (4.1) has been removed.

7.3(b) THE I.R. DIFFRACTION COEFFICIENT APPLIED TO A CONDUCTING STRIP.

The secondary diffraction coefficients $P_{m,n}(\theta,\psi,w)$ and $Q_{m,n}(\theta,\psi,w)$ are applied to the perfectly conducting strip. In order to compare some results with those of Yu and Rudduck[65], use is made of their normalization factor:

$$\frac{e^{-jkr}}{\sqrt{2\pi jkr}}\,. \qquad (7.32)$$

Consider the perfectly conducting strip of width 2a in Fig. 7.2. The incident plane wave $\vec{U}^{i}$ is given by

$$\vec{U}^{i} = \hat{z}\, U^{i}, \quad U^{i} = e^{jkr\cos(\theta-\theta_o)}\,, \qquad (7.33)$$

in the (r,θ,z) cylindrical polar co-ordinate system with origin at the centre of the strip. The G.T.D. primary diffracted field $\vec{U}^{p}_{gtd}$ is found from (1.42) and (1.43) to be

$$\vec{U}^{p}_{gtd} = \hat{z}\, U^{p}_{gtd}, \quad U^{p}_{gtd}(\theta,\theta_o) = \frac{-\cos[ka(\sin\theta+\sin\theta_o)]}{\cos(\frac{\theta-\theta_o}{2})}$$

$$\pm \frac{j\,\sin[ka(\sin\theta+\sin\theta_o)]}{\sin(\frac{\theta+\theta_o}{2})}\,, \qquad (7.34)$$

where the normalization factor in (7.32) has been removed, and the upper (lower) sign in (7.34) holds when the field is magnetically (electrically) polarized. In the reflection direction $\theta = -\theta_o$, the expression in (7.34) reduces to

$$U^p_{gtd}(-\theta_o,\theta_o) = -\sec(\theta_o) \pm j2ka\cos(\theta_o), \qquad (7.35)$$

which is in agreement with the form of (4.15) and (4.29) when $\theta_o = 0$.

By including with U^p_{gtd} the I.R. secondary diffracted fields defined in (7.16) and (7.28), the new estimate of the diffracted field is found to be

$$A(\theta,\theta_o) = A_{gtd}(\theta,\theta_o) + 4j\left[e^{-jka(\sin\theta-\sin\theta_o)}\, P_{2,2}(\tfrac{\pi}{2}-\theta,\tfrac{3\pi}{2}-\theta_o,2a)\right.$$

$$\left. + e^{jka(\sin\theta-\sin\theta_o)}\, P_{2,2}(\tfrac{\pi}{2}+\theta,\tfrac{3\pi}{2}+\theta_o,2a)\right], \qquad (7.36)$$

when the field is electrically polarized, and

$$H(\theta,\theta_o) = H^p_{gtd}(\theta,\theta_o) + 4j\left[e^{-jka(\sin\theta-\sin\theta_o)}\, Q_{2,2}(\tfrac{\pi}{2}-\theta,\tfrac{3\pi}{2}-\theta_o,2a)\right.$$

$$\left. + e^{jka(\sin\theta-\sin\theta_o)} Q_{2,2}(\tfrac{\pi}{2}+\theta,\tfrac{3\pi}{2}+\theta_o,2a)\right], \qquad (7.37)$$

when the field is magnetically polarized.

$A_{gtd}(\theta,\theta_o)$ is the complete G.T.D. electrically polarized diffracted field surrounding the strip. When the field is magnetically polarized, the sum of the primary and secondary diffracted field of the G.T.D. is given by H^s_{gtd}, where

$$H^{s}_{gtd}(\theta,\theta_o) = H^{p}_{gtd}(\theta,\theta_o) + \frac{e^{-j2ka}}{\sqrt{j\pi ka}} \left[\frac{e^{jka(\sin\theta-\sin\theta_o)}}{\cos(\frac{\theta+\theta_o}{2})-\sin(\frac{\theta-\theta_o}{2})} \right.$$

$$\left. + \frac{e^{-jka(\sin\theta-\sin\theta_o)}}{\cos(\frac{\theta+\theta_o}{2})+\sin(\frac{\theta+\theta_o}{2})} \right]. \qquad (7.38)$$

Since each side of the strip provides a direct ray path between the edges, a factor of 2 is included with the secondary field terms in (7.36), (7.37), and (7.38).

7.3(c) NUMERICAL CONSIDERATIONS.

The integrations in (7.17) and (7.29) for $P_{m,n}(\theta,\psi,w)$ and $Q_{m,n}(\theta,\psi,w)$ can be performed numerically. By removing the odd parts of the integrands, the expressions reduce to

$$P_{m,n}(\theta,\psi,w) = C \sin(\frac{\psi}{m}) \sin(\frac{\theta}{n}) \int_0^{\infty} \frac{\sinh v \sinh(\frac{mv}{n}) e^{-jkw\cosh(mv)}}{D(v)} dv, \qquad (7.39)$$

$$Q_{m,n}(\theta,\psi,w) = C \int_0^{\infty} \frac{\left[\cosh v \cos(\frac{\psi}{m})+\cos(\frac{\pi}{m})\right]}{D(v)}$$

$$\cdot\left[\cos(\frac{\pi}{n})-\cosh(\frac{mv}{n})\cos(\frac{\theta}{n})\right] e^{-jkw\cosh(mv)} dv, \qquad (7.40)$$

where

$$C = \frac{-j\ \varepsilon_n(\theta)}{\pi n} \sin(\frac{\pi}{m}) \sin(\frac{\pi}{n}), \qquad (7.41)$$

$$D(v) = \left[\left[\cosh v \cos(\frac{\pi}{m})+\cos(\frac{\psi}{m})\right]^2+\left[\sinh v \sin(\frac{\pi}{m})\right]^2\right]$$

$$\cdot\left[\cosh(\frac{mv}{n})-\cos(\frac{\theta-\pi}{n})\right]\left[\cosh(\frac{mv}{n})-\cos(\frac{\theta+\pi}{n})\right]. \qquad (7.42)$$

When v is large, the integrands of (7.39) and (7.40) are of order e^{-2v} and decrease rapidly in magnitude as v increases.

By expressing the exponential term in the integrands in trigonometric functions, the integrands are immediately separable into real and imaginary parts. The real parts oscillate as cos[kwcosh(mv)], and the imaginary parts as sin[kwcosh(mv)]. Consequently the zeros of the real part of the integrands are located at

$$v = \frac{1}{m} \cosh^{-1} \left[\frac{(2p-1)\pi}{2kw}\right] , \qquad (7.43)$$

where, within the range of integration, p is any integer satisfying

$$p \geq \frac{kw}{\pi} + \tfrac{1}{2}. \qquad (7.44)$$

Similarly, the zeros of the imaginary part of the integrands are located at

$$v = \frac{1}{m} \cosh^{-1} \left[\frac{p\pi}{kw}\right] \qquad (7.45)$$

where, within the range of integration, p is any integer satisfying

$$p \geq \frac{kw}{\pi}. \qquad (7.46)$$

The integrations have been evaluated by performing a Simpson's rule integration over each half cycle or "hump" of the real and imaginary parts of the integrands. The convergence of the calculation is indicated from a comparison of the area under a hump with both the sum of the areas under all preceeding humps, and the area under the preceeding hump. Convergence is attained when either the area under a hump is small compared with the sum of the areas

under all preceeding humps, or the sum of the areas under two consecutive humps is small. In the latter case, only one half of the area under the final hump is included in the area summation.

7.3(d) RESULTS.

Figures 7.3 and 7.4 indicate the difference between the I.R. and G.T.D. secondary diffracted fields given in (7.29) and (7.25) respectively. Fig. 7.3 shows the secondary diffracted field from edge 2 of the truncated wedge of Fig. 6.4 when only edge 1 is directly illuminated by the incident magnetically polarized field, and Fig. 7.4 shows the sum of the primary and secondary diffracted fields from edge 2 when both edges are directly illuminated. It is evident that there is an appreciable difference between the I.R. and G.T.D. secondary diffracted fields when w is small, and that this difference is not negligible when compared with the primary diffracted field.

The curves in Fig. 7.5 compare the G.T.D. diffracted field, the primary G.T.D. diffracted field, the field obtained by using the I.R. secondary diffraction coefficient as in (7.31), and the magnetically polarized field given by the S.C.R. technique for a symmetrically truncated wedge. The increased accuracy of the I.R. secondary diffraction coefficient over the other approximate methods is evident.

The expression in (7.30) has been evaluated for a symmetrically truncated wedge with $2\chi = 94^{o}$, $w = 0.1\lambda$, and

is plotted in Fig. 7.6. Also plotted are the G.T.D. diffracted field, the diffracted field of Burke and Keller[47,91], the field from an undeformed wedge with $2\chi = 94^{\circ}$, and the accurate value of the diffracted field as calculated from the S.C.R. technique. Again, the increased accuracy of the I.R. secondary diffraction coefficient over other approximate methods is evident. Similar remarks apply to the curves in Fig. 7.7.

The curves in Figs. 7.5, 7.6 and 7.7 may be compared with those in Figs. 4.22, 4.21 and 4.23 respectively.

The expressions in (7.30) and (7.31) involving the I.R. secondary diffraction coefficient have been evaluated for seven values of w in the range $0.05\lambda \leqslant w \leqslant 1.0\lambda$ for the case of normal backscattering from the truncated wedges appropriate to Figs. 4.25 - 4.30. When the curves obtained are plotted on these figures, they are indistinguishable from the accurate curves.

The three sets of curves in Fig. 7.8 show estimates of the diffraction from a perfectly conducting strip illuminated normally by an electrically polarized field. The results obtained from (7.36) are compared with the geometrical theory of diffraction estimate. It is apparent that the inclusion of the I.R. secondary diffracted fields in (7.36) only slightly modifies the G.T.D. estimate when $w > 0.5\lambda$, except near $\theta = \pm\frac{\pi}{2}$. The expression in (7.36) has not been evaluated in these two directions.

The curves in Fig. 7.9 show the field diffracted by a perfectly conducting strip illuminated normally by a magnetically polarized field. The figures show the primary G.T.D. field (7.34), the sum of the primary and secondary G.T.D. fields (7.38), the sum of the primary G.T.D. and I.R. secondary fields (7.37), and the diffracted field of Moshen and Hamid[62]. The use of the I.R. secondary diffraction coefficient results in a significantly better estimate of the field in the vicinity of $\theta = \pm \frac{\pi}{2}$ than does the G.T.D. or the method of Moshen and Hamid. A similar improvement is noticeable in Fig. 7.10 where the magnetically polarized incident field is not normal to the strip.

It is concluded from the above results that when the separation between edges is small, use of the I.R. secondary diffraction coefficients results in significantly increased accuracy over the asymptotic coefficients of the G.T.D., and also over the coefficient of Moshen and Hamid for the strip.

7.4(a) MODIFIED PHYSICAL OPTICS.

Before a modification is suggested to the physical optics estimate of the surface current density on a perfectly conducting body with edges, the current density on the perfectly conducting wedge of Fig. 1.1 will be derived from (1.16) and (1.33). The surface $\phi = 0$ of the wedge is called surface 1, and the surface $\phi = 2\pi - \beta$ is called surface 2.

Consider the wedge illuminated by the electrically polarized plane wave given by

$$\vec{A}^i = \hat{z}\, A^i, \quad A^i = e^{jk\rho\cos(\phi-\psi)}. \tag{7.47}$$

An expression for the surface current density $\vec{K}_2(r)$ at $\rho = r$ on surface 2 is derived in section 6.2(a). The surface current density $\vec{K}_1(r)$ at $\rho = r$ on surface 1 can be derived in a similar manner. Thus,

$$\vec{K}(r) = \hat{z}\, K(r), \quad K_1(r) = \gamma(\psi), \quad K_2(r) = \gamma(m\pi-\psi), \tag{7.48}$$

where

$$\gamma(\xi) = \frac{-2jk}{\mu}\,\varepsilon(\xi)\,\sin\xi\; e^{jkr\cos\xi} + \gamma_m^c(r,\xi), \quad 0 \leq \xi \leq m\pi, \tag{7.49}$$

$$\gamma_m^c(r,\xi) = \frac{-k}{\mu\pi}\sin\left(\frac{\xi}{m}\right)\int_\infty^\infty \frac{\sinh(mv)\,e^{-jkr\cosh(mv)}}{\cos\left(jv+\frac{\pi}{m}\right)-\cos\left(\frac{\xi}{m}\right)}\,dv, \tag{7.50}$$

$$m\pi = 2\pi-\beta, \quad \varepsilon(\xi) = 1, \quad 0 < \xi < \pi, \quad = 0, \quad \pi < \xi \leq m\pi. \tag{7.51}$$

The physical optics surface current densities $\vec{K}_1^P(r)$ and $\vec{K}_2^P(r)$ on surfaces 1 and 2 respectively are given in (4.40) and (4.41). It follows from (7.48) and (7.49) that

$$K_1(r) = K_1^P(r) + \gamma_m^c(r,\psi), \qquad K_2(r) = K_2^P(r) + \gamma_m^c(r,m\pi-\psi). \tag{7.52}$$

Consider the wedge illuminated by the magnetically polarized plane wave given by

$$\vec{H}^i = \hat{z}\, H^i, \quad H^i = e^{jk\rho\cos(\phi-\psi)}. \tag{7.53}$$

An expression for the surface current density $\vec{L}_2(r)$ at $\rho = r$ on surface 2 is derived in section 6.2(b). The surface current density $\vec{L}_1(r)$ at $\rho = r$ on surface 1 can be derived in a similar manner. Thus,

$$\vec{L}_1(r) = \hat{r}_1\, \delta(\psi), \quad \vec{L}_2(r) = -\hat{r}_2\, \delta(m\pi-\psi), \tag{7.54}$$

where

$$\delta(\xi) = 2\varepsilon(\xi)e^{jkr\cos\xi} + \delta_m^c(r,\xi), \tag{7.55}$$

$$\delta_m^c(r,\xi) = \frac{1}{\pi}\int_{-\infty}^{\infty} \frac{\sin(jv+\frac{\pi}{m})\, e^{-jkr\cosh(mv)}}{\cos(jv+\frac{\pi}{m})-\cos(\frac{\xi}{m})}\, dv, \tag{7.56}$$

$$\hat{r}_1 = \hat{\rho}\cos\phi-\hat{\phi}\sin\phi, \quad \hat{r}_2 = \hat{\rho}\cos(\phi+\beta)-\hat{\phi}\sin(\phi+\beta), \tag{7.57}$$

and m and $\varepsilon(\xi)$ are defined in (7.51). The physical optics surface current densities $\vec{L}_1^P(r)$ and $\vec{L}_2^P(r)$ on surfaces 1 and 2 respectively are given in (4.67) and (4.69). It follows from (7.54) and (7.55) that

$$\vec{L}_1(r) = \vec{L}_1^P(r) + \hat{r}_1\, \delta_m^c(r,\psi), \quad \vec{L}_2(r) = \vec{L}_2^P(r)-\hat{r}_2\delta_m^c(r,m\pi-\psi). \tag{7.58}$$

The application of the method of stationary phase[15] to the expressions for $\gamma_m^c(r,\xi)$ and $\delta_m^c(r,\xi)$ shows that at a large distance from the wedge apex,

$$\gamma_m^c(r,\xi) \approx 0, \quad \delta_m^c(r,\xi) \approx 0, \quad kr \gg 1, \tag{7.59}$$

and thus,

$$K_1(r) \approx K_1^p(r),\ K_2(r) \approx K_2^p(r),\ \vec{L}_1(r) \approx \vec{L}_1^p(r),$$

$$\vec{L}_2(r) \approx \vec{L}_2^p(r),\ kr \gg 1. \qquad (7.60)$$

It is shown in section 3.1(a) that when the field is electrically polarized, the surface current density tends to infinity as the wedge apex is approached. (This behaviour can also be seen by substituting the expression in (3.11) into (2.28).) The P.O. approximations $\vec{K}_1^p(r)$ and $\vec{K}_2^p(r)$ do not predict this current density behaviour. Similarly, it follows from section 3.1(c) that when the field is magnetically polarized, the surface current density is continuous around the wedge apex. (This behaviour can also be seen by substituting the expression in (3.11) into (2.58).) The physical optics approximations $\vec{L}_1^p(r)$ and $\vec{L}_2^p(r)$ are discontinuous around the wedge apex if only one surface of the wedge is illuminated.

The expressions in (7.60) emphasize that the physical optics approximation to the surface current density on a perfectly conducting body is equivalent to regarding each point on the body as a point on an infinite perfectly conducting plane. In the case of the perfectly conducting wedge, $\gamma_m^c(r,\psi)$ and $\delta_m^c(r,\psi)$ may be regarded as a perturbation

to the physical optics current density on surface 1 due to that surface terminating in an edge at r = 0. Similarly, $\gamma_m(r,m\pi-\psi)$ and $\delta_m(r,m\pi-\psi)$ may be regarded as a perturbation to the physical optics current density on surface 2 due to that surface terminating in an edge at r=0. These perturbations have little effect beyond a distance of about one wavelength from the edge[89]. This suggests that the perturbations could be used with the physical optics current density to approximate the current density on a perfectly conducting body with edges.

The Modified Physical Optics (M.P.O.) current density on a perfectly conducting body is derived by adding a term of the form $\gamma_m(r,\xi)$ or $\delta_m(r,\xi)$ (depending upon the polarization of the field) to the expression for the physical optics current density in the vicinity of an edge. This approximation is equivalent to regarding each edge of the body as the apex of an infinite perfectly conducting wedge.

For example, consider the perfectly conducting body in Fig. 7.1. The geometry of the body is described in section 7.2(a), and m and n are defined in (7.18). When the incident field is electrically polarized in the z-direction, the M.P.O. current density $\vec{K}^c(r)$ at s = r on the surface θ= 0 is

$$\vec{K}^c(r) = \hat{z}\, K^c(r),\ K^c(r) = K^p(r) + A^i_\beta\, \gamma^c_m(a-r, m\pi-\psi_\beta)$$

$$+ A^i_\alpha\, \gamma^c_n(r, \psi_\beta+\beta-\pi), \qquad (7.61)$$

where A^i_α and A^i_β are the incident fields on the edges of internal angles α and β respectively, and $K^p(r)$ is the physical optics current density.

When the incident field is magnetically polarized in the z-direction, the M.P.O. current density $\vec{L}^c(r)$ at s=r on the surface $\theta = 0$ is

$$\vec{L}^c(r) = \vec{L}^p(r) + \hat{r}\left[H^i_\beta\, \delta^c_m(a-r, m\pi-\psi_\beta) + H^i_\alpha\, \delta^c_n(r, \psi_\beta+\beta-\pi)\right], \qquad (7.62)$$

where $\vec{L}^p(r)$ is the physical optics current density, and

$$\hat{r} = \hat{s}\cos\theta - \hat{\theta}\sin\theta. \qquad (7.63)$$

H^i_α and H^i_β are the incident fields on the edges of internal angles α and β respectively.

Notice that while physical optics predicts no current density if the surface is not directly illuminated, M.P.O. predicts no current density only if neither edge at the ends of the surface is directly illuminated.

If in the approximation to the current density given in (7.61) and (7.62) the functions $\gamma_\tau(x,\xi)$ and $\delta_\tau(x,\xi)$ are defined to exist only for $0 \leq x < a$, the correct behaviour of the surface currents at the edges is obtained.

However, in this case the approximation to the current density would be discontinuous at at least one point on the surface. The M.P.O. current density is continuous on the surface, and predicts an infinite current density at the edges when the field is electrically polarized. When the field is magnetically polarized, the M.P.O. current density is continuous around the edges if a is large.

7.4(b) SOME DEFINITIONS.

It is convenient at this point to make some definitions. Define

$$\Gamma_m(w,\xi,\eta) = \frac{-j\mu}{4}\int_o^w \gamma_m^c(r,\xi)\, e^{jkr\cos\eta}\,dr, \qquad 0 \leqslant \eta \leqslant 2\pi. \tag{7.64}$$

Substitution of the expression in (7.50) and evaluation of the integral results in

$$\Gamma_m(w,\xi,\eta) = \frac{\sin(\frac{\xi}{m})}{4\pi}\int_{-\infty}^{\infty} \frac{\sinh(mv)\{1-e^{-jkw[\cosh(mv)-\cos\eta]}\}}{[\cos(jv+\frac{\pi}{m})-\cos(\frac{\xi}{m})][\cosh(mv)-\cos\eta]}\,dv, \tag{7.65}$$

which, by substituting $x = j(\eta-\pi)$ into Appendix 7, reduces to

$$\Gamma_m(w,\xi,\eta) = \frac{j}{2}\left[\frac{\varepsilon(\xi)\sin\xi}{\cos\xi+\cos\eta} + \frac{\sin(\frac{\xi}{m})}{m[\cos(\frac{\pi-\eta}{m})-\cos(\frac{\xi}{m})]}\right] + \Xi_m(w,\xi,\eta), \tag{7.66}$$

where $\varepsilon(\xi)$ is defined in (7.51), and

$$\Xi_m(w,\xi,\eta) = -\frac{\sin(\frac{\xi}{m})}{4\pi}\int_{-\infty}^{\infty}\frac{\sinh(mv)\ e^{-jkw[\cosh(mv)-\cos\eta]}}{[\cos(jv+\frac{\pi}{m})-\cos(\frac{\xi}{m})][\cosh(mv)-\cos\eta]}dv \tag{7.67}$$

if w is finite. When w is infinite, it follows from (4.46) that the result of the integration with respect to r in (7.64) requires

$$\Xi_m(\infty,\xi,\eta) = 0. \tag{7.68}$$

Define

$$\Delta_m(w,\xi,\eta) = \frac{k}{4}\sin(\eta)\int_0^w \delta_m^c(r,\xi)\ e^{jkr\cos\eta}dr, \quad 0 \leq \eta \leq 2\pi. \tag{7.69}$$

By substituting the expression in (7.56), evaluating the integral with respect to r, and using Appendix 8 with $x = j(\eta-\pi)$,

$$\Delta_m(w,\xi,\eta) = -\frac{j}{2}\left[\frac{\varepsilon(\xi)\sin\eta}{\cos\xi+\cos\eta} + \frac{\sin(\frac{\pi-\eta}{m})}{m[\cos(\frac{\pi-\eta}{m})-\cos(\frac{\xi}{m})]}\right] + T_m(w,\xi,\eta), \tag{7.70}$$

where the definition

$$T_m(w,\xi,\eta) = \frac{j\sin\eta}{4\pi}\int_{-\infty}^{\infty}\frac{\sin(jv+\frac{\pi}{m})\ e^{-jkw[\cosh(mv)-\cos\eta]}}{[\cos(jv+\frac{\pi}{m})-\cos(\frac{\xi}{m})][\cosh(mv)-\cos\eta]}dv \tag{7.71}$$

holds if w is finite. When w is infinite,

$$T_m(\infty,\xi,\eta) = 0. \tag{7.72}$$

7.4(c) M.P.O. APPLIED TO A TRUNCATED WEDGE.

Consider the perfectly conducting truncated wedge of Fig. 4.1 in the presence of an electrically polarized field. The fields A_1^i and A_2^i incident upon edges 1 and 2 respectively are defined in (4.9). The notation used in this section follows that in Chapter 4.

Using the definition in (7.61), the M.P.O. surface current density $\vec{K}_1^c(r)$ at $\rho = r$ on the surface $\phi = 0$ is given by

$$\vec{K}^c(r) = \hat{z}\, K^c(r), \quad K_1^c(r) = K_1(r) + A_1^i\, \gamma_\tau^c(r-a_1, \psi), \qquad (7.73)$$

where $K_1(r)$ is the P.O. surface current density defined in (4.40). The M.P.O. surface current density $K_2^c(r)$ at $\rho = r$ on the surface $\phi = m\pi$ is given by

$$K_2^c(r) = K_2(r) + A_2^i\, \gamma_\gamma^c(r-a_2, m\pi-\psi), \qquad (7.74)$$

where $K_2(r)$ is the P.O. surface current density defined in (4.41). The M.P.O. surface current density $K_3^c(x)$ at a distance x from edge 1 on the surface of length w between edge 1 and edge 2 is

$$K_3^c(x) = K_3(x) + A_1^i\, \gamma_\tau^c(x, \tau\pi-\psi) + A_2^i\, \gamma_\gamma^c(w-x, \psi+\beta-\pi), \qquad (7.75)$$

where $K_3(x)$ is the P.O. surface current density defined in (4.50).

The field radiated by the P.O. current density on the truncated wedge is evaluated in Chapter 4. The magnetic vector potential $\vec{A}^c$ radiated by the "modifying"

current density on the wedge is found from (1.36), (7.73)-(7.75), and (1.21) to be

$$\vec{A}^c = \hat{z}A^c, \quad A^c = A_1^i\, e^{jka_1\cos\phi}[\Gamma_\tau(\infty,\psi,\phi) + \Gamma_\tau(w,\tau\pi-\psi,\tau\pi-\phi)]$$

$$+ A_2^i\, e^{jka_2\cos(m\pi-\phi)}[\Gamma_\gamma(\infty,m\pi-\psi,m\pi-\phi) + \Gamma_\gamma(w,\psi+\beta-\pi,\phi+\beta-\pi)], \quad \rho \gg r, \tag{7.76}$$

where $\Gamma_m(w,\xi,\eta)$ is defined in (7.64), and the normalization factor in (4.1) has been removed.

The M.P.O. field A_{mpo} scattered by the truncated wedge is given by (7.76) and (4.57) as

$$A_{mpo} = A_{po} + A^c. \tag{7.77}$$

Straightforward but laborious algebraic manipulation enables A_{mpo} to be reduced to

$$A_{mpo} = A_{gtd} + A_1^i\, e^{jka_1\cos\phi}\, \Xi(w,\tau\pi-\psi,\tau\pi-\phi)$$

$$+ A_2^i\, e^{jka_2\cos(m\pi-\phi)}\, \Xi(w,\psi+\beta-\pi,\phi+\beta-\pi), \tag{7.78}$$

where A_{gtd} defined in (4.14) is the geometrical theory of diffraction field surrounding the truncated wedge. $\Xi(w,\xi,\eta)$ is defined in (7.67) and (7.68).

Now consider the perfectly conducting truncated wedge of Fig. 4.1 in the presence of a magnetically polarized field. The fields H_1^i and H_2^i incident upon edges 1 and 2 respectively are defined in (4.9) with the symbol A replaced by H. Using the definition in (7.62), the M.P.O.

surface current density $\vec{L}_1^c(r)$ at $\rho = r$ on the surface $\phi=0$ is given by

$$\vec{L}_1^c(r) = \vec{L}_1(r) + H_1^i \hat{r}_1 \delta_\tau^c(r-a_1,\psi), \tag{7.79}$$

where $\vec{L}_1(r)$ is the physical optics current density defined in (4.67), and $\hat{r}_1$ is defined in (4.68). The M.P.O. surface current density $\vec{L}_2^c(r)$ at $\rho = r$ on the surface $\phi = m\pi$ is given by

$$\vec{L}_2^c(r) = \vec{L}_2(r) - H_2^i \hat{r}_2 \delta_\gamma^c(r-a_2,m\pi-\psi), \tag{7.80}$$

where the physical optics current density $\vec{L}_2(r)$, and $\hat{r}_2$, are both defined in (4.69). The M.P.O. surface current density $\vec{L}_3^c(x)$ at a distance x from edge 1 on the surface of length w of the truncated wedge is

$$\vec{L}_3^c(x) = \vec{L}_3(x) + \hat{r}_3 \left[H_1^i \delta_\tau^c(x,\tau\pi-\psi) + H_2^i \delta_\gamma^c(w-x,\psi+\beta-\pi)\right], \tag{7.81}$$

where $\vec{L}_3(x)$ is the physical optics current density defined in (4.74), and

$$\hat{r}_3 = -\hat{\rho}\cos(\phi+\beta)+\hat{\phi}\sin(\phi+\beta). \tag{7.82}$$

The field radiated by the P.O. current density on the truncated wedge is evaluated in Chapter 4. The magnetic field intensity $\vec{H}^c$ radiated by the "modifying" current density is found from (1.36), (7.79) - (7.81), and (1.21) to be

$$\vec{H}^c = \hat{z}H^c, \quad H^c = H_1^i \, e^{jka_1\cos\phi}[\Delta_\tau(\infty,\psi,\phi) + \Delta_\tau(w,\tau\pi-\psi,\tau\pi-\phi)]$$

$$+ H_2^i \, e^{jka_2\cos(m\pi-\phi)}[\Delta_\gamma(\infty,m\pi-\psi,m\pi-\phi) + \Delta_\gamma(w,\psi+\beta-\pi,\phi+\beta-\pi)], \tag{7.83}$$

where $\Delta_m(w,\xi,\eta)$ is defined in (7.69), and the normalization factor in (4.1) has been removed.

The M.P.O. field H_{mpo} scattered by the truncated wedge is given by (7.83) and (4.79) as

$$H_{mpo} = H_{po} + H^c. \tag{7.84}$$

Straightforward but laborious algebraic manipulation enables H_{mpo} to be reduced to

$$H_{mpo} = H_{gtd}^p + H_1^i \, e^{jka_1\cos\phi} \, T_\tau(w,\tau\pi-\psi,\tau\pi-\phi)$$

$$+ H_2^i \, e^{jka_2\cos(m\pi-\phi)} \, T_\gamma(w,\psi+\beta-\pi,\phi+\beta-\pi). \tag{7.85}$$

The primary diffracted field H_{gtd}^p of the G.T.D. is given by $(H_1^1 + H_2^1)$ in (4.17) after normalization by the factor in (4.1).

7.4(d) DISCUSSION AND RESULTS.

It is shown in section 7.4(c) that the M.P.O. approximation to the surface current density on the truncated wedge is equivalent to adding to the primary field of the geometrical theory of diffraction two fields for each edge. Each of these fields is a function of

the length of one side of the body adjacent to the edge, and is zero if that side is of infinite extent. However, these fields are dependent only upon the internal angle of one edge of the body, and therefore do not describe any interactive effects between the edges. Unlike physical optics, M.P.O. predicts a polarization sensitive back-scattered field.

The numerical evaluation of the integrals in (7.78) and (7.85) was accomplished by using a technique similar to that described in section 7.3(c). The curves in Figs. 7.11-7.13 compare the fields radiated by the P.O. current density, the M.P.O. current density, and the field diffracted by the undeformed wedge, with the field diffracted by the symmetrically truncated wedge illuminated by an electrically polarized field. The three figures apply to the wedges appropriate to Figs. 4.21 and 7.6, 4.23 and 7.7, and 4.24 respectively. It can be seen that the M.P.O. current density gives a more accurate estimate of the diffracted field than does the P.O. current density, although in certain regions Fig. 7.11 shows the most accurate estimate is that of the field diffracted from the undeformed wedge.

The magnetically polarized field diffracted by a symmetrically truncated wedge is shown in Fig. 7.14. It is apparent that the field radiated by the M.P.O. current density is a more accurate estimate of the scattered field than that radiated by the P.O. current density.

The M.P.O. approximation has also been used to estimate the normally backscattered field from the wedges appropriate to Figs. 4.25 - 4.30, with w in the range $0.05\lambda \leqslant w \leqslant 1.0\lambda$. When the curves obtained are plotted on these figures they are indistinguishable from the accurate curves.

It is concluded from these and other curves, that although the M.P.O. approximation results in a more accurate estimate of the scattered field than does P.O., it is in general less accurate than the use of the I.R. secondary diffraction coefficients defined in sections 7.2(a) and 7.2(b).

7.5(a) SUGGESTIONS FOR FURTHER RESEARCH.

The application of the S.C.R. technique to bodies other than the deformed wedge would give further insight into the effect of boundary perturbations on scattering patterns. In particular, the scattering from deformed circular cylinders and spheres could be compared with the G.T.D. and P.O. approximations and could also be used to evaluate the Fock approximation[78,79]. It may be possible to use the formulation of scattering from a deformed wedge to augment present knowledge on diffraction phenomena associated with the propagation of radio waves over mountain ranges[92].

The P.C.R. technique has yet to be applied to a scattering problem. The scattering by dielectric cylinders could be found using this technique, and the results used to evaluate the accuracy of approximate methods of determining

the scattering.

The results of applying the I.R. secondary diffraction coefficient to other scattering bodies such as polygonal cylinders and thick half-planes could be compared with results obtained by other methods[20,51,88,90]. The increased accuracy of the I.R. secondary diffraction coefficients over that of the G.T.D. encourages further investigation of the series in (6.2) with the aim of finding higher-order edge diffraction coefficients. A study of the convergence of this series is also warranted.

It has been shown how the application of the I.R. technique to the truncated wedge gives rise to the I.R. secondary diffraction coefficients. Similarly, the application of the I.R. technique to scattering bodies such as those of Fig. 6.6 may give further insight into the nature of the diffraction from the edge formed by two curved surfaces, or a curved and a flat surface[56].

The M.P.O. approximation to the surface current density on a perfectly conducting rectangular cylinder could be compared with other results[20,21,89] in an attempt to further improve the current density representation.

The volume of recent literature concerned with the derivation and evaluation of simple approximate methods of determining scattered fields shows that this is currently a most rewarding avenue of research. These approximate methods not only enable estimates of the field scattered by complicated bodies to be calculated quickly and with little programming effort, but can also provide an insight into the nature of scattering phenomena.

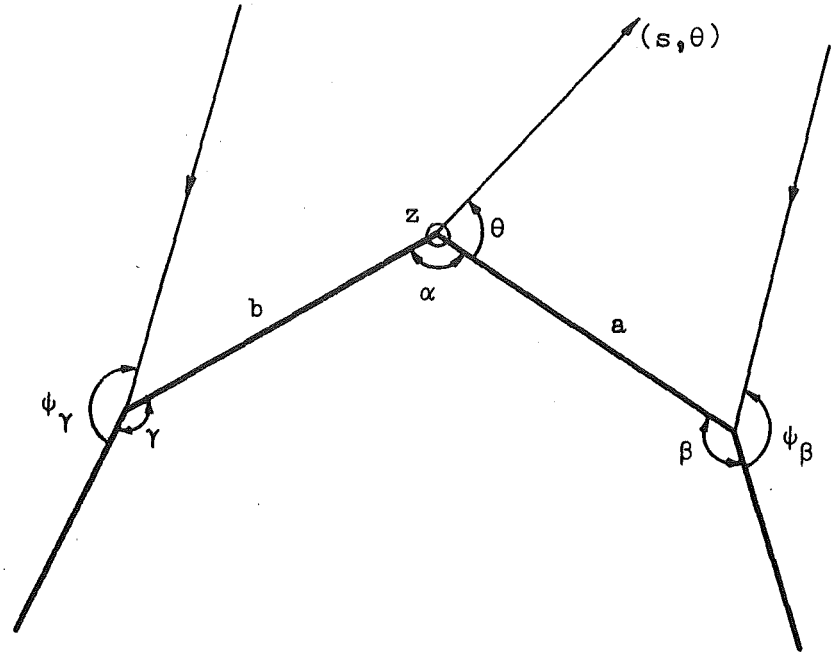

Figure 7.1 z axis perpendicular to the paper.

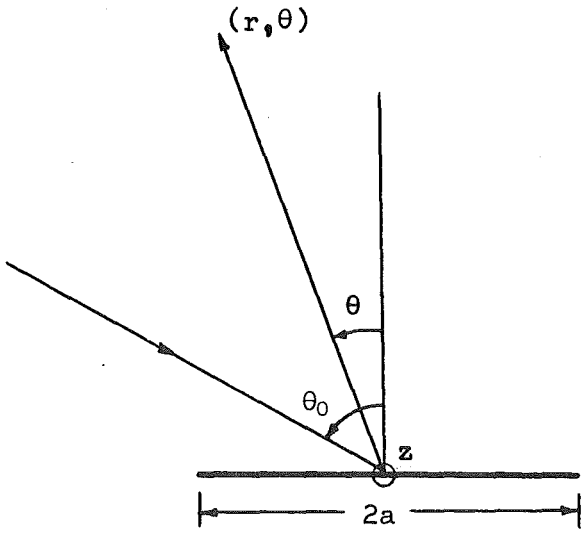

Figure 7.2 Scattering from a strip.

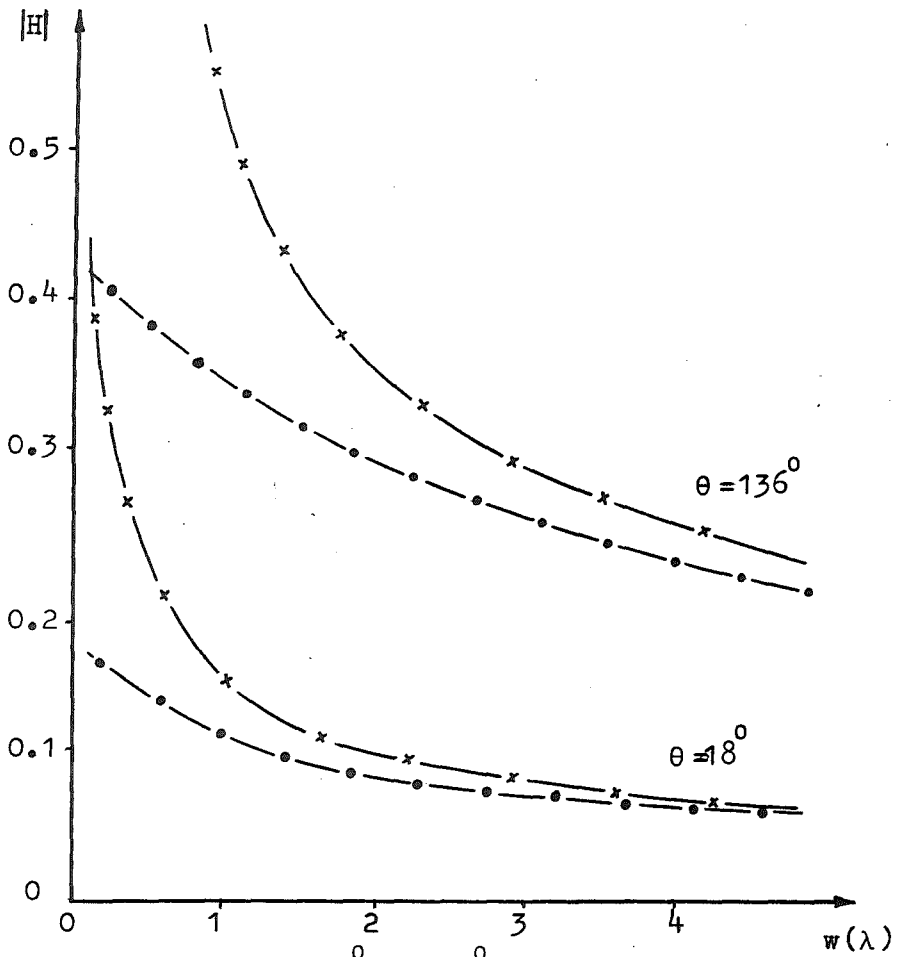

Figure 7.3 ($2\chi=94^{\circ}$, $\psi=20^{\circ}$)

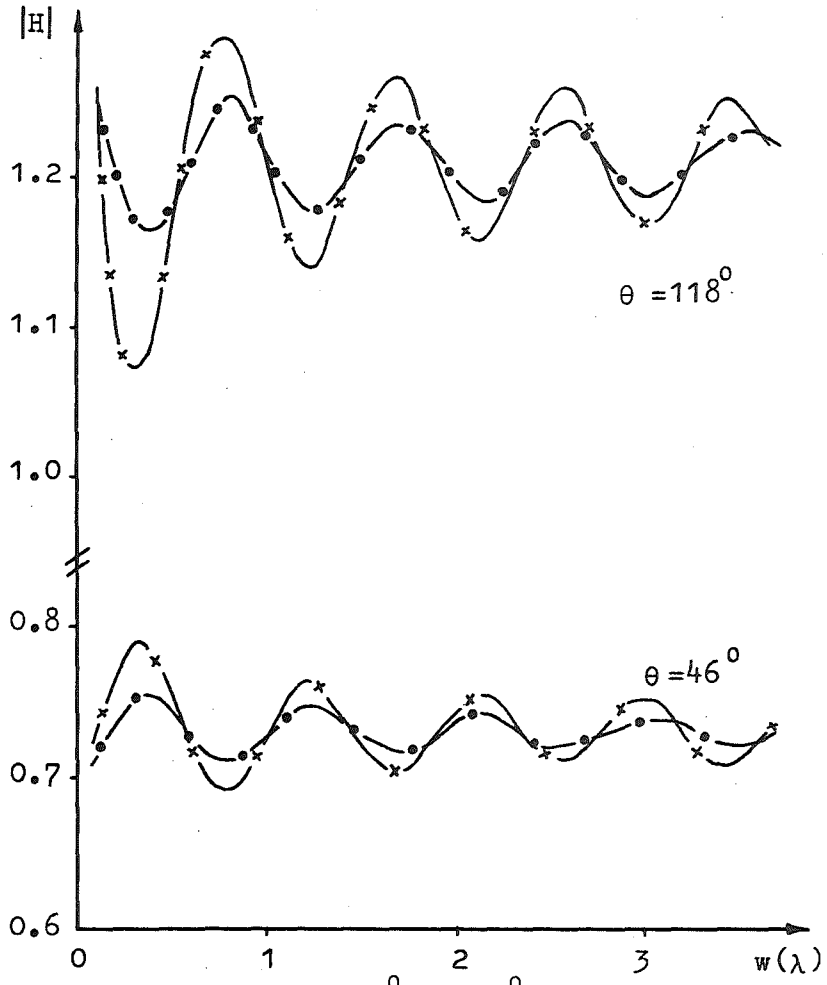

Figure 7.4 ($2\chi=94^{\circ}$, $\psi=60^{\circ}$)

Diffraction from edge at s=0. Legend on p 235.

Symmetrically Truncated Wedge. Magnetic Polarization.

LEGEND FOR FIGURES 7.3-7.7, 7.11-7.14

———————	from S.C.R. technique
—— —— ——	from Physical Optics
— △ ——— △ —	from the undeformed wedge
— ○ ——— ○ —	G.T.D. diffracted field
— □ ——— □ —	G.T.D. primary diffracted field
— × ——— × —	G.T.D. sum of primary and secondary diffracted fields
— ◆ ——— ◆ —	from Burke and Keller [47,91]
— • ——— • —	using I.R. secondary diffraction coefficient
— ⊙ ——— ⊙ —	from M.P.O.

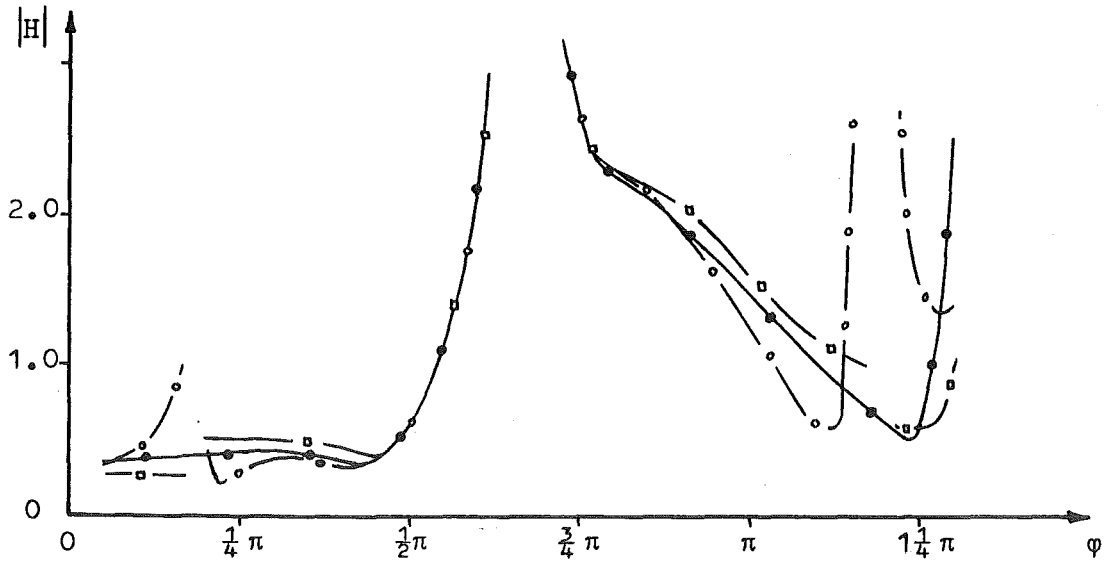

Figure 7.5 ($2\chi=114^0$, $\psi=60^0$, $w=0.1\lambda$)

Symmetrically Truncated Wedge. Magnetic Polarization.

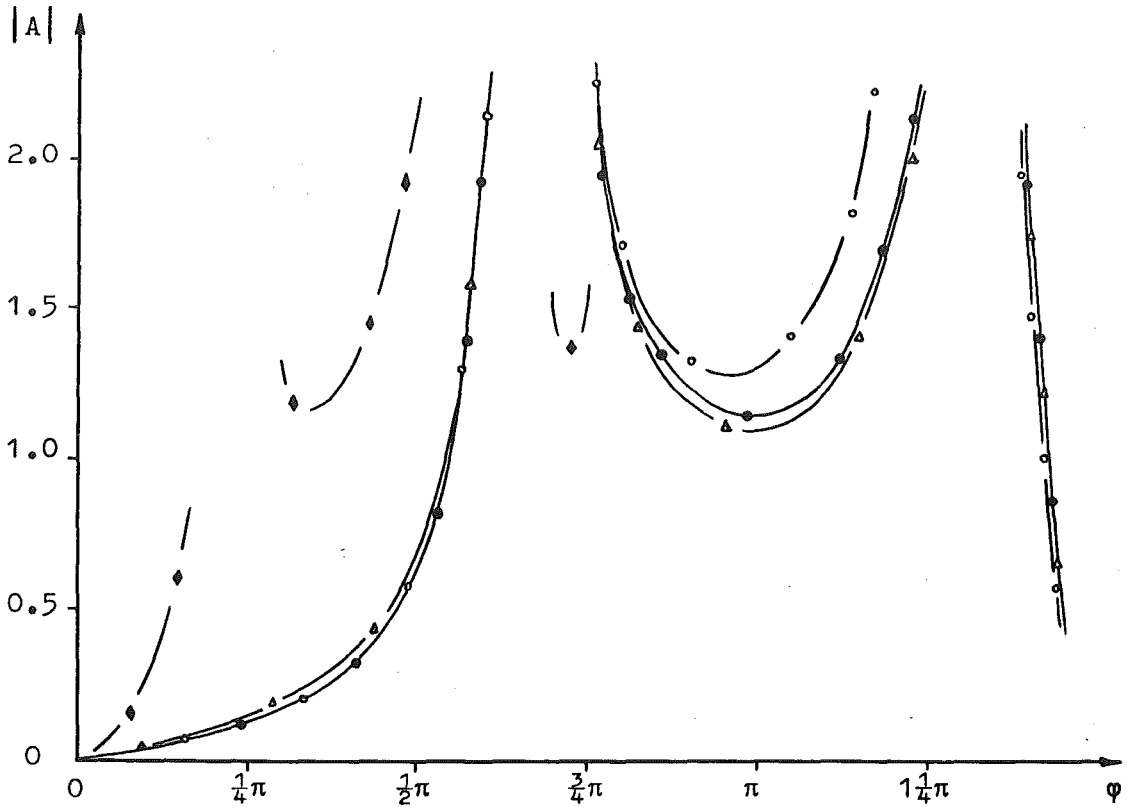

Figure 7.6 ($2\chi=94^0$, $\psi=60^0$, $w=0.1\lambda$) Legend on p 235.

Symmetrically Truncated Wedge. Electric Polarization.

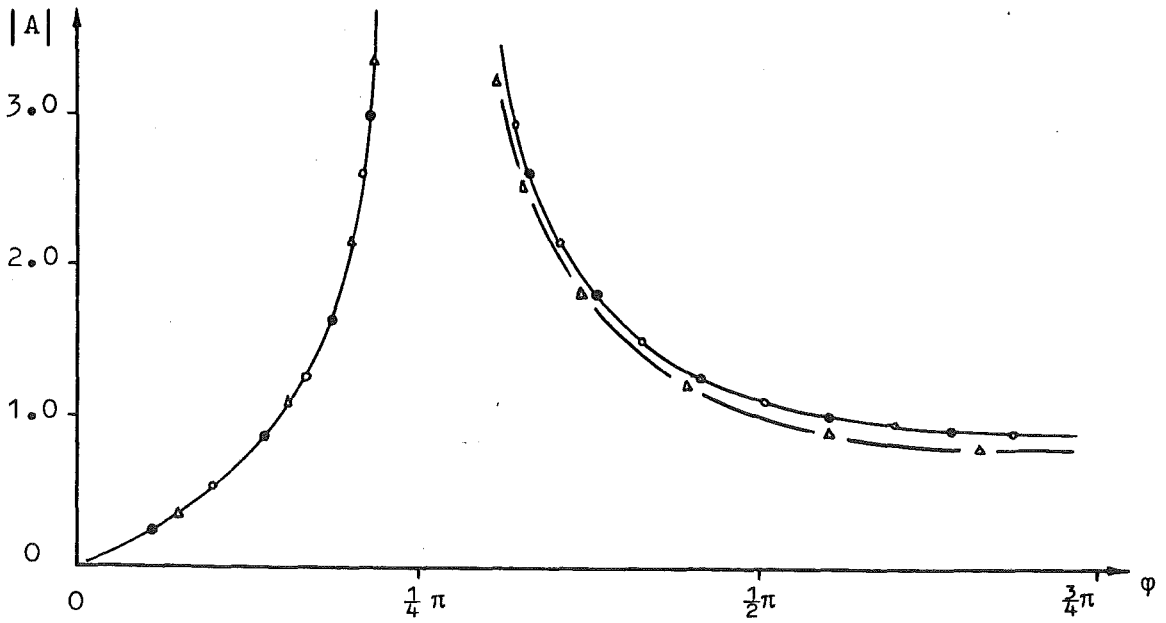

Figure 7.7 ($2\chi=94^0$, $\psi=133^0$, $w=0.1\lambda$) Legend on p 235.

Symmetrically Truncated Wedge. Electric Polarization.

LEGEND FOR FIGURES 7.8-7.10

———————	from Yu and Rudduck [65]
— ∘ ——— ∘ —	G.T.D. diffracted field
— ▫ ——— ▫ —	G.T.D. primary diffracted field
— × ——— × —	G.T.D. sum of primary and secondary diffracted fields
— ♦ ——— ♦ —	from Moshen and Hamid [62]
— • ——— • —	using I.R. secondary diffraction coefficient

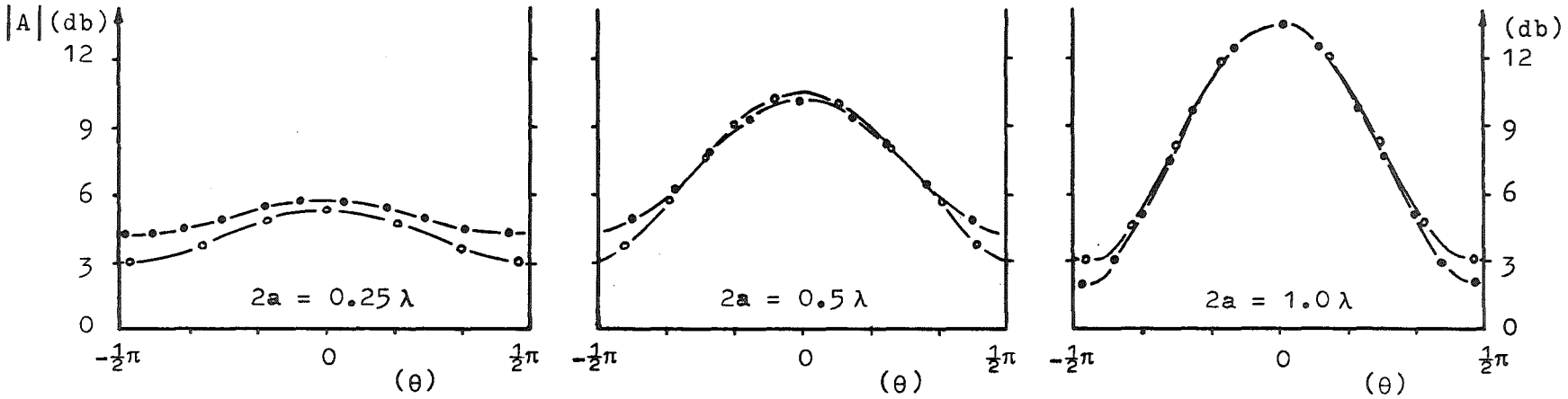

Figure 7.8 ($\theta_0 = 0$)

Strip Diffraction. Electric Polarization.

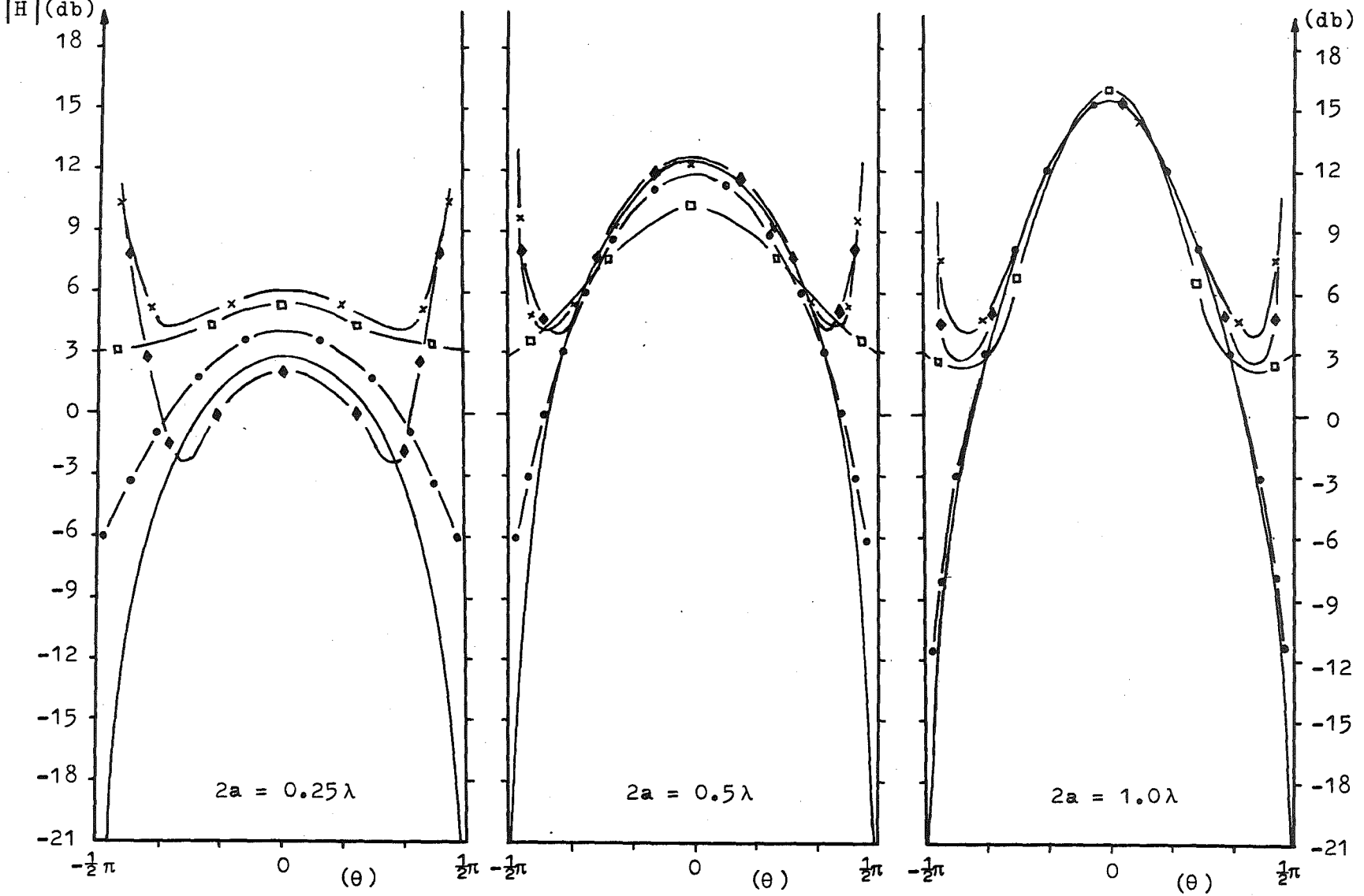

Figure 7.9 ($\theta_0 = 0$) Legend on p 237.

Strip Diffraction. Magnetic Polarization.

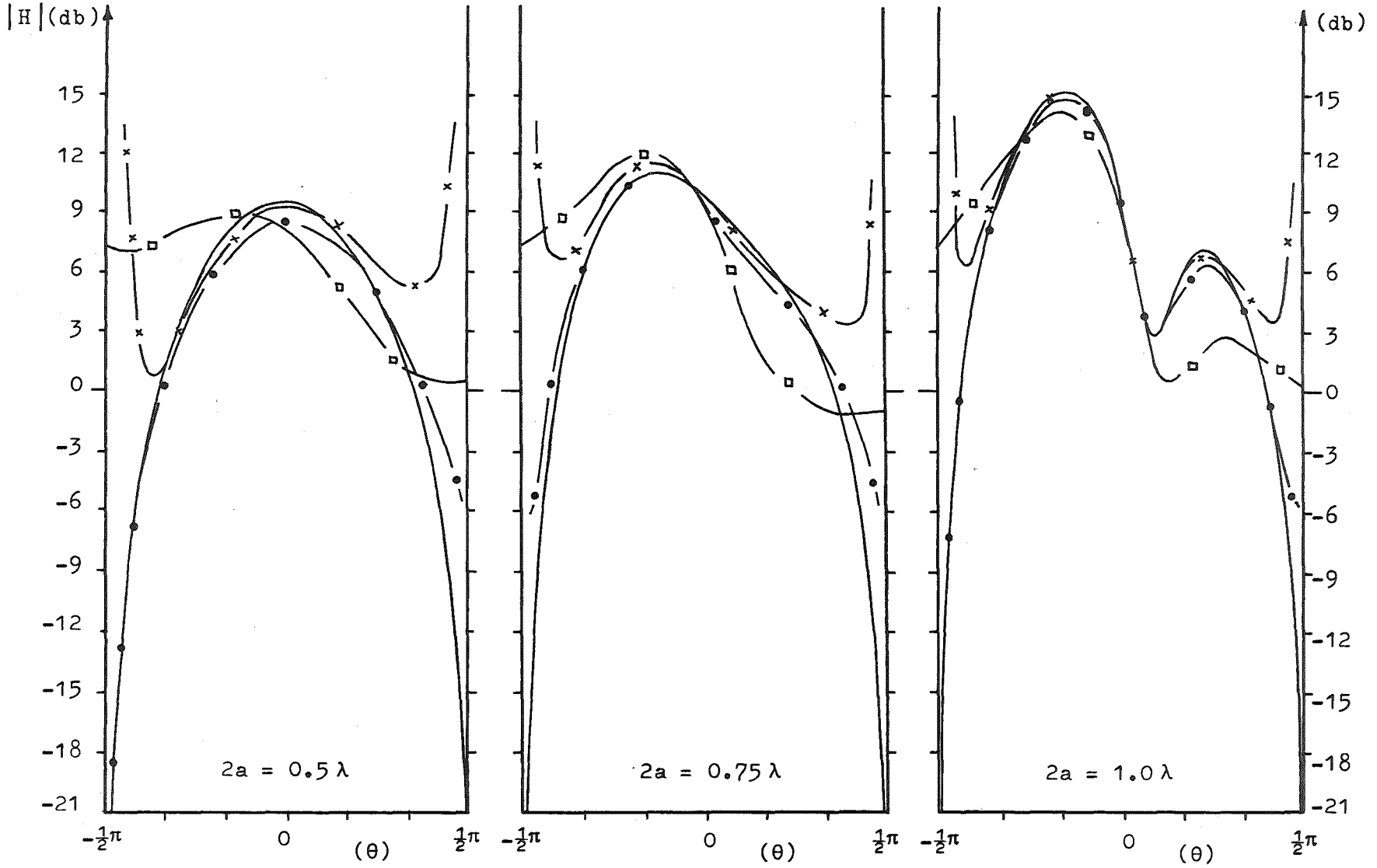

Figure 7.10 ($\theta_0=40^0$) Legend on p 237.

Strip Diffraction. Magnetic Polarization.

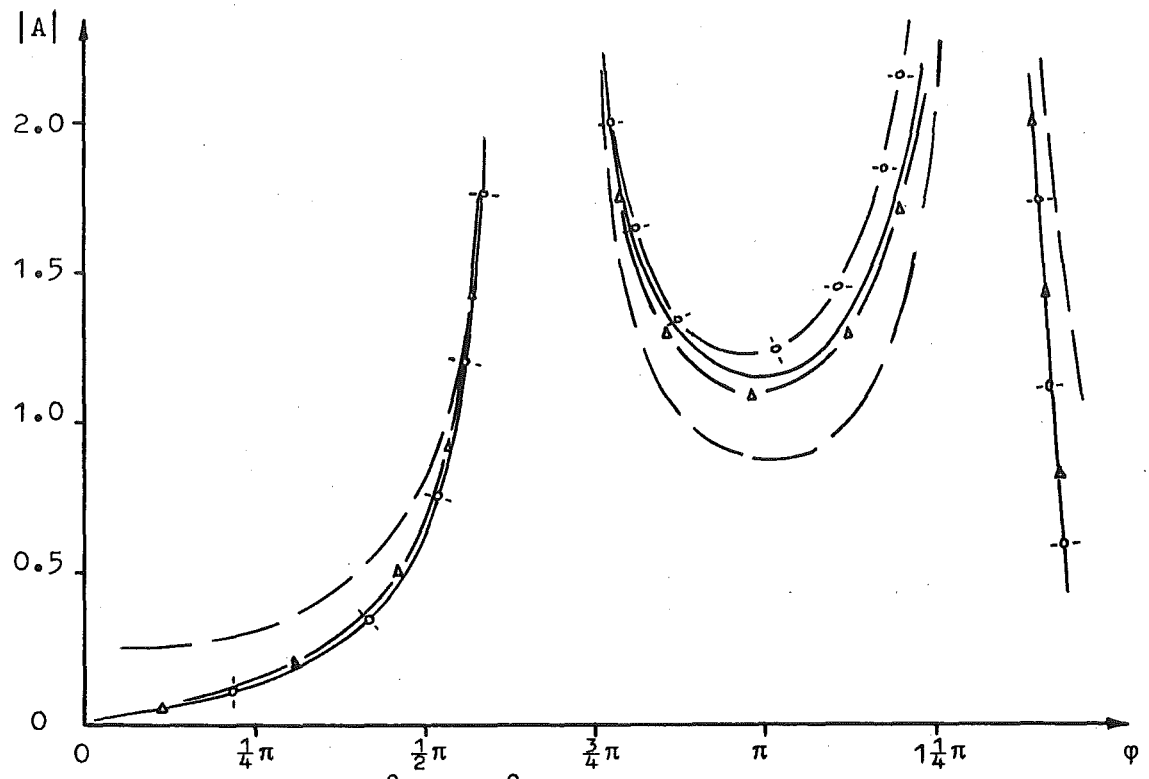

Figure 7.11 ($2\chi=94^0$, $\psi=60^0$, $w=0.1\lambda$) Legend on p 235.

Symmetrically Truncated Wedge. Electric Polarization.

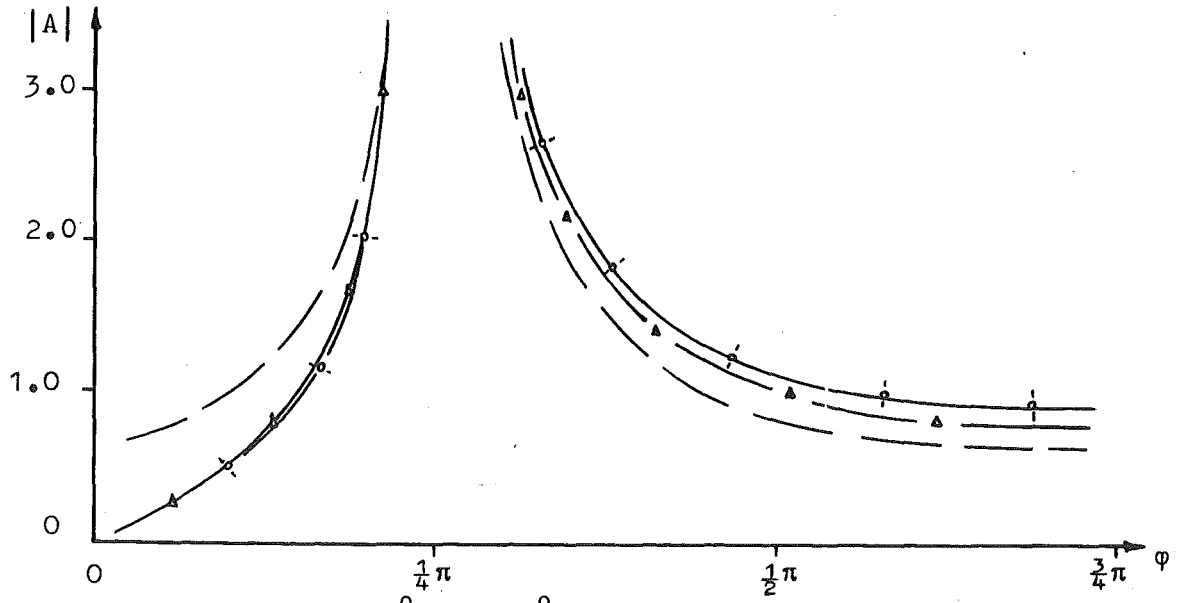

Figure 7.12 ($2\chi=94^0$, $\psi=133^0$, $w=0.1\lambda$) Legend on p 235.

Symmetrically Truncated Wedge. Electric Polarization.

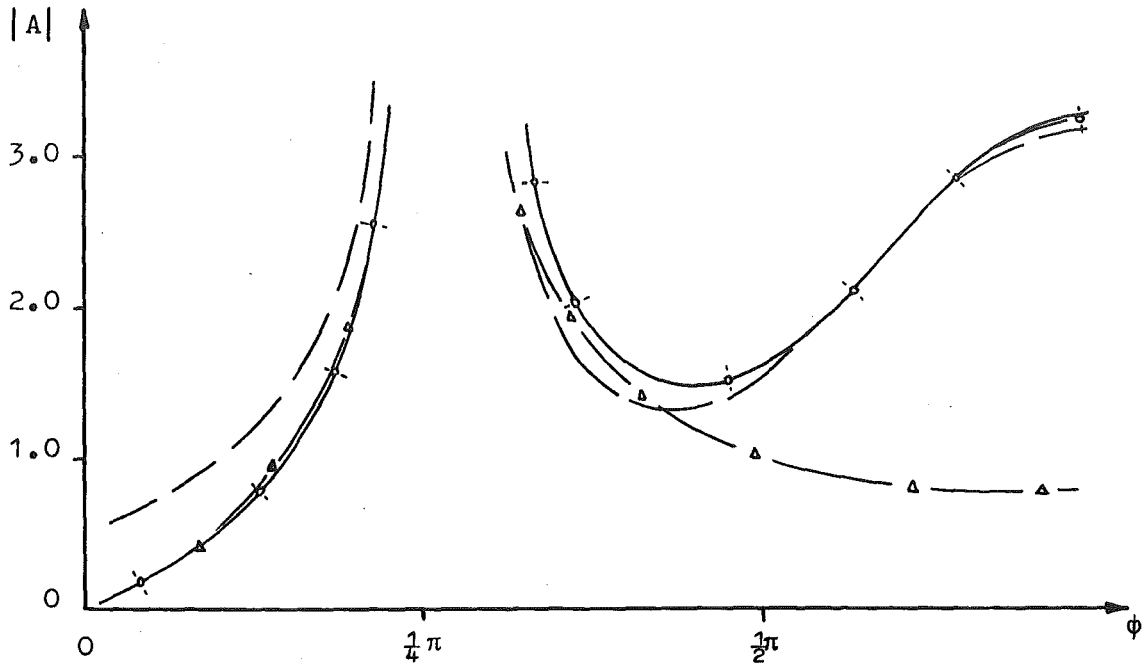

Figure 7.13 ($2\chi=94^0$, $\psi=133^0$, $w=1.0\lambda$) Legend on p 235.

Symmetrically Truncated Wedge. Electric Polarization.

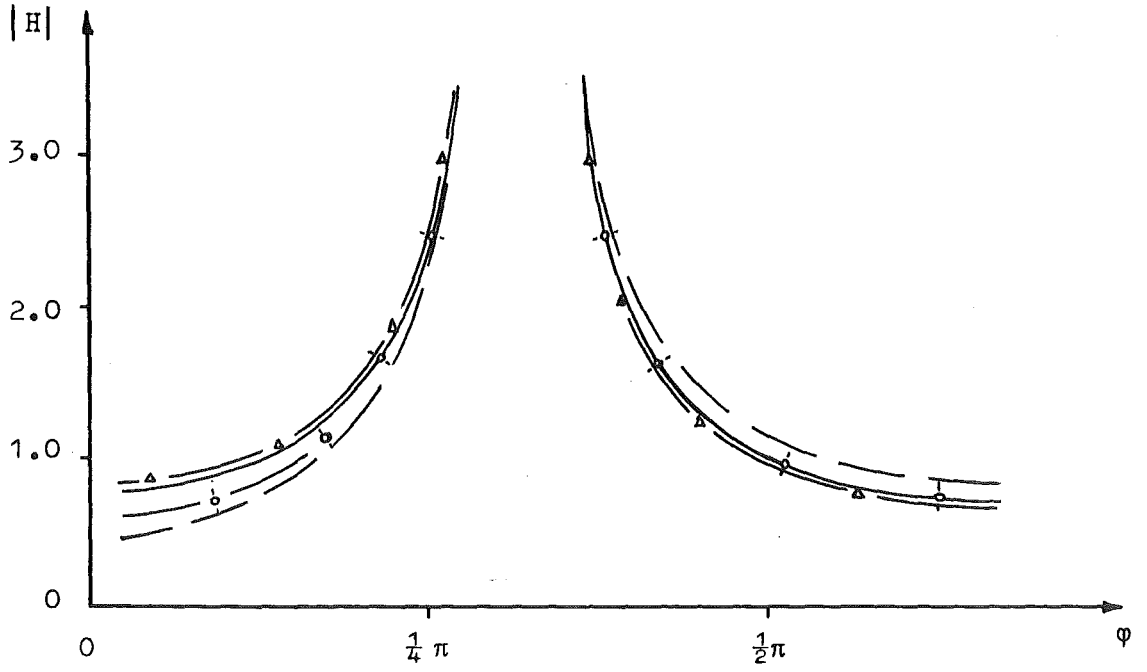

Figure 7.14 ($2\chi=114^0$, $\psi=123^0$, $w=0.1\lambda$) Legend on p 235.

Symmetrically Truncated Wedge. Magnetic Polarization.

APPENDIX 1

Consider

$$S = J_p(kb) \int_b^\infty \frac{H_\mu^{(2)}(kr)\, H_p^{(2)}(kr)}{r}\, dr$$

$$+ H_p^{(2)}(kb) \int_a^b \frac{H_\mu^{(2)}(kr)\, J_p(kr)}{r}\, dr \,.$$

By using (2.46), and letting k have a small negative imaginary part such that

$$k = (\alpha - j\varepsilon), \quad \varepsilon \to 0,$$

S can be expressed as

$$S = \frac{kb\, H_\mu^{(2)}(kb)}{\mu^2 - p^2} \left[H_p^{(2)}(kb)\, J_{p+1}(kb) - J_p(kb)\, H_{p+1}^{(2)}(kb) \right]$$

$$+ \frac{ka\, H_p^{(2)}(kb)}{\mu^2 - p^2} \left[H_{\mu+1}^{(2)}(ka)\, J_p(ka) - H_\mu^{(2)}(ka)\, J_{p+1}(ka) \right]$$

$$- \frac{H_p^{(2)}(kb)\, H_\mu^{(2)}(ka)\, J_p(ka)}{\mu + p} \,.$$

But[14],

$$H_{p+1}^{(2)}(z)\, J_p(z) - H_p^{(2)}(z)\, J_{p+1}(z) = \frac{2j}{\pi z},$$

and therefore

$$S = \frac{-2j\, H_{\mu}^{(2)}(kb)}{\pi(\mu^2-p^2)} + H_p^{(2)}(kb) \left[\frac{ka}{\mu^2-p^2} \{H_{\mu+1}^{(2)}(ka)\, J_p(ka) - H_{\mu}^{(2)}(ka)\} J_{p+1}(ka)\} - \frac{H_{\mu}^{(2)}(ka)\, J_p(ka)}{\mu+p}\right].$$

APPENDIX 2

Let $C_m(x)$, $\tilde{C}_m(x)$ be any two cylindrical Bessel functions of order m and argument x. Then

$$S = \sum_{m=-\infty}^{\infty} [C_{m-1}(x)\, \sin\{(m-1)\alpha\} + C_{m+1}(x)\, \sin\{(m+1)\alpha\}]\tilde{C}_m(z)$$

$$= \sum_{m=-\infty}^{\infty} [C_m(x)\, \sin\{m\alpha\}\tilde{C}_{m+1}(z) + C_m(x)\, \sin\{m\alpha\}\tilde{C}_{m-1}(z)]$$

$$= \sum_{m=-\infty}^{\infty} \frac{2m}{z}\, \tilde{C}_m(z) C_m(x) \sin\{m\alpha\}$$

$$= \sum_{m=1}^{\infty} \frac{4m}{z}\, \tilde{C}_m(z) C_m(x) \sin\{m\alpha\}.$$

APPENDIX 3

Consider

$$F = \xi(\ell)\, \frac{\partial^q}{\partial \delta^q} J_{\ell}(k\delta)\Big|_{\delta=0}, \quad \ell = 0,1,2,\text{---}, \qquad (A3.1)$$

where $\xi(\ell)$ is some function of ℓ. Repeated use of the recurrence relation for Bessel functions[14]

$$\frac{\partial}{\partial \delta} J_{\ell}(k\delta) = \frac{k}{2} \left[J_{\ell-1}(k\delta) - J_{\ell+1}(k\delta)\right],$$

shows that F may be written as

$$F = \xi(\ell) \left(\frac{k}{2}\right)^{q} \sum_{n=0}^{q} a_n J_{\ell-q+2n}(k\delta) \Bigg|_{\delta=0},$$

where the a_n are non-zero constants, and $a_o = 1$. Since

$$J_o(0) = 1; \quad J_p(0) = 0, \quad p \neq 0,$$

where p is any integer, ℓ is restricted to the values

$$\ell = q - 2n, \quad n \leq \frac{q}{2},$$

for F to be non-zero. The restriction on n arises from the condition in (A3.1) that ℓ be positive or zero.

If the function $\xi(\ell)$ is defined such that

$$\xi(\ell) = 0, \ \ell = q - 2n, \quad \forall n: 1 \leq n \leq \frac{q}{2},$$

then

$$F = 0, \ \ell \neq q,$$
$$= \xi(q) \left(\frac{k}{2}\right)^{q}, \ \ell = q.$$

APPENDIX 4

Consider the convex reflecting surface C in Fig. A1, illuminated by the incident plane wave $U^i(T)$ at the point T. The radius of curvature of the surface is R. The angles

made by the incident field with the normals OP, OQ to the surface at P and Q are ξ and $\xi+\delta\phi$ respectively, where $\angle POQ = \delta\phi$.

Let $|U^i(T)| = A_o$, and $|U^r(S)| = A$, where $U^r(S)$ is the reflected field at S. The conservation of energy flux in a cone of the reflected field requires

$$\rho_1 \, \delta\theta \, A_o^2 = (\rho_1 + r)\, \delta\theta \, A^2. \qquad (A4.1)$$

From ΔOQX,

$$\delta\theta = 2\,\delta\phi,$$

and since

$$R\,\delta\phi \rightarrow \frac{\rho_1 \, \delta\theta}{\cos\xi}, \quad \delta\phi \rightarrow 0,$$

$$\rho_1 \rightarrow \frac{R}{2}\cos\xi, \quad \delta\phi \rightarrow 0. \qquad (A4.2)$$

From (A4.1) and (A4.2),

$$\frac{A}{A_o} = \sqrt{\frac{R\cos\xi}{2r}} \qquad r >> R,$$

and hence

$$U^r(S) = \pm\, U^i(T) \sqrt{\frac{R\cos\xi}{2r}}\; e^{-jkr}, \quad r >> R,$$

where the upper (lower) sign applies when the field is magnetically (electrically) polarized in the z-direction.

APPENDIX 5.

Consider the functions $I(\theta-\pi)$ and $I(\theta+\pi)$ where

$$I(\xi) = \int_{-\infty}^{\infty} \frac{\sin\left(j\omega+\frac{\pi}{n}\right)}{\left[\cos\left(j\omega+\frac{\pi}{n}\right)-\cos\left(\frac{\xi}{n}\right)\right]\left[\cosh(n\omega)+\cosh x\right]}\, d\omega,$$

$$0 < \theta < n\pi, \quad n\pi = 2\pi - \alpha, \quad 1 < n < 2. \qquad (A5.1)$$

This integral can be evaluated by performing two contour integrations in the complex ω plane of Fig. A2. C_1 is the contour along the real axis from $-\infty$ to ∞, C_2 is the semicircle of radius R closing C_1 in the upper half-plane (U.HP.), and C_3 is the semicircle of radius R closing C_1 in the lower half-plane (L.HP.). In abbreviated notation,

$$I(\xi) = \int_{C_1}, \quad \int_{C_1} + \int_{C_2} = \sigma_{uhp}, \quad \int_{C_1} + \int_{C_3} = \sigma_{lhp}, \tag{A5.2}$$

where σ_{uhp} and σ_{lhp} are the sum of the residues in the upper and lower half-planes respectively. Examination of the integrand of $I(\xi)$ shows that

$$\int_{C_2} = \int_{C_3} = 0, \qquad R \to \infty,$$

and thus, from (A5.2),

$$2\, I(\xi) = \sigma_{lhp} + \sigma_{uhp}. \tag{A5.3}$$

(i) Consider the poles located at

$$\omega = j\left[\pm\frac{\xi}{n} + \frac{\pi}{n} + 2p\pi\right], \tag{A5.4}$$

where p is any integer or zero. The notation $p^{\pm}$ is used to denote the pole located by p with the $\pm$ sign in (A5.4). The residues $\delta_p^{\pm}$ at the $p^{\pm}$ poles in the U.HP. are

$$\delta_p^{\pm} = \frac{2\pi}{\cos(\pm\xi+2pn\pi)-\cosh x},$$

and the residues $\gamma_p^{\pm}$ in the L.HP. are

$$\gamma_p^{\pm} = \frac{-2\pi}{\cos(\pm\xi+2pn\pi)-\cosh x}.$$

Hence,

$$\delta_p^{+} = -\gamma_{-p}^{-}, \quad \delta_p^{-} = -\gamma_{-p}^{+}. \tag{A5.5}$$

(a) When $\xi = (\theta-\pi)$, examination of (A5.4) subject to the restrictions on θ and n in (A5.1) shows that the $p^{\pm}$ ($p \geq 0$) poles all lie in the U.HP., and the $p^{\pm}$ ($p < 0$) poles all lie in the L.HP.

The sum σ_1 of the residues $\delta_p^{\pm}$, $\gamma_p^{\pm}$ in the upper and lower half-planes reduces, with the use of (A5.5), to

$$\sigma_1 = \delta_o^{+} + \delta_o^{-} = \frac{-4\pi}{\cos\theta+\cosh x}, \tag{A5.6}$$

when $\xi = (\theta-\pi)$.

(b) When $\xi = (\theta+\pi)$, the $p^{\pm}$ ($p \geq 1$) poles and the 0^{+} pole located by (A5.4) lie in the U.HP. The $p^{\pm}$ ($p < 0$) poles and the 0^{-} pole lie in the L.HP. provided $\theta < 2\pi-2\alpha$. If $\theta > 2\pi-2\alpha$, the -1^{+} pole lies in the U.HP. Then, using (A5.5),

$$\sigma_1 = \varepsilon_o(\delta_1^{-} + \delta_{-1}^{+}) = \frac{-\varepsilon_o\, 4\pi}{\cos(\theta+2\alpha)+\cosh x}, \tag{A5.7}$$

where

$$\varepsilon_o = 1, \quad 2\pi-2\alpha < \theta < n\pi,$$
$$= 0, \quad 0 < \theta < 2\pi-2\alpha.$$

(ii) Consider the poles located by

$$\omega = \pm \frac{x}{n} + j(2p+1)\frac{\pi}{n}, \qquad (A5.8)$$

where p is any integer or zero. The notation $p^{\pm}$ is used to denote the pole located by p with the ± sign in (A5.8). The residues $\delta_p^{\pm}$ at the $p^{\pm}$ poles in the U.HP. are

$$\delta_p^{\pm} = \frac{2\pi \sinh(\pm\frac{x}{n} + j\frac{2p\pi}{n})}{n \sinh(\pm x)\left[\cosh(\pm\frac{x}{n}+j\frac{2p\pi}{n}) - \cos(\frac{\xi}{n})\right]},$$

and the residues $\gamma_p^{\pm}$ at the $p^{\pm}$ poles in the L.HP. are

$$\gamma_p^{\pm} = \frac{-2\pi \sinh(\pm\frac{x}{n}+j\frac{2p\pi}{n})}{n \sinh(\pm x)\left[\cosh(\pm\frac{x}{n}+j\frac{2p\pi}{n}) - \cos(\frac{\xi}{n})\right]}.$$

Comparison of $\delta_p^{\pm}$ and $\gamma_p^{\pm}$ shows that the expressions in (A5.5) are valid.

The locations of the poles given by (A5.8) are independent of ξ. The $p^{\pm}$ $(p \geqslant 0)$ poles lie in the U.HP., and the $p^{\pm}$ $(p < 0)$ poles lie in the L.HP. Using (A5.5), the sum σ_2 of the residues $\delta_p^{\pm}, \gamma_p^{\pm}$ in the upper and lower half planes is given by

$$\sigma_2 = \delta_o^{+} + \delta_o^{-} = \frac{4\pi \sinh(\frac{x}{n})}{n \sinh x\left[\cosh(\frac{x}{n}) - \cos(\frac{\xi}{n})\right]}. \qquad (A5.9)$$

Notice from the position of the poles that σ_2 is unchanged if x is replaced by $j(y-\pi)$, $0 \leqslant y \leqslant 2\pi$.

From (A5.3)

$$I(\xi) = \frac{\sigma_1 + \sigma_2}{2} ,$$

and thus, from (A5.6), (A5.7), and (A5.9),

$$I(\theta-\pi) = 2\pi\left[\frac{\sinh(\frac{x}{n})}{n \sinh x\left[\cosh(\frac{x}{n})-\cos(\frac{\theta-\pi}{n})\right]} - [\cos\theta+\cosh x]^{-1}\right],$$

$$I(\theta+\pi) = 2\pi\left[\frac{\sinh(\frac{x}{n})}{n \sinh x\left[\cosh(\frac{x}{n})-\cos(\frac{\theta+\pi}{n})\right]} - \varepsilon_o[\cos(\theta+2\alpha)+\cosh x]^{-1}\right].$$

APPENDIX 6

Consider the functions $J(\theta-\pi)$ and $J(\theta+\pi)$ where

$$J(\xi) = \int_{-\infty}^{\infty} \frac{\sinh(n\omega)}{[\cos(j\omega+\frac{\pi}{n})-\cos(\frac{\xi}{n})][\cosh(n\omega)+\cosh x]} d\omega,$$

$$0 < \theta < n\pi, \quad n\pi = 2\pi-\alpha, \quad 1 < n < 2.$$

This integral is similar to that evaluated in Appendix 5, and since the integration is performed in a similar manner, only the essential steps are noted here. The location of the poles of $J(\xi)$, and $I(\xi)$ of Appendix 5, are identical.

(i) Consider the poles located by

$$\omega = j[\pm\frac{\xi}{n} + \frac{\pi}{n} + 2p\pi],$$

where p is any integer or zero. The residues $\delta_p^{\pm}$ at the $p^{\pm}$ poles in the U.HP. are

$$\delta_p^{\pm} = \frac{2\pi j \sin(\pm\xi+2p\pi n)}{\sin(\pm\frac{\xi}{n})[\cos(\pm\xi+2p\pi n)-\cosh x]},$$

and the residues $\gamma_p^{\pm}$ in the L.HP. are

$$\gamma_p^{\pm} = \frac{-2\pi j \sin(\pm\xi+2p\pi n)}{\sin(\pm\frac{\xi}{n})[\cos(\pm\xi+2p\pi n)-\cosh x]},$$

and hence

$$\delta_p^{+} = -\gamma_p^{-}, \quad \delta_p^{-} = -\gamma_{-p}^{+}. \tag{A6.1}$$

(a) When $\xi = (\theta-\pi)$, the sum σ_1 of the residues $\delta_p^{\pm}$, $\gamma_p^{\pm}$ in the upper and lower half-planes reduces, with the use of (A6.1), to

$$\sigma_1 = \delta_o^{+} + \delta_o^{-} = \frac{4\pi j \sin\theta}{\sin(\frac{\theta-\pi}{n})[\cos\theta+\cosh x]}. \tag{A6.2}$$

(b) When $\xi = (\theta+\pi)$,

$$\sigma_1 = \varepsilon_o(\delta_1^{-} + \delta_{-1}^{+}) = \frac{\varepsilon_o\, 4\pi j \sin(\theta+2\alpha)}{\sin(\frac{\theta+\pi}{n})[\cos(\theta+2\alpha)+\cosh x]}, \tag{A6.3}$$

where

$$\varepsilon_o = 1, \quad 2\pi-2\alpha < \theta < n\pi,$$
$$= 0, \quad 0 < \theta < 2\pi-2\alpha.$$

(ii) Consider the poles located by

$$\omega = \pm \frac{x}{n} + j(2p+1)\frac{\pi}{n},$$

where p is any integer or zero. The residues $\delta_p^{\pm}$ at the $p^{\pm}$ poles in the U.HP. are

$$\delta_p^{\pm} = \frac{2\pi j}{n\left[\cosh(\pm\frac{x}{n} + j\frac{2p\pi}{n}) - \cos(\frac{\xi}{n})\right]},$$

and the residues $\gamma_p^{\pm}$ at the $p^{\pm}$ poles in the L.HP are

$$\gamma_p^{\pm} = \frac{-2\pi j}{n\left[\cosh(\pm\frac{x}{n} + j\frac{2p\pi}{n}) - \cos(\frac{\xi}{n})\right]}.$$

Comparison of $\delta_p^{\pm}$ and $\gamma_p^{\pm}$ shows that the expressions in (A6.1) are valid.

The sum σ_2 of the residues $\delta_p^{\pm}$ and $\gamma_p^{\pm}$ in the upper and lower half-planes is

$$\sigma_2 = \delta_o^{+} + \delta_o^{-} = \frac{4\pi j}{n\left[\cosh(\frac{x}{n}) - \cos(\frac{\xi}{n})\right]} \qquad (A6.4)$$

Notice the σ_2 remains unchanged if x is replaced by $j(y-\pi)$, $0 \leq y \leq 2\pi$. Since

$$J(\xi) = \frac{\sigma_1 + \sigma_2}{2},$$

from (A6.2), (A6.3), and (A6.4),

$$J(\theta-\pi) = 2\pi j\left[\frac{\sin\theta}{\sin(\frac{\theta-\pi}{n})\left[\cos\theta+\cosh x\right]} + \frac{1}{n}\left[\cosh(\frac{x}{n}) - \cos(\frac{\theta-\pi}{n})\right]^{-1}\right],$$

$$J(\theta+\pi) = 2\pi j \left[\frac{\varepsilon_o \sin(\theta+2\alpha)}{\sin(\frac{\theta+\pi}{n})[\cos(\theta+2\alpha)+\cosh x]} \right.$$

$$\left. + \frac{1}{n}\left[\cosh(\frac{x}{n})-\cos(\frac{\theta+\pi}{n})\right]^{-1}\right].$$

APPENDIX 7

Consider the expression $J(\xi)$ defined in Appendix 6, but subject to the restrictions

$$1 < n < 2, \quad 0 \leqslant \xi \leqslant n\pi.$$

(i) Consider the poles located by

$$\omega = j[\pm \frac{\xi}{n} + \frac{\pi}{n} + 2p\pi].$$

Using the notation of Appendix 6, the $p^{\pm}$ $(p \geqslant 1)$ poles and the 0^+ pole lie in the U.HP.; and the $p^{\pm}$ $(p < 0)$ poles and the 0^- pole lie in the L.HP., provided $\xi > \pi$. If $\xi < \pi$, the 0^- pole lies in the U.HP. and σ_1, the sum of the residues in the upper and lower half-planes is

$$\sigma_1 = \frac{\varepsilon(\xi)\ 4\pi j \sin\xi}{\sin(\frac{\xi}{n})[\cos\xi-\cosh x]}, \qquad \text{(A7.1)}$$

where

$$\varepsilon(\xi) = 1, \quad 0 \leqslant \xi < \pi,$$
$$= 0, \quad \pi < \xi \leqslant n\pi.$$

(ii) Consider the poles located by

$$\omega = \pm \frac{x}{n} + j(2p+1)\frac{\pi}{n}.$$

The sum σ_2 of the residues in the upper and lower half-planes

is given in (A6.4).

Hence, from (A6.4) and (A7.1)

$$J(\xi) = 2\pi j\left[\frac{\varepsilon(\xi)\ \sin\xi}{\sin(\frac{\xi}{n})[\cos\xi-\cosh x]} + \frac{1}{n}\left[\cosh(\frac{x}{n})-\cos(\frac{\xi}{n})\right]^{-1}\right].$$

APPENDIX 8

Consider the expression $I(\xi)$ defined in Appendix 5, but subject to the restrictions

$$1 < n < 2, \quad 0 \leqslant \xi \leqslant n\pi.$$

(i) Consider the poles located by

$$\omega = j[\pm\frac{\xi}{n} + \frac{\pi}{n} + 2p\pi].$$

Using the notation of Appendix 5, the $p^{\pm}$ $(p \geqslant 1)$ poles and the 0^{+} pole lie in the U.HP.; and the $p^{\pm}$ $(p < 0)$ poles and the 0^{-} pole lie in the L.HP. provided $\xi > \pi$. If $\xi < \pi$, the 0^{-} pole lies in the U.HP. and σ_1, the sum of the residues in the upper and lower half-planes is

$$\sigma_1 = \frac{\varepsilon(\xi)\ 4\pi}{\cos\xi-\cosh x}, \tag{A8.1}$$

where

$$\varepsilon(\xi) = 1, \quad 0 \leqslant \xi < \pi$$
$$= 0, \quad \pi < \xi \leqslant n\pi.$$

(ii) Consider the poles located by

$$\omega = \pm\frac{x}{n} + j(2p+1)\ \frac{\pi}{n}.$$

The sum σ_2 of the residues in the upper and lower half-planes is given in (A5.9).

Hence, from (A5.9) and (A8.1)

$$I(\xi) = 2\pi\left[\frac{\varepsilon(\xi)}{\cos\xi-\cosh x} + \frac{\sinh(\frac{x}{n})}{n\ \sinh x[\cosh(\frac{x}{n})-\cos(\frac{\xi}{n})]}\right].$$

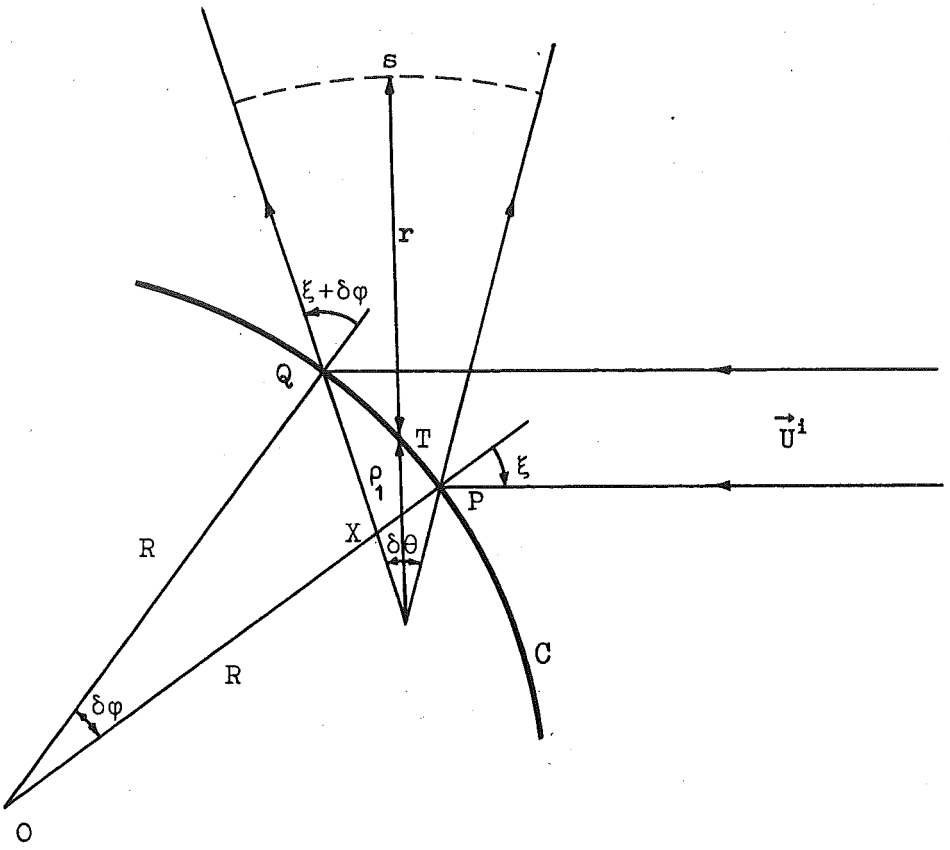

Figure A1 Reflection from a cylindrical surface.

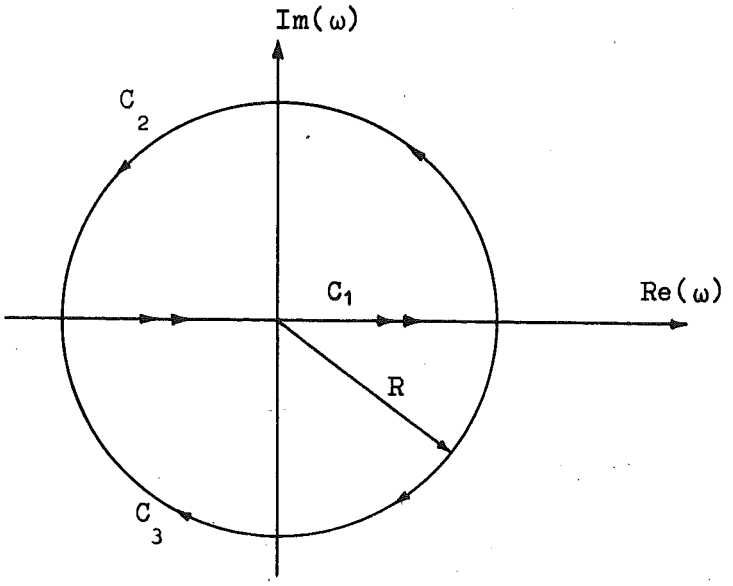

Figure A2

REFERENCES

1 Hunter J.D. and Bates R.H.T. "Computation of Scattering From a Class of Bodies of Unrestricted Size". To appear in J. Eng. Maths., 4, No 2, 1970.

2 Hunter J.D. "Computer Aided Design in Perturbed Boundary Value Problems" Proc. 3rd Hawaii Int'l Conference on System Sciences, 1970, 694-697.

3 Bates R.H.T. and Hunter J.D. "Scattering from Perfectly Conducting Wedges excited by Transversely Polarized Line Sources" Int. J. Electronics, 26, 1969, 91-94.

4 Morse P.M. and Feshbach H. Methods of Theoretical Physics, McGraw-Hill, N.Y., 1953.

5 Noble B. Methods Based on the Wiener-Hopf Technique for the Solution of Partial Differential Equations, Pergamon, London, 1958.

6 Bowkamp C.J. "Diffraction Theory" Rpts. Prog. Phys., XVII, 1954, 35.

7 Sommerfeld A. Math. Ann., 47, 1896, 317.

8 Macdonald H.M. Electric Waves, Cambridge University Press, 1902.

9 Macdonald H.M. "A Class of Diffraction Problems" Proc. London Math. Soc., 14, 1915, 410-427.

10 Pauli W. "On Asymptotic Series for Functions in the Theory of Diffraction of Light" Phys. Review, 54, 1938, 924-931.

11 Oberhettingher F. "On Asymptotic Series for Functions Occurring in the Theory of Diffraction of Waves by Wedges" J. Math. and Phys., 34, 1955, 245-255.

12 Kontorowich M.J. and Lebedev N.N. "On a Method of Solution of Some Problems of the Diffraction Theory". J. Phys. U.S.S.R., 1, 1939, 229.

13 Jones D.S. The Theory of Electromagnetism, Pergamon, London, 1964, § 9.14.

14 Abramowitz M. and Stegun I.A. Handbook of Mathematical Functions, Dover, N.Y., 1965, Chap. 9.

15 Jones D.S. The Theory of Electromagnetism, Pergamon, London, 1964, § 8.5.

16 Richmond J.H. "Scattering by a Dielectric Cylinder of Arbitrary Cross Section Shape" IEEE Trans. Ant. and Prop., AP-13, 1965, 334-341.

17 Harrington R.F. Field Computation by Moment Methods, Macmillan, N.Y., 1968.

18 Hashimoto M. and Fujisawa K. "Considerations on Matrix Methods and Estimation of their Errors" to be published in IEEE Trans. Micro. Theory and Tech.

19 Andreason M.G. "Scattering from Parallel Metallic Cylinders with Arbitrary Cross Sections" IEEE Trans. Ant. and Prop., AP-12, 1964, 746-754.

20 Mei K.K. and van Bladel J.G. "Scattering by Perfectly-Conducting Rectangular Cylinders" IEEE Trans. Ant. and Prop., AP-11, 1963, 185-192.

21 Iizuka K. and Yen J.L. "Surface Currents on Triangular and Square Metal Cylinders" IEEE Trans. Ant. and Prop., AP-15, 1967, 795-801.

22 Andreasen M.G. "Comments on 'Scattering by Conducting Rectangular Cylinders'" Trans. Ant. and Prop., AP-12, 1964, 235-236.

23 Copley L.G. "Fundamental Results Concerning Integral Representations in Acoustic Radiation" J.A.S.A., 44, 1968, 28-32.

24 Hönl H, Maue A.W., and Westpfahl K. Handbuch der Physik, 25, Springer-Verlag, Berlin, 1961, 240.

25 Waterman P.C. "Matrix Formulation of Electromagnetic Scattering" Proc. IEEE, 53, 1965, 805-812.

26 Waterman P.C. "New Formulation of Acoustic Scattering" J.A.S.A., 45, 1969, 1417-1429.

27 Yee H.Y. and Audeh N.F. "Uniform Waveguides with Arbitrary Cross-Section considered by the Point-Matching Method" IEEE Trans. Micro. Theory and Tech., MTT-13, 1965, 847-851.

28 Fuller J.A. and Audeh N.F. "The Point-Matching Solution of Uniform Nonsymmetric Waveguides" IEEE Trans. Micro. Theory and Tech., MTT-17, 1969, 114-115.

29 Bates R.H.T. "The Theory of the Point-Matching Method for Perfectly Conducting Waveguides and Transmission Lines" IEEE Micro. Theory and Tech., MTT-17, 1969, 294-301.

30 Bates R.H.T. "Radiation Pattern of Line Sources on a Wedge Covered with Finite Distributions of Dielectric" Proc. IEEE, 55, 1967, 1650-1651.

31 Richmond J.H. "TE-Wave Scattering by a Dielectric Cylinder of Arbitrary Cross-Section Shape" IEEE Trans. Ant. and Prop., AP-14, 1966, 460-464.

32 Jones D.S. The Theory of Electromagnetism, Pergamon, London, 1964, § 9.2.

33 Kay A.F. and Nihen J.F. "Scattering and Currents Induced on Sharp and Rounded Corners" IEEE Trans. Ant. and Prop., AP-14, 1966, 112-114.

34 Bates R.H.T. "Modal Expansions for Electromagnetic Scattering from Perfectly Conducting Cylinders of Arbitrary Cross-section". Proc. IEE, 115, 1968, 1443-1445.

35 Mautz J.R. and Harrington R.F. "Radiation and Scattering from Bodies of Revolution" Appl. Sci. Res., 20, 1969, 405-435.

36 Mullin C.R., Sandburg R., and Velline C.O. "A Numerical Technique for the Determination of Scattering Cross Sections of Infinite Cylinders of Arbitrary Geometrical Cross Section" IEEE Trans. Ant. and Prop., AP-13, 1965, 141-149.

37 Burrows M.L. "Equivalence of the Rayleigh Solution and the Extended-Boundary-Condition Solution for Scattering Problems" Electron. Lett., 5, 1969, 277-278.

38 Millar R.F. "Rayleigh Hypothesis in Scattering Problems" Electron. Lett., 5, 1969, 416-418.

39 Bates R.H.T. "Rayleigh Hypothesis, the Extended Boundary Condition and Point Matching" Electron Lett., 5, 1969, 654-655.

40 Burrows M.L. "Example of the Generalized-Function Validity of the Rayleigh Hypothesis" Electron. Lett., 5, 1969, 694-695.

41 Millar R.F. and Bates R.H.T. "On the Legitimacy of An Assumption Underlying the Point-Matching Method" to appear in IEEE Micro. Theory and Tech.

42 Weiner S.D. and Borison S.L. "Radar Scattering from Blunted Cone Tips" IEEE Trans. Ant. and Prop., AP-14, 1966, 774-781.

43 Waterman P.C. "Scattering by Dielectric Obstacles" Mitre Corp. Rpt., MTP-84, 1968.

44 Senior T.B.A. "Impedance Boundary Conditions for Imperfectly Conducting Surfaces" Appl. Sci. Res., Sec. B, 8, 418-436.

45 Richmond J.H. "Digital Computer Solutions of the Rigorous Equations for Scattering Problems" Proc. IEEE, 53, 1965, 796-804.

46 Jones D.S. The Theory of Electromagnetism, Pergamon, London, 1964, § 6.15, § 6.16.

47 Keller J.B. "Geometrical Theory of Diffraction" J. Opt. Soc. Am., 52, 1962, 116-130.

48 Levy B.R. and Keller J.B. "Diffraction by a Smooth Object" Commun. Pure and Appl. Math., XII, 1959, 159-209.

49 Felsen L.B. "Backscattering from Wide-Angle and Narrow-Angle Cones" J. Appl. Phys., 26, 1955, 138-151.

50 Keller J.B. "Diffraction by an Aperture" J. Appl. Phys., 28, 1957, 426-444.

51 Morse B.J. "Diffraction by Polygonal Cylinders" J. Math. Phys., 5, 1964, 199-214.

52 Kapany N.S., Burke J.J. and Frame K. "Diffraction by Apertures of Wavelength Dimensions" Applied Optics, 4, 1965, 1229-1238.

53 Ross R.A. "Radar Cross Section of Rectangular Flat Plates as a Function of Aspect Angle" IEEE Trans. Ant. and Prop., AP-14, 1966, 329-335.

54 Yee H.Y., Felsen L.B., and Keller J.B. "Ray Theory of Reflection from the Open End of a Waveguide" SIAM J. Appl. Math., 16, 1968, 268-300.

55 Yee H.Y. and Felsen L.B. "Ray Optics - A Novel Approach to Scattering by Discontinuities in a Waveguide" IEEE Trans. Micro. Theory and Tech., MTT-17, 1969, 73-85.

56 Pimenov Y.V. and Kravtsova G.V. "Diffraction of a Plane Electromagnetic Wave by an Ideally Conducting Spherical Segment" Radiotekhnika 24. English Translation in Telecom. and Radio Eng., 24, 1969, 101-106.

57 Ryan C.E. and Peters L. "Evaluation of Edge-Diffracted Fields Including Equivalent Currents for the Caustic Regions" IEEE Trans. Ant. and Prop., AP-17, 1969, 292-299.

58 Ahluwalia D.S., Lewis R.M., and Boersma J. "Uniform Asymptotic Theory of Diffraction by a Plane Screen" SIAM J. Appl. Math., 16, 1968, 783-807.

59 Hamid M.A.K. "Near Field of a Conducting Wedge" IEEE Trans. Ant. and Prop., AP-15, 1967, 490-492.

60 Mohsen A. and Hamid M.A.K. "Higher Order Asymptotic Terms of the Two-Dimensional Diffraction by a Small Aperture" Radio Sci., 3, 1968, 1105-1108.

61 Keller J.B., Lewis R.M., and Seckler B.D. "Asymptotic Solution of Some Diffraction Problems" Comm. Pure and Appl. Math., IX, 1956, 207-265.

62 Mohsen A. and Hamid M.A.K. "Modified Asymptotic Solution for the 2-dimensional Scattering by a Conducting Strip" Electron. Lett., 6, 1970, 12-13.

63 Ryan C.E. and Rudduck R.C. "A Wedge Diffraction Analysis of the Radiation Patterns of Parallel Plate Waveguides" IEEE Trans. Ant. and Prop., AP-16, 1968, 490-491.

64 Rudduck R.C. and Wu D.C.F. "Slope Diffraction Analysis of TEM Parallel-Plate Guide Radiation Patterns" IEEE Trans. Ant. and Prop., AP-17, 1969, 797-799.

65 Yu J.S. and Rudduck R.C. "On Higher-Order Diffraction Concepts Applied to a Conducting Strip" IEEE Trans. on Ant. and Prop., AP-15, 1967, 662-668.

66 Karp S.N. and Russek A. "Diffraction by a Wide Slit" J. Appl. Phys., 27, 1956, 886-894.

67 Millar R.F. "An Approximate Theory of the Diffraction of an Electromagnetic Wave by an Aperture in a Plane Screen" Proc. IEE, 103C, 1955, 177-185.

68 Millar R.F. "The Diffraction of an Electromagnetic Wave by a Circular Aperture" Proc. IEE, 104C, 1957, 87-95.

69 Millar R.F. "The Diffraction of an Electromagnetic Wave by a Large Aperture" Proc. IEE, 104C, 1957, 240-250.

70 Ryan C.E. and Peters L. "Evaluation of Edge-Diffracted Fields Including Equivalent Currents for the Caustic Regions" IEEE Trans. Ant. and Prop., AP-17, 1969, 292-299.

71 Moullin E.B. and Phillips F.M. "On the Current Induced in a Conducting Ribbon by the Incidence of a Plane Electromagnetic Wave" Proc. IEE, 99 (IV), 1952, 137-150.

72 Keller J.B. and Hansen E.B. "Survey of the Theory of Diffraction of Short Waves by Edges" Acta Physica Polonica, XXVII, 1965, 217-234.

73 Kouyoumjian R.G. "Asymptotic High-Frequency Methods" Proc. IEEE, 53, 1965, 864-876.

74 Felsen L.B. "Quasi-optical Methods in Microwave Propagation and Diffraction" Appl. Optics, 4, 1965, 1217-1228.

75 Lewin L. "Wedge Diffraction functions and their use in Quasioptics" Proc. IEE, 116, 1969, 71-76.

76 Harrington R.F. "On Scattering by Large Conducting Bodies" IRE Trans. Ant. and Prop., AP-7, 1959, 150-153.

77 Bates R.H.T. "Simulation Techniques for Evaluation of Space Vehicle Identification Radar Systems" Sperry Rand Research Center, SRRC 526-38, 1965.

78 Fock V.A. "The Distribution of Currents induced by a Plane Wave on the Surface of a Conductor" J. Phys. USSR, 10, 1946, 130-136.

79 Goodrich R.F. "Fock Theory - An Appraisal and Exposition" IRE Trans. Ant. and Prop., AP-7, 1959, 28-36.

80 Waterman P.C. "Elementary Source Description of Scattering and Diffraction" Avco Corp. Tech. Rpt., RAD-TR-62-13, 1962.

81 Waterman P.C. "Exact Theory of Scattering by Conducting Strips" Avco Corp. Tech. Memo., RAD-TM-63-78, 1963.

82 Plonsey R. "Diffraction by Cylindrical Reflectors" Proc. IEE, 105C, 1958, 312-318.

83 Clemmow P.C. The Plane Wave Spectrum Representation of Electromagnetic Fields, Pergamon Press, London, 1966.

84 Jones D.S. The Theory of Electromagnetism, Pergamon, London, 1964, § 1.27.

85 Watson G.N. A Treatise on the Theory of Bessel Functions, Cambridge Univ. Press, 1922, Chapter 5.

86 Cole W.J., Nagelberg E.R. and Nagel C.M. "Iterative Solution of Waveguide Discontinuity Problems" B.S.T.J., 46, 1967, 649-672.

87 Abramowitz M. and Stegun I.A. Handbook of Mathematical Functions, Dover, N.Y. 1965, Chap. 25.

88 Jones D.S. "Diffraction by a Thick Semi-infinite Plate" Proc. Roy. Soc. London, 217, 1953, 153-175.

89 Schretter S.J. and Bolle D.M. "Surface Currents Induced on a Wedge Under Plane Wave Illumination: an Approximation" IEEE Trans. Ant. and Prop., AP-17, 1969, 246-248.

90 Russo P.M., Rudduck R.C., and Peters L. "A Method for Computing E-Plane Patterns of Horn Antennas" IEEE Trans. Ant. and Prop., AP-13, 1965, 219-224.

91 Burke J.E. and Keller J.B. Research Rept. EDL-E48, Electronic Defense Laboratories, Sylvania Electronic Systems, Mountain View, California, 1960.

92 See for example "Proc. Conf. on Tropospheric Wave Propagation", IEE, London, 1968.